

Unit Commitment Models and Algorithms for the Simulation of the European Power System under many Weather Scenarios

**Modellen en algoritmen voor generator planning ten behoeve van
simulatie van het Europese elektriciteitssysteem onder verschillende
weersomstandigheden**

(met een samenvatting in het Nederlands)

Proefschrift

ter verkrijging van de graad van doctor aan de
Universiteit Utrecht
op gezag van de
rector magnificus, prof.dr. H.R.B.M. Kummeling,
ingevolge het besluit van het college voor promoties
in het openbaar te verdedigen op

vrijdag 25 augustus 2023 des middags te 2.15 uur

door

Rogier Hans Wuijts

geboren op 14 april 1993
te Zevenaar

Promotoren:

Prof. dr. E. Worrell

Dr. ir. J.M. van den Akker

Copromotor:

Dr. ir. M.A. van den Broek

Beoordelingscommissie:

Prof. dr. G.T. Barkema

Prof. dr. ir. E. Delarue

Prof. dr. M. Gibescu

Prof. dr. J.L. Hurink

Prof. dr. M.M. de Weerd

Dit proefschrift is onderdeel van het onderzoeksprogramma “Energie: Systeem Integratie en Big Data” met project nummer 647.003.005, gefinancierd door de Nederlandse Organisatie voor Wetenschappelijk Onderzoek (NWO) in samenwerking met KNMI en TenneT.

Contents

1	Introduction	7
1.1	Introduction	8
1.1.1	Climate Change and Climate Policy	8
1.1.2	Electric Power System	8
1.1.3	Power System Modeling	11
1.1.4	Unit Commitment Problem	12
1.1.5	Solving the Unit Commitment Problem	13
1.1.6	Main Research Questions of this Thesis	14
2	Effect of Modelling Choices in the Unit Commitment Problem	21
2.1	Abstract	23
2.2	Introduction	23
2.3	Unit Commitment Problem	25
2.3.1	Decision Variables	25
2.3.1.1	Commitment and dispatch decision variables	25
2.3.1.2	Auxiliary commitment variables	27
2.3.1.3	Alternative dispatch decision variable	27
2.3.2	Objective Function	27
2.3.2.1	Quadratic Generation Cost	27
2.3.2.2	Piece-wise linear generation cost function	28
2.3.2.3	Cycle Cost	29
2.3.2.4	System Costs	30
2.3.3	Thermal generator constraints	31
2.3.3.1	Generation Limits	31
2.3.3.2	Tighter generation limits	31
2.3.3.3	Ramp up and down limits	31
2.3.3.4	Minimum up- and downtime	32
2.3.4	Variable renewable energy and storage	32
2.3.4.1	Storage constraints	32
2.3.4.2	Variable Renewable Energy	33
2.3.5	Power Balance Constraint	33
2.3.6	Reserve Constraints	34
2.3.7	Transmission Constraints	35
2.3.7.1	DC model	35

2.3.7.2	Trade-Based	36
2.3.7.3	Copperplate	37
2.3.8	Clustering	37
2.3.9	Uncertainty	37
2.4	Methods	38
2.4.1	Instances	38
2.4.2	Experimental Setup	39
2.4.3	Indicators to measure performance	42
2.5	Results	44
2.5.1	(Tight) Linear relaxation	44
2.5.2	Impact of Relaxations	46
2.5.2.1	Ramping limits and reserve requirements	46
2.5.2.2	Minimum up- and down time and startup-costs	48
2.5.2.3	Overall Trend	48
2.5.3	Impact of resolution of piece-wise approximation	50
2.5.4	Impact of transmission modelling	50
2.5.5	Impact of alternative objective function	52
2.6	Discussion	53
2.6.1	Implications of key findings and comparison with existing literature	53
2.6.2	Limitations	54
2.7	Conclusion	55
3	An Improved Algorithm for Single-Unit Commitment with Ramping Limits	65
3.1	Abstract	66
3.2	Introduction	66
3.3	Outlook	67
3.4	Problem Definition	68
3.5	First Recurrence Relation	69
3.6	Constructing F_t^τ	71
3.7	Algorithm $RRF(+)$	73
3.7.1	Time Complexity	74
3.8	Second Recurrence Relation	74
3.9	Algorithm RRH	76
3.10	Computational Results	78
3.10.1	Results	79
3.11	Conclusion	81
4	New efficient ADMM algorithm for the Unit Commitment Problem	85
4.1	Abstract	86
4.2	Introduction	87
4.3	UC problem description	89
4.4	ADMM Example on simple UC problem	91
4.4.1	Multi-block Gauss Seidel	92

4.5	New ADMM Algorithm for UC	93
4.5.1	Solving the subproblems	94
4.5.1.1	Generator subproblem 1UC	94
4.5.1.2	Renewable generation subproblem 1RES	95
4.5.1.3	Storage subproblem 1Storage	96
4.5.1.4	Transmission subproblem	96
4.5.2	Our ADMM algorithm	98
4.6	Computational Experiments	100
4.6.1	Results	101
4.7	Discussion	109
4.8	Conclusion	109
5	Pitfalls of Power Systems Modelling Metrics	117
5.1	Abstract	118
5.2	Introduction	118
5.3	Methods	119
5.3.1	Metrics	120
5.3.2	Unit Commitment Instances	120
5.3.3	Procedure	122
5.4	Results	123
5.4.1	Loss of Load Hours	123
5.4.2	Capacity Factor	125
5.4.3	CO ₂ Emissions	126
5.5	Discussion	126
5.6	Conclusion	127
6	Linking Unserved Energy to Weather Regimes	131
6.1	Abstract	132
6.2	Introduction	132
6.3	Methods & Modelling	133
6.3.1	Energy System Scenarios	133
6.3.2	Power System Model	135
6.3.3	Modelling weather dependent variables	136
6.3.3.1	Energy conversion models for wind and solar	136
6.3.3.2	Hydro inflow data	137
6.3.4	Weather Regimes	138
6.3.5	Weather dependent demand	138
6.4	Results	139
6.4.1	Scenario dependency	139
6.4.2	Sequence of Weather Regimes	142
6.4.3	Driving factors for Unserved Energy during Weather Regimes	145
6.4.4	Role of storage	148
6.4.5	Validation of power system model formulation	148
6.5	Limitations and discussion	150
6.6	Conclusion	152

7	Conclusion	159
7.1	Summary	160
7.2	Research Question 1: How do modeling decisions influence the outcomes and computational performance of the UC in power system modeling?	164
7.3	Research Question 2: How can solving the unit commitment problem be algorithmically improved?	165
7.4	Research Question 3: What is the relationship between adequacy of European power systems and weather regimes?	166
7.5	Key Contributions and Impact	167
7.6	Future Work	167
7.7	Nederlandse Samenvatting	168
8	Appendices	177
8.1	Appendix Chapter 2	178
8.1.1	Additional Tight Constraints	178
8.1.2	Additional Figures and Tables	179
8.2	Appendix Chapter 3	192
8.3	Appendix Chapter 4	192
8.3.1	Multi-block ADMM by Variable Splitting	192
8.3.2	Gauss Seidel Compared to Variable Splitting	195
8.4	Appendix Chapter 5	196
8.4.1	UC problem description	196
8.4.2	Overview of experiments	197
8.4.3	Additional Figures	197
8.5	Appendix Chapter 6	200
8.5.1	Open Research	200
8.5.2	Region definition and naming convention	201
8.5.3	Specified capacity of the main bidding zones used	203
8.5.4	Unit Commitment Model	204
8.5.5	Validating Assumptions	205
8.5.6	Method for determining photovoltaic panel generation potential	206
8.5.7	Method for determining wind turbine generation potential	206
8.5.8	Method for determining Hydropower generation potential	207
8.5.9	Classification of weather into regimes	208
8.5.10	Summary of relative occurrence of weather regimes for all bidding zones	210
8.5.11	Meteorological changes between different weather regimes	214

Chapter 1

Introduction

1.1 Introduction

1.1.1 Climate Change and Climate Policy

An energy transition is currently taking place across the world driven by the global endeavor to decrease greenhouse gas emissions. In 2022, anthropogenic greenhouse gas emissions are estimated to already have caused approximately 1.0°C of warming to the average global surface temperature compared to pre-industrial levels (1850–1900) [19]. CO₂ emissions specifically are the primary driver of global climate change [33]. To avoid the worst consequences of climate change, the world needs to rapidly reduce its greenhouse gas emissions and in particular its CO₂ emissions.

As a result, almost every country in the world has ratified the Paris Agreements and is committed to keep the rise in mean global temperature well below 2 °C and to pursue efforts to limit the temperature increase to 1.5 °C above pre-industrial levels [30]. According to IPPC modeling pathways, this means that the world needs to reach net zero greenhouse gas emissions around 2050 or 2070 in order to limit the temperature increase to 1.5°C or 2.0°C respectively [20]. Following this, the EU aims to be net-zero by 2050 [13] meaning that in 2050 total production of greenhouse gases in Europe is offset by removal of greenhouse gas from the atmosphere.

The production of electricity is a large contributor to global greenhouse gas emissions (Figure 1.1). Around one third of global CO₂-eq ¹ GHG emissions are currently produced to generate electricity (heat is often also produced as a byproduct, i.e. district heating and process heat). Consequently, significant changes in electricity production are necessary for achieving net zero and mitigating climate change.

1.1.2 Electric Power System

An electric power system is a system that produces, transfers, and consumes electricity. Most electricity generation comes from thermal generation where heat energy is converted into electrical energy. This heat for thermal generation can come from a variety of sources such as nuclear fission, geothermal power, concentrated solar power, biofuels, and waste incineration, but most comes from fossil fuels (Figure 1.2). In order to reduce emissions, the power system needs to shift from one that is dominated by fossil fuels towards one that is dominated by low carbon thermal generation and renewable energy sources [18].

A large part of these renewable energy sources (RES) are intermittent such as solar photovoltaics (PV), onshore and offshore wind, and run-of-river hydro power. The relative share of RES in the total production of electricity is increasing. 10.5% of the global electricity generation in 2021 came from solar and wind compared to less than 1% in 2012 [6]. Moreover, more than 80% of the new installed capacity in

¹CO₂-eq is a metric measure used to compare the emissions from various greenhouse gases on the basis of their global-warming potential, by converting amounts of other gases to the equivalent amount of carbon dioxide with the same global-warming potential.

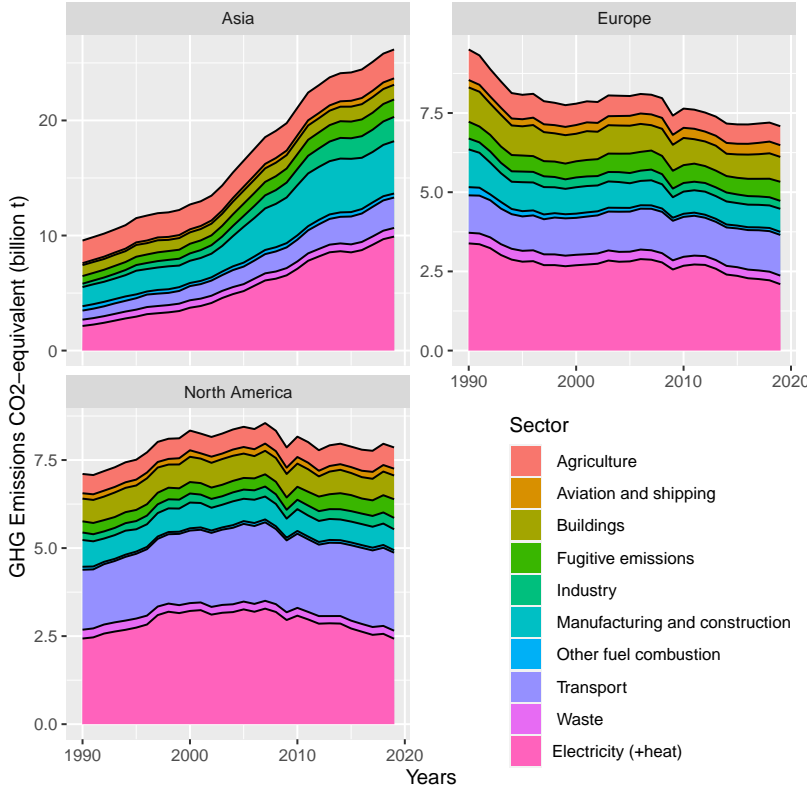


Figure 1.1: GHG emissions in CO₂-eq for different sectors for Asia, Europe and North America. Data from [33].

power systems around the world in 2021 were based on renewable energy sources (Figure 1.3).

These intermittent renewable energy sources are characterized by uncertain production and more importantly a large variability caused by their weather dependence and therefore make the power system increasingly weather dependent. Moreover, the electrification of heating exacerbates this weather dependence [12]. With this variability the uninterrupted availability of electricity is more challenging to achieve. To account for this variability of generation and demand, a power system must have sufficient flexibility to respond to the variability. Flexibility is the ability of a power system to adjust electricity demand or generation in response to anticipated and unanticipated variability [5]. In the past the main sources of flexibility were dispatchable generators, but energy storage, transmission expansion and reinforcement, and demand side response can also provide flexibility to the power system.

The need for hour-to-hour flexibility² in the power system doubles in 2030

²Flexibility needs are represented by the hour-to-hour ramping requirements after removing

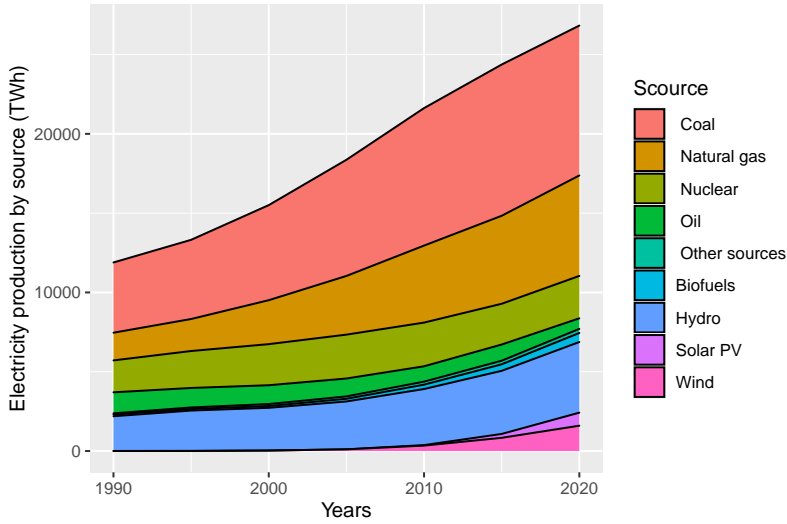


Figure 1.2: The total global electricity generation per type of source. Data from [34].

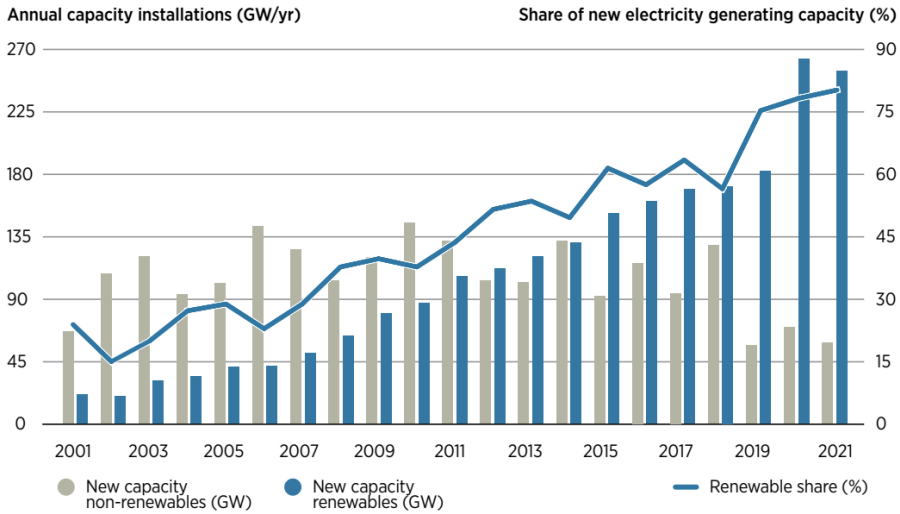


Figure 1.3: Renewable share of annual power capacity expansion. Figure taken from World Energy Transitions Outlook 2022: 1.5°C Pathway [21].

(Figure 1.4) and doubles again in 2050 if all aspirational targets announced by governments to tackle climate change are met [18]. If dispatchable thermal gener-

hourly wind and solar PV production from hourly electricity demand, divided by the average hourly demand for the year [18].

ators are not the main source of flexibility anymore, then storage and transmission capacity are needed to balance the uneven residual demand, i.e. the demand minus the intermittent renewable generation, over time and space. There are multiple ways to ensure the system has sufficient flexibility. For example, there is a large variety of proven and novel energy storage technologies (e.g. (pumped) hydro storage, lithium-ion battery storage, flow batteries, hydrogen energy storage) [24], but which role they will play in a future power system remains uncertain. **To analyze the impact of this transition and to assess whether possible pathways to achieve a net zero future are adequate, power system models are crucial [10].**

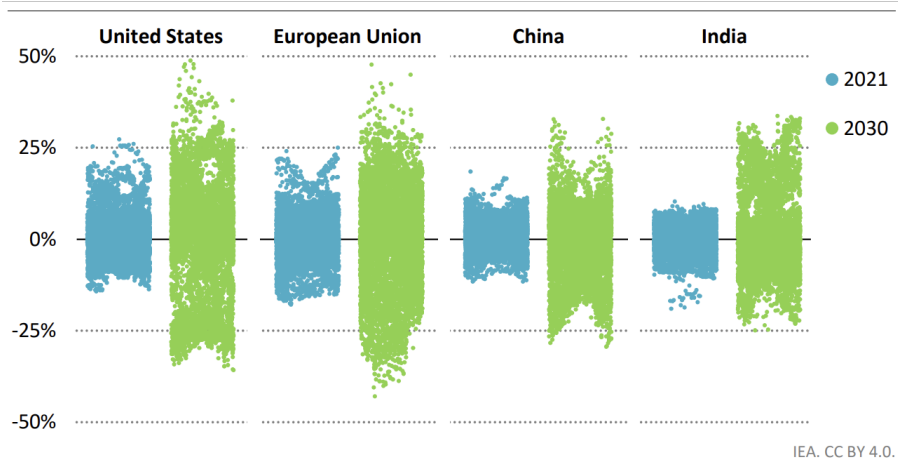


Figure 1.4: Hour-to-hour flexibility (ramping requirements) needs in the United States, European Union, China and India in 2021 and in the *Announced Pledges* scenario 2030 of the World Energy Outlook [18]

1.1.3 Power System Modeling

Power system modeling is the process of building, programming, and running mathematical models of power systems to analyze current and future power systems. Power system models (PSM) can be based on different model methodologies and serve different purposes [32]. For example, a PSM can be top-down (macro-behavior is enforced) or bottom-up (macro-behavior is emergent), simulation or optimization, and prescriptive or descriptive. In practice, PSMs often have a mixture of these characteristics [32]. For instance, a prescriptive PSM that uses optimization to find the best operation of the system also provides insight into the limits of the system. For example, if the optimal operation of the European power system results in a large amount of unserved energy, the power system can be described as inadequate.

Power system models are important for policy-making. For example, an important reliability indicator for power systems is Energy Not Served (ENS). ENS is the amount of energy demand in MWh which is not supplied in a given region and time period due to insufficient resources. The expected ENS in a year (EENS), is one of the two key reliability indicators which must be calculated in the EU as part of the European Resource Adequacy Assessment (ERAA), a European power system model study [14]. The other reliability indicator is loss of load expectation (LOLE), i.e., the expected number of hours ENS occurs in a year. Both indicators are calculated by simulating a power system for multiple years and taking the average of the yearly ENS and loss of load hours. Both reliability indicators are important because any EU member state that wishes to implement a capacity mechanism to safeguard security of supply, is only allowed to do so if the ERAA shows that the national LOLE is above a specified reliability standard [2, 11].

As the future power system will be more weather dependent, its operation will be influenced by weather variability. It is important to capture this weather variability in power system models as well. Therefore, power systems should be simulated for multiple weather years. This in turn means that the time horizons or the number of model runs of the power system model increases, and hence the computation time associated with it. Moreover, in order to accurately model the effect of the weather variability on the power system a high temporal resolution is needed [32]. To simulate hourly market operation by optimization with high technical detail often the unit commitment problem is used [38, 1].

1.1.4 Unit Commitment Problem

The unit commitment problem (UC), sometimes called the unit commitment and economic dispatch problem (UCED), is a family of optimization problems about deciding on the operation of electrical generators. The goal is to find a minimum cost schedule of generators that satisfies the electricity demand at each time step. UC is a widely researched topic in Operations Research and is commonly used in power system studies. UC is solved for time horizons ranging from days to years, in order to support market decisions and evaluate the adequacy of the system [31, 39, 40, 8, 16, 15].

A solution of the UC is a schedule that for each timestep dictates which electrical generators should be on and how much energy should be dispatched by each of them. Additionally, the solution can contain information on power flows in the grid, curtailment of intermittent renewable energy, loss of load, allocation of reserves, storage, and demand response.

Finding an optimal schedule is not easy. Individual generators have limits on the quantity they can produce and by how much they can change their production over time. Ramping limits determine how much a generator can change their energy production over time, which are set by physical and economical constraints, i.e. ramping can induce cost due to wear and tear [37]. Moreover, generators can only produce between their maximum capacity and minimum stable generation which could be between 30%-50% of maximum capacity depending on the type of generator [17]. Moreover, some generators have minimum up- and downtime,

a specified number of hours or days that the generators need to be turned off or on to ensure safe or economically viable operation. All of these factors contribute to the amount of flexibility of a generator and must be taken into account when finding an optimal schedule in the UC.

1.1.5 Solving the Unit Commitment Problem

The UC has been extensively researched in academia but is not considered to be well solved [3]. It exhibits a lot of characteristics that makes optimization problems hard, it is nonlinear, nonconvex and has a combinatorial characteristic due to the binary commitment variables [3]. UC is an NP-hard problem [25]. This means that there currently does not exist an algorithm with a polynomial time complexity that returns the optimal answer for any input and it is considered unlikely that such an algorithm exists. Various optimization techniques have been applied that try to solve the UC. This can be seen in the numerous papers cited in various surveys on the topic [3, 35, 29] spanning multiple algorithm paradigms, from exact methods to heuristic evolutionary algorithms. However, since UC has a mixed combinatorial and continuous statespace, mathematical programming techniques have been most successful in finding near optimal solutions [3]. Until the early 2000s, Lagrangian Relaxation was the method of choice for solving UC [7]. However, this has changed. In the past 15 years, Mixed Integer Linear Programming (MILP) problem formulations have been a very active area of research [23] and popular tool for solving the UC [4, 36, 26]. Additionally, it has been stated that in the industry, UC is commonly solved using MILP and that the shift from Lagrangian Relaxation to MILP was considered beneficial [27, 9, 28]. **However, even MILP has its limits when the number of timesteps or generators becomes too large, as is the case when modeling the power system in Europe.**

Therefore, in power system studies, the UC problems are sometimes simplified to save computation time. For example, the ramping limits, minimum up- and downtime, reserve requirements or integer requirements are relaxed in adequacy studies [16, 15]. Moreover, when solving the UC for a whole year the problem is often broken down into smaller parts. First, a whole year is solved with a simplified model that omits most unit commitment constraints in order to fix certain variables such as storage levels and planned outages [39, 22, 31]. Next, with those fixed values, a more detailed UC is solved on much smaller time horizons of a few days. **A drawback is that all these simplifications often are made without analyzing their effect on the quality of the solution.**

This illustrates that power system modeling inherently has an important trade-off between detailed models with long time horizons on the one hand and computation time on the other [32]. A reduction in the computation time of a power system model will in turn mean we can assess larger power systems, longer time horizons, or include more details in the model. **Therefore, the increase of efficiency of the underlying algorithm of a power system model based on UC will eventually improve the power system model in more than only in the efficiency.**

1.1.6 Main Research Questions of this Thesis

To summarize, the need for climate change mitigation results in a shift of electricity production in future power systems from fossil fuels towards low carbon and renewable energy sources. A large part of these renewable energy sources, i.e. wind, solar and run-of-river hydro, are intermittent. This together with the electrification of heating introduces variable generation and demand in the power system that depends on weather. There are multiple pathways to introduce the required flexibility and decarbonization into the system. However, operation of these potential future power systems need to be simulated by power system models to assess their system adequacy and identify potential problems.

Ideally, these power system models have high spatial and temporal resolutions in order to capture the full dynamic of regions that are under stress as they need to rely on their storage and transmission to spread the uneven residual demand over time and space. Moreover, due to the weather dependence of the power system and the variability of weather, this power system needs to be simulated under a large variety of weather years.

The unit commitment problem (UC) is used to simulate the operation of the power system with high levels of technical detail and captures the characteristics of flexibility of thermal generators and of the transmission and storage in the system. Solving these UC problems is not trivial as it is a hard optimization problem, and the size of the power system models makes solving it even harder. This results in incredibly high computation times which can be addressed by either increasing the efficiency of the algorithms or performing justified simplifications to the UC problem.

Power system modeling based on UC is used as a tool to evaluate the power system by different parties such as transmission system operators (TSO's) and policy makers. This thesis investigates how to use this tool, investigates how to improve it, and with the gained knowledge appropriately applies the tool itself. This thesis investigates how to use the power system modeling with the UC by studying the effect of model simplification on the computation time and outcome of the UC and investigates the sensitivity of important model metrics produced by the UC. This thesis also investigates how to improve solving the UC problem by creating new algorithms that produce high quality solutions with low computation time without simplifying the UC model. In the end we use the power system modeling with the UC by simulating a future European power system and investigate the relationship of adequacy and different weather regimes with the gained knowledge from the previous two points.

The main research question of this thesis therefore is: **How can power system modeling with the underlying unit commitment problem be used and improved to assess future power systems under a large variety of weather scenarios?** This research question is subdivided into the following sub-research questions which are answered throughout this thesis:

- RQ1: How do modeling decisions influence the outcomes and computational performance of the UC in power system modeling?

- RQ2: How can solving the unit commitment problem be algorithmically improved?
- RQ3: What is the relationship between adequacy in the European power systems and weather regimes?

These sub questions are addressed in multiple chapters in the thesis with some overlap (Table 1.1).

Chapter	Topic	Research Question		
		RQ1	RQ2	RQ3
2	Effect of power system model choices	✓		
3	Improved algorithms for 1UC		✓	
4	Improved algorithm for UC		✓	
5	Pitfalls of modeling metrics	✓		
6	Relationship ENS and weather regimes	✓		✓

Table 1.1: How the sub research questions related to the chapters.

Chapter 2, titled “*Effect of Modeling Choices in the Unit Commitment Problem*” thoroughly investigates the impacts of simplifications of UC formulations on solution quality and computation time. In power system studies, the UC problems are sometimes simplified to save computation time. However, these simplifications often are made without analyzing their effect on the solution quality. In this chapter a benchmark set consisting of almost all the available problem instances in the UC literature is introduced. On these problem instances we performed multiple experiments with the full UC problem formulation and 21 different model simplifications. We then used several indicators to compare the computation time and quality of the solutions between the different UC formulations.

Chapter 3, titled “*An Improved Algorithm for Single-Unit Commitment with Ramping Limits*” presents two efficient dynamic programming algorithms for the single unit commitment problem (1UC). 1UC is a subproblem that appears in many decomposition algorithms that solve the UC. 1UC is the problem of finding a cost optimal schedule for a single generator given a time series of electricity prices subject to generation limits, minimum up- and downtime and ramping limits. To solve the 1UC we maintain a set of functions for each time step, which represent the cost of the optimal schedule up to that time step. We show that we can combine a subset of these functions by only considering their minimum. We can construct this minimum either implicitly or explicitly. We have conducted experiments to demonstrate the efficiency of our algorithm and have analyzed how the computation time increases with an increase in the time horizon.

Chapter 4, titled “*New efficient ADMM algorithm for the Unit Commitment Problem*” introduces a new and efficient way to heuristically solve the UC with the Alternating Direction Method of Multipliers (ADMM). Our algorithm has a low computation time due to our efficient algorithm for the single UC subproblem introduced in Chapter 3 and our newly created algorithm to solve the transmission

subproblems. Our new algorithm is tested on a large set of UC problem instances and compared to the state-of-the-art MIP formulation for the UC.

Chapter 5, titled “*Pitfalls of Power Systems Modeling Metrics*” explores the possible variety of (sub)-optimal solutions to the UC. It shows that characteristics of these solutions that were not included in the optimization objective might get arbitrary values. Conclusions about such characteristics might therefore be presumptuous. For example, loss of load hours is part of one of the key reliability indicators used in the EU. However, equivalent optimal UC solutions in terms of the objective cost can have different loss of load hours. We illustrate this by multiple experiments on a future European power system. Each scenario was run multiple times by adding additional terms to the objective function such as the minimization and maximization of generator capacity factors, carbon emissions, and loss of load hours.

Chapter 6, titled “Linking Energy not Served with Weather Regimes” explores the relationship between Energy Not Served (ENS) and weather regimes. ENS is the total energy demand that cannot be supplied by electricity. Weather regimes are classifications of common atmospheric circulation regimes. Since weather regimes of Europe influence the renewable generation and the energy demand in Europe it is to be expected that for certain (sequences of) weather regimes it is more difficult to supply all energy demand. In this chapter we explore this relationship by simulating a large variety of weather scenarios on multiple future European power system scenarios created by ENTSO-E.

The last chapter summarizes the findings of these chapters and relates them to the research questions introduced here.

Bibliography

- [1] Saleh Y Abujarad, Mohammad Wazir Mustafa, and Jasrul Jamani Jamian. “Recent approaches of unit commitment in the presence of intermittent renewable energy resources: A review”. In: *Renewable and Sustainable Energy Reviews* 70 (2017), pp. 215–223.
- [2] ACER. *Methodology for Calculating the Value of Lost Load, the Cost of New Entry and the Reliability Standard*. 2020.
- [3] Wim van Ackooij et al. “Large-scale unit commitment under uncertainty: an updated literature survey”. In: *Annals of Operations Research* (2018), pp. 1–75.
- [4] Semih Atakan, Guglielmo Lulli, and Suvrajeet Sen. “A state transition MIP formulation for the unit commitment problem”. In: *IEEE Transactions on Power Systems* 33.1 (2017), pp. 736–748.
- [5] Olubayo Moses Babatunde, Josiah L Munda, and YJER Hamam. “Power system flexibility: A review”. In: *Energy Reports* 6 (2020), pp. 101–106.
- [6] BloombergNEF. *Power Transition Trends*. 2022.
- [7] Alberto Borghetti et al. “Lagrangian heuristics based on disaggregated bundle methods for hydrothermal unit commitment”. In: *IEEE Transactions on Power Systems* 18.1 (2003), pp. 313–323.
- [8] Anne Sjoerd Brouwer et al. “Least-cost options for integrating intermittent renewables in low-carbon power systems”. In: *Applied Energy* 161 (2016), pp. 48–74.
- [9] Brian Carlson et al. “MISO unlocks billions in savings through the application of operations research for energy and ancillary services markets”. In: *Interfaces* 42.1 (2012), pp. 58–73.
- [10] Miguel Chang et al. “Trends in tools and approaches for modelling the energy transition”. In: *Applied Energy* 290 (2021), p. 116731.
- [11] European Commission. “Regulation (EU) 2019/943 of the European Parliament and of the Council of 5 June 2019 on the Internal Market for Electricity”. In: *Off. J. Eur. Union* 158 (2019), pp. 54–124.
- [12] Matteo De Felice et al. *Power system flexibility in a variable climate*. Publications Office of the European Union, 2020.

- [13] A EC. “Clean Planet for all: a European strategic long-term vision for a prosperous, modern, competitive and climate neutral economy”. In: (2018).
- [14] ENTSO-E. *European Resource Adequacy Assessment - 2021 Edition*. 2021.
- [15] ENTSO-E. *Mid Term Adequacy Forecast (MAF)*. 2018. URL: https://docstore.entsoe.eu/Documents/SDC_20documents/MAF/2018/MAF_202018_20Executive_20Report.pdf.
- [16] ENTSO-E. *Pentalateral Energy Forum Support Group 2 Generation Adequacy Assessment*. 2018. URL: https://www.bmwi.de/Redaktion/DE/Downloads/P-R/plaf-sg2-generation-adequacy-assessment-2018.pdf?__blob=publicationFile&v=4.
- [17] ENTSO-E and ENTSO-G. *TYNDP2020—Scenario building guidelines*. 2020. URL: https://2020.entsos-tyndp-scenarios.eu/wp-content/uploads/2020/06/TYNDP_2020_Scenario_Building_Guidelines_Final_Report.pdf.
- [18] International Energy Agency. *World Energy Outlook 2022*. 2022, p. 524. DOI: <https://doi.org/https://doi.org/10.1787/3a469970-en>. URL: <https://www.oecd-ilibrary.org/content/publication/3a469970-en>.
- [19] IPCC. “Summary for Policymakers”. In: *Climate Change 2021: The Physical Science Basis. Contribution of Working Group I to the Sixth Assessment Report of the Intergovernmental Panel on Climate Change*. Ed. by V. Masson-Delmotte et al. Cambridge, United Kingdom and New York, NY, USA: Cambridge University Press, 2021, pp. 3–32. DOI: 10.1017/9781009157896.001.
- [20] IPoCC IPCC. “Summary for Policymakers” in Global warming of 1.5° C. An IPCC Special Report on the impacts of global warming of 1.5° C above pre-industrial levels and related global greenhouse gas emission pathways, in the context of strengthening the global response to the threat of climate change, sustainable development, and efforts to eradicate poverty”. In: *Sustainable Development, and Efforts to Eradicate Poverty*. Geneva, Switzerland: World Meteorological Organization 32 (2018).
- [21] IRENA. *World Energy Transitions Outlook 2022: 1.5° C Pathway*. 2022.
- [22] Konstantinos Kavvadias et al. *Integrated modelling of future EU power and heat systems-The Dispa-SET v2. 2 open-source model*. Tech. rep. European Commission, 2018.
- [23] Bernard Knueven, James Ostrowski, and Jean-Paul Watson. “A novel matching formulation for startup costs in unit commitment”. In: *Mathematical Programming Computation* (2020), pp. 1–24.
- [24] Chun Sing Lai et al. “A review on long-term electrical power system modeling with energy storage”. In: *Journal of Cleaner Production* 280 (2021), p. 124298.
- [25] Alexander C Melhorn et al. “Validating unit commitment models: A case for benchmark test systems”. In: *Power and Energy Society General Meeting (PESGM), 2016*. IEEE. 2016, pp. 1–5.

- [26] Germán Morales-España, Jesus M Latorre, and Andres Ramos. “Tight and compact MILP formulation of start-up and shut-down ramping in unit commitment”. In: *IEEE Transactions on Power Systems* 28.2 (2013), pp. 1288–1296.
- [27] Richard P O’Neill, Thomas Dautel, and Eric Krall. “Recent ISO software enhancements and future software and modeling plans”. In: *Federal Energy Regulatory Commission, Tech. Rep* (2011).
- [28] RP O’Neill. “It’s getting better all the time (with mixed integer programming)”. In: *HEPG Forty-Ninth Plenary Session* 16 (2007), p. 49.
- [29] Narayana Prasad Padhy. “Unit commitment-a bibliographical survey”. In: *IEEE Transactions on power systems* 19.2 (2004), pp. 1196–1205.
- [30] *Paris Agreement*. URL: https://treaties.un.org/pages/ViewDetails.aspx?src=TREATY&mtdsg_no=XXVII-7-d&chapter=27&clang=_en (visited on 03/28/2019).
- [31] Matija Pavičević et al. “The potential of sector coupling in future European energy systems: Soft linking between the Dispa-SET and JRC-EU-TIMES models”. In: *Applied Energy* 267 (2020), p. 115100.
- [32] Stefan Pfenninger, Adam Hawkes, and James Keirstead. “Energy systems modeling for twenty-first century energy challenges”. In: *Renewable and Sustainable Energy Reviews* 33 (2014), pp. 74–86.
- [33] Hannah Ritchie, Max Roser, and Pablo Rosado. “CO₂ and Greenhouse Gas Emissions”. In: *Our World in Data* (2020). URL: <https://ourworldindata.org/co2-and-other-greenhouse-gas-emissions>.
- [34] Hannah Ritchie, Max Roser, and Pablo Rosado. “Energy”. In: *Our World in Data* (2022). <https://ourworldindata.org/energy>.
- [35] B Saravanan et al. “A solution to the unit commitment problem—a review”. In: *Frontiers in Energy* 7.2 (2013), pp. 223–236.
- [36] Raouia Taktak and Claudia D’Ambrosio. “An overview on mathematical programming approaches for the deterministic unit commitment problem in hydro valleys”. In: *Energy Systems* 8.1 (2017), pp. 57–79.
- [37] Kenneth Van den Bergh and Erik Delarue. “Cycling of conventional power plants: technical limits and actual costs”. In: *Energy Conversion and Management* 97 (2015), pp. 70–77.
- [38] Manuel Welsch et al. “Incorporating flexibility requirements into long-term energy system models—A case study on high levels of renewable electricity penetration in Ireland”. In: *Applied Energy* 135 (2014), pp. 600–615.
- [39] William Zappa, Martin Junginger, and Machteld van den Broek. “Is a 100% renewable European power system feasible by 2050?” In: *Applied energy* 233 (2019), pp. 1027–1050.
- [40] Bas van Zuijlen et al. “Cost-optimal reliable power generation in a deep decarbonisation future”. In: *Applied Energy* 253 (2019), p. 113587.

Chapter 2

Effect of Modelling Choices in the Unit Commitment Problem

Published as:

Effect of modelling choices in the unit commitment problem.

Rogier Hans Wuijts, Marjan van den Akker & Machteld van den Broek
Energy Systems (2023)

Nomenclature

Decision variables

pc_{st}	amount of charging of storage unit s at time t
pd_{st}	amount of discharging of storage unit s at time t
p'_{gt}	power production of generator g at time t that is above the minimum generation
p_{gt}	power output of generator g at time t
p_{rt}	production of renewable energy source r at time t
u_{gt}	commitment variable that is 1 when generator g is on at time t and 0 otherwise
v_{gt}	start variable that is 1 when generator g starts at time t and 0 otherwise
w_{gt}	stop variable that is 1 when generator g stops at time t and 0 otherwise

Functions

SC_g^d	step-wise function of start-up cost of generator g after l timesteps since the generator has been turned off
----------	--

Generator Parameters

\bar{P}_g	maximum power output of generator g
RD_g	ramp down limit of generator g
RU_g	ramp up limit of generator g
SD_g	shutdown limit of generator g
SU_g	start-up limit of generator g
\underline{P}_g	minimum power output of generator g
AT_{rt}	availability factor of renewable energy source r at time t
DT_g	minimum downtime of generator g
UT_g	minimum uptime of generator g

Auxiliary variables

δ_{nt}	voltage angle of node n and time t used in an DC approximation
γ_t	loss of reserve at time t
r_{gt}^+	the spinning reserve generator g provides at time t
f_{lt}	amount of power that flows on the transmission line l

inj_{nt}	amount of power node n draws from the transmission system at time step t .
------------	--

LL_t	loss of load at time t
SC_{gt}	Cost of starting generator g at time t
SR_t	the spinning reserve requirement at time t
v_{gt}^s	start variable that is 1 when generator g at time t has a start-up of type s

Model Generator Parameters

\bar{P}_{gk}	maximum power output of generator g at piece-wise linear segment k
p_{gtk}	power output of generator g at time t at piece-wise linear segment k
s_{gk}	slope of line segment k of the linear approximation of the cost function of generator g
SI_{gs}	beginning of start-upcost interval s

Sets

G	set of generators
K_g	set of line segment of the linear approximation of the cost function of generator g
L	set of indices of the transmission lines
S	set of storage units
T	set of timesteps

System Parameters

\bar{f}_l	maximum flow on transmission line l
\underline{f}_l	maximum negative flow on transmission line l
B_l	susceptance of transmission line l
$PTDF_{ln}$	power transfer distribution matrix, a linear relation between the nodal injection on node n and the flow on transmission line l

VOLL	value of lost load
VOLR	value of lost reserve

Storage Parameters

η_s^c	charge efficiency of storage unit s
η_s^d	discharge efficiency of storage unit s
\bar{PC}_s	maximum charging limit of storage unit s
\bar{PD}_s	maximum discharging limit of storage unit s
\bar{PE}_s	maximum energy of storage unit s
\underline{PE}_s	minimum energy of storage unit s

2.1 Abstract

In power system studies the unit commitment problem (UC) is solved to support market decisions and assess system adequacy. Simplifications are made to solve the UC faster, but they are made without considering the consequences on solution quality. In this study we thoroughly investigated the impacts of simplifications on solution quality and computation time on a benchmark set consisting of almost all the available instances in the literature.

We found that omitting the minimum up- and downtime and simplifying the startup cost resulted in a significant quality loss without reducing the computation time. Omitting reserve requirements, ramping limits and transmission limits reduced the computation time, but degraded the solution significantly. However, the linear relaxation resulted in less quality loss with a significant speed-up and resulted in no difference when unserved energy was minimized. Finally, we found that the average and maximum capacity factor difference is large for all model variants.

2.2 Introduction

The unit commitment problem (UC) is a family of optimization problems about deciding on the operation of electrical generators. The goal is to find a minimum cost schedule of generators that satisfies the demand at each timestep. In power system studies, the UC is being solved for time horizons of days to years to support market decisions or assess system adequacy [66, 93, 96, 12, 22, 21]. For some time now UC has been an active research topic and many algorithms have been proposed [1, 74, 61]. Mathematical programming techniques have been the most successful to find near optimal schedules for this NP-hard problem [1, 51]. For example, the UC is often formulated as a Mixed Integer Linear Programming (MILP) problem and solved with commercial solvers such as Gurobi or CPLEX.

Constraints in a UC model represent essential characteristics of the power system. However, the set of constraints and associated characteristics included in UC models varies for different formulations. Table 2.1 demonstrates the large variety of algorithms and formulations that have been implemented to solve UC problems.

In power system studies, the UC problems are sometimes simplified to save computation time. For example, the ramping limits, minimum up- and downtime, reserve requirements or integer requirements are relaxed in adequacy studies [22, 21]. Moreover, when solving the UC for a whole year the problem is often broken into smaller parts. First, a whole year is solved with a simplified model that omits most unit commitment constraints, to fix certain variables such as storage levels and planned outages [93, 41, 66]. Next, with those fixed values, a more detailed UC is solved on a much smaller time horizon of a few days. *A drawback is that all these simplifications often are made without analyzing their effect on solution quality.*

In a related problem, the generation expansion problem, UC constraints have also been omitted to save computation time [62, 75, 68]. For these generation

expansion problems, numerous studies investigated to what extent errors arise from simplifications in the context of those expansion decisions. These studies have emphasized on power system simplifications, in terms of omitting unit commitment constraints, in the context of a generation expansion problem as opposed to the unit commitment problem itself. Moreover, almost all studies focus on a single power system [68, 63, 69, 19, 62].

Therefore, it is valuable to gain insights into the effect of omitting power system constraints on the solution quality, the violation of the omitted constraints, and the computational speed-up in the context of the UC. Furthermore, it is important to investigate this thoroughly by using a large and variate set of power systems. this chapter addresses the following question: “What is the influence of choices in power system modeling on the results and performance of the UC problem?”

To answer this question, we created and published a benchmark set of UC instances consisting of almost all the available UC instances in the literature¹. On those instances we performed multiple experiments with the full UC problem and its simplifications. We then used several indicators to compare the computation time and quality of the solutions between the different UC formulations. Our research paper contributes to the existing literature in the following way:

- We performed a comprehensive study of model simplifications in the unit commitment problem. In total in this chapter, we present the effect of 21 different model simplifications and variants; We investigated the linear relaxation of the model, the relaxation of the ramping limits, minimum up- and downtime and the removal of the reserve requirements. We also studied the model variants where energy not served instead of the total cost is minimized. Moreover, we investigated multiple piece-wise linear approximation of the quadratic generation cost function and, furthermore, we studied 4 different methods of modeling the transmission system.
- We performed our computational experiments on a large and variate data set, 17 in total consisting of almost all available UC instances in the literature. Moreover, we performed every experiment 30 times with a slight perturbation of the electricity demand to get robust results.
- Our systematic research gives insight into which model simplifications result in a computation gain with little or no loss in quality, which simplifications results in a trade-off between computation time and quality and which model simplifications results in no computational gain at all.
- We also complemented the existing literature by studying these simplifications in the context of the unit commitment problem and not in the context of the generation expansion problem.
- We published the benchmark, we collected from existing literature and put it into a single format. This benchmark can be used to compare algorithms that solve the UC, for which there is a need (see [51]), or it can be used for other power system studies.

¹<https://github.com/rogierhans/UCBenchmark>

The remainder of this chapter is organized as follows. In Section 2.3 we provide an overview of the different aspects of the power systems modeled in UC problems together with their mathematical formulation. Next, we describe our methodology, experimental setup, and present the benchmark of UC instances in Section 2.4. Our results are presented in Section 2.5, and we conclude with our findings, limitations, and comparison with existing literature in Section 2.6.

2.3 Unit Commitment Problem

In this section we discuss which characteristics of the power system can be included in UC problems and how they can be mathematically formulated. Characteristics relate to the efficiency and flexibility limits of the thermal electrical generators, and limitations to the supply of hydropower plants, variable renewable energy sources (VRES) and storage units. Furthermore, it must be ensured that the electricity demand is always met in each region, that sufficient reserves are available, and that transmission constraints are dealt with.

In Section 2.3.1 we introduce the decision variables in the UC and associated variables and in Section 2.3.2 the components of the objective function. In Section 2.3.3-2.3.7 the constraints of the UC are presented.

2.3.1 Decision Variables

A solution of the UC is a schedule that dictates which electrical generators should be on and how much energy they should generate at each timestep. Time here is discretized into timesteps and in the literature usually represents either hours or 15 min. Additionally, the solution can contain information on electrical flows in the grid, curtailment of VRES, energy not served, allocation of reserves, storage, and demand response. These variables will be defined in the corresponding sections.

2.3.1.1 Commitment and dispatch decision variables

The main decision variables in UC are defined as follows. Let G be the set of generators and T the set of timesteps. For every generator $g \in G$ and every timestep $t \in T$, p_{gt} is defined as the power level of generator g at time t . Moreover, $u_{gt} \in \{0, 1\}$ prescribes the commitment decision, where $u_{gt} = 1$ when generator g is on at time t . Let S be the set of storage units, and pc_{st} and pd_{st} describe the amount of charge and discharge of storage unit $s \in S$ at time t . Let R be the set of all renewable energy sources and p_{rt} the production of renewable energy source $r \in R$ at time t .

Besides decision variables, an UC model can include “auxiliary variables” such as start and stop variables. These variables are not necessary to implement a schedule obtained by solving the UC problem but can help to formulate constraints and analyze the solution. These variables will be introduced on the fly.

Table 2.1: The algorithm, included modelling characteristics, and data on which the experiments were performed are presented for a selection of UC articles. They are sorted on date of publication. (LR=Lagrangian Relaxation, B&B=Branch and Bound, Ben=Benders Decomposition, ANN=Artificial Neural Network, GA=Genetic Algorithm, CLP=Constraint Logic Programming, CG=Column Generation, SA= Simulated Annealing, Tabu = Tabu Search, DP=Dynamic Programming, NN=Neural Network, Ant = Ant Colony algorithm, MI(L)P= Mixed Integer (Linear) Programming, Memetic = Memetic Algorithm, PSO=Particle Swarm Optimization, Prior = Priority listing, Cut = Cut generation)

Algorithm	Piecewise Approx.	Up- and downtime	Ramping Limits	Reserves	Transmission	Hydro (Storage)	Time Dep. start cost	Number of Units	Timesteps	Instance name (created in this chapter)	Source
B&B, Ben	+	+	+				+	10	24	A10	[83]
ANN	+	+	?				+	26	24	RTS26	[88]
GA	+						+	10	24	GA10	[42]
B&B,CLP		+	+	+				4-38	8,24	TAI38,other	[34]
GA		+		?			+	10-110	24	A10,A110	[58]
CG	+			+	+			17	24	other	[2]
LP		+						26-104	24	RTS26	[50]
SA		+		+			+	10	24	A10	[38]
LR		+		+				10-100	24,168	various	[25]
LR,Tabu		+						10-60	24	GA	[9]
LR, DP	+	+	+				+	10	24	GA10	[23]
GA		+	+	+			+	45	24	-	[5]
Ant		+		+				10	24	GA10	[80]
LR			+	+				120	24	-	[11]
LR		+	+			+	+	70	24	GA70	[10]
LR		+		+			+	10-100	24	GA	[57]
LR		+	+		+			54	168	RTS54	[30]
LR,Ben		+	+	+	+		+	12	24	RTS54	[49]
NN,DP		+		+			+	10-20	24	GA	[48]
MILP	+		?	+			+	100	24	GA100	[14]
GA,LR		+	?	+			+	10	24	GA10	[16]
GA,LR		+	?	+	+		+	20-100	24	GA	[94]
MILP	+	+	+			+		10-100	24	RCUC	[29]
MILP		+		+				?	?	?	[82]
Ant, LR		+	?	+			+	20-60	24	GA	[92]
Memetic		+	+				+	4-110	4,24	A10,A110	[20]
LR,MILP	+	+	+			+		10-300	24	RCUC	[28]
PSO		+		+			+	10-100	24	GA,SING35	[39]
MIQP,B&B		+	+	+	+	+	+	54	24	?	[76]
LR,Ben			+	+	+		+	16	24	RTS16	[32]
PSO			+	+				3-38	24	various	[15]
MILP	+	+	+	+	+			242	24	-	[60]
LR		+	+	+	+		?	54	24	RTS16-54	[91]
MILP		+	+				+	28-187	24	OSTRO	[59]
MILP	+	+	+	+				10-200	24	RCUC	[40]
PSO		+	+	+		+		40-100	24,168	GA,TAI40	[17]
MILP		+	+	+				10	24	ADAP10	[55]
PSO+MILP	+	+	+	+			+	10-100	24	GA	[72]
Prior		+	+	+			+	10-100	24	GA10,RTS26,RTS54,KOR140	[53]
MILP	+	+	+	+			+	20-150	24	RCUC	[27]
MILP			+		+		+	54-223	24-444	HUB223,RTS54	[78]
CR		+	+	+	+			60	24	-	[24]
MILP		+	+	+	+			10	64,128,2	ADAP10,RTS54,IEEE78	[31]
MILP	+	+	+	+		+	+	28-1870	24,168	OSTRO,FERC	[6]
MILP		+	+			+		806	?	-	[52]
MILP	+	+	+	+	+	+	+	8	24	?	[3]
MILP		+	+	+			+	679	24	?	[77]
Cut	+	+	+	+			+	459-492	24	FERC459-FERC492	[44]

2.3.1.2 Auxiliary commitment variables

In the 3 binary commitment variables (3-bin) formulation, shutdown and startup events have their own commitment variables w_{gt} and v_{gt} when generator g stops (starts) at time t . Although these auxiliary variables are not essential as their values can be inferred from the commitment decisions, they make the constraints more readable. Furthermore, the 3-bin formulation is tighter than the 1-bin formulation [54]. This means that linear relaxation of the 3-bin formulation results in an objective value closer to that of the MILP problem than the linear relaxation of the 1-bin formulation. This stronger objective value can then be used as a lower bound in the MILP problem. In the 3-bin formulation we define the logical relation between the three types of commitment variables by the following “logic” constraint:

$$u_{gt} - u_{gt-1} = v_{gt} - w_{gt} \quad \forall t \in T, \forall g \in G \quad (2.1)$$

2.3.1.3 Alternative dispatch decision variable

In most UC formulations p_{gt} is used as the dispatch variable in the constraints. However, Knueven et al. [45] found that using an alternative dispatch decision variable p'_{gt} representing the power level above the minimum stable level leads to a computational faster model. This variable can be related to p_{gt} in the following way:

$$p_{gt} = p'_{gt} + \underline{P}_g u_{gt} \quad (2.2)$$

2.3.2 Objective Function

The objective of the UC is to minimize the total cost of operating the power system over a time horizon. The total cost includes the cost of the operation of generators and when applicable a penalty cost for energy not served and loss of reserves. The objective function is defined as:

$$\min \sum_{g \in G, t \in T} cost_{gt}^{gen} + cost_{gt}^{cycle} + cost_t^{system} \quad (2.3)$$

where $cost_{gt}^{gen}$ is the generation cost and $cost_{gt}^{cycle}$ is the cycling cost of unit g at time step t i.e. the cost of starting up and shutting down. The system cost $cost_t^{system}$ is the cost of energy not served and loss of reserve.

2.3.2.1 Quadratic Generation Cost

The generation cost consists of a constant term for running a generator and a cost that increases with the power level due to higher fuel cost, CO₂ emission cost, and variable operational and maintenance costs [87]. The relation between

the generation cost and the power level can be characterized by the following quadratic cost function [90]:

$$cost_{gt}^{gen} = a_g u_{gt} + b_g p_{gt} + c_g p_{gt}^2 \quad (2.4)$$

where a_g is the parameter that represents the constant cost and b_g and c_g represent the linear and quadratic cost dependent on the power level p_{gt} . This quadratic cost function can be a simplification of a nonconvex [90], non-monotonic [26] ‘rippled’ function reflecting the sequential opening of different valves in a power plant to increase the power output. Thermal power plants often have lower efficiencies at partial load resulting in relatively higher costs. The generation cost function captures this property when $a_g > 0$ [36]. In most UC problems, the parameters a_g , b_g , and c_g are constant, but in reality they may change per time step [14, 87, 71].

When solving the UC problem with MILP the quadratic cost function is approximated with a piece-wise linear [14] or linear [87, 13, 71] cost function. The piece-wise linear approximation can capture the characteristics of the quadratic cost function accurately [95], but some authors argue that even a linear approximation is accurate enough [13, 84].

2.3.2.2 Piece-wise linear generation cost function

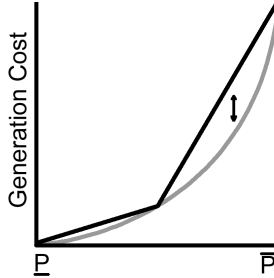


Figure 2.1: The piece-wise approximation of the convex quadratic cost generation cost function always overestimates the cost.

To solve the UC problem with a MILP solver the generation cost function needs to be linearized. A quadratic cost function can be split into multiple pieces which can each be approximated by a linear cost function. This piece-wise linear approximation consists of $|K|$ linear segments with their own maximum \bar{P}_{gk} :

$$p_{gtk} \leq \bar{P}_{gk} \quad \forall g \in G, \forall t \in T, \forall k \in K \quad (2.5)$$

Each segment k has its own power level variable p_{gtk} such that their sum is equal to the power level of the generator:

$$p'_{gt} = \sum_{k \in K} p_{gtk} \quad \forall g \in G, \forall t \in T \quad (2.6)$$

Each segment has its own slope s_k . The slope s_k is based on the additional generation cost divided by the additional production between the start and end of the segment. Since the cost function is convex, the slopes are increasing in k . Hence, the segments will be used in increasing order which implies that equation (6) is valid. This approximation will always overestimate the convex quadratic generation cost that is not on the boundary of a segment (Figure 2.1). Quadratic costs can be linearized with alternative methods, but these are often not explicitly described in the literature [29]. The cost of a generator can be specified as:

$$cost_{gt}^{gen} = (a_g + b_g \underline{P}_g + c_g \underline{P}_g^2) u_{gt} + \sum_{k \in K} s_{gk} p_{gkt} \quad (2.7)$$

Where $(a_g + b_g \underline{P}_g + c_g \underline{P}_g^2)$ is the cost of the quadratic cost function evaluated at \underline{P} .

2.3.2.3 Cycle Cost

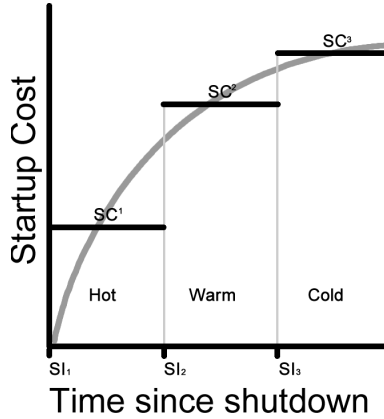


Figure 2.2: The relation between the startup cost and time since last shutdown. In this example, the relation is approximated by a step-function with 3 startup types with corresponding intervals and cost.

Cycling is changing the power level of thermal generators by ramping, starting up and shutting down [85]. Cycle cost can be modeled as:

$$cost_{gt}^{cycle} = SC_{gt} + SDC_{gt} \quad \forall g, \forall t \quad (2.8)$$

where SC_{gt} and SDC_{gt} are the startup and shutdown cost, respectively. However, the shutdown is often not modelled explicitly [1] and could be included in the startup cost. Some authors also include ramping cost [87] but this is not included in our models.

The startup cost can depend on the time since the generator was last shutdown. To take into account the fact that a recent shutdown a thermal generator needs less fuel to return to the desired temperature and that less temperature fluctuation

leads to less operational and maintenance costs [85]. In this time-dependent formulation, a variable cost component is added to the fixed startup cost component as follows [90]:

$$SC_{gt} = VSC_g(1 - e^{-\lambda_g l}) + FSC_g \quad (2.9)$$

where λ_g is the heat-loss coefficient and l is the time since the generator last shutdown, VSC is the variable startup cost and FSC is the fixed startup cost.

Often this exponential function is approximated with a monotonic increasing step-function (Figure 2.2) in which the time after last shutdown is split into intervals. Each interval belongs to a startup type s that has a startup cost SC^s associated with it. Then for each startup type a new decision variable v_{gt}^s is created and $v_{gt}^s = 1$ when interval s is used. Each startup needs to have exactly one startup type:

$$\sum_{s \in S} v_{gt}^s = v_{gt} \quad \forall t, \forall g \quad (2.10)$$

The startup cost can then be defined as:

$$SC_{gt} = \sum_s v_{gt}^s SC_g^s \quad \forall t, \forall g \quad (2.11)$$

However, we can only use the startup type s if the time since the last shutdown is in the interval $[SI_s, SI_{s+1})$. This is formulated as follows:

$$v_{gt}^s \leq \sum_{i=SI_s}^{SI_{s+1}-1} w_{gt-i} \quad \forall t, \forall g, \forall s \quad (2.12)$$

Silbernagl et al. introduced additional analysis variables representing the temperature and ‘applied heat’ of a generator at every timestep. In that way the startup cost can be modeled even tighter which in turn provides a smaller integrality gap [78]. However, we did not include this into our model.

2.3.2.4 System Costs

At last, there is the cost of the system as a whole which is not attributable to individual generators. Most UC models include the possibility to not meet the demand at a penalty cost. This is modeled with a variable ENS_t which stands for the Energy Not Served at time t with an associated cost being the Value Of Lost Load (VOLL). If this is not included in the model the model simply would be infeasible if there is an hour in which the demand is not met. For similar reasons a variable γ_t , the loss of reserve at time t , and a penalty $VOLR$ (Value Of Lost Reserve) can be added for hours in which the reserve requirements cannot be met. Note that $VOLR < ENS$. We now obtain

$$cost_t^{system} = VOLL \ ENS_t + VOLR \ \gamma_t \quad (2.13)$$

2.3.3 Thermal generator constraints

The power level range and flexibility properties (i.e. ability to ramp up or down, or startup or shutdown) of generators are modelled by thermal generator constraints.

2.3.3.1 Generation Limits

Every electrical generator has a minimum and maximum power output. When a generator is on it must operate within this power range, and when it is off the power level is zero. Maximum power level is modeled by the following constraint:

$$p'_{gt} \leq u_{gt}(\overline{P}_g - \underline{P}_g) \quad \forall g \in G, \forall t \in T \quad (2.14)$$

Minimum power level is implied by our ‘above minimum power level variable’ formulation (2.2).

2.3.3.2 Tighter generation limits

Recently Knueven et al. [45] experimented with different formulations of the UC. One of their formulations was called **tight** and combined different constraints from the literature as well as novel ones. The idea is to provide more accurate generation bounds by combining start up, shut down and ramping limits. In our model variant, we implemented their additional constraints related to the maximum generation. These additional equations describe the same set of MILP solutions but the linear relaxation of this formulation should be better. The additional constraints are in the appendix 8.1.1.

2.3.3.3 Ramp up and down limits

The difference in power output levels between consecutive timesteps is constraint by ramping limits. These limits represent physical and economic constraints. If power output levels would change too fast, high temperature and pressure variations can lead to accelerated component failure and forced outages [85]. These limits can also be imposed by an insurance company as part of an insurance policy to prevent failure of components. Moreover, ramping limits are sometimes also modelled with a cost, the higher the difference the higher the price you pay.

The ramping limits are modeled for all two consecutive timesteps:

$$p'_{gt+1} \leq p'_{gt} + u_{gt}RU_g \quad \forall t \in \{1 \dots n-1\}, \forall g \in G \quad (2.15)$$

$$p'_{gt} \leq p'_{gt+1} + u_{gt+1}RD_g \quad \forall t \in \{1 \dots n-1\}, \forall g \in G \quad (2.16)$$

where RD_g is the maximum ramping down between two timesteps of unit g and RU_g is the maximum ramping up between two timesteps of unit g .

When a unit is off it produces zero power. When a unit is on it must produce more than its minimum stable generation. Therefore, since the ramp up and ramp down limits could be smaller than the minimum stable generation, other ramping

limits apply when the generator starts or stops, i.e. the startup SU and shutdown SD limits. The ramping constraints can be extended with these limits with the following elegant and tight formulation of Damci-Kurt et al. [18]:

$$p'_{gt} - p'_{gt-1} \leq (SU_g - \underline{P}_g - RU_g)v_{gt} + RU_g u_{gt} \forall t \in \{1 \dots n-1\}, \forall g \in G \quad (2.17)$$

$$p'_{gt-1} - p'_{gt} \leq (SD_g - \underline{P}_g - RD_g)w_{gt} + RD_g u_{gt-1} \forall t \in \{1 \dots n-1\}, \forall g \in G \quad (2.18)$$

2.3.3.4 Minimum up- and downtime

Because some generators cannot be started up or shut down arbitrarily in consecutive hours [35], minimum up- and downtime constraints are included in most models. The reasons why a generator cannot cycle arbitrarily, are related to physical limitations, safety and economics. Frequent cycling can have a huge effect on the wear and tear of a generator in the long term [85].

Pierre et al. [67], however, report the minimum downtime of most conventional generators to be almost non-existent. Huber argues that due to safety reasons a power plant should always be able to shut down [36] and therefore the minimum uptime constraint could possibly be ignored in the UC problem.

Rajan et al. [73] gives an efficient formulation for the minimum up- and downtime:

$$\sum_{i=t-UT_g+1}^t v_{gi} \leq u_{gt} \quad \forall t \in T, \forall g \in G \quad (2.19)$$

$$\sum_{i=t-DT_g+1}^t w_{gi} \leq 1 - u_{gt} \quad \forall t \in T, \forall g \in G \quad (2.20)$$

where UT_g is the minimum uptime of unit g and DT_g is the minimum downtime of unit g .

2.3.4 Variable renewable energy and storage

Future power systems will rely more on VRES such as solar, wind, and run-off-river hydro power with the major downside that these sources are unpredictable and intermittent. Flexibility needs to be included in a power system to make the power system as reliable as a controllable thermal fleet. This is mostly done by introducing storage systems.

2.3.4.1 Storage constraints

Energy storage technology could include battery, compressed air, flywheel energy and pumped hydro storage.

They can be modeled with a minimum and maximum storage $\underline{PE}, \overline{PE}$, an efficiency of charging η^c and discharging η^d and a maximum charging capacity \overline{PC} , and a maximum discharging capacity \overline{PD} [87]. They are modelled by the following equations.

$$pe_{st} = pe_{st-1} + pc_{st} * \eta_{st}^c - \frac{pd_{st}}{\eta_{st}^d} \quad t \in T, s \in S \quad (2.21)$$

$$0 \leq pc_{st} \leq \overline{PC}_s \quad t \in T, s \in S \quad (2.22)$$

$$0 \leq pd_{st} \leq \overline{PD}_s \quad t \in T, s \in S \quad (2.23)$$

$$\underline{PE}_s \leq pe_{st} \leq \overline{PE}_s \quad t \in T, s \in S \quad (2.24)$$

Pumped hydro storage can be modeled as a battery and a hydropower plant with a dam and reservoir as a battery that cannot be charged but has hourly inflow. However, hydro plants can also be modeled in more detail with constraints related to capacity bounds, flow equations, flow delay, ramp rate, turbine pumping compatibility and forbidden zones [1].

2.3.4.2 Variable Renewable Energy

VRES are modeled with time series of availability factors which indicate for each timestep the ratio of the maximum capacity at which the source can produce. Often in UC models it is assumed that VRES can be curtailed. The availability factors AF_{rt} of VRES r at time t can be implemented by the following constraint:

$$p_{rt} \leq AF_{rt} \overline{P}_{rt} \quad \forall r \in R, t \in T \quad (2.25)$$

2.3.5 Power Balance Constraint

The power balance, also called supply-demand equilibrium or market clearing condition, is the essential UC constraint that models that every demand (at each location, region, bus, or node) should be met with equal supply at every timestep. When the power system consists of a single region (with only thermal generation) this can be modeled with the following equation:

$$\sum_{g \in G} (p'_{gt} + u_{gt} \underline{P}_g) = D_t \quad \forall t \in T \quad (2.26)$$

where p'_{gt} is the dispatch of generator g at time t and D_t is the demand at time t .

However, in a more complex power system with transmission every region or node has its own supply-demand equilibrium. The supply can additionally consist of VRES, discharge from batteries or pumped hydro storage, and nodal injections from the transmission system. The demand can also include the power needed for charging batteries or pumping water in a pumped hydro storage facility. This results in the following constraint:

$$\sum_{g \in G_n} (p'_{gt} + u_{gt} P_g) + \sum_{r \in R_n} p_{rt} + \sum_{s \in S_n} p d_{st} + inj_{nt} = \quad (2.27)$$

$$D_{nt} + \sum_{s \in S_n} p c_{st} - ENS_{nt}, \forall t \in T, \forall n \in N \quad (2.28)$$

where G_n , R_n and S_n are the set of generators, VRES and storage units at node n . Where p_{rt} and $p c_{st}$ is the dispatch or discharge of generator g , renewable energy source r or storage unit s and charge of storage unit s at time t . Finally, D_{nt} , inj_{nt} and ENS_{nt} are the demand, nodal injection from the transmission grid and energy not served of node n at time t .

2.3.6 Reserve Constraints

The supply and demand of electricity are uncertain. Even when consumption and generation of electricity is known in one timestep, the power production and consumption within a timestep is not constant. Therefore, ancillary services are in place that ensure grid stability and security. In most literature of the UC, of the different types of ancillary services only spinning reserves are modelled. Spinning reserves are extra generation capacity that is available by increasing the power output of generators already connected to the power grid. However, it is often unclear what this “extra generation capacity” entails. The extra generation capacity is restricted by the difference of the maximum generation capacity and the actual generation. However, ramping limits also affect the available extra generation capacity. Moreover, the available extra generation capacity is limited by ramping limits plus the generation in the previous timestep. When a generator just used its maximum ramping capacity to go from the generation level in the previous timestep to the current generation level, it does not have extra capacity for the current timestep.

To model the spinning reserves an additional variable is included. The upward spinning reserve provided by generator g at time t is represented by r_{gt}^+ . Suppose SR_t is the spinning reserve requirement, and γ_t the amount by which the system fails to meet this requirement or so-called loss of reserve. Then the reserve requirement is modeled as:

$$\sum_{g \in G} r_{gt}^+ + \gamma_t \geq SR_t \quad t \in T \quad (2.29)$$

When part of the capacity of a generator is used for spinning reserves, this cannot simultaneously be used for dispatch. Therefore, when spinning reserves are included in the UC model, constraint (2.14) is adjusted to:

$$p_{gt} + r_{gt}^+ \leq \bar{P}_g \quad u_{gt} \quad \forall g \in G, \forall t \in T \quad (2.30)$$

The capacity a generator can provide as spinning reserve is also limited by its ramping limits.

$$r_{gt}^+ \leq u_{gt}RU_g \quad \forall g \in G, \forall t \in T \quad (2.31)$$

Some authors [54, 14, 59] limit the reserve capacity by its ramp up limit but also take into account the generation from the previous timestep:

$$p'_{gt+1} + r_{gt}^+ \leq p'_{gt} + u_{gt}RU_g \quad \forall t \in \{1 \dots n-1\}, \forall g \in G \quad (2.32)$$

Even more ramping limits could be applied. Arroyo and Conejo [4] define the maximum generation \bar{p}_{gt} of a generator g at time t as:

$$\bar{p}_{gt} = \min \begin{cases} \bar{P}_g(u_{gt} - w_{gt+1}) + SDw_{gt+1} \\ p_{gt-1} + RU_g u_{gt-1} + SU_g v_{gt} \end{cases} \quad (2.33)$$

With this definition generation limits, ramp up, startup and shutdown limits are respected. The reserve constraint of Morales et al. [54] also respects those limits. Ostrowski et al. [59] only include generation limits, ramp up and startup limits. In the **tight** model of Knueven et al. [45] ramp down limits are partly included.

2.3.7 Transmission Constraints

Every element of the power system is connected to a power grid (the transmission system). The characteristics of the grid limit the power flow between supply and demand. The power grid is a complex network respecting physical laws. As noted by Ackooij et al. [1] transmission systems can typically be modeled at three levels of approximation: AC model, DC approximation, or copperplate. However, a simplified version of the DC approximation, namely the trade-based model, is also used [87]. The AC model based on all Kirchhoff laws is usually not implemented in UC problems and is therefore not considered in this study. The associated non-linear and non-convex constraints of this transmission model already make the economic dispatch problem intractable.

2.3.7.1 DC model

The DC power flow model is widely used as a power flow model simplification in techno-economic studies related to electricity markets [70].

The DC model includes the topology of the grid and the capacities of the transmission lines but simulates the Kirchhoff laws in a simplified and linearized way. This model assumes lossless transmission lines, a flat voltage profile and small voltage angles between neighboring nodes [70]. For real power flow these assumptions do not hold, but if the actual power characteristic violate these assumptions only a small amount then the overall error is also small [70]. The error on individual

transmission lines however can be much larger and therefore the DC model should not be used to draw conclusions about individual lines [70, 86].

To incorporate DC power flows in the UC model, the nodes have positive, negative or zero network injection i.e. they are either an exporter or an importer.

$$inj_{nt} = \sum_{n'} f_{(n' \rightarrow n)t} \quad \forall t \in T, n \in N \quad (2.34)$$

where inj_{nt} is the amount of power node n draws from the transmission system at time t and $f_{(n' \rightarrow n)t}$ is the power flow from node n to node n' . the sum of all imports and exports over all nodes should be zero:

$$\sum_n inj_{nt} = 0 \quad \forall t \in T \quad (2.35)$$

In the DC approximation, the flow on a line $l = n \rightarrow n'$ is determined by the voltage angle difference of node n and n' times the susceptance B_l of the line:

$$f_{lt} = B_l(\delta_{nt} - \delta_{n't}) \quad \forall l \in L \quad (2.36)$$

At last, the flow on a transmission line l is restricted by its thermal capacity limits:

$$\underline{f}_l \leq f_{lt} \leq \overline{f}_l \quad \forall l \in L \quad (2.37)$$

The difference in voltage angles between nodes solely determines the flow on the transmission line between them. Moreover, if we know the nodal injection of the transmission system then we do not need voltage angles to determine the power flow. In fact, a linear relationship exists between nodal injections and power flows on lines which can be described in a power transfer distribution factor (PTDF) matrix[86]. Thus two equivalent methods are available for DC power approximation in an UC model: one based on voltage angles and one based on a PTDF matrix.

A $PTDF_{L \times N}$ matrix dictates how a power injection at node n influences the power flow at line l . We can now rewrite (2.36) to:

$$f_{lt} = \sum_n PTDF_{l,n} inj_{nt} \quad \forall t \in T \quad (2.38)$$

With the above formulation we can also choose to only model a subset of critical transmission lines.

Van den Bergh et al. [86] argue that using a linear DC grid model instead of a more accurate nonlinear AC grid model is justified, because the resulting error is smaller than the deviation between the power flows in the AC power flow simulation and the real power flows.

2.3.7.2 Trade-Based

In a trade-based model only constraints (2.34), (2.37) and (2.35) are used [87]. The transmission network is represented by a graph with nodes where power is generated and consumed and edges who represent power lines that can transmit power between nodes to compensate for the power imbalances at individual nodes.

2.3.7.3 Copperplate

In the literature a transmission system is often neglected in the UC models [81, 87]. Instead a copperplate is assumed in which everything is connected to one single bus and power flows between supply and demand are not limited by grid constraints.

2.3.8 Clustering

Sometimes² similar generators are clustered to reduce the complexity of the UC model. Instead of individual generators with binary unit commitment variables u_{gt} , the units are combined and have a single integer commitment variable u_t that keep track of the number of generators that are on at a specific moment. Most constraints can easily be changed from the binary case to the integer case (u_{gt} changes from $\in \{0, 1\}$ to $\in \{1 \dots \text{number-of-units}\}$). Only the ramping limits (2.15), (2.16), (2.31) and minimum up- and downtime (2.19), (2.20) need small adjustments [52]. However, generator clustering can introduce approximation errors. Meus et al. [52] showed that due to specific interactions of startup and shutdown limits combined with ramping limits and minimum up time, the flexibility may be overestimated when clustering identical generators.

2.3.9 Uncertainty

In this section we have presented a deterministic UC problem formulation, in which the patterns of demand, renewable energy supply, water inflow into the hydro reservoirs, and availability of generators are all known in advance. This is not the case in the real world and multiple methods have been proposed in the literature to account for the uncertainty of these entities.

One of these methods is robust optimization in which the solution must be feasible for all values of the input entities in a so-called uncertainty set. For example, the set of valid import and export patterns for nodes can depend on the outages of transmission lines. In robust optimization, an n-1 transmission system constraint can be included that enforces the import and export pattern to be valid in case of transmission outage of a single line [56].

Another method is Stochastic Programming in which usually the expected value of a UC solution is minimized [8]. This requires that the probability distribution over the uncertain scenarios is known, which is a strong assumption. A Stochastic Programming model contain 2 types of decision variables: 1) variables modelling the initial decisions and 2) recourse variables representing the decisions after the scenario has been revealed. For example, suppose many different renewable supply scenarios exist, where each scenario has a given probability. A solution to the stochastic UC problem could consist of two stages (other stochastic optimization variants exist). In the first stage one on/off pattern for each generator is determined that is valid for every renewable supply scenario. In the second stage,

²In our experiments only for the 2 largest instances

the power output of the generators is determined separately for each specific renewable supply scenario. Finally, the value of the objective function is a weighed (based on the probability) sum of objective values of all scenarios.

Other methods exist to deal with uncertainty in the UC: for example, by doing chance constraint optimization where some constraints only have to hold with a certain probability. Moreover, in the deterministic case, if the model includes reserve requirements, then this reserve constraint already account for the unpredictably and variability of uncertain elements in the UC [1]. See Ackooij et al. [1] for a more detailed explanation of research on how to deal with uncertainty in the UC problem. Finally, a deterministic UC can be combined with a Monte Carlo simulation to capture the variability of the scenarios when UC is used in a power system model.

We have decided for our experiments in this chapter to focus on the impact of simplifications on solution quality and computation time on a deterministic optimization model of the UC problem. Main reason is that model simplifications are usually applied in large-scale power system modeling. Here the UC is performed on large power system models to evaluate the system adequacy of current and future electricity generation portfolios and to support investment decisions. The size of these models prohibits the use of a stochastic model, which would make the models and our study even larger.

2.4 Methods

In this study we applied 21 different formulations of the UC model on a benchmark set of 17 power system instances to assess the impact of different formulations on the result quality and computation time. The different formulations were obtained from a base model with all relevant power system constraints and a set of variations (mainly relaxations) of it. We solved these models with state-of-the-art software for solving large-scale MILP problems, namely, the commercial solver, Gurobi [33].

For each model we solved every instance with a time limit of 10 minutes and a MIP-gap³ of 0.00001⁴ and repeated every experiment 30 times with a slight perturbation of the electricity demand (uniform random within 1% of the total demand, at each timestep).

2.4.1 Instances

Table 2.2 presents an overview of all the power system instances that we collected from the literature. We used this benchmark of instances in our experiments and it is published online⁵. An instance can contain the following items (Not every power system instance includes every item, see Table 2.2 for more details):

³MIP-Gap = $\frac{\text{bestbound} - \text{solution}}{\text{solution}}$

⁴This means the solves stop when it finds a solution and a lower bound that is only a factor 0.00001 apart from each other.

⁵<https://github.com/rogierhans/UCBenchmark>

- A set of generators specified with generation limits, ramping limits (including start and shutdown limits), minimum up- and downtime, generation cost (either linear or quadratic), startup cost (either time dependent or constant over time).
- Time series of demand for each node, availability factors for renewable energy and hourly inflows for hydro.
- Transmission system which includes a topology and lines characterized by susceptance and capacity.
- A set of storage units with charge and discharge limits, charging and discharging efficiency and capacity.
- Renewable Energy Sources with availability factors.

2.4.2 Experimental Setup

We studied the following 21 models, each based on a MILP formulation. Table 2.3 gives an overview of the items included in each of the models and Table 2.4 shows which cost functions or constraints were used for modelling each of the items.

- The base *Model* contains all relevant power system equations: it includes generation limits, minimum up- and downtimes, ramping limits, power balance, reserve requirements (set at 10% of total demand), transmission network model based on DC-approximation with PTDF matrix, transmission limits, linear approximation of the quadratic function and time-dependent startup cost. This base *Model* is used as the reference point for the other, mostly simpler, formulations.
- *Model^{Tight}* is used to investigate how the addition of tight constraints to the base *Model* affect the computation time.
- Seven models are designed to study the impact of simplifications of the base *Model*. *Model_{LP}* and *Model_{LP}^{Tight}* are the LP relaxation of *Model* and *Model^{Tight}* respectively, in which the binary requirements of the variables are relaxed. *Model^{Ramp}* and *Model^{MUMD}* are the base model without the ramping limits and minimum up- and downtime, respectively. In *Model^{TDSUC}* the time-dependent startup cost was replaced with a fixed startup cost. In *Model^{Reserve}* the reserve requirement was set to 0% instead of the normal 10% of the total demand. Finally, *Model^{All}* has no ramping limits, minimum up- and downtime, time-dependent startup cost and no reserve requirement.
- In *2-Model* ... *10-Model* the number of linear segments to approximate the quadratic cost function by a piece-wise linear function are varied from 2 to 10 in contrast with the base model with only one segment. These models are only applied to the 8 instances with a quadratic generation cost function.

	Quadratic Cost	TDSUC	Transmission	Storage	RES	Source	Description
GA10	+	+	-	-	-	[42][72]	Instance from Kazarlis et al. [42] with the ramping limits proposed by Rahman et al. [72].
TAI38	+	-	-	-	-	[34]	Instance from Huang et al. [34] that models the power system from Taiwan Power Company.
A110	+	+	-	-	-	[58]	Instance from Orero et al. [58] with the the ramping limits proposed by Dimitroulas and Georgilakis [20].
KOR140	+	+	-	-	-	[65][53]	Instance from Park et al. [65] with the minimum up- and downtime and startup cost proposed by Moradi et al. [53].
OSTRO187	+	+	-	-	-	[59]	With generator data based on GA10 [42].
HUB223	-	+	-	-	+	[37]	Models the German power system of 2014 as published by the German Federal Network Agency. The system contains renewable energy in the form of wind, solar, hydro and biofuel
RCUC50	+	-	-	-	-	[29]	The parameters of the generators were randomly generated but within a realistic range according to the authors.
RCUC200	+	-	-	-	-	[29]	It is a Western Europe power system. It models 6 countries which are interconnected but within a country it is assumed to be a copperplate.
DSET304	-	-	+	+	+	[41]	
D2SET1442	-	-	+	+	+	[41]	This instance includes 31 countries and 1443 units but most of them are identical and therefore can be clustered.
ZUI1905	-	-	+	+	+	[96]	Outcome of a generation capacity planning model from Zuijlen et al. [96]. It models Western Europe.
FERC978	-	+	-	-	+	[45][47]	Instance from Wang et al. [89] with the ramping limits from an earlier paper from Wang and Shahidehpour [88]. This instance has a transmission system based on the modified IEEE 24-bus system [79].
CA610	-	+	-	-	+	[45]	
GMLC73	-	+	-	-	+	[7]	
RTS26	+	+	+	-	-	[89][88]	
RTS54	-	+	+	-	+	[37]	The instance RTS54 comes from Silbernag et al. [78]. This instance has a transmission system based on the modified IEEE 118-bus system. (There exist multiple variants of this IEEE 118-bus system in the literature of the UC with different generation portfolios and demand series.)
RTS96	-	-	+	-	-	[64]	The instances RTS96 comes from Pandzic et al. [64]. This instance has a transmission system based on the IEEE RTS-96 system. We linearized the piece-wise generation cost.

Table 2.2: Overview of the instances in the benchmark set. All instances have thermal generators with techno-economic characteristics but only some have a quadratic generation cost, time dependent startup cost, a transmission system, storage or a renewable energy with availability factors.

- In contrast to the DC-approximation with a PTDF matrix in the base *Model*, in *Model^{Angles}*, *Model^{Trade}* and *Model^{Copper}* the transmission system is modeled with DC-approximation using volt angles, a trade- based approximation, and a copperplate assumption, respectively.
- At last, with the models *ENS-Model*, *ENS-Model_{LP}*, *ENS-Model^{Tight}*, and *ENS-Model_{LP}^{Tight}* the objective function is changed from cost minimization in the base model to energy not served minimization. The latter is relevant for adequacy studies in which only the occurrence of energy not served matters and not the costs [22, 21]. These 4 models further differ in whether or not a tight formulation or linear relaxation of binary variables were adopted. Furthermore, when these 4 models were applied to the instances in the benchmark set, all demands in these instances were increased to a level resulting in a 0.1% energy not served in the optimal solution. The reason is that the original demands would never result in a energy not served as the instances were all designed with sufficient generation capacity.

	Generation Cost	Cycle Cost	System Cost	Binary	Logic	Generation Limits	RES & Hydro	Power Balance	Tight	Ramp	UDT	TDSUC	Reserve	PTDF	Tradebased	Volt Angle	Segments	Model Compared To
<i>Model</i>	+	+	+	+	+	+	+	+		+	+	+	+	+			1	-
<i>Model^{Tight}</i>	+	+	+	+	+	+	+	+	+	+	+	+	+	+			1	<i>Model</i>
<i>Model_{LP}</i>	+	+	+		+	+	+	+		+	+	+	+	+			1	<i>Model</i>
<i>Model_{LP}^{Tight}</i>	+	+	+		+	+	+	+	+	+	+	+	+	+			1	<i>Model</i>
<i>Model_{LP}^{Ramp}</i>	+	+	+	+	+	+	+	+			+	+	+	+			1	<i>Model</i>
<i>Model^{MUMD}</i>	+	+	+	+	+	+	+	+		+		+	+	+			1	<i>Model</i>
<i>Model^{TDSUC}</i>	+	+	+	+	+	+	+	+		+	+		+	+			1	<i>Model</i>
<i>Model^{Copper}</i>	+	+	+	+	+	+	+	+		+	+	+	+				1	<i>Model</i>
<i>Model^{Trade}</i>	+	+	+	+	+	+	+	+		+	+	+	+		+		1	<i>Model</i>
<i>Model^{Angles}</i>	+	+	+	+	+	+	+	+		+	+	+	+			+	1	<i>Model</i>
<i>Model^{Reserve}</i>	+	+	+	+	+	+	+	+		+	+	+		+			1	<i>Model</i>
<i>Model^{All}</i>	+	+	+	+	+	+	+	+						+			1	<i>Model</i>
<i>2-Model</i>	+	+	+	+	+	+	+	+		+	+	+	+	+			2	<i>Model</i>
<i>3-Model</i>	+	+	+	+	+	+	+	+		+	+	+	+	+			3	<i>Model</i>
<i>4-Model</i>	+	+	+	+	+	+	+	+		+	+	+	+	+			4	<i>Model</i>
<i>5-Model</i>	+	+	+	+	+	+	+	+		+	+	+	+	+			5	<i>Model</i>
<i>10-Model</i>	+	+	+	+	+	+	+	+		+	+	+	+	+			10	<i>Model</i>
<i>ENS-Model</i>	+		+	+	+	+	+	+		+	+	+	+	+			1	-
<i>ENS-Model^{Tight}</i>	+		+	+	+	+	+	+	+	+	+	+	+	+			1	<i>ENS-Model</i>
<i>ENS-Model_{LP}</i>	+				+	+	+	+		+	+	+	+	+			1	<i>ENS-Model</i>
<i>ENS-Model_{LP}^{Tight}</i>	+				+	+	+	+	+	+	+	+	+	+			1	<i>ENS-Model</i>

Table 2.3: Overview of the different models. For each model it shows which characteristic is included (+).

For the largest instances, D2SET1442 and ZUI1905, we used a clustered formulation, and these instances are only considered in the experiments with different transmissions constraints. Moreover, not every instance was used for every model variant because some instances do not have all the characteristics, only some have a

transmission system, quadratic generation cost functions or time dependent start-up cost.

Characteristic	Equation
Generation Cost	(2.5),(2.6),(2.7)
Cycle Cost	(2.11),(2.12)
System Cost	(2.13)
Logic	(2.1)
Generation Limits	(2.30)
RES	(2.25)
Hydro	(2.21),(2.22),(2.23),(2.24)
Power Balance	(2.28)
Tight	(8.1)-(8.5)
Ramp	(2.15),(2.16),(2.31)
UDT	(2.19),(2.20)
TDSUC	(2.10)
Reserve	(2.29),(2.30)
PTDF	(2.35),(2.37),(2.38)
Trade Based	(2.35),(2.37), (2.34)
Volt Angle	(2.35),(2.37),(2.34),(2.36)

Table 2.4: Overview of the power system equations in each of the 21 UC models corresponding to the included power system characteristics in Table 2.3

2.4.3 Indicators to measure performance

To measure the impact of alternative UC formulations besides total computation time and speed-up factor in computation time, we choose 6 indicators related to the cost and solution properties of the UC solutions:

- Cost-Gap.

This Cost-Gap shows how much the total cost of a model differs from that of the Base model and is defined as

$$\text{Cost-Gap} = \frac{Z_{base} - Z_{relaxed}}{Z_{base}} \quad (2.39)$$

where Z_{base} is the total cost of the best-found solution of the base model, and $Z_{relaxed}$ is the total cost of the best-found solution of the relaxed model.

- Quadratic-Gap.

The Quadratic-Gap measures how much the piece-wise approximation of the generation cost function alters the generation cost by comparing it with the cost calculated with the quadratic cost function at the power levels in the solution found with the piece-wise approximation as cost function. This gap is defined as

$$\text{Quadratic-Gap} = \frac{Z_{\text{Quadratic}} - Z_{\text{Base}}}{Z_{\text{Quadratic}}}$$

Where Z_{Base} is the total cost of the best-found solution of the piece-wise linear model, and $Z_{\text{Quadratic}}$ is the score of the same solution evaluated with the original quadratic generation cost.

- Capacity factor difference.

Every generator has a capacity factor that indicates how much a generator is used. This is relevant for power system studies that want to know whether a generator is economically viable. The capacity factor is 100%, if the generator is always producing at maximum capacity and it is lower otherwise. The capacity factor is defined as:

$$CF_g = \frac{\sum_{t \in T} p_{gt}}{|T| \bar{P}_g}$$

The capacity factor difference is defined as $|CF_g^{\text{base}} - CF_g^{\text{relaxed}}|$. The average capacity factor difference (ACFD) is defined as:

$$ACFD = \sum_{g \in G} \frac{|CF_g^{\text{base}} - CF_g^{\text{relaxed}}|}{|G|} \quad (2.40)$$

here CF_g^{relaxed} of capacity factor of generator g for the relaxed model which is compared to the base model. The maximum capacity factor difference (MCFD) is defined as:

$$MCFD = \max_{g \in G} |CF_g^{\text{base}} - CF_g^{\text{relaxed}}|$$

For the capacity factor difference we only look at thermal generators and not solar, wind or hydro generators.

- Normalized L_1 norm of the commitment variables

The hamming distance between two bit-strings is the number of positions at which the bits are different. However, in case binary constraints are relaxed, we cannot use the hamming distance, but must use the L_1 norm. In this norm we only consider the commitment variables and define it as follows:

$$L_1 \text{norm} = \frac{\sum_{t \in T} \sum_{g \in G} |u_{gt}^{\text{base}} - u_{gt}^{\text{relax}}|}{|G|}$$

Because we want to compare the L_1 norm of different power system instances, we normalize it by dividing by the total number of variables.

- Constraint violation indicators

The ramping limit violation indicator reports how many times the difference of two consecutive power outputs exceeds the imposed ramping limit. The up/down time violation constraint reports how many times a unit is illegally turned on or off at a timestep. Finally, the different transmission violation constraints report how often and in how many lines the line flow constraints are exceeded (2.37) if the configuration of import and export of nodes were modeled with a PTDF DC-approximation.

2.5 Results

Model	Speed-up
<i>Model</i>	1
<i>Model^{Tight}</i>	1.09
<i>Model_{LP}</i>	32.2
<i>Model_{LP}^{Tight}</i>	25.5
<i>Model^{Ramp}</i>	2.1
<i>Model^{MUD}</i>	0.6
<i>Model^{TDSUC}</i>	1.1
<i>Model^{Reserve}</i>	1.9
<i>Model^{All}</i>	8.9

Table 2.5: The geometric average of the speed-up factor ($\frac{Time_{Base}}{Time_{Relaxed}}$) of every instance and every of the 30 runs for each model compared to the Base model.

Figure 2.3, and Table 2.5 provide a summary based on the aggregated results of 30 runs for all instances. More detailed figures can be found in the next subsections and appendix 8.1.2.

In Section 2.5.1 we present our results from the (tight) linear relaxation. Then, in Section 2.5.2.1 we show the ramping limits and reserve requirements relaxation. Subsequently, in Section 2.5.2.2 we present the results from omitting time dependent startup cost and removing minimum up- and downtime and in 2.5.2.3 we present the overall trends of all the model simplifications. Finally, in Section 2.5.3, 2.5.4 and 2.5.5 we present the results from the experiments with different numbers of segments for piece-wise approximation, different ways of transmission modeling, and the alternative objective function based on adequacy.

2.5.1 (Tight) Linear relaxation

The base *Model* with the binary commitment variables is compared with *Model_{LP}* and *Model_{LP}^{Tight}* without the binary variables. We found that this relaxation results in a large speed-up while having a similar total cost. However, the solutions differ with respect to the capacity factor and fractional variable indicators.

Figure 2.3a and Figure 2.3b show that the linear relaxation, *Model_{LP}* and *Model_{LP}^{Tight}*, is solved, respectively, on average 32.2 and 25.5 faster than the base

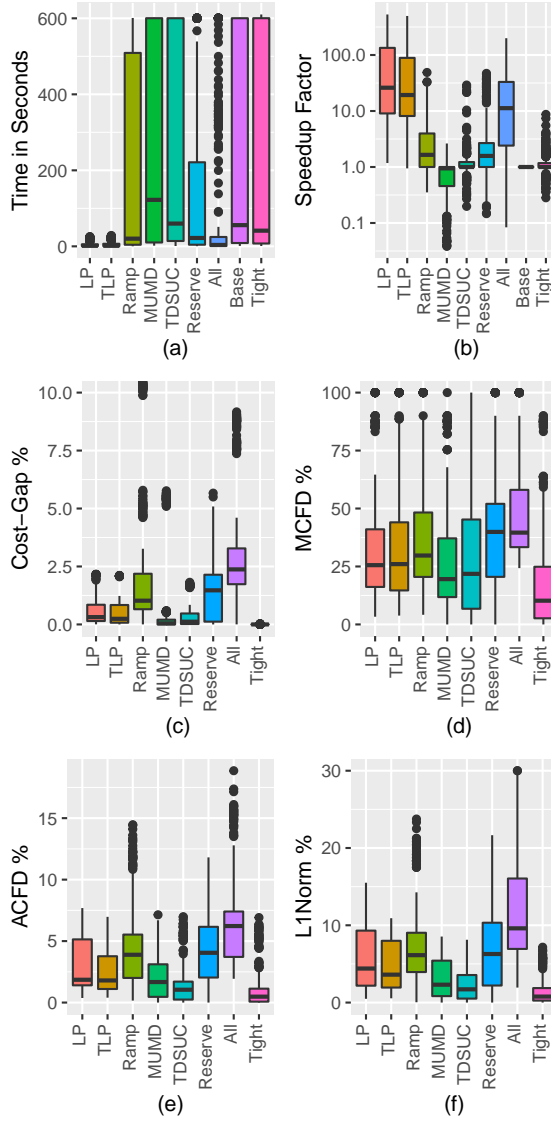


Figure 2.3: (a) Computation time in seconds, (b) the speed-up factor, (c) the Cost-Gap, (d) MCFD, (e) ACFD and (f) L_1 norm of the models of all the instances and 30 runs.

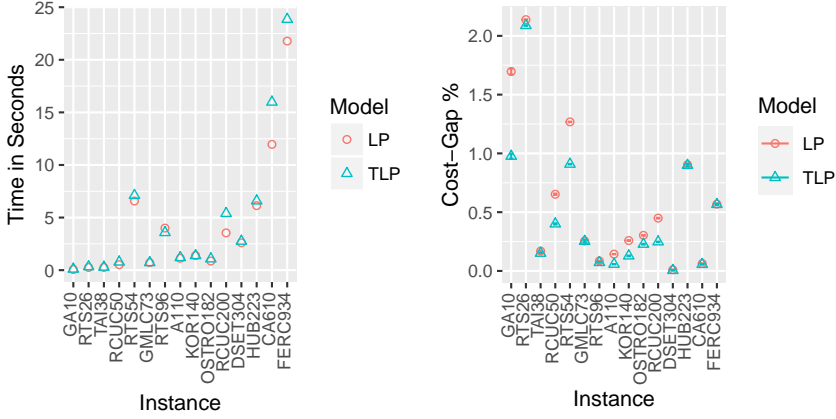


Figure 2.4: Average computation time and average Cost-Gap for $Model_{LP}$ and $Model_{LP}^{Tight}$ for 15 different instances and 30 runs.

Model. The base *Model* cannot solve the instance KOR140 within the 10 minute time limit, while $Model_{LP}$ solves it within 1.39 seconds on average. This is not surprising since the problem is convex and thus can be solved efficiently by Gurobi. Similarly, the computation time to solve $Model_{LP}^{Tight}$ is significantly lower than the base *Model* and only a little higher than $Model_{LP}$ (Figure 2.4).

Figure 2.3c and Figure 2.4 show the impact of the relaxation on the solution quality. The Cost-Gap is small for the binary relaxation ($Model_{LP}$) and even smaller for the tight binary relaxation ($Model_{LP}^{Tight}$). In all but one instance, the gap on average is below 1% and for one third of the instances it was below 0.1% for $Model_{LP}^{Tight}$.

However, the capacity factor indicators can be large in both relaxations. For example, the instance OSTRO182 has an average ACFD of 6.4% and an average MCFD of 37.7% (Table 8.1). Thus on average a single generator uses the capacity 37.7% less or more in the relaxed model compared to the base *Model*.

The boxplot in Figure 2.5 shows that in more than half of the models the percentage of fractional variables is higher than 10% for $Model_{LP}$ and $Model_{LP}^{Tight}$. Figure 2.5 suggest that a tight formulation can reduce this ratio considerably for some instances. For example, on average 32.4% of the binary variables are fractional when solving the instance RCUC50 with $Model_{LP}$ compared to 23.9% with $Model_{LP}^{Tight}$.

2.5.2 Impact of Relaxations

2.5.2.1 Ramping limits and reserve requirements

Without the ramping limits, the UC problem can be solved on average 2.1 times faster, and even 10 times faster for one instance (see Fig. 8.3 in the appendix). Similarly, without the reserve requirements, the UC problem can be solved on

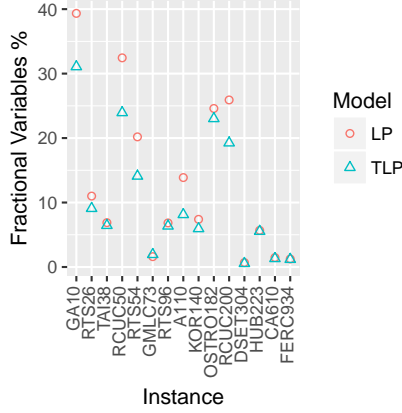


Figure 2.5: Ratio of fractional variables of 30 runs for each instance.

average 1.9 times faster for all instances except for one instance, OSTRO182, which has a longer computation time.

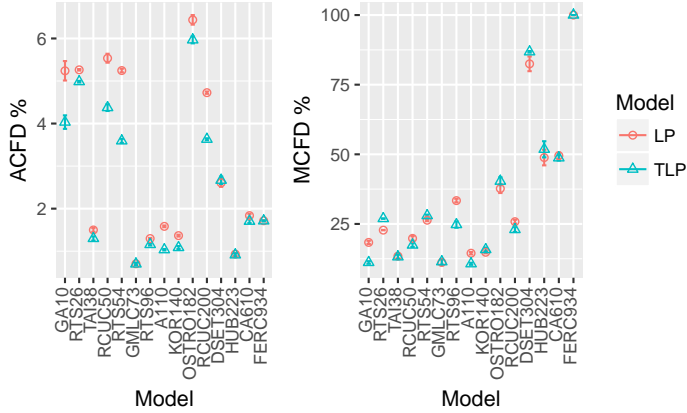


Figure 2.6: ACFD and MCFD for $Model_{LP}$ and $Model_{LP}^{Tight}$.

This decrease in computation time comes at the expense of the quality of the solutions. The Cost-Gap, ACFD and MCFD are all much larger than those of $Model_{LP}$ and $Model_{LP}^{Tight}$. For example, the Cost-Gap of $Model^{Ramp}$ or the instances GA10 and KOR140 show that the total system costs are estimated respectively, 5.1% and 3.2% too low when ramping limits are not taken into account. The ACFD for $Model^{Ramp}$ is as high as 12.2% and 8.3% for the instance GA10 and OSTRO182. The MCFD for these instances is 25.9% and 46.5%, respectively. The revenue of an individual generator could, therefore, be almost 50% higher or lower when the ramping constraints are omitted. Similar results can be found for the omission of reserve requirements (see appendix).

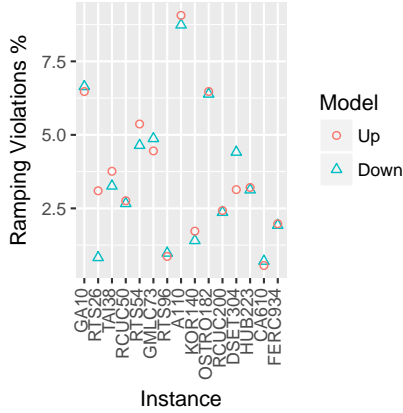


Figure 2.7: Ratio of ramping violations of 30 runs for each instance.

Figure 2.7 presents the number of times the ramping limits were violated in $Model^{Ramp}$ which varies per instance between 0.1% and 10%. The highest is for the instance A110 where both ramp-up and ramp-down limits were exceeded on average for around 9% of the generators every timestep.

In summary, $Model^{Ramp}$ and $Model^{Reserve}$ and variants result in a significant speed-up at the cost of quality loss.

2.5.2.2 Minimum up- and down time and startup-costs

For $Model^{TDSUC}$ and $Model^{MUMD}$, where the time dependent startup cost or minimum up- and downtime constraints are removed, computation time is not clearly improved. In some cases, $Model^{MUMD}$ even has a larger computation time (Figure 2.3b).

However, the removal of those constraints still comes at a cost. When the minimum up- and downtime are removed, the Cost-Gap and the other quality measures are still high (Figure 2.3c-e). The number of times the up-/downtime limits are violated is presented in Figure 2.8. It varies per instance and is between 0% and 25%. For example, with the instance FER934 on average the minimum up and minimum downtime are exceeded in 3.3% and 23.4% of the time.

2.5.2.3 Overall Trend

One of the reasons the UC is hard is because of the interdependency between time steps caused by generator properties like ramping limits, minimum up- and down time, and startup cost. If we were to remove this dependency the problem decomposes into easier subproblems.

As we can see from the results of $Model^{All}$, if we remove most of this dependency, the solver is much faster Figure 2.3a&b, but the solution quality also degrades the most as is shown by the Cost-Gap,ACFG,MCFD and L_1 norm Figure 2.3.

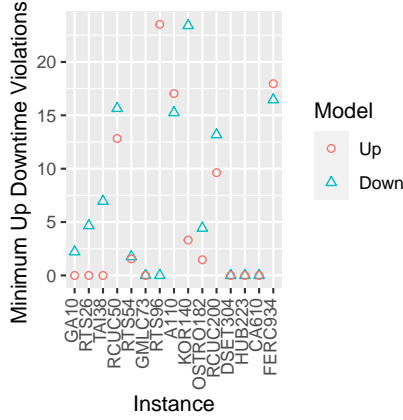


Figure 2.8: Ratio of minimum up/down time violations of 30 runs for each instance

The ACFD but especially the MCDF are very large for all models (Figure 2.3d&e), even when $Model$ and $Model^{Tight}$ are compared the MCDF is incredibly large. The base $Model$ and $Model^{Tight}$ have the same feasible search space and Gurobi returns cost values which are really close to each other (see Cost-Gap in Table 8.1). However, even if the cost difference of these solutions is very small the solutions themselves could be far apart. For example, on average the Cost-Gap is 0.01% for OSTRO182 but the MCDF is as high as 40%.

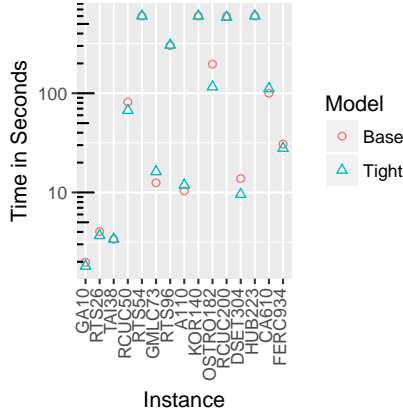


Figure 2.9: Average computation time of 30 runs for the Base and Tight model for 15 different instances

The average computation time of the $Model$ and $Model^{Tight}$ model is almost the same for every instance. For some instances the tight formulation is noticeable faster on average but the converse is also true for two instances (Figure 2.9).

2.5.3 Impact of resolution of piece-wise approximation

The experiments with piece-wise linear approximation show that for a single piece-wise linear, i.e. linear approximation, the Quadratic-Gap is already quite small ranging from 0.008% to 0.49 % (Figure 2.10). When more pieces are added the Quadratic-Gap becomes even smaller but the time also increases significantly (Figure 2.10). Although 0.5 % can be a lot of money in a larger system, it is important to note that the solutions for one piece and more pieces are similar and this similarity does not disappear when the number of pieces increases.

The other performance indicators of the models with more segments (see all indicators in Table 8.4 in the appendix) indicate that more segments hardly improve the quality of the solution compared to *Model*. For example, the Cost-Gap between one and two pieces in the piece-wise linear approximation on average is small $< 0.5\%$. But as shown in Figure 2.10 additional segments increase the computation time considerably.

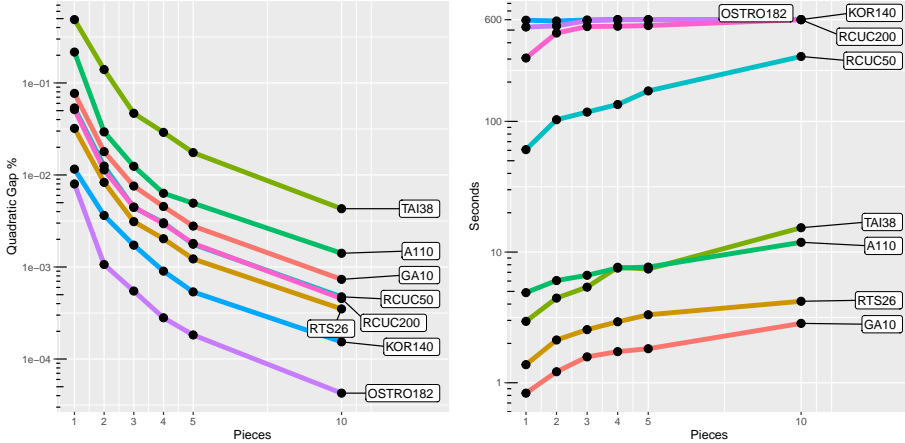


Figure 2.10: Quadratic-Gap and computation time of models with increasing number of pieces to approximate the Quadratic cost function.

2.5.4 Impact of transmission modelling

The experiments with the 3 alternative transmission models show that computation time of the solution process can speed-up when normal DC approximation with PTDF is replaced by the trade-based or copperplate model. At the same time quality is lost, except for instances where transmission plays a limited role (Figure 2.11 and appendix Table 8.5). For example, in the instances RTS26 and RTS96, the capacities of transmission lines are large in comparison with the demand. Furthermore, the demand size at the different nodes and location of generator capacity at these nodes agree sufficiently to avoid an overload of transmission lines. However, for the other instances this is not the case, and substantial quality loss is revealed by the scores of the performance indicators (see Figure 2.11).

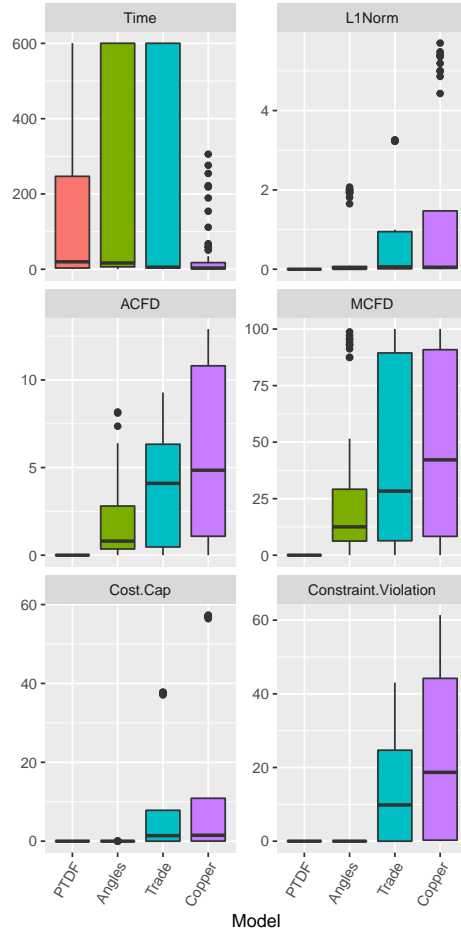


Figure 2.11: The ACFD, MCFD, Cost-Gap and Constraint violation of 30 runs for $Model^{Copper}$, $Model^{Trade}$ and $Model^{Angles}$.

Especially, the violation of the transmission constraints for more than 60% of the lines of all timesteps show that the simplifications is far from legitimate.

Using volt angles hardly differs from using PTDF when you look at the Cost-Gap, but the impact on the computation time differs as the use of volt angles is faster in some instances while the PTDF use is faster in others (Figure 2.11).

2.5.5 Impact of alternative objective function

When using energy not served as cost function, there was no difference in the cost of the models with all system constraints, i.e., in every experiment $ENS-Model$, $ENS-Model^{Tight}$, $ENS-Model_{LP}$ and $ENS-Model_{LP}^{Tight}$ had the same cost. Moreover, the computation time was also similar (Table 2.6) . However, this does not imply the models are equal in general. UC is an NP-hard problem. Therefore it cannot be expected to be solvable by an LP and it is rather easy to find counter examples where the LP-relaxation, $ENS-Model_{LP}$, gives a different optimal solution than $ENS-Model$ even when minimizing energy not served.

Instance	$ENS-Model$	$ENS-Model_{LP}$	$ENS-Model^{Tight}$	$ENS-Model_{LP}^{Tight}$
GA10	0.05	0.05	0.07	0.04
RTS26	0.08	0.07	0.1	0.07
TAI38	0.14	0.13	0.16	0.14
RCUC50	0.17	0.17	0.2	0.18
RTS54	0.23	0.23	0.3	0.23
GMLC73	0.17	0.16	0.27	0.15
RTS96	0.33	0.31	0.47	0.3
A110	0.43	0.43	0.46	0.43
KOR140	0.59	0.58	0.71	0.6
OSTRO182	0.44	0.34	0.92	0.33
RCUC200	1.14	1.05	1.25	1.08
HUB223	0.33	0.32	0.67	0.31
DSET304	0.91	0.85	1.67	0.84
CA610	1.93	1.75	2.99	1.78
FERC934	12.52	10.99	15.25	11.25

Table 2.6: Computation time in seconds of solving the 4 adequacy models for 15 instances averaged over 30 runs.

2.6 Discussion

2.6.1 Implications of key findings and comparison with existing literature

We found a decrease in computation time when we omitted ramping limits, reserve requirements or a detailed transmission system, but at the same time a decrease in quality, i.e. a large deviation in cost and capacity factors. This is in line with findings from Schwele et al. [75] who developed a generation expansion planning model incorporating UC constraints and showed that without ramping constraints the optimization causes a large error. Knueven et al. [46] also found that omitting reserve requirements can shorten computation time as the inclusion of these requirements significantly increases the difficulty of solving UC problem. Palmintier [62] concluded that one of the most important aspects were reserve requirements but stated that ramping constraints are less important. This difference in conclusions, whether ramping limits play a significant role, highlights, how specific assumptions of the techno-economic characteristics of the power system influence the impact of the model simplifications. Poncelet et al. [68] also argued that the impact of integrating UC constraints in the generation expansion problem strongly depends on the flexibility parameters of the generators in the power system that is being modelled.

In contrast to the omission of constraints, linear relaxation always significantly improves computation time while the cost differ relatively little from the full model. However, the solution of this relaxed model will always be infeasible in the real world, due to the fractional commitment variables. But infeasibility, can be argued, holds for every model simplification. For certain applications in power system modeling the actual schedule is less important since the schedule is not always implemented, but only need to provide sufficient insight in the relevant properties of the schedule. Our analysis reveals that if the LP-relaxation has a certain cost value, we may expect that there exists a schedule with cost very close to that value. Therefore, using a linear relaxation could be a good approach to shave off a large amount of time while losing less quality than removing other aspects such as the ramping limits or reserve requirements. This is in line with findings from Palmintier [62] and Poncelet et al. [68], who both found that the LP relaxation of the full model results in a small deviation from the total system cost of the full MILP model when generation expansion with UC constraints is modelled.

We also found that for all model simplifications and even for equivalent tight model variants the capacity factor difference is always large. This is in line with the comments from Kim et al. which report that suboptimal generator schedules (even with small optimality gap) can deviate significantly from an optimal schedule [43]. This means that statements about individual generators, in terms of how much they produce and consequently how much they earn and whether they are economically viable, cannot be justified from a solution produced by an UC model.

We found that the linear approximation of the quadratic generation function with a single segment is already a good approximation for the quadratic functions in the UC instances we studied. This confirms the comments of Bruninx and Van

den Bergh [13, 84] which stated that a linear approximation is already accurate given the quadratic functions found in the literature of the UC.

In all instances where we only minimized the energy not served the results of the full model and the linear relaxed model were equal. This finding has major implications for adequacy studies that use the UC problem to find the energy not served probability of current and future power systems [22, 21]. Most of the time these studies use a Monte Carlo approach, i.e. multiple UC problems are run, to get the expectation of the energy not served of a power system. For each run certain elements of the power system have forced outages and different demand patterns are drawn from a pool of different weather years. The ability to solve these UC problems faster without loss in quality means you can perform more Monte Carlo runs and get more accurate results.

Some studies first solve the UC problem for a whole year with a simplified model that omits most unit commitment constraints to fix certain variables such as storage levels and planned outages [93, 41, 66]. Since, as was shown in this chapter, model simplifications and especially the removal of multiple constraints can cause errors, these errors can propagate to the shorter time horizons when modelling with a rolling horizon.

2.6.2 Limitations

We have performed multiple experiments with different models on a large variety of UC instances. Some of those instances are artificially created (RCUC50, RCUC200) while others are based on real power systems (HUB223, DSET). For others (GA10) it is not clear where the generators characteristics come from. Moreover, for some instances the characteristics such as storage technologies or VRES which we could include in our model, were not provided (Table 2.2). Furthermore, for some instances certain characteristics are irrelevant in the sense that they do not have an impact. For example, in the instances DSET, GLMC and FERC, most generators have ramping limits that are so large that a unit could go from its minimum to maximum generation within 1 hour, which makes the ramping constraint obsolete.

We only looked at a small time horizon of 24 timesteps. We did further investigation of the instances that finished within 10s and ran the same experiments for 168 timesteps. The results are roughly the same except for the measures MCFD, MIPGap and computation time, which were all higher. It still has to be investigated if these results still hold for larger time horizons of months to years but we see no reason why it would not scale. Although for some instances a larger time horizon was available (Table 2.2), we fixed the run length to a day. Most data sets had their start time in January (in the winter). For longer horizon instances the results could differ if we choose to start in another season where demand and renewable energy generation would be different.

In our experiments, we choose to perform an elaborate set of runs on an elaborate set of instances. Therefore, we could not calculate the optimum of every UC instance exactly within a reasonable computation time. We applied a state-of-the-art MILP formulation but even then, for almost half of the instances the time limit of 10 minutes was reached. Moreover, in order to do a reasonable amount of

testing we terminated the branch and bound algorithm of Gurobi when a solution within the predefined MIPGap was reached. Therefore, calculating and comparing different solutions of the models introduced an inaccuracy since we were not able to compare optimal solutions.

In this chapter all experiments were performed on a deterministic UC problem. In Section 2.3.9 we mentioned that uncertainty plays an important role in the UC. Besides looking at reserve requirements, uncertainty is not investigated in this chapter. This is a limitation of our study since inclusion or exclusion of uncertainty can play a large role in power system models. A large-scale analysis of different approaches of including uncertainty (e.g. robust optimization, adjustable robustness, two-phase stochastic programming) and of the effect of model choices (objective functions, constraints) for the unit commitment with uncertainty would be a valuable addition to the literature of the UC. Note, however, that UC models with uncertainty can often be viewed as extensions of deterministic UC models. This might imply that the effect of model choices that are being studied in this chapter on a deterministic power system would have a similar effect on a non-deterministic power system.

2.7 Conclusion

We created a UC benchmark consisting of almost all available UC instances in the literature and representing power systems with a large variety of characteristics. We made this benchmark publicly available in a single format so that it can be used to evaluate the effectiveness of different algorithms and formulations of the UC in a robust way. In this study, we used this benchmark to compare the quality of solutions and computation times between a base UC model and variants of this model with less constraints. The base UC model is formulated as a MILP problem with generators characterized by a linear generation cost function, minimum up- and downtime, time dependent startup costs, and ramping limits. Furthermore, additional constraints guarantee sufficient reserves in the system and a DC approximation of the power flows is applied in the UC instances with transmission. Quality of the solutions were evaluated by comparing total system costs, capacity factors, and the number of times omitted constraints were violated in the relaxed models.

We found that some simplifications can speed-up solving the UC with no or only a small loss in quality. First, linear relaxation of the UC model, i.e. changing the MILP into an LP by relaxing the constraints that the commitment variables are binary, results in a significant speed-up, 32 times as fast on average, while having only a small cost gap. Moreover, the cost gap is even smaller when using a tighter formulation that contains additional inequalities for the maximum generation. The system cost gap for the tight linear relaxation for all instances except one was below 1% and for one third of the instances even below 0.1%. However, the actual schedule is not realistic, as the solution has fractional commitment decisions and when the solution is compared to the full model capacity factors of individual generators significantly differ. On average of 30 runs the average capacity factor

difference of the generators for one instance was 6.4% and the maximum capacity factor difference was 37.7%. Secondly, when the objective is to minimize energy not served instead of total system cost the linear relaxation gave the same cost for ever UC instance and for every of the 30 runs. Thirdly, we found that the piece-wise linear approximation of the quadratic generation cost functions used in the literature of the UC, a single piece already gave good results. Adding more pieces reduced the gap between the real evaluation and the piece-wise linear approximation of the solution even more but at a significant computation time increase.

All other simplifications of the UC model are not recommended:

- Omission of minimum up- and downtime mostly increased computation time and making start-up costs time-independent did not speed up the process, while both simplifications resulted in quality loss with regard to costs and differences in capacity factors.
- Omission of ramping limits and reserve constraints result in a 2.1- and 1.9-times speed-up on average, but at the expense of too much quality loss. Without the ramping limits the total cost for one instance was 5% lower on average and the capacity factors differed on average 12.2%.
- Although simplification of the transmission system may speed up the computation, quality loss with respect to the cost is too high. For one instance on average the total cost was 50% lower when transmission constraints were omitted.

Finally, we found that the average and maximum capacity factor difference is large for all model relaxations and even for the tight formulation, which is equivalent to the base model. These results imply that there are many different solutions with similar cost. This indicates that the actual generation pattern produced by the UC should not be considered as the unique way to achieve cost-efficient operation.

Bibliography

- [1] Wim van Ackooij et al. “Large-scale unit commitment under uncertainty: an updated literature survey”. In: *Annals of Operations Research* (2018), pp. 1–75.
- [2] Muhamed Aganagic and Sasan Mokhtari. “Security constrained economic dispatch using nonlinear Dantzig-Wolfe decomposition”. In: *IEEE Transactions on Power Systems* 12.1 (1997), pp. 105–112.
- [3] Gonzalo E Alvarez, Marian G Marcovecchio, and Pío A Aguirre. “Security-Constrained Unit Commitment Problem including thermal and pumped storage units: An MILP formulation by the application of linear approximations techniques”. In: *Electric Power Systems Research* 154 (2018), pp. 67–74.
- [4] José M Arroyo and Antonio J Conejo. “Optimal response of a thermal unit to an electricity spot market”. In: *IEEE Transactions on power systems* 15.3 (2000), pp. 1098–1104.
- [5] José Manuel Arroyo and Antonio J Conejo. “A parallel repair genetic algorithm to solve the unit commitment problem”. In: *IEEE Transactions on Power Systems* 17.4 (2002), pp. 1216–1224.
- [6] Semih Atakan, Guglielmo Lulli, and Suvrajeet Sen. “A state transition MIP formulation for the unit commitment problem”. In: *IEEE Transactions on Power Systems* 33.1 (2018), pp. 736–748.
- [7] Clayton Barrows et al. “The IEEE reliability test system: A proposed 2019 Update”. In: *IEEE Transactions on Power Systems* (2019).
- [8] John R Birge and Francois Louveaux. “Introduction to stochastic programming”. In: (2011).
- [9] A Borghetti et al. “Lagrangian relaxation and tabu search approaches for the unit commitment problem”. In: *2001 IEEE Porto Power Tech Proceedings (Cat. No. 01EX502)*. Vol. 3. IEEE. 2001, 7–pp.
- [10] A Borghetti et al. “Using of a cost-based unit commitment algorithm to assist bidding strategy decisions”. In: *2003 IEEE Bologna Power Tech Conference Proceedings*, vol. 2. IEEE. 2003, 8–pp.
- [11] Alberto Borghetti et al. “Lagrangian heuristics based on disaggregated bundle methods for hydrothermal unit commitment”. In: *IEEE Transactions on Power Systems* 18.1 (2003), pp. 313–323.

- [12] Anne Sjoerd Brouwer et al. “Least-cost options for integrating intermittent renewables in low-carbon power systems”. In: *Applied Energy* 161 (2016), pp. 48–74.
- [13] Kenneth Bruninx. “Improved modeling of unit commitment decisions under uncertainty”. In: (2016).
- [14] Miguel Carrión and José M Arroyo. “A computationally efficient mixed-integer linear formulation for the thermal unit commitment problem”. In: *IEEE Transactions on power systems* 21.3 (2006), pp. 1371–1378.
- [15] K Chandrasekaran and Sishaj P Simon. “Binary/real coded particle swarm optimization for unit commitment problem”. In: *2012 International Conference on Power, Signals, Controls and Computation*. IEEE. 2012, pp. 1–6.
- [16] Wenping Chang and Xianjue Luo. “A solution to the unit commitment using hybrid genetic algorithm”. In: *TENCON 2008-2008 IEEE Region 10 Conference*. IEEE. 2008, pp. 1–6.
- [17] Po-Hung Chen. “Two-level hierarchical approach to unit commitment using expert system and elite PSO”. In: *IEEE Transactions on Power Systems* 27.2 (2012), pp. 780–789.
- [18] Pelin Damcı-Kurt et al. “A polyhedral study of production ramping”. In: *Mathematical Programming* 158.1-2 (2016), pp. 175–205.
- [19] JP Deane et al. “Soft-linking of a power systems model to an energy systems model”. In: *Energy* 42.1 (2012), pp. 303–312.
- [20] Dionisios K Dimitroulas and Pavlos S Georgilakis. “A new memetic algorithm approach for the price based unit commitment problem”. In: *Applied energy* 88.12 (2011), pp. 4687–4699.
- [21] ENTSO-E. *Mid Term Adequacy Forecast (MAF)*. 2018. URL: https://docstore.entsoe.eu/Documents/SDC_20documents/MAF/2018/MAF_202018_20Executive_20Report.pdf.
- [22] ENTSO-E. *Pentalateral Energy Forum Support Group 2 Generation Adequacy Assessment*. 2018. URL: https://www.bmwi.de/Redaktion/DE/Downloads/P-R/plef-sg2-generation-adequacy-assessment-2018.pdf?__blob=publicationFile&v=4.
- [23] Wei Fan, Xiaohong Guan, and Qiaozhu Zhai. “A new method for unit commitment with ramping constraints”. In: *Electric Power Systems Research* 62.3 (2002), pp. 215–224.
- [24] Salar Fattahi et al. “Conic relaxations of the unit commitment problem”. In: *Energy* 134 (2017), pp. 1079–1095.
- [25] Stefan Feltenmark and Krzysztof C Kiwiel. “Dual applications of proximal bundle methods, including Lagrangian relaxation of nonconvex problems”. In: *SIAM Journal on Optimization* 10.3 (2000), pp. 697–721.

- [26] Eric S Fraga, Lingjian Yang, and Lazaros G Papageorgiou. “On the modelling of valve point loadings for power electricity dispatch”. In: *Applied energy* 91.1 (2012), pp. 301–303.
- [27] Antonio Frangioni and Claudio Gentile. *New MIP formulations for the single-unit commitment problems with ramping constraints*. 2015.
- [28] Antonio Frangioni, Claudio Gentile, and Fabrizio Lacalandra. “Sequential Lagrangian-MILP approaches for unit commitment problems”. In: *International Journal of Electrical Power & Energy Systems* 33.3 (2011), pp. 585–593.
- [29] Antonio Frangioni, Claudio Gentile, and Fabrizio Lacalandra. “Tighter approximated MILP formulations for unit commitment problems”. In: *IEEE Transactions on Power Systems* 24.1 (2009), pp. 105–113.
- [30] Yong Fu, Mohammad Shahidehpour, and Zuyi Li. “Long-term security-constrained unit commitment: hybrid Dantzig-Wolfe decomposition and sub-gradient approach”. In: *IEEE Transactions on Power Systems* 20.4 (2005), pp. 2093–2106.
- [31] Claudio Gentile, Germán Morales-España, and Andrés Ramos. “A tight MIP formulation of the unit commitment problem with start-up and shut-down constraints”. In: *EURO Journal on Computational Optimization* 5.1-2 (2017), pp. 177–201.
- [32] Sangang Guo. “A quick method for judging the feasibility of security-constrained unit commitment problems within Lagrangian relaxation framework”. In: *Energy Power Eng* 4 (2012), pp. 432–438.
- [33] LLC Gurobi Optimization. *Gurobi Optimizer Reference Manual*. 2019. URL: <http://www.gurobi.com>.
- [34] Kun-Yuan Huang, Hong-Tzer Yang, and Ching-Lien Huang. “A new thermal unit commitment approach using constraint logic programming”. In: *Power Industry Computer Applications., 1997. 20th International Conference on*. IEEE. 1997, pp. 176–185.
- [35] Yuping Huang, Panos M Pardalos, and Qipeng P Zheng. *Electrical power unit commitment: deterministic and two-stage stochastic programming models and algorithms*. Springer, 2017.
- [36] Matthias Huber. “Flexibility in Power Systems-Requirements, Modeling, and Evaluation”. PhD thesis. Technische Universität München, 2017.
- [37] Matthias Huber and Matthias Silbernagl. “Modeling start-up times in unit commitment by limiting temperature increase and heating”. In: *European Energy Market (EEM), 2015 12th International Conference on the*. IEEE. 2015, pp. 1–5.
- [38] Einar Stale Huse, Ivar Wangensteen, and Hans H Faanes. “Thermal power generation scheduling by simulated competition”. In: *IEEE Transactions on Power Systems* 14.2 (1999), pp. 472–477.

- [39] JC Inostroza and VH Hinojosa. “Short-term scheduling solved with a particle swarm optimiser”. In: *IET generation, transmission & distribution* 5.11 (2011), pp. 1091–1104.
- [40] RA Jabr. “Tight polyhedral approximation for mixed-integer linear programming unit commitment formulations”. In: *IET Generation, Transmission & Distribution* 6.11 (2012), pp. 1104–1111.
- [41] Konstantinos Kavvadias et al. *Integrated modelling of future EU power and heat systems-The Dispa-SET v2. 2 open-source model*. Tech. rep. European Commission, 2018.
- [42] Spyros A Kazarlis, AG Bakirtzis, and Vassilios Petridis. “A genetic algorithm solution to the unit commitment problem”. In: *IEEE transactions on power systems* 11.1 (1996), pp. 83–92.
- [43] Kibaek Kim, Audun Botterud, and Feng Qiu. “Temporal decomposition for improved unit commitment in power system production cost modeling”. In: *IEEE Transactions on Power Systems* 33.5 (2018), pp. 5276–5287.
- [44] Ben Knueven, Jim Ostrowski, and Jianhui Wang. “The ramping polytope and cut generation for the unit commitment problem”. In: *INFORMS Journal on Computing* 30.4 (2018), pp. 739–749.
- [45] Bernard Knueven, James Ostrowski, and Jean Paul Watson. “On mixed integer programming formulations for the unit commitment problem”. In: *E-print, Department of Industrial and Systems Engineering University of Tennessee, Knoxville, TN 37996* (2018).
- [46] Bernard Knueven, James Ostrowski, and Jean-Paul Watson. “A novel matching formulation for startup costs in unit commitment”. In: *Mathematical Programming Computation* (2020), pp. 1–24.
- [47] Eric Krall, Michael Higgins, and Richard P O’Neill. “RTO unit commitment test system”. In: ().
- [48] S Senthil Kumar and V Palanisamy. “A new dynamic programming based hopfield neural network to unit commitment and economic dispatch”. In: *2006 IEEE International Conference on Industrial Technology*. IEEE. 2006, pp. 887–892.
- [49] Bo Lu and Mohammad Shahidehpour. “Unit commitment with flexible generating units”. In: *IEEE Transactions on Power Systems* 20.2 (2005), pp. 1022–1034.
- [50] Marcelino Madrigal and Victor H Quintana. “An interior-point/cutting-plane method to solve unit commitment problems”. In: *Power Industry Computer Applications, 1999. PICA’99. Proceedings of the 21st 1999 IEEE International Conference*. IEEE. 1999, pp. 203–209.
- [51] Alexander C Melhorn et al. “Validating unit commitment models: A case for benchmark test systems”. In: *Power and Energy Society General Meeting (PESGM), 2016*. IEEE. 2016, pp. 1–5.

- [52] Jelle Meus, Kris Poncelet, and Erik Delarue. “Applicability of a clustered unit commitment model in power system modeling”. In: *IEEE Transactions on Power Systems* 33.2 (2018), pp. 2195–2204.
- [53] Saeed Moradi et al. “A semi-analytical non-iterative primary approach based on priority list to solve unit commitment problem”. In: *Energy* 88 (2015), pp. 244–259.
- [54] Germán Morales-España, Jesus M Latorre, and Andres Ramos. “Tight and compact MILP formulation of start-up and shut-down ramping in unit commitment”. In: *IEEE Transactions on Power Systems* 28.2 (2013), pp. 1288–1296.
- [55] Germán Morales-España, Andres Ramos, and Javier García-González. “An MIP formulation for joint market-clearing of energy and reserves based on ramp scheduling”. In: *IEEE Transactions on Power Systems* 29.1 (2014), pp. 476–488.
- [56] Richard P O’Neill et al. “Economic analysis of the N-1 reliable unit commitment and transmission switching problem using duality concepts”. In: *Energy Systems* 1.2 (2010), pp. 165–195.
- [57] Weerakorn Ongsakul and Nit Petcharak. “Unit commitment by enhanced adaptive Lagrangian relaxation”. In: *IEEE Transactions on Power Systems* 19.1 (2004), pp. 620–628.
- [58] SO Orero and MR Irving. “Large scale unit commitment using a hybrid genetic algorithm”. In: *International Journal of Electrical Power & Energy Systems* 19.1 (1997), pp. 45–55.
- [59] James Ostrowski, Miguel F Anjos, and Anthony Vannelli. “Tight mixed integer linear programming formulations for the unit commitment problem”. In: *IEEE Transactions on Power Systems* 27.1 (2012), pp. 39–46.
- [60] James Ostrowski and Jianhui Wang. “Network reduction in the transmission-constrained unit commitment problem”. In: *Computers & Industrial Engineering* 63.3 (2012), pp. 702–707.
- [61] Narayana Prasad Padhy. “Unit commitment-a bibliographical survey”. In: *IEEE Transactions on power systems* 19.2 (2004), pp. 1196–1205.
- [62] Bryan Palmintier. “Flexibility in generation planning: Identifying key operating constraints”. In: *2014 power systems computation conference*. IEEE. 2014, pp. 1–7.
- [63] Bryan Palmintier and Mort Webster. “Impact of unit commitment constraints on generation expansion planning with renewables”. In: *2011 IEEE power and energy society general meeting*. IEEE. 2011, pp. 1–7.
- [64] Hrvoje Pandzic et al. *Unit commitment under uncertainty-GAMS models. Library of the Renewable Energy Analysis Lab (REAL), University of Washington, Seattle, USA*.
- [65] Jong-Bae Park et al. “An improved particle swarm optimization for nonconvex economic dispatch problems”. In: *IEEE Transactions on Power Systems* 25.1 (2010), pp. 156–166.

- [66] Matija Pavičević et al. “The potential of sector coupling in future European energy systems: Soft linking between the Dispa-SET and JRC-EU-TIMES models”. In: *Applied Energy* 267 (2020), p. 115100.
- [67] Inge Pierre et al. “Flexible generation: Backing up renewables”. In: *Eurelectric, Tech. Rep.* (2011).
- [68] Kris Poncelet, Erik Delarue, and William D’haeseleer. “Unit commitment constraints in long-term planning models: Relevance, pitfalls and the role of assumptions on flexibility”. In: *Applied Energy* 258 (2020), p. 113843.
- [69] Kris Poncelet et al. “Impact of the level of temporal and operational detail in energy-system planning models”. In: *Applied Energy* 162 (2016), pp. 631–643.
- [70] Konrad Purchala et al. “Usefulness of DC power flow for active power flow analysis”. In: *Power Engineering Society General Meeting, 2005. IEEE. IEEE. 2005*, pp. 454–459.
- [71] Sylvain Quoilin, Ignacio Hidalgo Gonzalez, and Andreas Zucker. “Modelling Future EU Power Systems Under High Shares of Renewables: The Dispa-SET 2.1 open-source model”. In: (2017).
- [72] Dewan Fayzur Rahman, Ana Viana, and Joao Pedro Pedroso. “Metaheuristic search based methods for unit commitment”. In: *International Journal of Electrical Power & Energy Systems* 59 (2014), pp. 14–22.
- [73] Deepak Rajan, Samer Takriti, et al. “Minimum up/down polytopes of the unit commitment problem with start-up costs”. In: *IBM Res. Rep* 23628 (2005), pp. 1–14.
- [74] B Saravanan et al. “A solution to the unit commitment problem—a review”. In: *Frontiers in Energy* 7.2 (2013), pp. 223–236.
- [75] Anna Schwele, Jalal Kazempour, and Pierre Pinson. “Do unit commitment constraints affect generation expansion planning? A scalable stochastic model”. In: *Energy Systems* 11.2 (2020), pp. 247–282.
- [76] M Shafie-Khah, M Parsa Moghaddam, and MK Sheikh-El-Eslami. “Unified solution of a non-convex SCUC problem using combination of modified branch-and-bound method with quadratic programming”. In: *Energy Conversion and Management* 52.12 (2011), pp. 3425–3432.
- [77] Jiaying Shi and Shmuel S Oren. “Stochastic unit commitment with topology control recourse for power systems with large-scale renewable integration”. In: *IEEE Transactions on Power Systems* 33.3 (2018), pp. 3315–3324.
- [78] Matthias Silbernagl, Matthias Huber, and René Brandenberg. “Improving accuracy and efficiency of start-up cost formulations in MIP unit commitment by modeling power plant temperatures”. In: *IEEE Transactions on Power Systems* 31.4 (2016), pp. 2578–2586.
- [79] Probability Methods Subcommittee. “IEEE reliability test system”. In: *IEEE Transactions on power apparatus and systems* 6 (1979), pp. 2047–2054.

- [80] T Sum-Im and W Ongsakul. “Ant colony search algorithm for unit commitment”. In: *IEEE International Conference on Industrial Technology, 2003*. Vol. 1. IEEE. 2003, pp. 72–77.
- [81] Milad Tahanan et al. “Large-scale unit commitment under uncertainty”. In: *4OR* 13.2 (2015), pp. 115–171.
- [82] Aidan Tuohy et al. “Unit commitment for systems with significant wind penetration”. In: (2009).
- [83] Andre Turgeon. “Optimal scheduling of thermal generating units”. In: *IEEE Transactions on Automatic Control* 23.6 (1978), pp. 1000–1005.
- [84] Kenneth Van den Bergh. “Impact of Energy and Climate Policies on Electricity Generation-Analysis based on Large-scale Unit Commitment Modeling”. In: (2016).
- [85] Kenneth Van den Bergh and Erik Delarue. “Cycling of conventional power plants: technical limits and actual costs”. In: *Energy Conversion and Management* 97 (2015), pp. 70–77.
- [86] Kenneth Van den Bergh, Erik Delarue, and William D’haeseleer. “DC power flow in unit commitment models”. In: *TMF Working Paper-Energy and Environment, Tech. Rep.* (2014).
- [87] Kenneth Van den Bergh et al. “LUSYM: a unit commitment model formulated as a mixed-integer linear program”. In: *KU Leuven, TME Branch Working Paper* 7 (2014).
- [88] Chunyan Wang and SM Shahidehpour. “Effects of ramp-rate limits on unit commitment and economic dispatch”. In: *IEEE Transactions on Power Systems* 8.3 (1993), pp. 1341–1350.
- [89] SJ Wang et al. “Short-term generation scheduling with transmission and environmental constraints using an augmented Lagrangian relaxation”. In: *IEEE Transactions on Power Systems* 10.3 (1995), pp. 1294–1301.
- [90] Allen J Wood and Bruce F Wollenberg. *Power generation, operation, and control*. John Wiley & Sons, 2012.
- [91] Hongyu Wu et al. “A systematic method for constructing feasible solution to SCUC problem with analytical feasibility conditions”. In: *IEEE Transactions on Power Systems* 27.1 (2012), pp. 526–534.
- [92] Derong Yu, Yongqiang Wang, and Rui Guo. “A hybrid ant colony optimization algorithm based Lambda-iteration method for unit commitment problem”. In: *2010 Second WRI Global Congress on Intelligent Systems*. Vol. 1. IEEE. 2010, pp. 19–22.
- [93] William Zappa, Martin Junginger, and Machteld van den Broek. “Is a 100% renewable European power system feasible by 2050?” In: *Applied energy* 233 (2019), pp. 1027–1050.

- [94] Xiaohua Zhang, Jinquan Zhao, and Xingying Chen. “A hybrid method of Lagrangian relaxation and genetic algorithm for solving UC problem”. In: *2009 International Conference on Sustainable Power Generation and Supply*. IEEE. 2009, pp. 1–6.
- [95] Qipeng P Zheng et al. “A decomposition approach to the two-stage stochastic unit commitment problem”. In: *Annals of Operations Research* 210.1 (2013), pp. 387–410.
- [96] Bas van Zuijlen et al. “Cost-optimal reliable power generation in a deep decarbonisation future”. In: *Applied Energy* 253 (2019), p. 113587.

Chapter 3

An Improved Algorithm for Single-Unit Commitment with Ramping Limits

Published as:

An Improved Algorithm for Single-Unit Commitment with Ramping Limits.

Rogier Hans Wuijts, Marjan van den Akker & Machteld van den Broek

Electric Power Systems Research (2021)

3.1 Abstract

The single-unit commitment problem (1UC) is the problem of finding a cost optimal schedule for a single generator given a time series of electricity prices subject to generation limits, minimum up- and downtime and ramping limits. In this chapter we present two efficient dynamic programming algorithms. For each time step we keep track of a set of functions that represent the cost of optimal schedules until that time step. We show that we can combine a subset of these functions by only considering their minimum. We can construct this minimum either implicitly or explicitly.

Experiments show both methods scale linear in the amount of time steps and result in a significant speedup compared to the state-of-the-art for piece-wise linear as well as quadratic generation cost. Therefore using these methods could lead to significant improvements for solving large scale unit commitment problems with Lagrangian relaxation or related methods that use 1UC as subproblem.

Nomenclature

$f_t(p)$	The cost of producing p at time t .
\underline{P}	Minimal stable generation
\overline{P}	Maximal stable generation
Δ^+	Ramp-up limit
Δ^-	Ramp-down limit
SU	Start-up ramp limit
SD	Shut-down ramp limit
M_{up}	Minimum up time
M_{down}	Minimum down time

3.2 Introduction

The unit commitment (UC) problem revolves around finding the least cost power generation schedule for a set of generators such that the demand is met at each time step subject to technical restrictions [1].

The single-unit commitment problem (1UC) is a special case of the UC problem in which the least cost schedule is searched for only one generator subject to its technical restrictions [4]. In this case, the generator is not required to meet a demand, but a time series of electricity prices is given that determines how much revenue the generator can make at each time step. In this chapter we will study 1UC with generation limits, minimum up- and downtime and ramping limits.

The relevance of 1UC lies in the fact that it arises as a subproblem in the Lagrangian relaxation or column generation, which have been shown to be competitive for UC [1]. For the efficiency of these algorithms, the efficiency of solving 1UC is crucial.

A solution to 1UC is a schedule that for every time step specifies whether the generator is on or off and how much power it is producing. The cost associated with power production is the generation cost and consists of the cost of operating the generator minus the revenue. The generation cost is assumed to be convex and

in the often modeled as a linear, piece-wise linear or quadratic function. When 1UC is used as a subproblem in the Lagrangian relaxation this revenue corresponds to the Lagrangian multipliers.

Fan, Xiaohong Guan, and Zhai [2] solved 1UC with piece-wise linear generation cost in $O(n^3)$ time by splitting the problem in two parts. The first part of the algorithm is to define *on-periods*. A *on-period* is a subsequence of time steps of where the generator is on and must be larger or equal to the minimum up time. Every *on-period* has an optimal power output subsequence. Finding the optimal power output subsequence for each *on-period* is an optimization problem. Fan et al. solved this with a dynamic programming algorithm that recursively partitions the continuous state space by finding corner points of the cost-to-go function. In the second part, these *on-periods* weighted by the optimal economic dispatch costs, are combined in an optimal schedule by solving a shortest path problem.

Frangioni and Gentile [4] improved this method by making it more general. Their method of calculating the optimal economic dispatch works for any convex cost function. Their algorithm calculates the optimal economic dispatch of all on-periods in $O(n^3)$ and finds the shortest path in another $O(n^3)$. Frangioni and Gentile [3] found that a redefinition of the commitment state space graph can speed up this second part to $O(n^2)$.

In 2010, Zhai, Xiaohong Guan and Gao [12] presented a similar algorithm in which 1UC is also split into two parts, but which has the advantage that it also works for non-convex piece-wise linear cost functions.

In 2018 Yongpei Guan, Pan, and Zhou [6] introduced an algorithm to solve 1UC in $O(n)$ time. However, as a restriction it only works with convex piece-wise linear generation cost and when the ramp up and ramp down limits are equal to each other. They solved 1UC by keeping track of a finite number of points where the power production could be optimal.

3.3 Outlook

In this chapter we present two algorithms for solving 1UC that improve upon previous algorithms in terms of generality, time complexity and computation time in practice. Both algorithms are based on two equivalent recurrence relations.

The idea for both relations is as follows: for each time step we define all states the generator can attain and all valid state transitions. After that we define the recurrence relation that represents for each state at each time step the value of the optimal schedule that ends in that state. However, since the amount of states is infinite as the power output is continuous we cannot solve these recurrence relations directly. Therefore, 1UC is reformulated in terms of recurrence relations on functions, later defined as F_t^τ and H_t^τ . These functions can be constructed by partitioning their domain as was previously done to calculate the optimal economic dispatch for on-periods¹. However, instead of computing the optimal economic dispatch of an on-period beforehand F_t^τ and H_t^τ represent the cost of the complete 1UC schedule from time 1 up until time t .

¹cost-to-go functions L^t in [2] and $z_{h,k}$ in [4]

The first dynamic programming algorithm we defined, enables the identification of superfluous functions F_t^τ that are always dominated by other functions i.e. for every power output level p_t there is another function with a lower cost. If we remove superfluous functions the overall computation time can be reduced. Identification of these functions comes at a cost and has a worst case time complexity of $O(n^3)$. However, in practice it has little computational overhead. Moreover, we describe the conditions in which this algorithm grows linear with the amount of time steps and show these conditions are met for the instances we studied. This results in a speedup of the algorithm of Frangioni and Gentile [4].

The second dynamic programming algorithm we defined, combines subsets of on-states and thus reduces the total amount of states. At the same time, the number of functions the recurrence relation consists of diminishes, as multiple functions are replaced by their combined minimum. When f_t is piece-wise linear we can create this function by only keeping track of a finite number of points similar to the algorithm of Guan et al. [6]. However, in contrast to the algorithm of Guan et al. our algorithm, is more generic as it also works for ramp up and ramp down rates which differ from each other. Moreover, we show how to efficiently compute the values at those points. This results in an improved algorithm in terms of generality and time complexity.

In section 3.4 we formally define the 1UC problem. In section 3.5 and section 3.6 we will state the recurrence relation that solves 1UC and section 3.7 we define and analyse a dynamic programming algorithm, *RRF+*, that uses this recurrence relation. In section 3.8 we show an equivalent recurrence relation and in section 3.9 we define and analyse a dynamic programming algorithm, *RRH*, that uses this recurrence relation when the generation cost function is piece-wise linear. At last we conclude this chapter in section 3.10 with experiments regarding our two algorithms for both piece-wise linear and quadratic generation cost and show that they significantly decrease the computation time compared to previous methods.

3.4 Problem Definition

The single-unit commitment problem (1UC) is a special case of the unit commitment problem in which the least cost schedule is searched for only one generator subject to its technical restrictions. A solution to the 1UC is represented as two vectors $\mathbf{x} \in \{0, 1\}^n$ and $\mathbf{p} \in \mathbb{R}^n$. Where $\mathbf{x} = x_1 \dots x_n$ represents the binary commitment variables i.e. x_t is 1 when the generator is on at time t and 0 otherwise. The vector $\mathbf{p} = p_1 \dots p_n$ represents the continuous power output variables that for each time step indicates how much power a generator provides at that time. The associated cost of a solution is determined by time dependent generation cost function f_t . Here $f_t(p_t)$ is a function that returns the generation cost of providing p_t power at time t . If the generator is on then the production must be between the minimum generation \underline{P} and the maximum generation \overline{P} . Moreover, if the generator is turned on(off), it must stay on(off) for at least $M_{\text{up}}(M_{\text{down}})$ time steps. Finally, there are four ramping limits. There is a ramp-up (Δ^+) and ramp-down (Δ^-) constraint that limits how much two consecutive power output levels p_t and p_{t+1} can differ from each other. These limits only hold for two consecutive time steps where the generator is on. Special ramping limits apply when a generator

starts or shuts down, the startup limit SU and shutdown limit SD . We assume the generator can be in any state at $t=1$ ². We can now define 1UC as the following mixed integer program:

$$\min c_{cycle}(x) + \sum_{t \in \{1, \dots, n\}} f_t(p_t) \text{ subject to} \quad (3.1)$$

$$\underline{P}x_t \leq p_t \leq \bar{P}x_t, t = 1 \dots n \quad (3.2)$$

$$p_{t+1} \leq p_t + x_t \Delta^+ + (1 - x_t)SU, t = 1 \dots n - 1 \quad (3.3)$$

$$p_t \leq p_{t+1} + x_{t+1} \Delta^- + (1 - x_{t+1})SD, t = 1 \dots n - 1 \quad (3.4)$$

$$x \in X, p_t \in \mathbb{R} \quad (3.5)$$

$c_{cycle}(x)$ consists of the start-up c_{start} and shutdown cost c_{down} of the commitment vector x . X is the set of feasible commitment vectors with respect to the minimum up- and downtime (3.5).

$$c(off_t^\tau) = 0 \quad t = 1 \quad (3.6)$$

$$c(off_t^\tau) = \min_{p_{t-1} \in [\underline{P}, SD]} \min_{\tau' \in \{M_{up} \dots t\}} c(on_{t-1}^{\tau'}, p_{t-1}) + c_{stop} \quad t > 1 \quad \tau = 1 \quad (3.7)$$

$$c(off_t^\tau) = c(off_{t-1}^{\tau-1}) \quad t > 1 \quad 1 < \tau < M_{down} \quad (3.8)$$

$$c(off_t^\tau) = \min\{c(off_{t-1}^{\tau-1}), c(off_{t-1}^\tau)\} \quad t > 1 \quad \tau = M_{down} \quad (3.9)$$

$$c(on_t^\tau, p_t) = f_t(p_t) \quad t = 1 \quad \underline{P} \leq p_t \leq \bar{P} \quad (3.10)$$

$$c(on_t^\tau, p_t) = f_t(p_t) + c(off_{t-1}^{M_{down}}) + c_{start} \quad t > 1 \quad \tau = 1, \underline{P} \leq p_t \leq SU \quad (3.11)$$

$$c(on_t^\tau, p_t) = f_t(p_t) + \min_{p_{t-1} \in [p_t - \Delta^+, p_t + \Delta^-]} c(on_{t-1}^{\tau-1}, p_{t-1}) \quad t > 1 \quad \tau > 1, \underline{P} \leq p_t \leq \bar{P} \quad (3.12)$$

$$c(.) = \infty \quad \text{otherwise} \quad (3.13)$$

$$F_t^\tau(p_t) = \begin{cases} f_t(p_t) & t = 1, \underline{P} \leq p_t \leq \bar{P} \\ f_t(p_t) + c(off_{t-1}^{M_{down}}) + c_{start} & t > 1, \tau = 1, \underline{P} \leq p_t \leq SU \\ f_t(p_t) + \min_{p_{t-1} \in [p_t - \Delta^+, p_t + \Delta^-]} F_{t-1}^{\tau-1}(p_{t-1}) & t > 1, \tau > 1, \underline{P} \leq p_t \leq \bar{P} \\ \infty & \text{otherwise} \end{cases} \quad (3.14)$$

3.5 First Recurrence Relation

In this section we define the state space and the corresponding recurrence relation that solves it.

The state space represents the possible states of the generator for each time step. Every state at time t has a set of feasible transitions to states at time $t + 1$ which depends on ramping limits and minimum up and down time. It is therefore necessary to keep track of how long a generator has been on or off, until the minimum up- or downtime is reached, and to keep track of the power output

²Here we ignore the transition constraints and cost between $t = 0$ and $t = 1$. Alternatively, the state at $t=0$ can also be provided as input to the problem.

$p_t \in [\underline{P}, \overline{P}]$ when a generator is on. The set of states that a generator can be in at time t is defined as:

$$S_t = \bigcup \left\{ \begin{aligned} &\{off_t^\tau \mid \tau \in \{1 \dots M_{\text{down}}\}\} \\ &\{(on_t^\tau, p_t) \mid \tau \in \{1 \dots \max(t, M_{\text{up}})\}, p_t \in [\underline{P}, \overline{P}]\} \end{aligned} \right\} \quad (3.15)$$

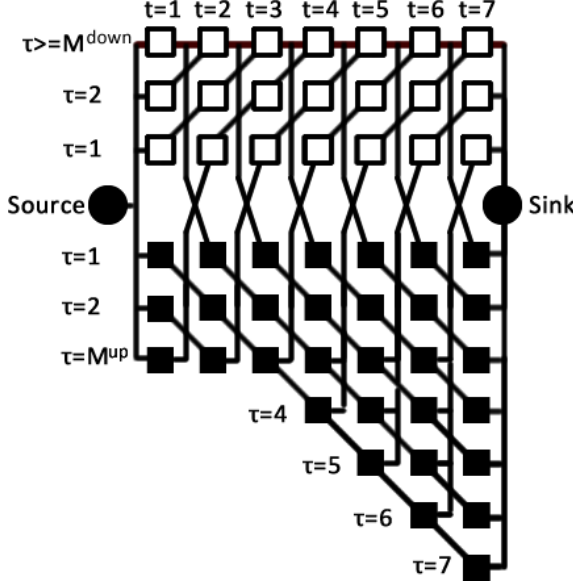


Figure 3.1: The commitment statespace and transitions of 7 time steps. The off-states are represented as white nodes and the on-states as black nodes.

See Figure 3.1 for the binary commitment variables statespace and transitions. The state off_t^τ represents the state at time t where the generator is off for τ time steps, but when $\tau = M_{\text{down}}$ it represents that the generator is off for at least M_{down} time steps. The state (on_t^τ, p_t) represents that at time t a generator is on for τ time steps and produces p_t at time t .

We will now define the recurrence relation $c(s_t)$ that for each state s_t returns the cost of the optimal IUC schedule at time t that ends in s_t (3.6)-(3.13). For each state s_t this is defined as the cost of that state, the minimum of $c(s_{t-1})$ over states s_{t-1} that can transition towards s_t and the transitions costs.

At $t = 1$ the generator can be in any state with only the cost of being in that state and no transition cost, (3.6) and (3.10).

For $t > 1$ we can formulate every possible state transition that respects ramping limits and minimum up- and downtime and define the recurrent part of the recurrence relation by (3.7)-(3.9) and (3.11)-(3.12).

There are three types of transitions to a state where the generator is off. First, we can get to the first off-state off_t^1 from an on-state (on_{t-1}^τ, p_t) where the generator is on for at least M_{up} time steps and produces less than the shutdown limit SD (3.7). Secondly we can get to the off-state off_t^τ that is off for $\tau > 1$ time steps

from an off-state that is off for $\tau - 1$ time steps (3.8). Thirdly, if $\tau = M_{\text{down}}$ we can also get to the last off-state $off_t^{M_{\text{down}}}$ from $off_{t-1}^{M_{\text{down}}}$ (3.9).

For the on-states it is almost similar. We can only get to the on-state (on_t^1, p_t) , where p_t is less than the startup limit SU , from an off-state $off_{t-1}^{M_{\text{down}}}$ where the generator is off for at least M_{down} time steps (3.11). We can get to on-state (on_t^τ, p_t) that is on for $\tau > 1$ time steps from an on-state $(on_{t-1}^{\tau-1}, p_{t-1})$ if the difference between p_t and p_{t-1} respects the ramp-up Δ^+ and ramp-down Δ^- limit (3.12).

3.6 Constructing F_t^τ

Because the set of on-states is infinite, we cannot calculate the cost of every possible on-state, (on_t^τ, p_t) , explicitly. Therefore we construct for every $t \in \{1, \dots, n\}, \tau \in \{1, \dots, \max(t, M_{\text{up}})\}$ a function F_t^τ such that $F_t^\tau(p_t) = c(on_t^\tau, p_t)$, the function is given by (3.14). Moreover, F_t^τ is a piece-wise function and is convex³.

In order to solve 1UC we need determine $c(off_t^\tau)$ and F_t^τ for each t and τ . Solving 1UC efficiently boils down to constructing F_t^τ efficiently for all t and τ . In this chapter we will present a method to construct F_t^τ equivalent to Frangioni and Gentile [4] but in a declarative way which is in our opinion more intuitive.

Constructing the first F_t^1 is easy since f_t is given as input and $c(off_{t-1}^{M_{\text{down}}})$ is just a single value. The hard part of constructing F_t^τ is taking the sliding window minimum of $F_{t-1}^{\tau-1}$. Suppose p_{t-1}^* is a point in $[\underline{P}, \overline{P}]$ for which $F_{t-1}^{\tau-1}$ is minimal:

$$p_{t-1}^* = \operatorname{argmin}_{p_{t-1} \in [\underline{P}, \overline{P}]} F_{t-1}^{\tau-1}(p_{t-1})$$

To find the value of $\min_{p_{t-1} \in [p_t - \Delta^+, p_t + \Delta^-]} F_{t-1}^{\tau-1}(p_{t-1})$ for a given p_t three cases can be identified equivalent to those of Frangioni and Gentile [4]:

$$\min_{p_{t-1} \in [p_t - \Delta^+, p_t + \Delta^-]} F_{t-1}^{\tau-1}(p_{t-1}) = \begin{cases} F_{t-1}^{\tau-1}(p_t + \Delta^-) & p_t < p_{t-1}^* - \Delta^- \\ F_{t-1}^{\tau-1}(p_{t-1}^*) & p_{t-1}^* - \Delta^- \leq p_t \leq p_{t-1}^* + \Delta^+ \\ F_{t-1}^{\tau-1}(p_t - \Delta^+) & p_t > p_{t-1}^* + \Delta^+ \end{cases} \quad (3.16)$$

In other words, if p_t can be reached from p_{t-1}^* within the ramping limits, i.e. with a subtraction smaller than Δ^- or an addition smaller than Δ^+ then

$$\min_{p_{t-1} \in [p_t - \Delta^+, p_t + \Delta^-]} F_{t-1}^{\tau-1}(p_{t-1}) = F_{t-1}^{\tau-1}(p_{t-1}^*)$$

. Otherwise p_t is either smaller than $p_{t-1}^* - \Delta^-$ or larger than $p_{t-1}^* + \Delta^+$. In the first case, since this function is convex, the largest feasible p_{t-1} is optimal. Which is given by $p_{t-1} = p_t + \Delta^-$. Similar for the second case the smallest feasible p_{t-1} is optimal. Which is given by $p_{t-1} = p_t - \Delta^+$. The idea is illustrated in Figure 2.

³Proof is omitted for brevity but convexity is easy to see if you look at the epigraph of the new function created in (3.16).

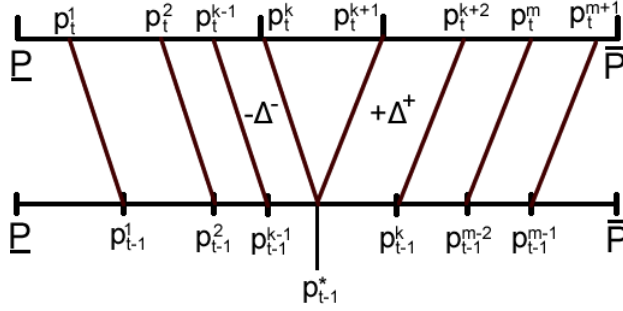


Figure 3.2: Visualising (3.16). Here the bottom axis represents how the domain of $F_{t-1}^{\tau-1}$ (3.17) is partitioned and how its mapped to the domain of $p_t \mapsto \min_{p_{t-1} \in [p_t - \Delta^+, p_t + \Delta^-]} F_{t-1}^{\tau-1}(p_{t-1})$ (3.19).

Suppose the function $F_{t-1}^{\tau-1}$ consists of m piece-wise functions $g_{t-1}^1 \dots g_{t-1}^m$ over m intervals:

$$[\underline{P}, p_{t-1}^1], [p_{t-1}^1, p_{t-1}^2], \dots, [p_{t-1}^{m-1}, \overline{P}] \quad (3.17)$$

$$g_{t-1}^i(p_{t-1}) = F_{t-1}^{\tau-1}(p_{t-1}) \quad p_{t-1} \in [p_{t-1}^{i-1}, p_{t-1}^i] \quad (3.18)$$

Suppose p_{t-1}^* falls in interval k , $p_{t-1}^* \in [p_{t-1}^{k-1}, p_{t-1}^k]$. We now observe that $p_t \mapsto \min_{p_{t-1} \in [p_t - \Delta^+, p_t + \Delta^-]} F_{t-1}^{\tau-1}(p_{t-1})$ consists of $m+2$ piece-wise functions $g_t^1 \dots g_t^{m+2}$ which we can explicitly construct from the previous intervals. These intervals are given by:

$$[\underline{P}, p_t^1], \dots, [p_t^k, p_t^{k+1}], \dots, [p_t^{m+1}, \overline{P}] \quad (3.19)$$

$$p_t^i = \begin{cases} \max(\underline{P}, p_{t-1}^i - \Delta^-) & i < k \\ \max(\underline{P}, p_{t-1}^* - \Delta^-) & i = k \\ \min(\overline{P}, p_{t-1}^* + \Delta^+) & i = k + 1 \\ \min(\overline{P}, p_{t-1}^{i-2} + \Delta^+) & i \geq k + 2 \end{cases} \quad (3.20)$$

$$g_t^i(p) = \begin{cases} g_{t-1}^i(p + \Delta^-) & i < k \\ g_{t-1}^{i-1}(p_{t-1}^*) & i = k + 1 \\ g_{t-1}^{i-2}(p - \Delta^+) & i \geq k + 2 \end{cases} \quad (3.21)$$

Intervals that become $[\underline{P}, \underline{P}]$ or $[\overline{P}, \overline{P}]$ are redundant and can be removed. Moreover if the optimal point lies on the end point of an interval, say $p_{t-1}^* = p_{t-1}^k$, then the $k+2$ st interval becomes a single point and can be removed. Also note that if $g_{t-1}^1 \dots g_{t-1}^m$ are linear functions then the optimal point always lies on a breakpoint. Therefore if f_t is piece-wise linear only one extra interval is introduced.

3.7 Algorithm $RRF(+)$

Solving c with F_t^τ is similar to the algorithm of Frangioni and Gentile [4]. The major difference is that instead of pre-calculating the optimal economic dispatch for on-periods we now inductively for each time step create a set of functions F_t^τ . These functions represent the optimal 1UC schedule up until time t which includes the optimal economic dispatch. This has the advantage that we can identify functions that will not lead to optimality and do not have to calculate the next function $F_{t+1}^{\tau+1}$. This is based on the following proposition:

Proposition 3.7.1. *If a function F_t^τ has the property $\forall p \in [\underline{P}, \overline{P}] F_t^\tau(p) > \min_{\tau' \in [M_{up}, t]} F_t^{\tau'}(p)$ then a schedule in which the generator at time t is on for τ time steps cannot be optimal.*

The idea is that for any t and $p_t \in [\underline{P}, \overline{P}]$ all states (on_t^τ, p_t) where $\tau \in \{M_{up}, t\}$ have equivalent state transitions. Therefore the antecedent implies there exists a better schedule for every $p_t \in [\underline{P}, \overline{P}]$. Therefore $F_t^\tau(p)$ can be forgotten and consequently all following $F_{t+i}^{\tau+i}$, $1 \leq i < n$.

Irrelevant functions can be identified in multiple ways. One way is to trace the minimum of all F_t^τ functions and mark those that are part of the minimum. After that we can remove those functions F_t^τ that are not marked. The minimum can be traced by finding the function F_t^τ that has the minimal value at \underline{P} . This function is part of the minimum and if it intersects with another function at any point in $[\underline{P}, \overline{P}]$ then that function is also part of the minimum. We can find every function by iteratively finding intersections.

We call the algorithm that solves the recurrent relation (3.6)-(3.13) by constructing the F_t^τ functions without removing irrelevant ones: RRF and the algorithm that removes the irrelevant functions $RRF+$. The whole procedure of RRF and $RRF+$ is outlined in Algorithm 1.

Algorithm 1 $RRF(+)$

- 1: Initialise F_1^τ and $c(off_1^\tau)$
 - 2: **for all** $t \in \{2, \dots, n\}$ **do**
 - 3: **for all** $\tau \in \{1, \dots, M_{down}\}$ **do**
 - 4: Determine $c(off_t^\tau)$ with (3.7), (3.8) and (3.9)
 - 5: **end for**
 - 6: **for all** $\tau \in \{1, \dots, \max(t, M_{up})\} / \text{Irrelevant}$ **do**
 - 7: Determine F_t^τ with (3.14), (3.19), (3.20) and (3.21)
 - 8: **end for**
 - 9: (Remove irrelevant functions by finding intersections)
 - 10: **end for**
 - 11: Backtrack to get the solution
-

3.7.1 Time Complexity

Let m be the maximum number of intervals of all F_t^τ functions at any time and let k be the maximum number of relevant functions at any time:

$$m = \max_{t \in \{1, \dots, n\}} \max_{\tau \in \{1, \dots, t\}} \text{intervals}(F_t^\tau) \quad (3.22)$$

$$k = \max_{t \in \{1, \dots, n\}} \left| \left\{ \tau \mid \begin{array}{l} \tau \in \{1, \dots, t\}, \exists p \in [\underline{P}, \overline{P}] \\ F_t^\tau(p) \leq \min_{\tau' \in \{1, \dots, t\}} F_t^{\tau'}(p) \end{array} \right\} \right| \quad (3.23)$$

Regarding the complexity of $RRF(+)$, Line 7 is repeated $O(nkm)$ times since the $O(k)$ relevant functions have $O(m)$ intervals. Line 9 is repeated $O(n)$ times and has a cost of $O(mk^2)$ since the maximum number of intersections that can occur for $O(k)$ functions with $O(m)$ intervals is $O(mk^2)$.

Therefore, the total time complexity of $RRF+$ is $O(nmk^2)$ and RRF is $O(n^2m)$ since line 9 is skipped in which irrelevant functions are removed. As the numbers k and m theoretically could both be $O(n)$ the time complexity of $RRF+$ and RRF are $O(n^4)$ and $O(n^3)$ respectively.

However, we found that every function only has a small number of intervals when we use generator data from specific UC problems described in the literature. Moreover only a small (most of the time only one) number of functions is minimal at some point $p_t \in [\underline{P}, \overline{P}]$. In this case our algorithm $RRF+$ runs in linear time (Table 3.1).

Author/ Name	f_t is convex		Note
	Time	Time Detailed	
Frangioni et al. [4]	$O(n^3)$		
Frangioni et al. [3]	$O(n^3)$	$O(n^2m)$	$m = \max \text{ intervals}$
RRF (this work)	$O(n^3)$	$O(n^2m)$	
$RRF+$ (this work)	$O(n^4)$	$O(nmk^2)$	$k = \max \text{ relevant functions}$

Table 3.1: Overview 1UC algorithms

3.8 Second Recurrence Relation

$$c'(of f_t^\tau) = \min_{p_{t-1} \in [\underline{P}, SD]} c'(on_{t-1}^{M_{up}}, p_{t-1}) + c_{stop} \quad t > 1, \tau = 1 \quad (3.24)$$

$$c'(on_t^\tau, p_t) = f_t(p_t) + \min_{p_{t-1} \in [p_t - \Delta^+, p_t + \Delta^-]} \min\{c'(on_{t-1}^{\tau-1}, p_{t-1}), c'(on_{t-1}^\tau, p_{t-1})\} \quad t > 1, \tau = M_{up} \quad (3.25)$$

$$H_t^\tau(p_t) = \begin{cases} f_t(p_t) & t = 1, \underline{P} \leq p_t \leq \overline{P} \\ f_t(p_t) + c'(of f_{t-1}^{M_{\text{down}}}) + c_{start} & t > 1, \tau = 1, \underline{P} \leq p_t \leq SU \\ f_t(p_t) + \min_{p_{t-1} \in [p_t - \Delta^+, p_t + \Delta^-]} H_{t-1}^{\tau-1}(p_{t-1}) & t > 1, 1 < \tau < M_{\text{up}} \\ f_t(p_t) + \min_{p_{t-1} \in [p_t - \Delta^+, p_t + \Delta^-]} \min\{H_{t-1}^{\tau-1}(p_{t-1}), H_{t-1}^\tau(p_{t-1})\} & t > 1, \tau = M_{\text{up}} \\ \infty & \text{otherwise} \end{cases} \quad (3.26)$$

In this section we present a different but equivalent recurrence relation that is based on the fact that it is only necessary to keep track of how long a generator has been on up until the minimum uptime is reached. Therefore we could reduce the state space by reformulating the states S_t (3.15) to S'_t :

$$S'_t = \bigcup \left\{ \{of f_t^\tau \mid \tau \in \{1 \dots M_{\text{down}}\}\} \right. \\ \left. \{ (on_t^\tau, p_t) \mid \tau \in \{1 \dots M_{\text{up}}\}, p_t \in [\underline{P}, \overline{P}] \} \right\} \quad (3.27)$$

See Figure 3.3 for the binary commitment variables statespace and transitions.

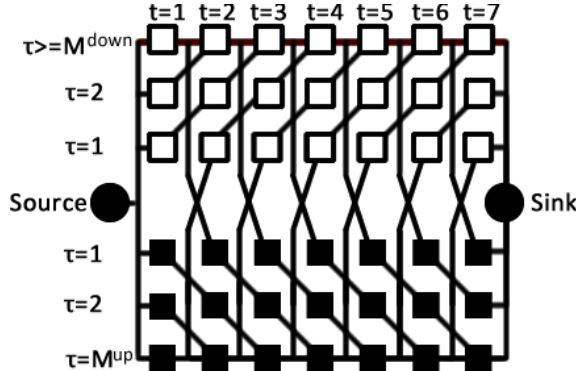


Figure 3.3: The new commitment statespace and transitions of 7 time steps. The off-states are represented as white nodes and the on-states as black nodes.

Now the state (on_t^τ, p) represents the state at time t where the generator is on for τ time steps and produces p_t at time t but when $\tau = M_{\text{up}}$ it represents that the generator is on for at least M_{up} time steps.

Besides reducing the state space this also introduces an additional type of state transition that can be made. Now we can also get to the last on-state $(on_t^{M_{\text{up}}}, p_t)$ from $(on_{t-1}^{M_{\text{up}}}, p_{t-1})$ if the difference between p_{t-1} and p_t respects the ramping limits. We define a new recurrence relation $c'(s_t)$ similar to $c(s_t)$. For brevity we only show the parts of the recurrence relation that differ from $c(s_t)$ in (3.24) and (3.25).

Again since we cannot compute the cost $c'(s)$ for every possible state s we need to construct a function H_t^τ such that: $H_t^\tau(p_t) = c'(on_t^\tau, p_t)$ and is defined in

(3.26). Now it is easy to see that $\forall t \in \{M_{\text{up}} \dots n\}$:

$$H_t^{M_{\text{up}}}(p) = \min_{\tau \in \{M_{\text{up}} \dots t\}} F_t^\tau(p) \quad \forall p \in [\underline{P}, \overline{P}] \quad (3.28)$$

For any time step t , $H_t^{M_{\text{up}}}$ is the minimum of multiple F_t^τ functions and this is the reason why we can remove irrelevant functions in Section 3.7. Effectively we are trying to find the smallest subset of F_t^τ that represents $H_t^{M_{\text{up}}}$.

We can solve 1UC either by constructing F_t^τ or H_t^τ . For F_t^τ there exists an efficient method to construct these functions and to identify redundant functions. Constructing H_t^τ for any convex function f_t is harder since we need to iteratively take the point-wise sliding minimum of two functions, one convex $H_{t-1}^{M_{\text{down}}-1}$ and one non-convex $H_{t-1}^{M_{\text{down}}}$ see (3.26).

3.9 Algorithm RRH

We will now show a way to construct H_t^τ when f_t is piece-wise linear by storing H_t^τ at a finite set of points. When solving the recurrence relation in this way the state space becomes equivalent to the state space of Guan et al. [6]. But we found a mistake in their formulation, fixed that mistake⁴ and made the algorithm more general. Our algorithm also works with non-equal ramping limits. Moreover, by a more in-depth analysis of the recurrence relation we make the algorithm more efficient.

When f_t is piece-wise linear we can represent H_t^τ by only storing a finite set of points that must contain the optimum of F_t^τ and, by a consequence of (3.28), of H_t^τ . This set also contains the points that are required to compute the optimum. These are the points that are computed when solving the recurrence relation, i.e. points that are on the path found by backtracking from optimal points. We use B^{f_t} to denote the set of breakpoints of the piece-wise linear cost function f_t . We use B to denote the set of all possible optimal points. We use Q to denote the set of all optimal points plus those points required to compute $H_t^\tau(b)$ for $b \in B$. Let the set B be defined as:

1. $\{\underline{P}, SU, \overline{P}\} \cup B^{f_t} \in B$
2. if $p \in B$ and $p + \Delta^+ < \overline{P}$ then $p + \Delta^+ \in B$
3. if $p \in B$ and $p - \Delta^- > \underline{P}$ then $p - \Delta^- \in B$

Let the set Q be defined as:

1. $B \cup \{SD\} \subseteq Q$
2. if $p \in Q$ and $p - \Delta^+ > \underline{P}$ then $p - \Delta^+ \in Q$
3. if $p \in Q$ and $p + \Delta^- < \overline{P}$ then $p + \Delta^- \in Q$

⁴For example the point $SU - \Delta$ where $\Delta = \Delta^+ = \Delta^-$ should also be included.

All proofs regarding B and Q are in the appendix 8.2. When we solve the recurrence relation c' we need to calculate $H_t^\tau(p_t)$ for every $t \in \{1, \dots, n\}$, $\tau \in \{1, \dots, M_{\text{up}}\}$ and $p_t \in Q$.

For a single function H_t^τ where $\tau > 1$ and for every $p_t \in Q$ we need to find the point $p_{t-1} \in [p_t - \Delta^+, p_t + \Delta^-] \cap Q$ where $H_{t-1}^{\tau-1}(p_{t-1})$ is minimal. Finding this point can be trivially done in $O(|Q|)$ resulting in a total time complexity of $O(|Q|^2)$.

However if $\tau < M_{\text{up}}$ then H_t^τ is still a convex function and the minimal point in Q is given as the argument of the minimum of (3.16) and can be computed in $O(1)$.

The case where $\tau = M_{\text{up}}$ could also be improved. We can make use of the property that for two consecutive points $p_t, p'_t \in Q$ the set representing the interval around the points $Q \cap [p_t - \Delta^+, p_t + \Delta^-]$ and $Q \cap [p'_t - \Delta^+, p'_t + \Delta^-]$ shares the majority of elements. To find to minimum value for all points is finding the sliding minimum over an array. All minimal points can be found with a double-ended queue in $O(|Q|)$. The full Algorithm *RRH* is described here:

Algorithm 2 RRH

```

1: Initialise  $H_1^\tau$  and  $c(off_1^\tau)$ 
2: for all  $t \in \{2, \dots, n\}$  do
3:   Compute  $c(off_t^\tau)$  with (3.7), (3.24) and (3.25)
4:   for all  $\tau \in \{2, \dots, M_{\text{up}} - 1\}$  do
5:     Determine  $H_t^\tau(p_t)$  with (3.26),(3.16) for all  $p_t \in Q$ 
6:   end for
7:   Create Dequeue  $D$ 
8:   for all  $p \in Q$  do
9:     for all  $q \in (Q \cap [p - \Delta^+, p + \Delta^-]) - D$  do
10:      Remove elements from end of D that
11:      have value  $> \max\{H_t^{M_{\text{up}}}(q), H_t^{M_{\text{up}}-1}(q)\}$ 
12:      Add q to the end of D
13:     end for
14:     Remove  $q \in D - (Q \cap [p - \Delta^+, p + \Delta^-])$  from D
15:      $q \leftarrow$  the front of D
16:      $H_t^\tau(p) = \max\{H_t^{M_{\text{up}}}(q), H_t^{M_{\text{up}}-1}(q)\} + f_t(p)$ 
17:   end for
18: end for
19: Backtrack to get the solution

```

Creating all H_t^τ has a time complexity of $O(n \cdot |Q|)$. The overall time complexity of *RRH* therefore becomes $O(n \cdot |Q|)$ which is an improvement to complexity of $O(n \cdot |Q|^2)$ from Guan et al. [6].

Author/ Name	f_t is convex piece-wise linear		Restrictions
	Time	Time Detailed	
Fan et al. [2]	$O(n^3)$		$\Delta^+ = \Delta^-$, $SU = SD$
Guan et al. [6]	$O(n)$	$O(n \cdot Q ^2)$	$\Delta^+ = \Delta^-$, $SU = SD$
RRH (this work)	$O(n)$	$O(n \cdot Q)$	

Table 3.2: Overview 1UC algorithms

3.10 Computational Results

To test the efficiency we have implemented five algorithms for linear and quadratic generation cost and tested it on generator data from instances in the UC literature. We gathered the generator data of power systems from the following sources:

- A110, 110 generator instance (Orero and Irving [9]).
- TAI38, 38 generator instance (Huang et al. [7]).
- GA10, 10 generator instance (Kazarlis et al. [8]).
- KOR140, 140 generator instance (Park et al. [11]).
- RCUC200, 200 generator instance (Frangioni et al. [5]).

For all instances we solved the problem with 10 different time series of electricity prices for every generator for 10 different horizons $\in \{100, 200, \dots, 1000\}$. For every time step, f_t is constructed from the generation cost of the generator and Lagrangian multipliers. In total we ran 49,900 different 1UC problems and compared the following algorithms:

- *RRF+*, here we solve the recurrence relation c by constructing F_t^τ and remove irrelevant functions as described in section 3.7.
- *RRH*, here we solve the recurrence relation c' by constructing H_t^τ with values in Q efficiently by the method described in section 3.9.
- *Guan**, here we solve the recurrence relation c' by constructing H_t^τ with values in Q but without the proposed time complexity improvements. Here the algorithm is equivalent to the algorithm of Guan et al. [6] if the formulation was complete and extended for non-equal ramping limits (hence the star).
- *RRF*, here we solve recurrence relation c by constructing F_t^τ without removing irrelevant functions. This algorithm is, therefore, comparable to Frangioni and Gentile [4] with the graph reduction mentioned in [3].
- *Gurobi*, at last we implemented the problem as a MIL(Q)P in Gurobi with a standard 3-bin formulation [10].

All algorithms were written in C# and run on an i7-8700K 3.70 GHz processor running on Windows 10.

3.10.1 Results

Instance	n	f_t is linear					f_t is quadratic		
		RRH	$Gurobi^*$	$RRF+$	RRF	$Gurobi$	$RRF+$	RRF	$Gurobi$
GA10	100	0.2	0.3	0.8	2.2	17.1	0.6	2.5	22.6
TAI38		1	37.2	0.4	1.7	16.1	0.4	2.1	100
A110		0.1	0.2	0.4	1.6	13.1	0.3	2.1	17.4
KOR140		0.2	0.8	0.4	1.5	12.4	0.3	2	141.4
RCUC200		2.3	101.5	0.5	1.9	20.9	0.4	2.3	105.4
GA10	500	0.7	1.6	3.5	55.1	162.9	2.7	60.3	453.4
TAI38		4.3	191.9	2.4	44.1	44.8	1.7	52.6	853.2
A110		0.5	0.7	1.5	38.8	56.8	1.2	51.2	317.4
KOR140		1.1	3.8	2.4	38.4	55.2	1.7	49.7	2436.5
RCUC200		11	497.4	2.5	49.5	141.2	1.9	57.3	3410.9
GA10	1000	1.4	3.5	6.7	213.4	395.5	5.3	237.7	1355.8
TAI38		8.7	380.7	4.7	167.9	112.8	3.4	208.4	3838.3
A110		0.8	1.3	2.9	148.5	128.2	2.4	198.3	977.2
KOR140		2.2	7.8	4.8	152	122.2	3.4	198.9	3398.6
RCUC200		21.8	991.1	4.9	192	391.2	3.8	225.7	4980

Table 3.3: Average computation time to solve 1UC of 10 time series of electricity prices for all generators in 5 instances for 3 horizons (100, 500, and 1000 time steps), both for the piece-wise linear and quadratic cost function (in milliseconds).

Instance	f_t is linear			f_t is quadratic	
	max $ Q $	max m	max k	max m	max k
GA10	15	6	5	9	5
TAI38	284	5	2	7	2
A110	12	6	5	9	5
KOR140	32	6	4	10	4
RCUC200	251	7	4	8	4

Table 3.4: Per instance, maximum values of m , k and $|Q|$ all generators in all time steps of 10 horizons with 10 time series of electricity prices.

The results are given in Table 3.3, Table 3.4, Figure 4 and Figure 5. Table 3.3 contains the average running time in milliseconds of the 1UC problems. Table 3.4 contains for each instance the maximum amount of points in Q , the maximum number of intervals and the maximum number of relevant functions for all experiments. Figure 4 shows the growth in computation time when the time horizon is increased and Figure 5 shows the ratio of problems solved for different performance ratios.

For all problem instances $RRF+$ and RRH outperform the other algorithms in terms of computation time. From Figure 5 you can see that in 40% of the cases RRH and in 60% of the cases $RRF+$ has the lowest computation time.

When the generation cost is linear the geometric average speed up of RRH compared to $RRF+$, $Gurobi^*$, RRF and $Gurobi$ is 1.3, 7.3, 17.6 and 45.8. The

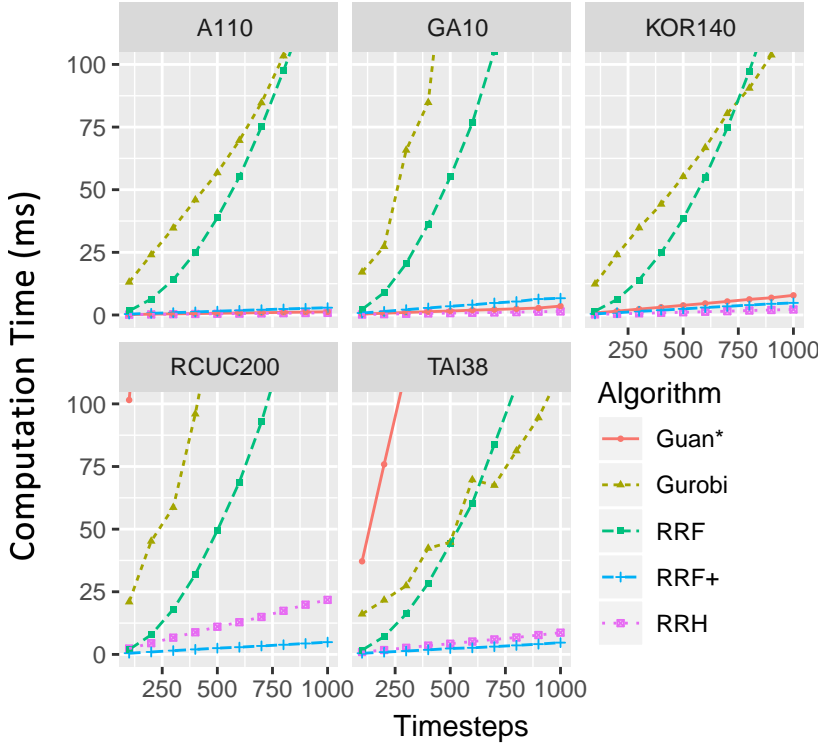


Figure 3.4: The growth of the average computation time in milliseconds when the amount of time steps increases when the generation cost function is linear.

geometric average speed up of $RRF+$ compared to $Guan^*$, RRF and $Gurobi$ is 5.7, 13.6 and 35.7. When the generation cost is quadratic the geometric average speed up of $RRF+$ compared to $Guan^*$, RRF and $Gurobi$ is 22.0 and 387.9. Table 3.3 shows that even for large time steps both algorithms solve 1UC in a few milliseconds.

The fact that $Gurobi$ performs as one of the worst is also not surprising since it is a general solver that tries to compete with algorithms specifically designed for 1UC.

$RRF+$ outperforms RRF as it is a direct improvement of RRF with a little computational overhead to identify redundant functions. In theory (for now) the worst case analysis of $RRF+$ is worse than RRF but in practice it reduces the amount of functions needed from $O(n)$ to some small amount. For these experiments we considered 49,900 different 1UC problems and k was at most 5 and m at most 10 (Table 3.4). These values were the same across all time horizons and did not increase when we increased n . We can also see the direct result of the linear vs quadratic growth in Figure 4.

The algorithm RRH is a direct improvement to $Guan^*$. For some instances

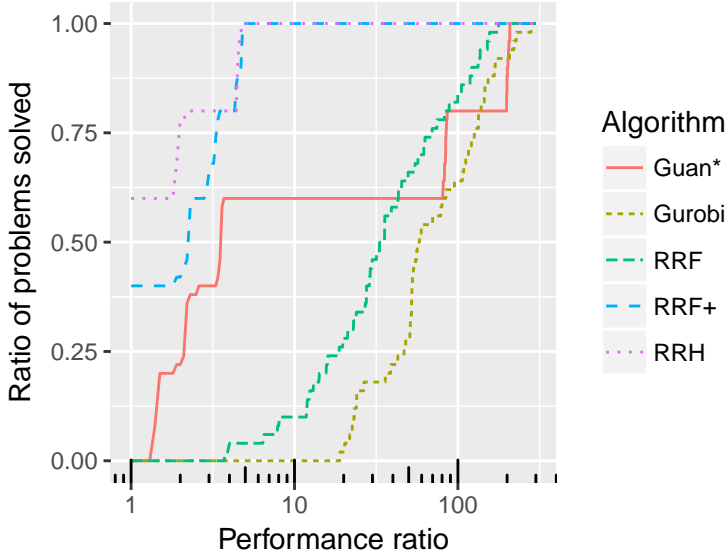


Figure 3.5: Graph that shows for increasing performance ratios the ratio of problems that are solved within a factor, the performance ratio, of the best performing algorithm for each instance.

where the set of optimal points Q is small (Table 3.4) there is little to no difference (A110,GA10) but for other instances where Q is much larger this difference becomes significant (see TAI38 and RCUC200 in Table 3.3).

3.11 Conclusion

We introduced a recurrence relation that solves 1UC. In order to solve this recurrence relation we created multiple functions F_t^τ that for each $p_t \in [P, \bar{P}]$ return the cost of the optimal schedule that is on at time t for τ time steps and produces p_t . By creating these functions inductively we were able to identify irrelevant functions and remove them. Resulting in a time complexity of $O(nmk^2)$ where k is the maximum number of relevant functions and m is the maximum number of intervals of those functions. We showed that for the instances studied k was at most 5 and m at most 10 and did not increase when we increased the amount of time steps. We show experimentally that this results in a computation time that grows linear in the amount of time steps which improves the previous quadratic growth

We introduced a different recurrence relation H_t^τ that requires fewer functions to be stored. These functions are harder to create than F_t^τ . However we showed that in the special case where generation cost is piece-wise linear we only need to keep track of a finite number of points Q to represent these functions. The method of representing cost only at a finite number of points is similar to the DP

algorithm of Guan et al. However our method works for non-equal ramping limits and we showed how to efficiently compute the value at Q , resulting in an improved algorithm in terms of generality and time complexity of $O(n \cdot |Q|)$.

We performed computational experiments with generator data from multiple power systems. The results show that our algorithm, *RRF+*, that identifies and removes irrelevant functions F_t^τ and our algorithm, *RRH*, of representing H_t^τ as a finite set points outperforms other methods with piece-wise linear and quadratic generation cost.

Both methods increase the efficiency and can solve the single-unit commitment problem for large time horizons in a few milliseconds. This could lead to significant improvements for solving large scale unit commitment problems with Lagrangian relaxation or related methods.

Bibliography

- [1] Wim van Ackooij et al. “Large-scale unit commitment under uncertainty: an updated literature survey”. In: *Annals of Operations Research* (2018), pp. 1–75.
- [2] Wei Fan, Xiaohong Guan, and Qiaozhu Zhai. “A new method for unit commitment with ramping constraints”. In: *Electric Power Systems Research* 62.3 (2002), pp. 215–224.
- [3] Antonio Frangioni and Claudio Gentile. *New MIP formulations for the single-unit commitment problems with ramping constraints*. 2015.
- [4] Antonio Frangioni and Claudio Gentile. “Solving nonlinear single-unit commitment problems with ramping constraints”. In: *Operations Research* 54.4 (2006), pp. 767–775.
- [5] Antonio Frangioni, Claudio Gentile, and Fabrizio Lacalandra. “Tighter approximated MILP formulations for unit commitment problems”. In: *IEEE Transactions on Power Systems* 24.1 (2009), pp. 105–113.
- [6] Yongpei Guan, Kai Pan, and Kezhao Zhou. “Polynomial time algorithms and extended formulations for unit commitment problems”. In: *IIEE Transactions* 50.8 (2018), pp. 735–751.
- [7] Kun-Yuan Huang, Hong-Tzer Yang, and Ching-Lien Huang. “A new thermal unit commitment approach using constraint logic programming”. In: *Power Industry Computer Applications., 1997. 20th International Conference on.* IEEE. 1997, pp. 176–185.
- [8] Spyros A Kazarlis, AG Bakirtzis, and Vassilios Petridis. “A genetic algorithm solution to the unit commitment problem”. In: *IEEE transactions on power systems* 11.1 (1996), pp. 83–92.
- [9] SO Orero and MR Irving. “Large scale unit commitment using a hybrid genetic algorithm”. In: *International Journal of Electrical Power & Energy Systems* 19.1 (1997), pp. 45–55.
- [10] J. Ostrowski, M. F. Anjos, and A. Vannelli. “Tight mixed integer linear programming formulations for the unit commitment problem”. In: *IEEE Transactions on Power Systems* 27.1 (2009), pp. 39–46.

- [11] Jong-Bae Park et al. “An improved particle swarm optimization for nonconvex economic dispatch problems”. In: *IEEE Transactions on Power Systems* 25.1 (2010), pp. 156–166.
- [12] Qiaozhu Zhai, Xiaohong Guan, and Feng Gao. “Optimization based production planning with hybrid dynamics and constraints”. In: *IEEE Transactions on Automatic Control* 55.12 (2010), pp. 2778–2792.

Chapter 4

New efficient ADMM algorithm for the Unit Commitment Problem

This chapter is in submission at: Annals of Operations Research
Rogier Hans Wuijts, Marjan van den Akker & Machteld van den Broek

Nomenclature

Decisions variables

- p_s Sum of charging and discharging of storage unit s at time t
- pc_{st}, pd_{st} Charging and discharging of storage unit s at time t
- f_{lt} The amount of power node that flows on the transmission line l . if $l = (n \rightarrow n')$ the power that flows from node n to node n'
- inj_{nt} The amount of power node n draws from the transmission system at time step t .
- p_{gt} Production of generator g at time t
- p_{rt} Production of renewable energy source r at time t
- u_{gt}, v_{gt}, w_{gt} Binary commitment, start and stop variable of generator g at time t .

Model Generator Parameters

- η_s^c, η_s^d Charge and discharge efficiency of storage unit s
- $\overline{PC}_s, \overline{PD}_s$ Charging and discharging limit of storage unit s
- $\underline{PE}_s, \overline{PE}_s$ The minimum and maximum energy of storage unit s
- $\overline{f}_l, \underline{f}_l$ Maximum flow and maximum negative flow on transmission line l
- $\overline{P}_g, \underline{P}_g$ maximum and minimum power output of generator g
- RU_g, RD_g Ramp up and down limit of generator g
- AT_{rt} Availability factor of renewable source r at time t
- SU_g, SD_g Start-up and shutdown limit of generator g
- UT_g, DT_g The minimum uptime and downtime of generator g

Sets

- G, R, T, S, L Set of the generators, renewable generators, time steps, storage units and transmission lines

4.1 Abstract

The unit commitment problem (UC) is an optimization problem concerning the operation of electrical generators. Many algorithms have been proposed for the UC and in recent years a more decentralized approach, by solving the UC with alternating direction method of multipliers (ADMM), has been investigated. For convex problems ADMM is guaranteed to find an optimal solution. However, because UC is non-convex additional steps need to be taken in order to ensure convergence to a feasible solution of high quality. Therefore, solving UC by a MIL(Q)P formulation and running an off-the-shelf solver like Gurobi until now seems to be the most efficient approach to obtain high quality solutions.

In this chapter, we introduce a new and efficient way to solve the UC with ADMM to near optimality. We relax the supply-demand balance constraint and deal with the non-convexity by iteratively increasing a penalty coefficient until we eventually force convergence and feasibility. At each iteration the subproblems are

solved by our efficient algorithm for the single UC subproblem developed in earlier work and our new ADMM algorithm for the transmission subproblems.

Computational experiments on benchmark instances demonstrated that our algorithm produces high-quality solutions. The computation time seems to grow practically linear with the length of the time horizon. For the case with quadratic generation cost our algorithm is significantly faster than solving the problem by a state-of-the-art MIL(Q)P formulation. For the case of linear generation cost, it outperforms the MILP approach for longer time horizons.

4.2 Introduction

The unit commitment problem (UC) is a family of NP-hard [2, 32] optimization problems for the operational planning of electrical generators. The goal is to find a minimum cost schedule of generators that satisfies the electricity demand at each time step. UC is a widely studied topic in Operations Research, but its significance extends beyond this field, as it plays a central role in detailed power system modeling, which is crucial in the ongoing global shift towards sustainable energy [50, 1].

The UC has been extensively researched in academia, with various optimization techniques applied to solve it. This can be seen in the numerous papers cited in various surveys on the topic [2, 45, 39] spanning multiple algorithm paradigms, from exact methods to heuristic evolutionary algorithms. However, since UC has a mixed combinatorial and continuous statespace, mathematical programming techniques have been most successful in finding near optimal solutions [2]. Until the early 2000's, Lagrangian Relaxation was the method of choice for solving UC [8]. However, this has changed. In the past 15 years, Mixed Integer Linear Programming (MILP) problem formulations have been a very active area of research [27] and popular tool for solving the UC [3, 46, 34]. Additionally, it has been stated that in the industry, UC is commonly solved using MILP and that the shift from Lagrangian Relaxation to MILP was considered beneficial [35, 10, 36].

The recent resurgence of interest in alternating direction method of multipliers (ADMM) [56] have also resulted in an increased application of augmented Lagrangian methods, such as ADMM, to the UC [15, 29, 43, 58, 57, 53].

ADMM is an augmented Lagrangian method that solves convex optimization problems. In ADMM, decision variables are split into two or more subsets, and the coupling constraints, i.e constraints involving variables from different subsets, are relaxed by moving them to the objective such that violation of these constraints results in a penalty cost. Next, at consecutive steps subproblems are solved over a subset of the variables. These subproblems are much easier to solve than the original problem and this can be done in a distributed and parallel way.

The UC problem can be decomposed in multiple ways. For example, ADMM can be applied to the UC by relaxing the demand coupling constraint at each node, which was done by [29, 57] and is also commonly used in existing literature on Lagrangian relaxation for UC [7, 13, 19]. The demand coupling constraint at a node ensures that the total production of electricity is equal to the consumption

of electricity. By relaxing this constraint, the problem decomposes into multiple subproblems for the generators, Renewable Energy Sources (RES), transmission, and storage units. These subproblems can then be solved by efficient algorithms [52, 18, 21, 14]. The Lagrange multipliers at each node corresponds to a nodal electricity price for each time step.

When the problem is decomposed at the transmission level [15, 43, 53, 58], the nodes of the power system are divided into regions, which are then decoupled by copying transmission variables at their boundaries and relaxing the equality between these copied variables. If you decompose at the transmission level, the subproblems at each node are (smaller) UC problems which contain a subset of the total generators, RES and storage units. These UC problems can still be hard to solve and are often solved with MILP.

There are several other possible decompositions. For example, duplicated dispatch variables can be used in different subproblems of the UC problem [6] or temporal constraints such as ramping limits or minimum up- and downtime can be relaxed [44].

Only for convex optimization problems, ADMM is guaranteed to find an optimal solution [9]. However, since UC is non-convex due to the binary commitment variables, researchers using ADMM to solve UC must be aware that it may not converge to the optimal solution, if at all. This is a general drawback of decomposition algorithms based on Lagrangian relaxation.

Some authors [15, 53] solved the issue of nonconvexity by embedding their ADMM algorithm into a larger heuristic that after some iterations fixes the binary commitment variables to make the problem convex. The ADMM algorithm can then converge towards the local optimal solution given these fixed binary variables. This process is called “release-and-fix”. It is not guaranteed that these fixed commitment variables are optimal or even result in feasible solutions.

Another approach is to repair the final solution provided by Lagrangian relaxation in an ad hoc way by fixing the binary variables with some heuristic [16, 55, 8, 19]. A convex economic dispatch problem is then solved with these fixed binary variables. For example, the heuristics proposed by [16] sequentially and greedily processes the timesteps, fixing binary variables while adhering to minimum up times. Which generators are being turned on or off is based on either a priority list or randomly sampled from a probability distribution calculated using information from their bundle methods. They introduce four variants, one of which is deterministic and the others use sampling. When sampling is used, the heuristics are repeated, and the best solution is retained. The authors found that three out of the four proposed heuristics frequently fail to produce feasible solution and the fourth one requires a lot of sampling steps (repeated 200 [17] or 1000 [16] times).

Note that in the above heuristics ramping limits are ignored. [19] and [8] both use a slight modification of one of the four heuristics proposed [16]. [19] studies the case of UC with ramping limits and only finds feasible solutions in roughly one out of ten dual iterations. Moreover, the authors state that incorporating ramping limits into their heuristic is non-trivial.

Other authors try to force feasibility by adding an additional penalty function [12]. However, solutions produced are still infeasible and far away from optimality.

Finally, others have chosen to just ignore the issue [6] and some authors chose to convexify the generator polytope, i.e. they remove the non-convexity by taking the convex-hull of the generator state space [29], again leading to infeasible solutions.

Our contribution: in this chapter we introduce a new and efficient way to solve UC with ADMM. We relax the demand coupling constraint and improve existing approaches in two ways. Firstly, we apply a different method to deal with the non-convexity by using an increasing penalty coefficient. This means that we do not need heuristic approaches to transfer the infeasible solution into a feasible one. Our algorithm is the first Lagrangian algorithm to force convergence and feasibility for the UC including ramping limits without requiring an ad-hoc repair heuristic. Secondly, we solve the subproblems very efficiently by applying our 1UC algorithm [52], which strongly outperforms earlier algorithms for 1UC especially on longer time horizons, and also our newly created algorithm to solve transmission sub problems. We performed computational experiments on all known benchmark instances. Although our ADMM algorithm needs many iterations to converge, each iteration has a low computation time due to our efficient 1UC algorithm.

Consequently, we have introduced a fast algorithm that produces high quality solutions respecting the ramping limits which experimentally outperforms solving UC with MIP formulations, the current state-of-the-art for the UC. Moreover, our method scales much better with the length of the planning horizon. In the experiments, we always found feasible solutions of a very good quality for a large set of UC instances.

The remainder of this chapter is organized as follows. In the following section, we present the problem formulation of UC. In Section 4.4, we describe how ADMM can be applied to a small power system. In Section 4.5, we describe how we applied ADMM to a full UC formulation, how we solve the individual subproblems and how we dealt with non-convexity. Our experiments and results are presented in Section 4.6, and we end the paper with a discussion in Section 4.7 and conclusions in Section 4.8.

4.3 UC problem description

In this section, we define the UC that we study in this chapter. Our UC description is based on a Mixed Integer Quadratic Program (MIQP) formulation with detailed thermal generators, RES, storage, and transmission lines. The decision variables p_{gt} , p_{rt} , p_{st} are the generation of thermal generator unit g , RES unit s and storage unit s at time step t . Other variables are created to specify the feasible state space of these variables. We use the well-known 3-bin formulation [27]. This means that we use binary variables u_{gt} , v_{gt} , and w_{gt} to signal that generator g respectively is

on, switched on, and switched off in time step t . The formulation is as follows:

$$\min \sum_{t \in T} \sum_{g \in G} a_g u_{gt} + b_g p_{gt} + c_g p_{gt}^2 + v_{gt} cost_{start} \quad (4.1a)$$

s.t.

$$p_{gt} \geq u_{gt} \underline{P}_g, g \in G, t \in T \quad (4.1b)$$

$$p_{gt} \leq \overline{P}_g u_{gt}, g \in G, t \in T \quad (4.1c)$$

$$\sum_{i=t-UT_g+1}^t v_{gi} \leq u_{gt}, t \in T, g \in G \quad (4.1d)$$

$$\sum_{i=t-DT_g+1}^t w_{gi} \leq 1 - u_{gt}, t \in T, g \in G \quad (4.1e)$$

$$p_{gt} - p_{gt-1} \leq (SU_g - RU_g) v_{gt} + RU_g u_{gt}, t \geq 2, g \in G \quad (4.1f)$$

$$p_{gt-1} - p_{gt} \leq (SD_g - RD_g) w_{gt} + RD_g u_{gt-1}, t \geq 2, g \in G \quad (4.1g)$$

$$p_{rt} \leq AF_{rt} \overline{P}_{rt}, r \in R, t \in T \quad (4.1h)$$

$$0 \leq pc_{st} \leq \overline{PC}_s, t \in T, s \in S \quad (4.1i)$$

$$0 \leq pd_{st} \leq \overline{PD}_s, t \in T, s \in S \quad (4.1j)$$

$$p_{st} = pd_{st} - pc_{st}, t \in T, s \in S \quad (4.1k)$$

$$\underline{PE}_s \leq pe_{st} \leq \overline{PE}_s, t \in T, s \in S \quad (4.1l)$$

$$pe_{st} = pe_{st-1} + pc_{st} * \eta_{st}^c - \frac{pd_{st}}{\eta_{st}^d}, t \in T, s \in S \quad (4.1m)$$

$$inj_{nt} = \sum_{l=(n' \rightarrow n), n' \in N} f_{lt}, t \in T, n \in N \quad (4.1n)$$

$$\underline{f}_l \leq f_{lt} \leq \overline{f}_l, l \in L, t \in T \quad (4.1o)$$

$$\sum_{g \in G_n} p_{gt} + \sum_{r \in R_n} p_{rt} + \sum_{s \in S_n} p_{st} + inj_{nt} = D_{nt}, t \in T, n \in N \quad (4.1p)$$

$$u_{gt} - u_{gt-1} = v_{gt} - w_{gt}, t \in T, g \in G \quad (4.1q)$$

$$u_{gt}, v_{gt}, w_{gt} \in \{0, 1\}, p_{gt}, p_{rt}, p_{st}, pe_{st}, inj_{nt}, f_{lt} \in \mathbb{R} \quad (4.1r)$$

(4.1a) is the objective function of the UC consisting of the generation cost and start cost, a_g is the constant cost, b_g is the linear cost coefficient and c_g is the quadratic cost coefficient. Constraint (4.1b) and (4.1c) ensure the minimum and maximum production of generators. Constraint (4.1d) and (4.1e) ensure the minimum up and downtime of generators. Constraint (4.1f) and (4.1g) ensure the ramping limits of generators between time steps. Constraint (4.1h) ensures that the RES production is lower than the availability at that hour. (4.1i), (4.1j) and (4.1l) ensure the charge, discharge and energy storage limits for storage units. Equation (4.1k) is the sum of charge and discharge i.e. the net storage production. Equation (4.1m) describes the relation between the charge, discharge and net power production of a storage unit. Equation (4.1q) describes the logic between the binary commitment,

start and stop variables of the generators. Equation (4.1n) describes the relation between the flow on transmission lines and the power injection at nodes. Constraint (4.1o) ensures flow limits on transmission lines. Equation (4.1p) ensures that the total generation meets the total demand at every node and time step. At last, the commitment variables are binary while the generation are real numbers (4.1r)

The difference between this formulation and the full model used in chapter 2 is that here we don't consider reserve requirements or start dependant startup cost. However, at the end of this chapter there is a discussion how this could be implemented.

4.4 ADMM Example on simple UC problem

To illustrate the application of ADMM to UC, we present here a simple UC example. Suppose we want to find the least cost power production schedule for a power system with a demand D and n generators with generation levels p_i and a convex generation cost function f_i for generator i . This optimization problem can be formulated as:

$$\min \sum_{1 \leq i \leq n} f_i(p_i) \quad (4.2)$$

s.t.

$$D - \sum_{1 \leq i \leq n} p_i = 0 \quad (4.3)$$

We can solve this problem by first taking the augmented Lagrange relaxation of the demand coupling constraint (4.3) and for a given ρ turning it in the following function:

$$\mathcal{L}(p_1, \dots, p_n, \lambda) = \sum_{1 \leq i \leq n} f_i(p_i) + \lambda(D - \sum_{1 \leq i \leq n} p_i) + \frac{\rho}{2}(D - \sum_{1 \leq i \leq n} p_i)^2 \quad (4.4)$$

we can define the corresponding dual problem as:

$$\max_{\lambda} g(\lambda) \quad (4.5)$$

$$\text{where } g(\lambda) = \inf_{\mathbf{p}} \mathcal{L}(\mathbf{p}, \lambda)$$

If strong duality holds, the optimal value of the dual problem (4.5) is the same as the optimal value of the primal problem (4.2). Then the optimal primal solution can be recovered from the optimal dual solution. We can find the optimal multiplier λ by doing dual descent, i.e. iteratively solving $\inf_{\mathbf{p}} \mathcal{L}(\mathbf{p}, \lambda)$ for a given λ and update λ in the direction of the gradient of g (4.5).

However, contrary to solving a standard Lagrangian iteration, we cannot determine the optimal generation p_i independently of the other production variables when solving an augmented Lagrangian iteration. Unfortunately, this makes the augmented Lagrangian dual iteration as difficult as solving the original primal problem.

A solution to deal with the interdependence of the subproblems is ADMM. The idea of ADMM is that you iteratively optimize one subproblem while the other subproblems stay fixed. In other words, only a subset of the decision variables can change while the rest of the decision variables remain fixed at the value of the previous iteration or, if they have already been updated, of the current iteration. At the end of the ADMM iteration the dual multipliers are updated (see [9] for a detailed explanation of ADMM).

When the original problem is convex and the problem is split into two sets of variables then this method will converge to a primal feasible solution with an optimal value [9]. However, a lot of optimization problems have a decomposable structure that consist of multiple sets or blocks. To decompose a problem that has a multi-block structure we can either use multi-block Gauss Seidel ADMM or variable splitting ADMM which at its core has a two-block structure [31]. The former ADMM method has been applied to practical problems [31] but lacks the converging guaranty of the latter [11].

4.4.1 Multi-block Gauss Seidel

We apply Gauss Seidel ADMM to determine the optimal Lagrange multipliers and generation for the UC example. At each iteration k we sequentially minimize p_i while keeping the other production values constant. The values p_j^{k+1} are used for generators j where $j < i$ and for generators $j > i$ we use the old value p_j^k of the previous iteration, resulting in each iteration in n statements of the form:

$$p_i^{k+1} \leftarrow \operatorname{argmin}_{p_i} \mathcal{L}(p_1^{k+1}, \dots, p_{i-1}^{k+1}, p_i, p_{i+1}^k, \dots, p_n^k, \lambda^k) \quad (4.6)$$

The strength of ADMM is that we remove the interdependence created by the cross term in (4.4) by optimizing only for p_i while keeping the other values constant.

At the end of each iteration, the multiplier is updated in the direction of the gradient of the relaxed constraint violation with step size ρ . For readability, we define the relevant residual load R_i for generator i :

$$R_i = D - \sum_{1 \leq j < i} p_j^{k+1} - \sum_{i < j \leq n} p_j^k \quad (4.7)$$

The full Gauss-Seidel multi-block ADMM that solves our small UC example with n generators is presented in Algorithm 3.

An alternative method of applying ADMM on a problem with a multi-block structure is by variable splitting, but we found that this ADMM performed much worse than the Gauss Seidel ADMM. More information is presented in the appendix 8.3.

Algorithm 3 Gauss-Seidel Multi-block ADMM

```

1: while Stopping criteria have not been met do
2:    $p_1^{k+1} \leftarrow \operatorname{argmin}_{p_1} \{f_1(p_1) - \lambda^k p_1 + \frac{\rho}{2}(R_1 - p_1)^2\} \triangleright \operatorname{argmin}_{p_1} \mathcal{L}(p_1, \dots, p_n^k, \lambda)$ 
3:    $\vdots$ 
4:    $p_i^{k+1} \leftarrow \operatorname{argmin}_{p_i} \{f_i(p_i) - \lambda^k p_i + \frac{\rho}{2}(R_i - p_i)^2\} \triangleright$ 
      $\operatorname{argmin}_{p_i} \mathcal{L}(p_1^{k+1} \dots p_i \dots p_n^k, \lambda)$ 
5:    $\vdots$ 
6:    $p_n^{k+1} \leftarrow \operatorname{argmin}_{p_n} \{f_n(p_n) - \lambda^k p_n + \frac{\rho}{2}(R_n - p_n)^2\} \triangleright$ 
      $\operatorname{argmin}_{p_n} \mathcal{L}(p_1^{k+1}, \dots, p_n, \lambda)$ 
7:    $\lambda^{k+1} \leftarrow \lambda^k + \rho(D - \sum_{1 \leq i \leq n} p_i^{k+1})$ 
8:    $k \leftarrow k + 1$ 
9: end while

```

4.5 New ADMM Algorithm for UC

After the application of ADMM to a simple UC example, we now apply ADMM to the full UC problem described in Section 4.3. Although the procedure is also based on the relaxation of the coupling constraint that links generation and demand, the individual subproblems are more detailed and thus more complicated than the simple UC example.

In the UC description (4.1a) - (4.1r) the only constraint that links the generation and demand is (4.1p). We obtain the following augmented Lagrangian by relaxing this constraint:

$$\begin{aligned}
\mathcal{L}(\vec{p_{gt}}, \vec{p_{rt}}, \vec{p_{st}}, \vec{inj_{nt}}, \vec{\lambda_{nt}}) &= \sum_{t \in T} \sum_{g \in G} [a_g + b_g p_{gt} + c_g p_{gt}^2 + v_{gt} cost_{start}] \\
&+ \sum_{t \in T} \sum_{n \in N} \left[\lambda_{nt} R D_{nt} + \frac{\rho}{2} R D_{nt}^2 \right]
\end{aligned} \tag{4.8a}$$

$$\text{s.t. (4.1b) - (4.1o)} \tag{4.8b}$$

where:

$$R D_{nt} = D_{nt} - \left(\sum_{g \in G_n} p_{gt} + \sum_{r \in R_n} p_{rt} + \sum_{s \in S_n} p_{st} + inj_{nt} \right)$$

λ_{nt} is the Lagrange multiplier of coupling constraint of node n at time t and ρ is the quadratic penalty coefficient on the residual demand.

At each iteration the optimal value of the decision variables will be determined while the rest of the decision variables remain fixed at the value of the previous iteration or, if they have already been updated, of the current iteration. Consequently, we iteratively solve the following subproblems: single unit commitment subproblem (1UC) for each generator $g \in G$, RES subproblem for each renewable resource $r \in R$, storage subproblem for each storage unit $s \in S$, and the transmission subproblem for each time step $t \in T$. This is depicted in (Figure 4.1). After

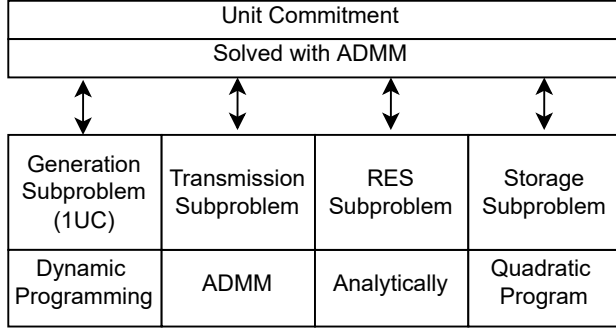


Figure 4.1: Flowchart of solving UC with ADMM by decomposing it into subproblems.

each iteration the Lagrange multipliers are updated in the direction of the subgradient which equals to the residual demand RD_{nt} . The ADMM Gauss-Seidel iteration proceeds according to Algorithm 4.

Algorithm 4 Gauss-Seidel ADMM iteration

```

1: for all  $g \in G$  do
2:    $\mathbf{p}_g \leftarrow \operatorname{argmin}_{p_g} \mathcal{L}(\dots, p_{g-1}^{k+1}, p_g, p_{g+1}^k \dots, \lambda^k)$        $\triangleright$  Solve 1UC subproblem
3: end for
4: for all  $r \in R$  do
5:    $\mathbf{p}_r \leftarrow \operatorname{argmin}_{p_r} \mathcal{L}(\dots, p_{r-1}^{k+1}, p_r, p_{r+1}^k \dots, \lambda^k)$        $\triangleright$  Solve 1RES subproblem
6: end for
7: for all  $s \in S$  do
8:    $p_s \leftarrow \operatorname{argmin}_{p_s} \mathcal{L}(\dots, p_{s-1}^{k+1}, p_s, p_{s+1}^k \dots, \lambda^k)$        $\triangleright$  Solve 1Storage subproblem
9: end for
10: for all  $t \in T$  do
11:    $\mathbf{inj}_t \leftarrow \operatorname{argmin}_{inj_t} \mathcal{L}(\dots, inj_t, \dots, \lambda^k)$        $\triangleright$  Solve Transmission subproblem
12: end for
13: for all  $t \in T$  do
14:   for all  $n \in N$  do
15:      $\lambda_{nt}^{k+1} \leftarrow \lambda_{nt}^k + \rho RD_{nt}^k$        $\triangleright$  Update Lagrangian multipliers
16:   end for
17: end for

```

4.5.1 Solving the subproblems

4.5.1.1 Generator subproblem 1UC

The 1UC problem is the problem of determining the optimal power schedule for a single generator. In each iteration of our Gauss-Seidel algorithm, we have to solve a number of 1UC problems (see Line 2 in Algorithm 4). For a given generator g

at node n , this problem can be defined as:

$$\operatorname{argmin}_{p_g} \mathcal{L}(\dots, p_{g-1}^{k+1}, p_g, p_{g+1}^k \dots, \lambda^k) \text{ s.t. (4.1b) - (4.1r)} \quad (4.9)$$

Only p_g is variable here, the other production variables p_g ($g \in G_n$) are constant.

Similar to the the small UC example in Section 4.4.1, we define the relevant residual load R_{gnt} for determining the optimal power output of generator g at node n and time t by

$$R_{gnt} = D_{nt} - \sum_{1 \leq i < g} p_{it}^{k+1} - \sum_{g < i \leq |G_n|} p_{it}^k - \sum_{r \in R_n} p_{rt}^k - \sum_{s \in S_n} p_{st}^k - in j_{nt}^k. \quad (4.10)$$

We can rewrite (4.9) to an equivalent problem formulation:

$$\min \sum_{t \in T} a_g + b_g p_{gt} + c_g p_{gt}^2 + v_{gt} cost_{start} - \lambda_t p_{gt} + \frac{\rho}{2} (R_{gnt} - p_{gt})^2 \quad (4.11)$$

$$\text{subject to (4.1b), (4.1c), (4.1d), (4.1e), (4.1q), (4.1f), (4.1g)} \quad (4.12)$$

Solving 1UC. Since we have to solve a series of 1UC problems in each iteration, solving these problems very efficiently is crucial. Here we use our dynamic programming algorithm *RRF+* [52], which significantly outperforms earlier 1UC algorithms in terms of computation time. This advanced dynamic programming algorithm models part of the states by convex functions instead of single values. This algorithm is based on a recurrence relation on functions that represents for each generator state at each time step the value of the optimal generator schedule that ends in that state. The RFF+ algorithm is very efficient because it does not need to compute the optimal economic dispatch for each possible ‘on-interval’ of a generator and it can identify superfluous functions which reduces the computation time significantly (see [52] for more details).

4.5.1.2 Renewable generation subproblem 1RES

The 1RES subproblem is the problem of finding the optimal renewable energy generation given its availability and is given by:

$$\operatorname{argmin}_{p_r} \mathcal{L}(\dots, p_{r-1}^{k+1}, p_r, p_{r+1}^k \dots, \lambda^k) \text{ s.t. (4.1b) - (4.1r)} \quad (4.13)$$

We define the relevant residual load R_{rnt} for RES r at node n and time t .

$$R_{rnt} = D_{nt} - \sum_{g \in G_n} p_{gt}^{k+1} - \sum_{1 \leq i < r} p_{it}^{k+1} - \sum_{r < i \leq |R_n|} p_{it}^k - \sum_{s \in S_n} p_{st}^k - in j_{nt}^k \quad (4.14)$$

Now (4.13) is equivalent to the following program:

$$\min \sum_{t \in T} -\lambda_t^k p_{rt} + \frac{\rho}{2} (R_{rnt} - p_{rt})^2 \quad (4.15)$$

$$\text{subject to } p_{rt} \leq AF_{rt} \bar{P}_{rt} \quad t \in T \quad (4.16)$$

We can easily solve this problem analytically since it is a simple minimization of a quadratic function with bounds, which results in:

$$p_{rt}^{k+1} = \begin{cases} 0 & \frac{\lambda_t^k}{R_{rnt}} < 0 \\ \frac{\lambda_t^k}{R_{rnt}} & 0 \leq \frac{\lambda_t^k}{R_{rnt}} \leq AF_{rt}\bar{P}_{rt} \\ AF_{rt}\bar{P}_{rt} & \frac{\lambda_t^k}{R_{rnt}} > AF_{rt}\bar{P}_{rt} \end{cases} \quad (4.17)$$

4.5.1.3 Storage subproblem 1Storage

The storage subproblem to find the least cost charging and discharging strategy is given by:

$$\operatorname{argmin}_{p_s} \mathcal{L}(\dots, p_{s-1}^{k+1}, p_s, p_{s+1}^k, \dots, \lambda^k) \quad \text{s.t. (4.1b) - (4.1r)} \quad (4.18)$$

We define the relevant residual load R_{snt} for storage unit s at node n and time t .

$$R_{snt} = D_{nt} - \sum_{g \in G_n} p_{gt}^{k+1} - \sum_{r \in R_n} p_{rt}^{k+1} - \sum_{1 \leq i < s} p_{st}^{k+1} - \sum_{s < i \leq |S_n|} p_{st}^k - inj_{nt}^k \quad (4.19)$$

To find the best storage schedule (4.18), we can simply solve the following quadratic program:

$$\min \sum_{t \in T} -\lambda_t^k p_{st} + \frac{\rho}{2} (R_{snt} - p_{st})^2 \quad (4.20)$$

$$\text{subject to (4.1l), (4.1i), (4.1j), (4.1m), (4.1k)} \quad (4.21)$$

Although other algorithms exist that solve this problem efficiently with dynamic programming [4], we solve this storage subproblem with the QP-solver Gurobi.

4.5.1.4 Transmission subproblem

The transmission subproblem is given by

$$\operatorname{argmin}_{inj_{nt}} \mathcal{L}(\dots, inj_{nt}, \dots, \lambda^k) \quad \text{s.t. (4.1b) - (4.1r)} \quad (4.22)$$

The transmission subproblem (4.22) is harder than the RES or storage subproblems but fortunately it consists of a set of the subproblems which are independent in time. We define the relevant residual load R_{nt} for the optimal nodal injection at node n and time t .

$$R_{nt} = D_{nt} - \sum_{g \in G_n} p_{gt}^{k+1} - \sum_{r \in R_n} p_{rt}^{k+1} - \sum_{s \in S_n} p_{st}^{k+1} \quad (4.23)$$

Moreover, we define a set L_n as $\{l \mid l \in L, n' \in N, l = (n' \rightarrow n)\}$ i.e. the set of transmission line going into n . For each time step $t \in T$ we have to solve the

transmission subproblem that is equivalent to (4.22):

$$\min \sum_{n \in N} -\lambda_n^k inj_n + \frac{\rho}{2} (R_{nt} - inj_n)^2 \quad (4.24a)$$

subject to

$$inj_n = \sum_{l \in L_n} f_l \quad \forall n \in N \quad (4.24b)$$

$$\underline{f}_l \leq f_l \leq \bar{f}_l \quad \forall l \in L \quad (4.24c)$$

This subproblem is a quadratic program that can be solved by a QP-Solver. However, computation time is long, since it needs to be solved for every time step at every ADMM iteration. We found that solving this subproblem with our own ADMM algorithm is much faster. Since (4.24) is a convex quadratic program we can solve it to optimality with a standard ADMM procedure by relaxing the injection and flow coupling constraint (4.24b). This results in the following augmented Lagrangian:

$$\begin{aligned} \mathcal{L}^{trans}(\vec{\pi}_n, \vec{inj}_n, \vec{f}_l) = & \quad (4.25) \\ \sum_{n \in N} \left(-\lambda_n^k inj_n + \frac{\rho}{2} (R_{nt} - inj_n)^2 + \pi_n (inj_n - \sum_{l \in L_n} f_l) + \frac{\rho_{trans}}{2} (inj_n - \sum_{l \in L_n} f_l)^2 \right) \end{aligned}$$

When we solve (4.25) with ADMM we iteratively need to solve two kinds of subproblems: determining the optimal injections and determining the optimal flow on transmission lines. The former is solved by finding the minimum of a quadratic function and the latter by finding the minimum of a quadratic function with bounds.

Algorithm 5 Transmission Subproblem Gauss-Seidel ADMM

```

1: for all  $n \in N$  do
2:    $inj_n \leftarrow \operatorname{argmin}_{inj_n} \mathcal{L}^{trans}(\dots, inj_{n-1}^{k+1}, inj_n, inj_{n+1}^k, \dots)$  ▷ see (4.26a)
3: end for
4: for all  $l \in L$  do
5:    $f_l \leftarrow \operatorname{argmin}_{f_l} \mathcal{L}^{trans}(\dots, f_{l-1}^{k+1}, f_l, f_{l+1}^k, \dots)$  ▷ see (4.27a)
6: end for
7: for all  $n \in N$  do
8:    $\pi_n \leftarrow \pi_n + \rho_{trans} (inj_n - \sum_{l \in L_n} f_l)$  ▷ Update Lagrangian multipliers
9: end for

```

When determining the optimal nodal injection of a single node n at ADMM iteration k , the other nodal injection and flows are constant. Determining the optimal injection is done by finding the minimal point of the following quadratic function:

$$\min \underbrace{(-\lambda_n^k - \rho R_{nt} + \pi_n - \rho_{trans} \sum_{l \in L_n} f_l^k)}_{\text{linear coefficient}} inj_n + \underbrace{\left(\frac{\rho}{2} + \frac{\rho_{trans}}{2} \right)}_{\text{quadratic coefficient}} inj_n^2 \quad (4.26a)$$

Similarly, determining the optimal flow for a single transmission line $l = (n', n)$ at the ADMM iteration, the other flows and nodal injections are constant. Determining the optimal flow is done by finding the minimal point of the following quadratic function within certain flow limits:

$$\underbrace{(-\pi_{n'} + \pi_n - \rho_{trans}(inj_{n'}^{k+1} - \sum_{l' \in L_{n'} \setminus \{l\}} f_{l'}^k) + \rho_{trans}(inj_n^{k+1} - \sum_{l' \in L_n \setminus \{l\}} f_{l'}^k) \underline{f}_l}_{\text{linear coefficient}} + \underbrace{\rho_{trans}}_{\text{quadratic coefficient}} \underline{f}_l^2 \quad (4.27a)$$

subject to

$$\underline{f}_l \leq f_l \leq \overline{f}_l \quad (4.27b)$$

4.5.2 Our ADMM algorithm

When all the subproblems are convex, ADMM will converge to the optimal solution after some iterations¹. But since 1UC is non-convex, optimality or convergence are not guaranteed. This means that after a certain number of iterations the residual load is still significant indicating that the current solution is infeasible due to the violation of the demand coupling constraint.

To solve the nonconvergence, we iteratively increase the penalty coefficient ρ to force convergence and feasibility. In [54], it was shown that this helps to achieve faster convergence of convex problems. Figure 4.2 shows in red the convergence of the solution when 1UC is convex² and the nonconvergence (at least not after 1000 iterations) in blue of the non-convex problem. It also shows the convergence of the non-convex problem in orange when ρ is increased. As ρ grows to ∞ the constraint violation is encouraged to go to 0. We start with a small ρ and then iteratively increase it after m iterations. We found that the slower this process goes the better the heuristic solution becomes. The whole procedure is presented in Algorithm 6.

Here m is the number of iterations after we increase ρ , by multiplying ρ times α . Varying α and m gives us a way to increase and decrease the rate of convergence and therefore the total computation time but at the expense of solution quality.

The intuition is as follows, when solving the subproblems the individual generators, RES and storage units are encouraged to produce power at every time step by the Lagrangian multipliers (when positive) and encouraged to minimize the total residual by the quadratic penalty. Our ADMM algorithm could be interpreted as a greedy algorithm that first steers to the (sub)optimal solution by the

¹For the optimal Exchange this is guaranteed and for the Gauss Seidel variant this is probable [31], i.e. there are theoretical cases where it does not converge but experimentally there have been success. In our experiments with multiple convex UC instances the Gauss Seidel variant always converged to the optimal solution.

²We convexified the 1UC problem by removing the binary requirement on the commitment variables.

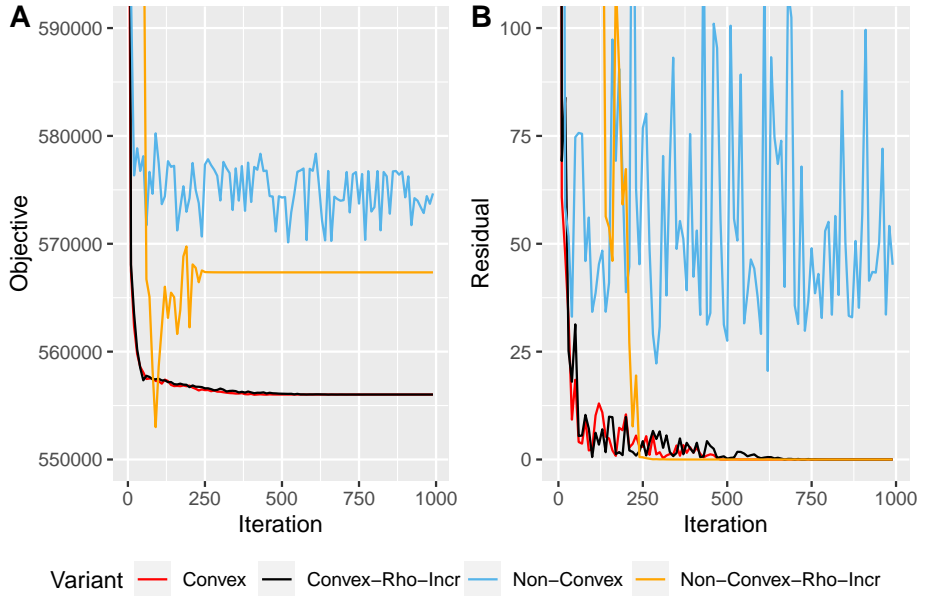


Figure 4.2: 1000 ADMM iterations on a convex and a non-convex UC instance with and without increasing ρ .

Algorithm 6 ADMM Increasing ρ

```

1:  $\rho \leftarrow$  initial  $\rho$ 
2: while  $\sum_{n \in N, t \in T} RD_{nt} > \epsilon \wedge k < \text{Max iterations}$  do
3:   for  $i \in \{1, \dots, m\}$  do
4:     Gauss Seidel ADMM Iteration
5:      $k \leftarrow k + 1$ 
6:   end for
7:    $\rho \leftarrow \alpha \rho$ 
8: end while

```

Lagrangian multipliers and then steers towards feasibility by increasing ρ . Theoretically not much is known about converges or the quality of the solution when applying ADMM to non-convex problems [9]. In the next section we will show experimentally that our proposed algorithm gives a fast feasible solution of good quality and scales well with the number of times steps.

4.6 Computational Experiments

Name	Quadratic Cost	Transmission	Storage	RES	Source
GA10	+	-	-	-	[25][42]
TAI38	+	-	-	-	[22]
RCUC50	+	-	-	-	[20]
GMLC73	-	-	-	+	[5]
A110	+	-	-	-	[37]
KOR140	+	-	-	-	[41][33]
OSTRO187	+	-	-	-	[38]
RCUC200	+	-	-	-	[20]
HUB223	-	-	-	+	[23]
CA426	-	-	-	+	[26]
FERC923	-	-	-	+	[26][28]
RTS26	+	+	-	-	[49][48]
RTS54	-	+	-	+	[23]
RTS96	-	+	-	-	[40]
DSET304	-	+	+	+	[24]

Table 4.1: Overview of the instances in the benchmark set. All instances have thermal generators with techno-economic characteristics but only some have a quadratic generation cost, a transmission system, storage or a renewable energy with availability factors. See [51] for more detail.

To test the efficiency of our proposed algorithms we have performed multiple experiments on 15 well-known benchmark instances³ found in the literature (Table 4.1) created by [51]. We solved the UC instances with our Gauss Seidel ADMM algorithm and with Gurobi with the presented MIL(Q)P formulation (4.1a) - (4.1r). Next, we compared the quality of the solutions and the computation times of these algorithms.

First, we experimented with different values of α , namely 1.01, 1.05, 1.1 or, 1.2. Due to the large number of experiments we needed to perform we chose to omit the instances with transmission. Note that as α increases that the computation time and number of iterations decreases. Finally, we performed more detailed

³<https://github.com/rogierhans/UCBenchmark>

experiments for the average value $\alpha = 1.1$. For the last experiments we also included the instances with transmission.

All experiments were repeated 10 times to account for the random order of updating the subproblems and the random initial Lagrange multipliers. We set the time horizon to 24, 48, \dots , 168 time steps. In all runs, ρ was initially set at 0.0001 and m at 1. If ρ was set lower or m higher then the solution quality is better but the algorithm takes more iterations to converge. In preliminary experiments we found that these parameters give a good trade-off between computation time and solution quality except for 1 instance which will be addressed in the next section. Both ADMM algorithms and Gurobi had a time limit of 1 hour.

Gurobi’s MIL(Q)P solver continuously finds heuristic upper bounds and lower bounds until the specified MIP-gap is reached. Our ADMM algorithm produces a single solution, which turned out to be feasible in all our experiments. To compare our ADMM algorithms to Gurobi, we ran the MIL(Q)P model with a MIP-gap of 0 and recorded the intermediate heuristic solutions along with a timestamp at which time they were found. We can then compare the computation times of our ADMM algorithm to the time that Gurobi needs to find a heuristic solution with at most the same value (see Figure 4.3).

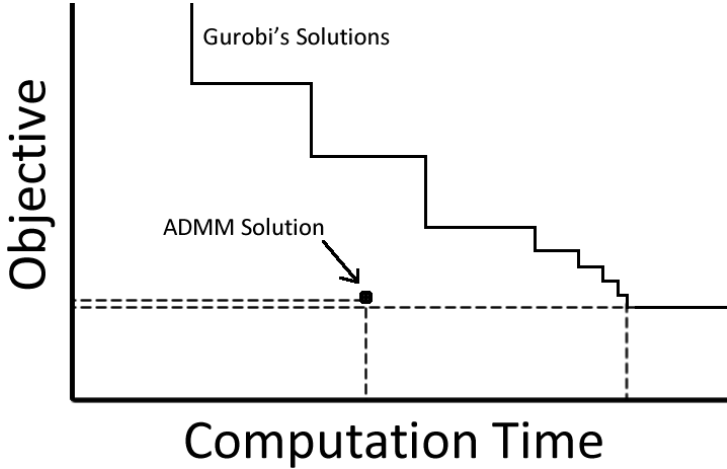


Figure 4.3: Comparing the ADMM solution to Gurobi.

4.6.1 Results

Figure 4.4 and Table 4.2 show the aggregated results for the instance without transmission and for varying values of α . We present the number of iterations, the gap with the optimal (or best known) solution, and the speed-up factor compared to solving the problem by Gurobi.

The figure shows that with increasing α the computation time and number of iterations decreases but the solution quality also gets worse. An α of 1.01 for example results in small gap indicating high quality solutions but it takes some

time for ρ to be of sufficient size that feasibility and convergence is forced. An α of 1.2 has the opposite effect, the algorithm converges fast, for one instance it was 5801.3 times faster for Gurobi to find a solution of similar quality. However, the average gap is rather large and it has outliers, for example, one solution for UC instance *KOR140* was 3.7% removed from the optimal value.

α	Iterations				Gap %				Speedup			
	avg	median	min	max	avg	median	min	max	avg	median	min	max
1.01	1229	1239	685	1696	0.07	0.03	0	0.9	29.6	6.0	0.1	271.9
1.05	287	292	154	393	0.09	0.04	0	0.9	108.4	19.4	0.5	1813.1
1.1	163	168	90	216	0.15	0.08	0	1.2	195.3	35.6	0.8	3109.4
1.2	104	100	60	255	0.54	0.13	0	3.7	310.4	43.3	1.0	5801.3

Table 4.2: Summary of the experiments with varying values of α for the 11 instances without transmission.

Figure 4.5, Figure 4.6 and Figure 4.7 show the results of the experiments where α was 1.1 in more detail. These results also include the four instances with transmission. Detailed results for α set at 1.01, 1.05 or 1.2 would show similar results but with a faster or slower running time and better or worse solution quality according to the trend presented in Table 4.2.

Figure 4.5 shows that for most instances the quality is good, for others it is a little worse but still close to optimal while for the instance *RTS54* the solutions are far away from the optimum. Even with those outliers on average the algorithm performs well, on average 0.08% away from the optimal value or the best known (Table 4.2). Moreover, if we choose a different value for α then these gaps would be a lot smaller. In some instances, the solutions produced by our algorithm was the best known. For the instances *TAI138*, *RCUC200*, *OSTRO178* and *KOR140* Gurobi could not find a better solution within the 1 hour time limit for time horizons > 48 .

Figure 4.6 presents the computation time increase of our ADMM Gauss Seidel Algorithm when the time horizon increases. For most instances it seems to grow linearly with the number of time steps while for others the growth seems slightly more than linear. Recall from Figure 4.4 that the number of iterations needed for convergence stays constant when the time horizons increases. However, the computation time of the underlying 1UC subproblem grows when the time horizon increases⁴.

Figure 4.7 shows how fast our algorithm can find a high quality solution compared to Gurobi. Speedup is defined as the ratio of the computation time of our algorithm and of Gurobi to find a similar solution. The computation time of Gurobi is set at the first time it finds a solution with an objective equal or better

⁴The time complexity of our 1UC algorithm was experimental established as linear [52] in the length of the time steps but also linear in the length of the minimum up and downtime. This is speculative but the superlinearity of *FERC923* could be explained by the fact that this instance has multiple units with minimum up and downtime of 168 hours. As the time horizon increases the computation time of the subproblem increases quadratically up until the point that the minimum up- and downtime is achieved but this needs more investigation in order to be confirmed.

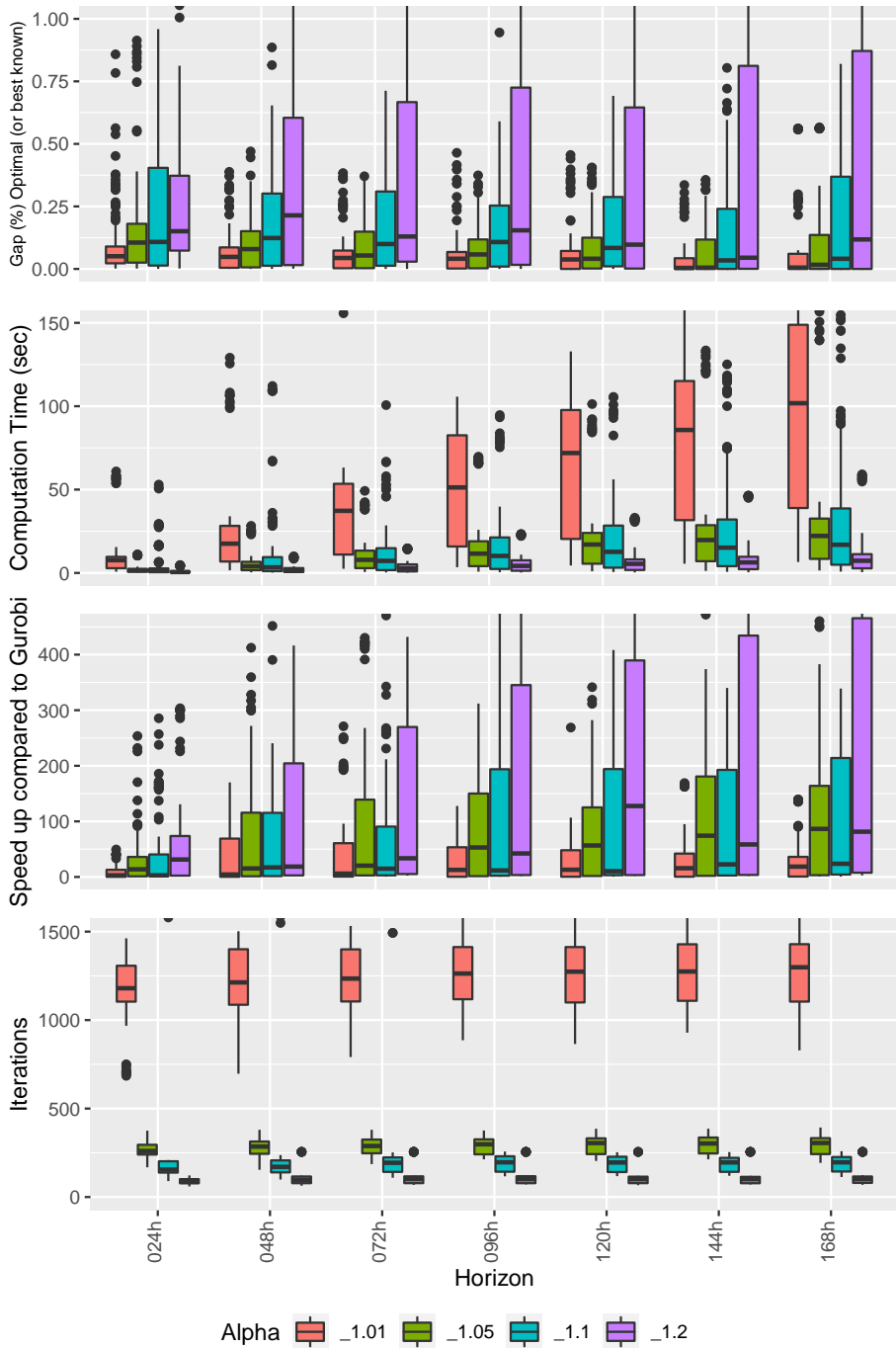


Figure 4.4: The gap, computation time, speed-up and the number of iterations for varying time horizons and values of α for the 11 instances without transmission.

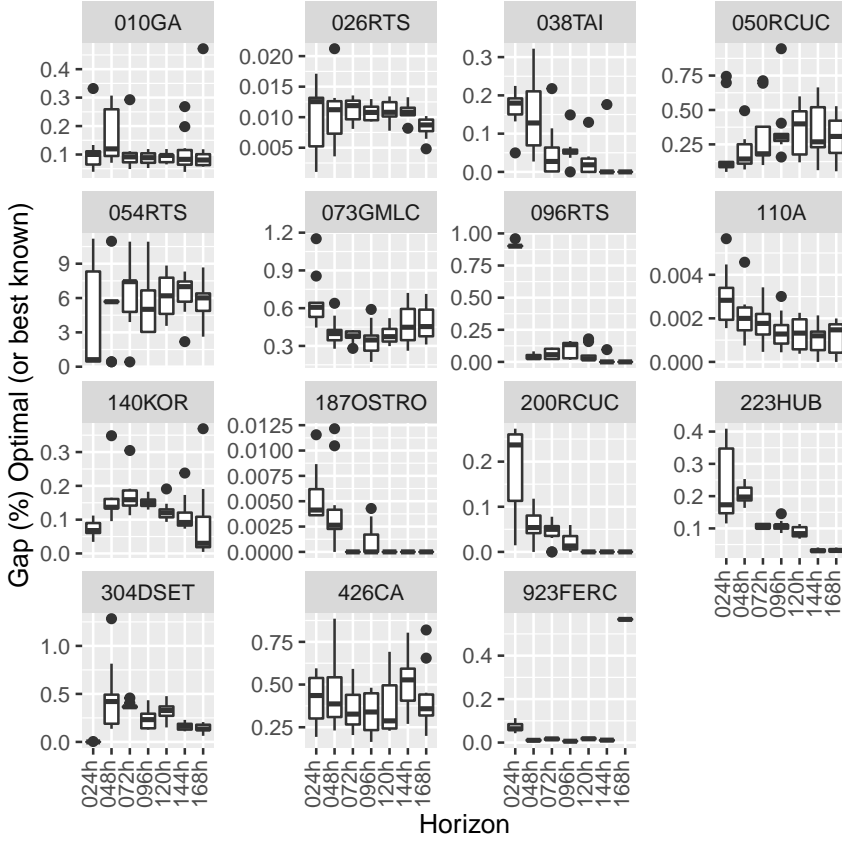


Figure 4.5: The gap of the objective value of the solution produced by our ADMM algorithm relative to the optimal or best known solution. For these experiments α was set at 1.1.

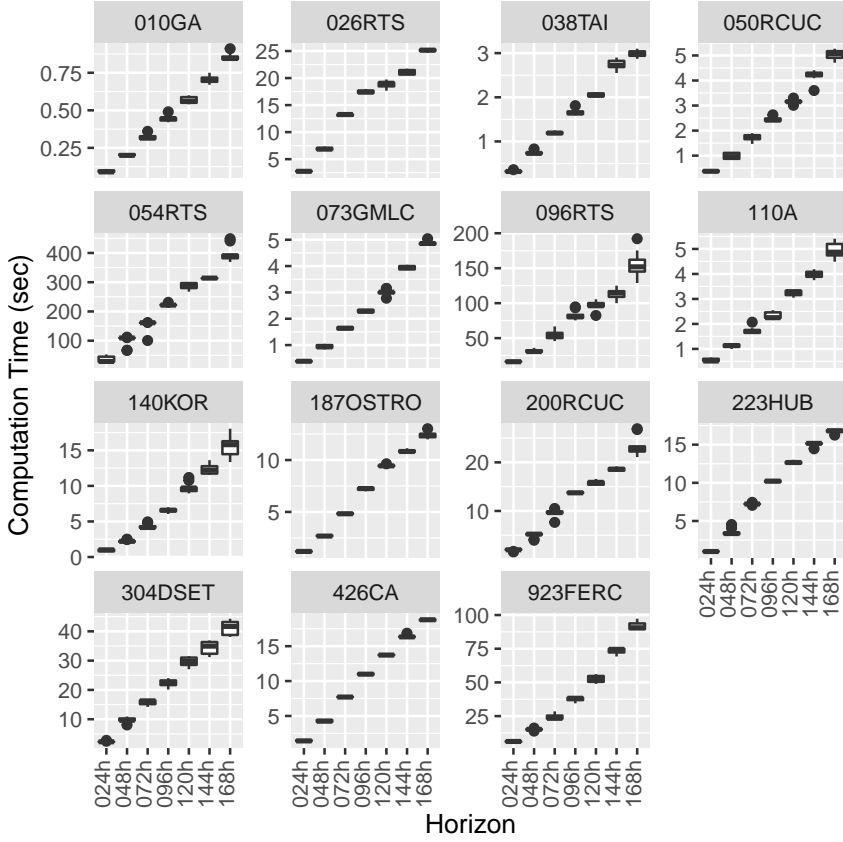


Figure 4.6: The computation time of all instances with a varying length of the time horizon. For these experiments α was set at 1.1 and for every instance and was repeated 10 times.

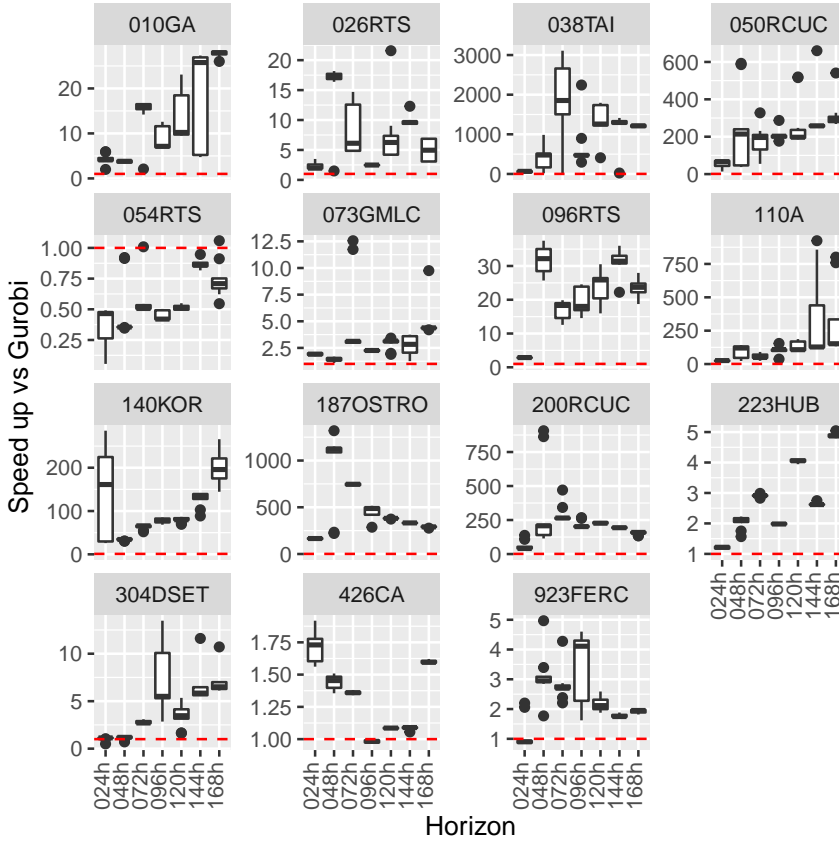


Figure 4.7: The speedup factor compared to the production of an equal solution by Gurobi. For these experiments α was set at 1.1 and for every instance in was repeated 10 times.

than our final objective. For most instances this ratio is large and indicates a large speedup. It seems that our algorithm performs much better than Gurobi on instances with quadratic generation cost. For some instances, especially the ones with linear generation cost, the ratio is smaller and even sometimes below 1. These are for example, *RTS54*, *GMLC73*, *HUB223*, *DSET304*, *CA426*, and *FERC923*. This highlights that for Gurobi solving a MILP is much faster than solving a MIQP. Still even for the instances with linear generation cost the speedup obtained by our algorithm is significant. Moreover, for some cases the speedup increases when the time horizon increases.

Because in the cases Gurobi could not find an equal or better solution within the time limit of 1 hour, we set the computation time to one hour, the real ratios for those instances are larger. Details are presented in Table 4.3. This also explains the seemingly downward trend of the instances *RCUC50*, *KOR140*, *OSTRO187* and *RCUC200*.

Time horizon	24h	48h	72h	96h	120h	148h	168h
GA10	1s	6s	35s	76s	171s	384s	551s
RTS26	59s	0.006%	0.029%	0.069%	0.1%	0.107%	0.111%
TAI38	0.516%	1.356%	1.746%	1.822%	1.922%	2.078%	2.166%
RCUC50	0.031%	0.106%	0.142%	0.177%	0.184%	0.202%	0.25%
RTS54	0.031%	0.084%	0.147%	0.21%	0.236%	0.296%	0.328%
GMLC73	3s	12s	188s	0.044%	0.08%	0.027%	0.078%
RTS96	1.601%	1.766%	1.835%	1.89%	1.921%	2.062%	2.536%
A110	0.001%	0.009%	0.012%	0.014%	0.015%	0.017%	0.02%
KOR140	0.64%	0.929%	1.026%	1.06%	1.109%	1.152%	1.206%
OSTRO187	0.029%	0.05%	0.063%	0.07%	0.115%	0.114%	0.337%
RCUC200	0.091%	0.163%	0.283%	0.308%	11.582%	20.613%	31.123%
HUB223	3s	0.001%	0.001%	0.002%	0.002%	0.001%	0.002%
DSET304	3s	1664s	0%	0%	0.031%	0.03%	0.063%
CA426	6s	62s	118s	197s	406s	615s	971s
FERC923	94s	96s	389s	378s	3601s	1043s	0.001%

Table 4.3: Computation time for Gurobi to find the optimal solution in seconds. If Gurobi failed to find the optimal solution within 1 hour computation time limit then the MIP-gap is shown.

As our ADMM algorithm with the setting of $\alpha = 1.1$ and $m = 1$ cannot find a good solution for the instance *RTS54*, we did additional experiments with α set at 1.05 and m at 5 and presented these much-improved results in Figure 4.8. However, Gurobi seems just to be very successful at solving this particular instance. But if we consider the speedup, as the time horizon increases, we see that our algorithm gets better relative to Gurobi. This suggests that if we would increase the time horizon even more then it favors our algorithm.

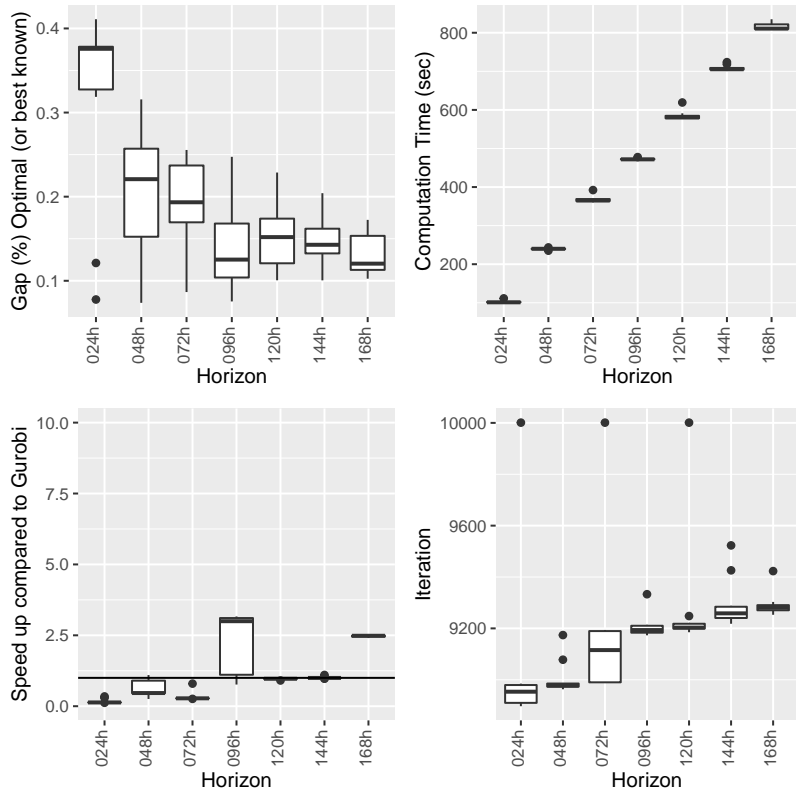


Figure 4.8: Additional experiments with the UC instance *RTS54* with $\alpha = 1.05$ and $m = 5$

4.7 Discussion

The results of our new ADMM algorithm for the UC looks promising in comparison with the competing state-of-the-art MIP approach. The advantages of the latter in general are that it can solve large programs, produce near optimal solutions, and can be easily extended. These three advantages also apply to our algorithm; the first two are demonstrated by our results and also our algorithm can easily be extended by implementing new subproblems as a QP or MIQP, as we have shown with the storage units. Additionally, our method has the advantage that solving subproblems can also be improved by using more specific sophisticated algorithms. For example, our 1UC algorithm on average was almost 400 times faster than the MIQP approach [52].

Moreover, our algorithm seems to scale well with the number of time steps. The previous section showed that the time complexity in practice was almost linear. When solving instances with long time horizons, as is needed in large scale power system modeling, our method can find a high-quality solution in seconds while the MIP solver could not find any good solution even after 1 hour.

For future work this algorithm can be extended or improved in the following way:

- Our algorithm currently does not include reserve requirements. Since reserve requirements are coupling constraints that includes decision variables from multiple components of the power system, we would need to relax these. Moreover, the addition of reserve requirements leads to additional Lagrange multipliers that we need to incorporate into our 1UC dynamic programming algorithm as was previously done by [30].
- Our algorithm currently does not include time dependent start-up cost for the 1UC subproblems but this could be easily incorporated [18].
- The subproblems can be modelled in a more complex but also more accurate way. For example, hydropower systems can be modelled in more detail [2], a more detailed transmission system (DC, AC) can be used, or a more robust transmission system that respect $n - 1$ criteria can be modelled [47]. Moreover, different power system assets such as demand response can easily be added as a subproblem.

4.8 Conclusion

In this chapter, we presented a new ADMM algorithm that heuristically solves UC. First, we transformed a standard UC formulation into an augmented Lagrangian formulation by relaxing the demand coupling constraints. Next, we solved this new problem with ADMM, an iterative algorithm. In each iteration we solved the subproblems induced by the relaxation of the demand coupling constraints. These subproblems were relatively easy to solve as there exist efficient solution methods for them. Especially, the use of our recently introduced fast algorithm for the

1UC subproblem enables many iterations in a limited time, so that ADMM can converge to a feasible solution of high quality.

Computational experiments on a large set of UC instances showed that our algorithm produces high quality solutions. For instances with linear generation cost it outperformed the state-of-the-art MILP formulation, especially with longer time horizons. For the instances with quadratic cost our algorithms solved those instances significantly faster compared to the state-of-the-art MIQP formulation. As the time complexity of our ADMM grew almost linearly with the number of time steps, it could find high-quality solutions in seconds for instances with long time horizons, while the MIP solver could not find any good solution within one hour.

Our ADMM, therefore, has potential to improve large scale power system modelling commonly based on UC with long time horizons, and planning of unit commitment in the short-term at high temporal resolution. Moreover, due to the decoupled nature of ADMM, the subproblem formulations can easily be adapted, for example to model elements of the power system in more detail or to improve the time complexity of solving the subproblems.

Bibliography

- [1] Saleh Y Abujarad, Mohammad Wazir Mustafa, and Jasrul Jamani Jamian. “Recent approaches of unit commitment in the presence of intermittent renewable energy resources: A review”. In: *Renewable and Sustainable Energy Reviews* 70 (2017), pp. 215–223.
- [2] Wim van Ackooij et al. “Large-scale unit commitment under uncertainty: an updated literature survey”. In: *Annals of Operations Research* (2018), pp. 1–75.
- [3] Semih Atakan, Guglielmo Lulli, and Suvrajeet Sen. “A state transition MIP formulation for the unit commitment problem”. In: *IEEE Transactions on Power Systems* 33.1 (2017), pp. 736–748.
- [4] CH Bannister and RJ Kaye. “A rapid method for optimization of linear systems with storage”. In: *Operations Research* 39.2 (1991), pp. 220–232.
- [5] Clayton Barrows et al. “The IEEE reliability test system: A proposed 2019 Update”. In: *IEEE Transactions on Power Systems* (2019).
- [6] J Batut and A Renaud. “Daily generation scheduling optimization with transmission constraints: a new class of algorithms”. In: *IEEE Transactions on Power Systems* 7.3 (1992), pp. 982–989.
- [7] A Borghetti et al. “Lagrangian relaxation and tabu search approaches for the unit commitment problem”. In: *2001 IEEE Porto Power Tech Proceedings (Cat. No. 01EX502)*. Vol. 3. IEEE. 2001, 7–pp.
- [8] Alberto Borghetti et al. “Lagrangian heuristics based on disaggregated bundle methods for hydrothermal unit commitment”. In: *IEEE Transactions on Power Systems* 18.1 (2003), pp. 313–323.
- [9] Stephen Boyd, Neal Parikh, and Eric Chu. *Distributed optimization and statistical learning via the alternating direction method of multipliers*. Now Publishers Inc, 2011.
- [10] Brian Carlson et al. “MISO unlocks billions in savings through the application of operations research for energy and ancillary services markets”. In: *Interfaces* 42.1 (2012), pp. 58–73.
- [11] Caihua Chen et al. “The direct extension of ADMM for multi-block convex minimization problems is not necessarily convergent”. In: *Mathematical Programming* 155.1-2 (2016), pp. 57–79.

- [12] Louis Dubost, Robert Gonzalez, and Claude Lemaréchal. “A primal-proximal heuristic applied to the French Unit-commitment problem”. In: *Mathematical programming* 104.1 (2005), pp. 129–151.
- [13] Wei Fan, Xiaohong Guan, and Qiaozhu Zhai. “A new method for unit commitment with ramping constraints”. In: *Electric Power Systems Research* 62.3 (2002), pp. 215–224.
- [14] Wei Fan, Xiaohong Guan, and Qiaozhu Zhai. “A new method for unit commitment with ramping constraints”. In: *Electric Power Systems Research* 62.3 (2002), pp. 215–224. ISSN: 0378-7796. DOI: [https://doi.org/10.1016/S0378-7796\(02\)00043-3](https://doi.org/10.1016/S0378-7796(02)00043-3). URL: <https://www.sciencedirect.com/science/article/pii/S0378779602000433>.
- [15] Mohammad Javad Feizollahi et al. “Large-scale decentralized unit commitment”. In: *International Journal of Electrical Power & Energy Systems* 73 (2015), pp. 97–106.
- [16] Stefan Feltenmark. “On optimization of power production”. In: (1997).
- [17] Stefan Feltenmark and Krzysztof C Kiwiel. “Dual applications of proximal bundle methods, including Lagrangian relaxation of nonconvex problems”. In: *SIAM Journal on Optimization* 10.3 (2000), pp. 697–721.
- [18] Antonio Frangioni and Claudio Gentile. “Solving nonlinear single-unit commitment problems with ramping constraints”. In: *Operations Research* 54.4 (2006), pp. 767–775.
- [19] Antonio Frangioni, Claudio Gentile, and Fabrizio Lacalandra. “Solving unit commitment problems with general ramp constraints”. In: *International Journal of Electrical Power & Energy Systems* 30.5 (2008), pp. 316–326.
- [20] Antonio Frangioni, Claudio Gentile, and Fabrizio Lacalandra. “Tighter approximated MILP formulations for unit commitment problems”. In: *IEEE Transactions on Power Systems* 24.1 (2009), pp. 105–113.
- [21] Xiaohong Guan, Qiaozhu Zhai, and Alex Papalexopoulos. “Optimization based methods for unit commitment: Lagrangian relaxation versus general mixed integer programming”. In: *Power Engineering Society General Meeting, 2003, IEEE*. Vol. 2. IEEE. 2003, pp. 1095–1100.
- [22] Kun-Yuan Huang, Hong-Tzer Yang, and Ching-Lien Huang. “A new thermal unit commitment approach using constraint logic programming”. In: *Power Industry Computer Applications., 1997. 20th International Conference on*. IEEE. 1997, pp. 176–185.
- [23] Matthias Huber and Matthias Silbernagl. “Modeling start-up times in unit commitment by limiting temperature increase and heating”. In: *European Energy Market (EEM), 2015 12th International Conference on the*. IEEE. 2015, pp. 1–5.
- [24] Konstantinos Kavvadias et al. *Integrated modelling of future EU power and heat systems-The Dispa-SET v2. 2 open-source model*. Tech. rep. European Commission, 2018.

- [25] Spyros A Kazarlis, AG Bakirtzis, and Vassilios Petridis. “A genetic algorithm solution to the unit commitment problem”. In: *IEEE transactions on power systems* 11.1 (1996), pp. 83–92.
- [26] Bernard Knueven, James Ostrowski, and Jean Paul Watson. “On mixed integer programming formulations for the unit commitment problem”. In: *E-print, Department of Industrial and Systems Engineering University of Tennessee, Knoxville, TN 37996* (2018).
- [27] Bernard Knueven, James Ostrowski, and Jean-Paul Watson. “A novel matching formulation for startup costs in unit commitment”. In: *Mathematical Programming Computation* (2020), pp. 1–24.
- [28] Eric Krall, Michael Higgins, and Richard P O’Neill. “RTO unit commitment test system”. In: ().
- [29] Matt Kraning et al. *Dynamic network energy management via proximal message passing*. Citeseer, 2014.
- [30] Zhigang Li et al. “Dynamic economic dispatch with spinning reserve constraints considering wind power integration”. In: *2013 IEEE Power & Energy Society General Meeting*. IEEE. 2013, pp. 1–5.
- [31] Lanchao Liu and Zhu Han. “Multi-block ADMM for big data optimization in smart grid”. In: *2015 International Conference on Computing, Networking and Communications (ICNC)*. IEEE. 2015, pp. 556–561.
- [32] Alexander C Melhorn et al. “Validating unit commitment models: A case for benchmark test systems”. In: *Power and Energy Society General Meeting (PESGM), 2016*. IEEE. 2016, pp. 1–5.
- [33] Saeed Moradi et al. “A semi-analytical non-iterative primary approach based on priority list to solve unit commitment problem”. In: *Energy* 88 (2015), pp. 244–259.
- [34] Germán Morales-España, Jesus M Latorre, and Andres Ramos. “Tight and compact MILP formulation of start-up and shut-down ramping in unit commitment”. In: *IEEE Transactions on Power Systems* 28.2 (2013), pp. 1288–1296.
- [35] Richard P O’Neill, Thomas Dautel, and Eric Krall. “Recent ISO software enhancements and future software and modeling plans”. In: *Federal Energy Regulatory Commission, Tech. Rep* (2011).
- [36] RP O’Neill. “It’s getting better all the time (with mixed integer programming)”. In: *HEPG Forty-Ninth Plenary Session* 16 (2007), p. 49.
- [37] SO Orero and MR Irving. “Large scale unit commitment using a hybrid genetic algorithm”. In: *International Journal of Electrical Power & Energy Systems* 19.1 (1997), pp. 45–55.
- [38] James Ostrowski, Miguel F Anjos, and Anthony Vannelli. “Tight mixed integer linear programming formulations for the unit commitment problem”. In: *IEEE Transactions on Power Systems* 27.1 (2012), pp. 39–46.

- [39] Narayana Prasad Padhy. “Unit commitment-a bibliographical survey”. In: *IEEE Transactions on power systems* 19.2 (2004), pp. 1196–1205.
- [40] Hrvoje Pandzic et al. *Unit commitment under uncertainty-GAMS models. Library of the Renewable Energy Analysis Lab (REAL), University of Washington, Seattle, USA.*
- [41] Jong-Bae Park et al. “An improved particle swarm optimization for nonconvex economic dispatch problems”. In: *IEEE Transactions on Power Systems* 25.1 (2010), pp. 156–166.
- [42] Dewan Fayzur Rahman, Ana Viana, and Joao Pedro Pedroso. “Metaheuristic search based methods for unit commitment”. In: *International Journal of Electrical Power & Energy Systems* 59 (2014), pp. 14–22.
- [43] Paritosh Ramanan et al. “Asynchronous decentralized framework for unit commitment in power systems”. In: *Procedia Computer Science* 108 (2017), pp. 665–674.
- [44] Farnaz Safdarian, Ali Mohammadi, and Amin Kargarian. “Temporal decomposition for security-constrained unit commitment”. In: *IEEE Transactions on Power Systems* 35.3 (2019), pp. 1834–1845.
- [45] B Saravanan et al. “A solution to the unit commitment problem—a review”. In: *Frontiers in Energy* 7.2 (2013), pp. 223–236.
- [46] Raouia Taktak and Claudia D’Ambrosio. “An overview on mathematical programming approaches for the deterministic unit commitment problem in hydro valleys”. In: *Energy Systems* 8.1 (2017), pp. 57–79.
- [47] Kenneth Van den Bergh, Erik Delarue, and William D’haeseleer. “DC power flow in unit commitment models”. In: *TMF Working Paper-Energy and Environment, Tech. Rep.* (2014).
- [48] Chunyan Wang and SM Shahidehpour. “Effects of ramp-rate limits on unit commitment and economic dispatch”. In: *IEEE Transactions on Power Systems* 8.3 (1993), pp. 1341–1350.
- [49] SJ Wang et al. “Short-term generation scheduling with transmission and environmental constraints using an augmented Lagrangian relaxation”. In: *IEEE Transactions on Power Systems* 10.3 (1995), pp. 1294–1301.
- [50] Manuel Welsch et al. “Incorporating flexibility requirements into long-term energy system models—A case study on high levels of renewable electricity penetration in Ireland”. In: *Applied Energy* 135 (2014), pp. 600–615.
- [51] R.H. Wuijts, M. van den Akker, and M. van den Broek. “Effect of modelling choices in the unit commitment problem”. In: *Energy Systems* (2023). DOI: 10.1007/s12667-023-00564-5.
- [52] Rogier Hans Wuijts, Marjan van den Akker, and Machteld van den Broek. “An improved algorithm for single-unit commitment with ramping limits”. In: *Electric Power Systems Research* 190 (2021), p. 106720.

- [53] Alinson S Xavier, Feng Qiu, and Santanu S Dey. “Decomposable formulation of transmission constraints for decentralized power systems optimization”. In: *arXiv preprint arXiv:2001.07771* (2020).
- [54] Yi Xu et al. “No More Fixed Penalty Parameter in ADMM: Faster Convergence with New Adaptive Penalization”. In: *Advances in Neural Information Processing Systems*. 2017, pp. 1267–1277.
- [55] Houzhong Yan et al. “Scheduling of hydrothermal power systems”. In: *IEEE Transactions on power Systems* 8.3 (1993), pp. 1358–1365.
- [56] Yu Yang et al. “A Survey of ADMM Variants for Distributed Optimization: Problems, Algorithms and Features”. In: *arXiv preprint arXiv:2208.03700* (2022).
- [57] Chen Zhang, Linfeng Yang, and Jinbao Jian. “Two-stage fully distributed approach for unit commitment with consensus ADMM”. In: *Electric Power Systems Research* 181 (2020), p. 106180.
- [58] Shaobo Zhang and Kory W Hedman. “A computational comparison of PTDF-based and phase-angle-based formulations of network constraints in distributed unit commitment”. In: *Energy Systems* (2021), pp. 1–26.

Chapter 5

Pitfalls of Power Systems Modelling Metrics

Published as:

Pitfalls of Power Systems Modelling Metrics.

Rogier Hans Wuijts, Marjan van den Akker & Machteld van den Broek
18th International Conference on the European Energy Market (2022)

5.1 Abstract

In power system modelling the unit commitment problem is used to simulate the wholesale electricity market. A solution to the unit commitment problem is a least-cost schedule that contains information regarding the capacity factors of each generator, the total CO₂ emissions, and unserved energy per hour. However, since there might be a large variety of (sub)-optimal solutions, these characteristics might be arbitrary and conclusions about them may be presumptuous. In this chapter, we illustrate this by running multiple experiments on a future European power system. Each scenario was run multiple times by adding additional terms to the objective function such as the minimization and maximization of generator capacity factors, carbon emissions, and loss of load hours. The results showed that schedules can be equivalent in terms of cost, but that relative capacity factors, emissions, and loss of load hours could differ by large factors.

5.2 Introduction

The unit commitment and economic dispatch (UC) problem is commonly used by academic researchers, Transmission and Distribution System Operators, energy companies, and policy makers to evaluate the resource adequacy of current and future electricity generation portfolios, and to support investment and operational decision-making ([12, 13, 14, 2, 6, 5]). As a result of the energy transition and increasing reliance on variable renewable energy sources, the need for robust power system modelling is becoming increasingly important.

A UC model finds the least-cost schedule for a generation portfolio under a set of hard and soft constraints. Outputs provide specific information regarding the schedule such as capacity factors of each generator, CO₂ emissions, and unserved energy per hour. However, conclusions about these characteristics are often presumptuous. This is caused by the fact that they are not explicitly included in the objective function, which implies that they can take an arbitrary value so long as they do not violate any hard constraints, or negatively influence the objective function.

For example, many countries use the Loss of Load Expectation (LOLE) metric, i.e., the average number of hours unserved energy occurred in a year based on a Monte Carlo simulation over many years to assess the system adequacy. The LOLE is one of the two key reliability indicators which must be calculated in the European Union (EU) as part of the European Resource Adequacy Assessment (ERAA) [4]. A second indicator is expected Energy Not Served (ENS), which represents the energy which is not supplied over a given period due to insufficient capacity resources to meet the demand. LOLE is an important adequacy indicator as any EU member state wishing to implement a capacity mechanism to safeguard security of supply can only do so if the ERAA shows that the national LOLE is above a specified reliability standard [1, 3], calculated according to a strict methodology but typically in the range of 3 - 8 h a year [4].

When a UC problem is solved to simulate the operation of the current European power system, the resulting power generation schedule has minimal generation

cost and minimal amount of unserved energy and specific hours in which loss of load occurs. These specific hours, however, might be arbitrary. For example, one schedule with all unserved energy in a single time step may cost as much as another schedule with the unserved energy distributed over several time steps [8]. However, these two schedules will have a different impact on the LOLE metric which in turn could imply divergent policy decisions.

Which (sub)-optimal solution you get out of an optimization can depend on random choices a solver or algorithm makes, the fact that an algorithm produces a heuristic solution, the stopping criteria of sub optimality, how solvers are configured, how the input data is structured, and much more. Two real-world examples we experienced of this are as follows:

- When adding valid inequalities to our Mixed Integer Linear Programming UC model to guide the solver by improving the relaxation bound, the optimal solution produced by the solver gave back very different capacity factors (Chapter 2). However, these valid inequalities were not expected to change the solution as they do not reduce the search space of the solution.
- The standard method of solving a LP in Gurobi is by concurrently running multiple algorithms such as Simplex, Dual Simplex, and the Barrier Method. When one of these methods finds a solution, the process is stopped, and the solution found by that method is returned. However, the other algorithms would have also resulted in an optimal solution. Thus, multiple runs of the same scenario on the same computer with the same program may randomly result in different solutions ([9] p. 748) with, for example, different LOLEs depending on the fastest algorithm in each run.

These are just a few examples of when the modelling metrics of a solution can be arbitrarily changed, and potentially lead analysts to draw non-robust conclusions from the results.

In this chapter, we illustrate this arbitrary effect by running multiple experiments on three scenarios of the European power system in the years 2030 and 2040 [7]. For these scenarios we ran the UC problem to find least-cost schedules that meet the electricity demand with unserved energy rated at a loss of load value of 10,000 Euro/MWh. Each scenario was run multiple times by adding additional objectives such as the minimization and maximization of capacity factors of generators, emissions and loss of load hours, while keeping the total dispatch costs equivalent. In this way, we demonstrate the maximum and minimum values of these indicators which could technically arise from the UC model, and hence the possible range of arbitrariness in the indicator results.

5.3 Methods

We want to test how arbitrary important metrics of power system modelling are. The metrics we investigate are Loss of Load Hours (LOLH), capacity factors (CF) of generators and total CO2 emissions. First, we will give a definition for every metric. Then, we will describe the power system instances on which we run the UC.

Finally, we will describe how we maximize the model metric differences between solutions of equivalent cost to analyse the different possible solutions.

5.3.1 Metrics

Loss of load occurs when generation capacity is insufficient in a given hour to meet the demand. This can be a result of insufficient generation on the supply side (e.g. due to power plant outage, or a shortage in renewable generation), or insufficient flexibility on the demand side. The metric of Loss of Load Hours (LOLH) is relevant to determine the system adequacy of a certain power system. The relationship with LOLE is that LOLE is the expected LOLH in a year which is the result of a Monte Carlo simulation over many years. Let's define a loss of load hours, $LOLH_{nt}$, as a binary variable that is 1 when is the Energy Not Served, ENS_{nt} , is above zero:

$$LOLH_{nt} = \begin{cases} 1 & ENS_{nt} > 0 \\ 0 & \text{otherwise} \end{cases} \quad (5.1)$$

is the demand of node n and time t that cannot be provided. Every generator has a capacity factor that indicates how much a generator is used. The capacity factor is 100%, if the generator is always producing at maximum capacity and it is lower otherwise. This metric is relevant for studies looking at the economic viability of power plants, which depends on the number of hours they run. The capacity factor of generator g is defined as:

$$CF_g = \frac{\sum_{t \in T} p_{gt}}{|T| \bar{P}_g}$$

where p_{gt} is the power production of generator g at time t . $|T|$ is the number of timesteps and \bar{P}_g is the maximum generation of generator g .

Many conventional thermal generators produce CO_2 when burning fossil fuels to generate power. Due to the negative greenhouse effect of CO_2 it is often of interest to investigate how much CO_2 is likely to result from electricity generation. The total CO_2 produced by a UC schedule is defined as:

$$\text{Total } CO_2 = \sum_{g \in G, t \in T} FCP_g u_{gt} + VCP_g p_{gt}$$

where p_{gt} is the power production of generator g at time t and FCP_g is the fixed and VCP_g is the variable CO_2 production of generator g .

5.3.2 Unit Commitment Instances

The UC instances we performed the experiments on are based on future European power system scenarios of the ‘‘TYNDP2020’’ created by the European Network of Transmission System Operators for Electricity (ENTSO-E) [7]. These scenarios

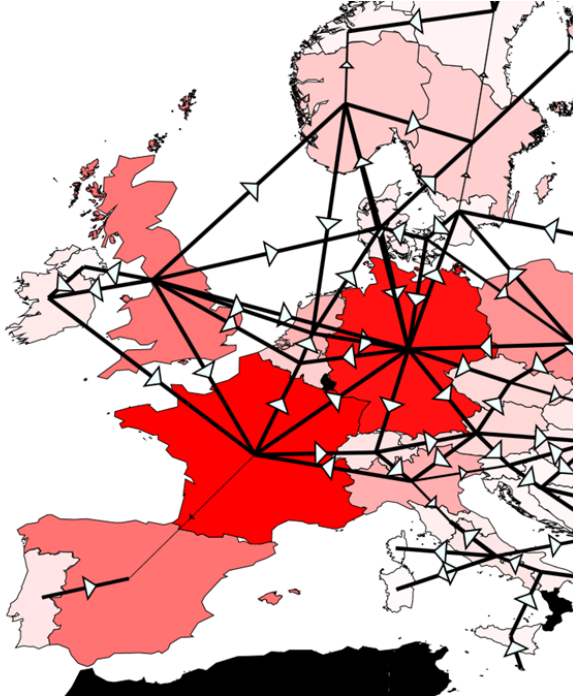


Figure 5.1: The bidding zones regions modelled in the TYNDP2020 scenarios

consist of 55 ‘nodes’ corresponding roughly to the current bidding zone configuration of Europe. In practice, most bidding zones correspond to a single country (Figure 5.1) but some countries such as Sweden and Italy are divided into multiple bidding zones. Table 5.1 gives an overview of the total generation capacity for each scenario. For our study we used six scenarios of the TYNDP2020 study, namely the three different pathways of National Trends (NT), Global Ambition (GA) and Distributed Energy (DE) for target years 2030 and 2040. These scenarios created by ENTSO provide insights into the possible energy system of the future and the effects of changes in supply and demand on the energy system [7].

In our experiments we used the climate years from 1950 till 2019 to simulate the variation in renewable energy generation. We used historic renewable energy availability factors for PV, onshore and offshore wind based on the ERA5 data set [10]. For the hydro inflow data, we used the scaled inflow data from another European power system study [12] which were obtained from the RESTORE 2050 project [11]. For our study we used a time horizon of 72 hours sliced from the yearly demand and renewable patterns of the scenarios. The start of these 72 hours periods were at the start of hour 0, 2400, 4800 and 7200 of the climate years 1950 to 2019 and from one of the 6 TYNDP scenarios. In total we used $4 \cdot 60 \cdot 6 = 1440$ UC instances of 72 timesteps. For the other experiments with CF and CO2 we used a smaller subset. Here we only looked at the years 1950, 1960, ..., 2010 and in total we used $4 \cdot 7 \cdot 6 = 168$ UC instances of 72 timesteps. The

Scenario	Capacity (GW)			DSR (GW)	Demand (TWh)
	Thermal	Storage	RES		
GA2030	576	125	794	38	4038
GA2040	544	148	1089	44	4296
DE2030	567	130	944	38	4214
DE2040	535	221	1480	44	5075
NT2030	587	121	818	26	3968
NT2040	554	170	1093	31	4402

Table 5.1: Summary of the capacity resources scenarios from TYNDP [7]

difference in the number of instances is because we expect not every UC instance to have ENS, leading to trivial results, but we do expect that every instance has some CFs and CO₂ emissions.

5.3.3 Procedure

We want to maximise the difference of a specific model metric between two solutions with equivalent costs. In order to calculate the maximal difference, we first find the optimal solution of the UC problem. This solution has a certain objective value (e.g., a total cost of $1 \cdot 10^8$) and a metric value (e.g., 2 hours LOLH). From this original solution, we want to find other solutions with the same objective function value, but with different values for a particular metric, e.g., a solution with a total cost of $1 \cdot 10^8$ but with 10 LOLH. In order to see the range of potential solutions which give rise to an equivalent objective function value but different metric values, we find a minimum and maximum metric using optimization. UC can be formulated compactly as follows (The full and precise formulation of the UC is in the appendix (8.17) - (8.37)):

$$\min f(x) \tag{5.2}$$

$$Ax = b \tag{5.3}$$

where x is the UC solution that contain all the relevant information that satisfies all the constraints, $Ax = b$. The objective $f(x)$ includes the generation cost, CO₂ emission certificate cost, start-up cost and system wide costs such as value of lost load multiplied by the ENS.

Suppose that the optimal solution of the optimization problem is x^* . Let g be our metric function that we want to minimize and maximize in order to find the largest difference. The following program gives an equivalent solution in terms of cost but minimizes the modeling metric g :

$$\min g(x) \tag{5.4}$$

$$Ax = b \tag{5.5}$$

$$f(x) \leq \alpha f(x^*) \tag{5.6}$$

if α is set to 1 then the solution to this problem has optimal cost. If $\alpha = 1.001$ then the solution is within 0.1% of optimality.

In this chapter we want to focus on the three metrics LOLH, CF and CO₂. For each of the three metrics we performed various experiments. For the LOLH experiments we kept α at 1, i.e. we only looked at optimal solutions, but at three levels of detail of the UC problem. The first level is a simplified *ENS-Model*, where the original objective is minimizing the total ENS and not the production cost of generators. Here we do not include flexibility constraints such as minimum up and down time and ramping limits. The second level is the *Cost-Model* in which production cost are minimized, but still without flexibility constraints. In the third level, the *Full-Model*, we take all the cost and flexibility constraints into account. Here, we also included a wheeling charge on the transmission lines, which implies that exporting and importing power between bidding zones has a small cost.

For the CF experiments we set $\alpha \in \{1.001, 1.005, 1.01\}$ and minimized and maximized the capacity factor of Gas, Coal and Nuclear-powered electrical generators. For the CO₂ experiments we set $\alpha \in \{1.001, 1.005, 1.01\}$ and minimized and maximized the total CO₂ produced by the power system. Table 8.6 in the appendix 8.4 presents the precise setup of the experiments, the definition of the original objective function f and the model metric function g we want to minimize or maximize.

5.4 Results

5.4.1 Loss of Load Hours

	Minimizing		Original		Maximizing		Factor difference		
	Avg	σ	Avg	σ	Avg	σ	Avg	σ	max
ENS-Model	16.0	11.4	27.1	14.8	45.3	13.4	5.1	5.4	38.0
Cost-Model	17.7	13.5	27.1	14.4	40.2	16.4	3.4	2.6	19.5
Full-Model	28.7	20.2	34.8	17.0	43.3	17.2	2.3	1.7	11.1

Table 5.2: Summary of the LOLH metric for the ENS-, Cost- and Full-Model

The results of our experiments with minimising and maximising the LOLH are presented in Table 5.2, Figure 5.2 and Figure 5.3, and additional figures in the appendix 8.4.

Table 5.2 presents the average LOLH of the three different models. The second of the column is the LOLH from the initial solution when we minimize the objective f . The first and third column are the minimized and maximised LOLH. Note that the original LOLH falls somewhere between the minimized and maximized variant. For some UC instances there was no ENS in any region or at any timestep. We removed those instances from our figures and tables.

For the ENS-Model the total difference of the average LOLH is a factor of $\frac{45.3}{16} \approx 2.8$, for the *Cost-Model* it is ≈ 2.3 and for the *Full-Model* this is a factor of ≈ 1.5 . The difference with single UC instances is much higher. If we look at individual instances, we can see that the average factor between the minimized and maximized LOLH is 5.1 for the *ENS-Model* and for the *Full-Model*. Furthermore,

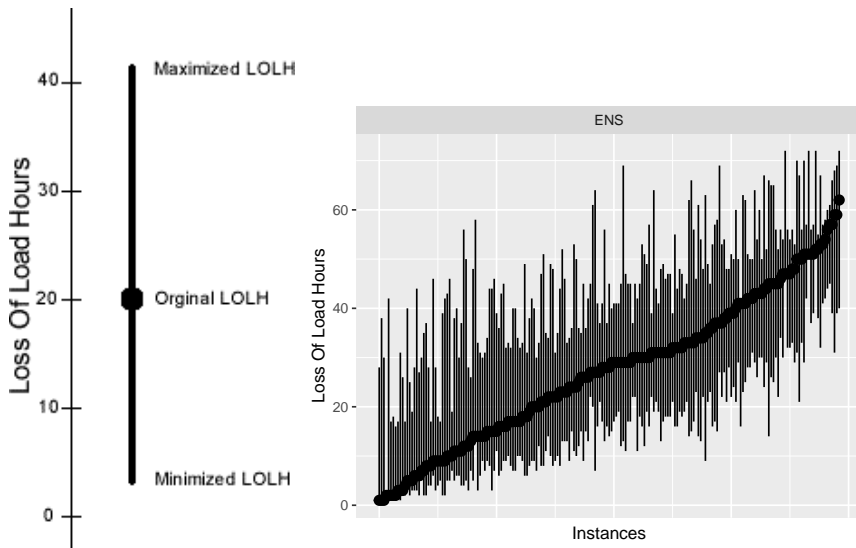


Figure 5.2: The LOLH for all instances, ordered by the LOLH, for the ENS-Model. The middle circle is the LOLH of the original optimization. The upper and lower value are the minimized and maximized LOLH. The whole range are the possible values of LOLH an equivalent solution can take on.

some specific runs have even more extreme differences such as one case with the *ENS-Model* where the maximum LOLH was 38 higher than the minimum one.

The difference of the LOLH in the different models of individual runs becomes more apparent in Figure 5.2. It shows the individual model runs (black dots) that had ENS sorted on the original LOLH. The black bar around the dot shows the minimized and maximised LOLH. This black bar can be interpreted as the possible LOLH that could come out of the model given the same ENS.

For the experiments with the *Cost-Model* and the *Full-Model* shows a similar pattern as Figure 5.2 but with one major difference (Figure 8.9 in the appendix). The black bar representing the possible range of LOLH given the same ENS and the same cost is a little smaller for the *Cost-Model* and even smaller for the *Full-Model*. This makes sense, as with more detail the model has less leeway for a solution to change while the objective function stays the same. It is to be expected that if we added even more detail to the Full-Model that this range would become even smaller.

Figure 5.2 shows the cause of such a discrepancy of LOLH between UC solutions. All the solutions have exactly the same ENS between the minimization and maximization run and the same primary objective function f . However, the total LOLH is different. When the LOLH is minimized the ENS is concentrated in a single node but when the LOLH is maximized it is spread out as evenly as possible between nodes and timesteps.

For the UC instance used in Figure 5.2, we can see that the amount of leeway

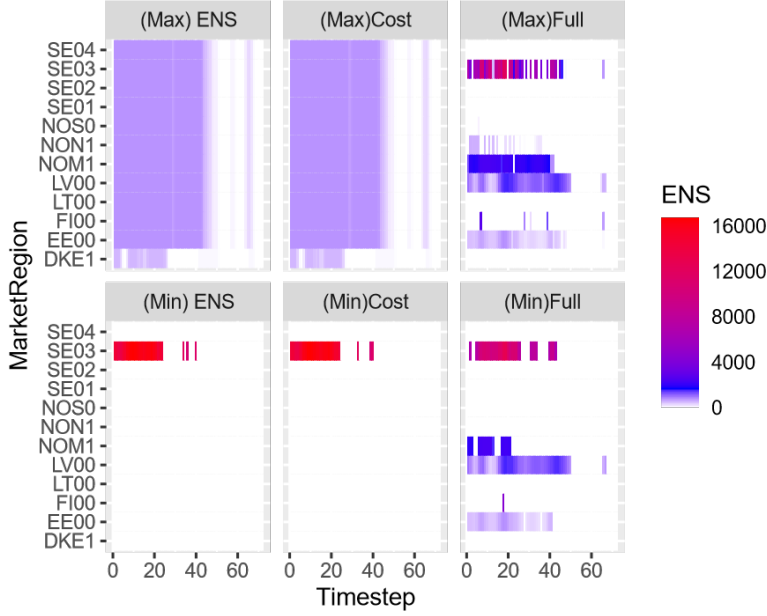


Figure 5.3: The difference in solutions where we maximize (upper figures) and minimize (lower figures) LOLH with the ENS-, Cost- and Full-Model

in the solution space is almost the same for the *ENS-Model* and the *Cost-Model* but that the *Full-Model* has significantly less ability to spread out the ENS.

5.4.2 Capacity Factor

The results of our experiments with maximizing the difference in capacity factors are summarized in Table 5.3, Figure 5.4, and figures in the appendix 8.4.

Table 5.3 shows that equivalent solutions for within a margin of 1% of the optimum on average can have a Coal CF that is either 4.3% or 23.0%, a factor 5.3 different. In some cases, the CF of coal became 0% when minimizing this metric resulting (see Figure 4).

For Gas the difference is still high but slightly lower than the coal generators. It seems that nuclear in these instances is the least flexible and on average could be a factor of 1.2 higher. If we reduce α to be closer to optimality, we can see that the difference reduces for all generator types. However, for gas and coal this difference at 0.1% removed from optimum is still relatively high. Figure 8.10 in the appendix shows the differences for all instances and all generator types. The figure shows that on average the difference is high but that also a lot of outliers exist where the difference is even higher. Even at 0.1% removed from optimum this difference sometimes is between zero production and some production for the coal-fired generators.

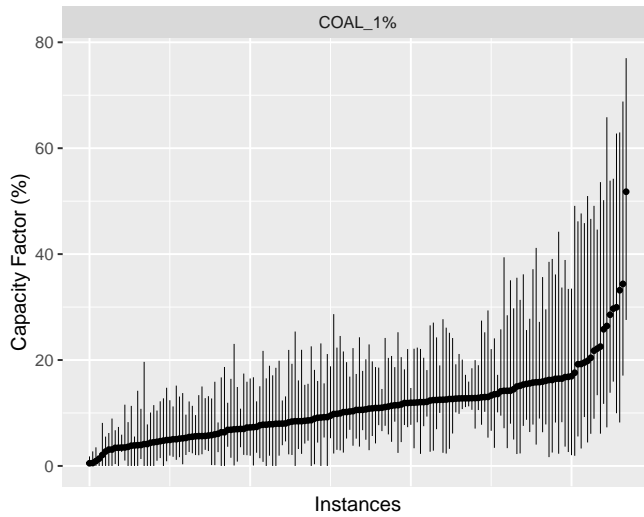


Figure 5.4: The CFs for all instances, ordered by the original total CF, for the solutions within 1% of the optimum.

5.4.3 CO₂ Emissions

The results of our experiments with maximizing the difference in CO₂ emissions are summarized in Table 5.4 and Figure 5.5. Table 5.4 shows that equivalent solutions within a margin of 1% of the optimum on average are a factor of 1.4 different and this factor can be as high as 2.5.

Figure 8.11 in the appendix shows the different percentages removed from optimum. The difference of total CO₂ is almost negligible when the solution is 0.1% removed from optimum. When LOLH, CF and CO₂ are compared, we can see that the difference in the CO₂ metric are much lower than those of the LOLH and CF metric. This difference might be attributed to the fact that the CO₂ is a part of the objective function as there is a tax on CO₂ emissions.

5.5 Discussion

In the previous section we showed the difference in the modeling metrics, LOLH, CF and CO₂ for equivalent solutions that are close or equal to the optimal solution. The way we maximised those differences with optimization is not something you would normally do in power system modelling analysis, but it does show the maximal error solutions produced by these methods. The next question that might come up is what the chance is, when running the model, one might get one solution or the other. The answer is that this is arbitrary. Or to be more specific: since the solutions have equivalent objective function values, it is equally valid for any solver or algorithm to produce either solution. Moreover, it would be an unintended consequence if they would prefer one solution over the other. If it was

	α	Minimizing		Original		Maximizing		Factor difference		
		Avg	σ	Avg	σ	Avg	σ	Avg	σ	max
Gas	0.001	8.3	6.0	9.6	6.8	10.8	7.5	1.7	1.8	21.0
	0.005	6.2	4.8	9.6	6.8	12.3	8.1	4.6	9.4	83.5
	0.01	4.9	4.0	9.6	6.8	13.6	8.7	-	-	-
Coal	0.001	8.5	5.6	11.1	6.9	14.2	8.7	-	-	-
	0.005	5.9	4.9	11.1	6.9	19.5	11.6	-	-	-
	0.01	4.3	4.1	11.1	6.9	23.0	13.7	-	-	-
Nuc	0.001	64.1	19.2	64.9	19.3	65.8	19.3	1	0	1.2
	0.005	62.6	19.1	64.9	19.3	68.0	19.4	1.1	0.1	1.9
	0.01	61.2	19.1	64.9	19.3	70.5	19.7	1.2	0.2	2.7

Table 5.3: Summary of the experiments with capacity factor

	α	Minimizing		Original		Maximizing		Factor difference		
		Avg	σ	Avg	σ	Avg	σ	Avg	σ	max
CO ₂	0.001	1.99	1.06	2.08	1.11	2.18	1.16	1.1	0.1	1.5
	0.005	1.88	1.02	2.08	1.11	2.35	1.26	1.3	0.2	2.1
	0.01	1.79	0.98	2.08	1.11	2.47	1.34	1.4	0.2	2.5

Table 5.4: Summary of the experiments with CO₂

intended, then it should be explicitly modeled.

In this chapter we showed that we could minimize the spread of LOLH in a more detailed model. The takeaway, however, from this chapter is that more detail should not be added to avoid these arbitrariness in these metrics but to be conscious and careful when using any metric that is not explicitly optimized. These metrics are secondary characteristics of the solution, and they are not the goal and therefore should not be used as the main subject of analysis of these solutions. The analysis might be better on the objective itself. For example, the total ENS as a metric for adequacy is more robust than LOLE. ENS is explicitly modeled in the objective with a high coefficient, the value of lost load, and therefore (sub)optimal solutions have the same or similar ENS.

5.6 Conclusion

In this chapter we investigated the arbitrariness of important modelling metrics such as LOLH, CF and CO₂ in power system modelling. These metrics are used to analyse current and future power systems. However, often when simulating these power systems with optimization, these metrics are not explicitly optimized for. Therefore, conclusions from these modeling metrics should not be drawn and if they are drawn people should at least be conscious of the arbitrariness of these metrics. Experimentally we showed the arbitrariness of the previously mentioned metrics. We used the 6 future European power systems with multiple climate years and simulated short term electricity market simulations by solving multiple

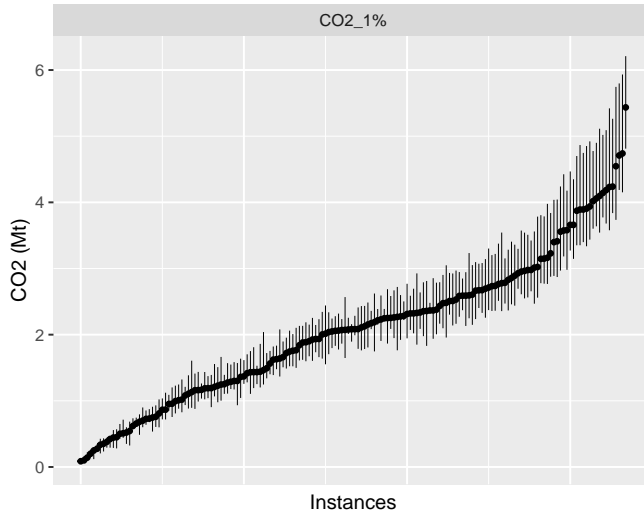


Figure 5.5: The total CO₂ emissions for all instances, ordered by the original total CO₂ emissions, for the solutions within 1% of the optimum.

72-hour long UC instances. With these instances we re-optimized these different modeling metrics given equivalent objective functions.

We found that the difference in the LOLH metric could be as high as a factor 38 for individual instances and the total difference, depending on the model, varied from a factor of 1.5 to 2.8. For the capacity factor of coal, gas- and nuclear-powered generators these differences depend on how close they are to the optimal solution. For individual instances the CF could be 0% when minimizing but more than 20% when maximizing, while both are within 1% of optimality. And in total the CF over all experiments for coal was a factor of 5.3 different. For gas and nuclear this was 2.8 and 1.2 respectively. For the CO₂ the difference was less pronounced, on average single instances had a factor difference of 1.1 to 1.4.

Bibliography

- [1] ACER. *Methodology for Calculating the Value of Lost Load, the Cost of New Entry and the Reliability Standard*. 2020.
- [2] Anne Sjoerd Brouwer et al. “Least-cost options for integrating intermittent renewables in low-carbon power systems”. In: *Applied Energy* 161 (2016), pp. 48–74.
- [3] European Commission. “Regulation (EU) 2019/943 of the European Parliament and of the Council of 5 June 2019 on the Internal Market for Electricity”. In: *Off. J. Eur. Union* 158 (2019), pp. 54–124.
- [4] ENTSO-E. *European Resource Adequacy Assessment - 2021 Edition*. 2021.
- [5] ENTSO-E. *Mid Term Adequacy Forecast (MAF)*. 2018. URL: https://docstore.entsoe.eu/Documents/SDC_20documents/MAF/2018/MAF_202018_20Executive_20Report.pdf.
- [6] ENTSO-E. *Pentalateral Energy Forum Support Group 2 Generation Adequacy Assessment*. 2018. URL: https://www.bmwi.de/Redaktion/DE/Downloads/P-R/plef-sg2-generation-adequacy-assessment-2018.pdf?__blob=publicationFile&v=4.
- [7] ENTSO-E and ENTSO-G. *TYNDP2020—Scenario Report*. 2020.
- [8] Energy Systems Integration Group. *Redefining Resource Adequacy for Modern Power Systems*. 2021.
- [9] LLC Gurobi Optimization. *Gurobi Optimizer Reference Manual*. 2022.
- [10] Hans Hersbach et al. “The ERA5 global reanalysis”. In: *Quarterly Journal of the Royal Meteorological Society* (2020). DOI: 10.1002/qj.3803.
- [11] A Kies, L von Bremen, and D Heinemann. *Hydro energy inflow for power system studies*. 2017.
- [12] Matija Pavičević et al. “The potential of sector coupling in future European energy systems: Soft linking between the Dispa-SET and JRC-EU-TIMES models”. In: *Applied Energy* 267 (2020), p. 115100.
- [13] William Zappa, Martin Junginger, and Machteld van den Broek. “Is a 100% renewable European power system feasible by 2050?” In: *Applied energy* 233 (2019), pp. 1027–1050.

- [14] Bas van Zuijlen et al. “Cost-optimal reliable power generation in a deep decarbonisation future”. In: *Applied Energy* 253 (2019), p. 113587.

Chapter 6

Linking Unserved Energy to Weather Regimes

This chapter is in submission at: Earth's Future

Rogier Hans Wuijts, Laurens Stoop, Jing Hu, Arno Haverkamp, Frank Wiersma, William Zappa, Gerard van der Schrier, Marjan van den Akker & Machteld van den Broek

6.1 Abstract

The integration of renewable energy sources into power systems is expected to increase significantly in the coming decades. This can result in critical situations related to the strong variability in space and time of weather patterns. During these critical situations the power system experiences a structural shortage of energy across multiple time steps and regions, leading to Energy Not Served (ENS) events.

Our research explores the relationship between weather regimes that describe the large scale atmospheric flow and ENS events in Europe by simulating future power systems. Our results indicate that most regions have a specific weather regime that leads to the highest number of ENS events. However, ENS events can still occur during any weather regime, but with a lower probability.

In particular, our findings show that ENS events in western and central European countries often coincide with either the positive Scandinavian Blocking (SB+), characterised by cold air penetrating Europe under calm weather conditions from north-eastern regions, or North Atlantic Oscillation (NAO+) weather regime, characterised by westerly flow and cold air in the southern half of Europe. Additionally, we found that the relative impact of one of these regimes reaches a peak 10 days before ENS events in these countries. In Scandinavian and Baltic countries, on the other hand, our results indicate that the relative prevalence of the negative Atlantic Ridge (AR-) weather regime is higher during and leading up to the ENS event.

6.2 Introduction

In 2022, anthropogenic greenhouse gas emissions are estimated to already have caused approximately 1.0°C of warming to the average global surface temperature compared to pre-industrial levels (1850–1900) [23]. To avoid the worst consequences of climate change, the world strives to rapidly reduce its greenhouse gas emissions [8, 1]. In order to reduce CO₂ emissions in the power system, supply needs to shift to renewable energy sources (RES) complemented by low carbon generators [22]. In the future a large part of RES are variable such as solar photovoltaic (PV), onshore and offshore wind, and run-of-river hydro power. The relative share of RES in the global production of electricity is increasing, 10.5% of the total generation of electricity in 2021 came from solar and wind compared to less than 1% in 2012 [4]. Moreover, more than 80% of the newly installed capacity in power systems around the world in 2021 came from RES [24]. However, the energy production of these sources is uncertain and variable. To mitigate this variability a power system must have sufficient storage, demand side response, low/non carbon emitting supply, and transmission capacity to spread the uneven power generation over time and space.

A critical situation in a power system may not always manifest as a high residual load at a single time step and place [41, 43, 9], but can also manifest as a structural shortage of energy over multiple time steps and across multiple

regions [39]. When these critical situations occur the power system cannot supply every demand, resulting in Energy Not Served (ENS).

ENS is an important reliability indicator for power systems. ENS is the part of demand which is not supplied in a given region over a given time period due to insufficient supply or demand-side resources, implying the Transmission System Operator (TSO) would need to curtail demand involuntary to maintain stable system operation. The expected Energy Not Served (EENS) is one of two key reliability indicators which must be calculated in the European Union as part of the European Resource Adequacy Assessment (ERAA) [13]. The other key reliability indicator is loss of load expectation (LOLE), i.e., the average number of hours ENS that is expected to occur per year based on simulations. However, in power system models, LOLE can take on arbitrary values making it a less robust indicator than EENS [46].

Weather regimes are classifications of common atmospheric states into quasi-stationary, persistent and recurrent large-scale atmospheric circulation patterns. As the weather in the winter period in Europe is more persistent, weather regimes are often defined for the extended winter [29, 31, 18], although other year-round definitions exist [20]. The circulation pattern over Europe, and thus a specific weather regime, influences the renewable generation and the energy demand in Europe. Therefore, it may be more difficult to supply all energy demand in certain weather regimes than others, potentially leading to ENS [43, 6, 32, 40].

In this chapter, we aim to investigate the relationship between ENS and weather regimes in Europe. Specifically, we want to determine which weather regimes lead to the highest levels of ENS in European countries. By identifying these critical weather regimes, we can better understand the factors that contribute to ENS and find directions to make the future European power system more resilient. We explore this relationship by simulating the scenarios of a future European power system created by ENTSO-E, incorporating 28 historical weather years in total. For these simulated years we calculate when and how much ENS occurs for each time step and region and if this ENS concurrently occurs with specific weather regimes.

6.3 Methods & Modelling

In this section, we provide an overview of our methods. We first describe the baseline capacity scenarios we used to model the future European power system. Next, we explain how we constructed our power system model and how we calculated weather-dependent variables, such as wind and solar generation and hydro inflow, for multiple weather years. In the following section we outline the weather regime classification we employed and finally we explain how we generated weather-dependent demand.

6.3.1 Energy System Scenarios

As basis of our power system model, we used the future European power system scenarios from the 2020 Ten Year Network Development Plan (TYNDP2020)

created by the European Network of Transmission System Operators for Electricity (ENTSO-E) and Gas (ENTSO-G) [15]. These scenarios provide insights into the possible energy system of the future and the effects of changes in supply and demand in the energy system.

For our study we used the three scenarios of the TYNDP2020 study as a starting point, namely the three different pathways of National Trends (NT), Global Ambition (GA) and Distributed Energy (DE) for the target year 2040. Table 6.1 gives an overview of the total generation capacity per technology for each scenario. Each scenario consists of 55 ‘nodes’ corresponding roughly to the current bidding zones in Europe. Each bidding zone usually covers an entire country except for Norway, Denmark, Sweden, and Italy as these are divided into multiple zones. In 8.5.2 an overview of the bidding zones, their region code, and the corresponding countries is provided. 8.5.3 presents an overview of the installed capacities for some bidding zones of the DE scenario as this is mainly used in this analysis.

Table 6.1: Total capacity (GW) in Europe for different generation technologies for the different TYNDP Scenarios in 2040.

	Thermal (Coal, Nuclear etc.)	Run of River	Closed pumped hydro storage	Open pumped hydro storage	Hydro Storage	Solar Photovoltaic	Offshore Wind	Onshore Wind	Battery
Distributed Energy (DE)	431	67	42	62	109	750	79	585	112
National Trends (NT)	451	67	42	62	109	489	131	406	61
Global Ambition (GA)	441	67	42	62	109	437	146	440	40

The TYNDP scenarios are comprehensive datasets that provide a detailed breakdown of the assumed generator capacities of different technologies in the different bidding zones. The datasets include generators of various fuel types and ages, which can impact their efficiency. However, technological details such as average unit size and ramping limits have been added from other sources [33, 16], as these were not included in the TYNDP datasets. The transmission capacity between regions is given by net transfer capacity (NTC) values, which are constant throughout the year but differ per scenario. All the capacity and grid data used and information about their origin is included in an online dataset¹.

The maximum residual load is defined as the remaining demand when renewable energy generation (i.e. from solar, wind and run-of-river hydro) is fully utilised

¹The capacity data and its source can be found here <https://github.com/rogierhans/TYNDP2040ScenarioData>.

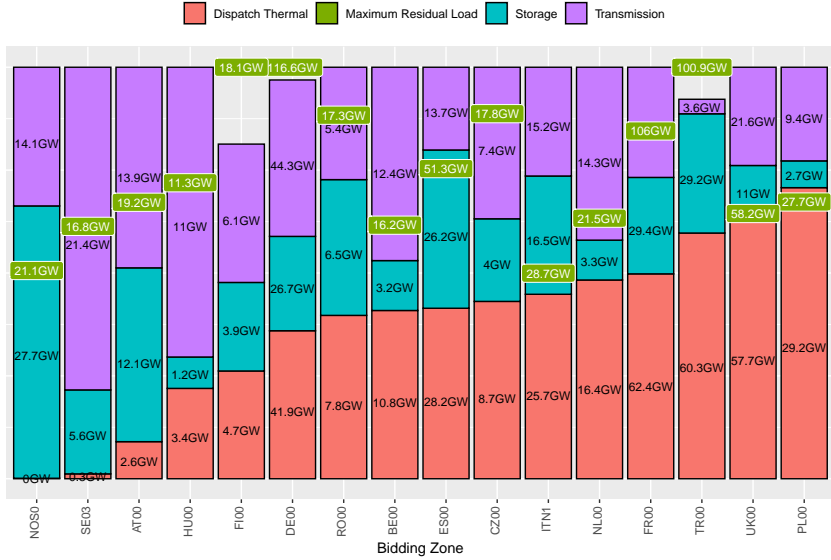


Figure 6.1: As a percentage of total capacity in the region, the total thermal dispatch capacity (red), the additional transmission capacity (purple), and storage capacity (blue) are shown for a subset of bidding zones with high residual load. In addition, the maximum residual load (green box) over 28 weather years for the scenario *Distributed Energy 2040* is shown. See 8.5.2 for the explanation of the codes.

to meet the demand. We found that for some bidding zones and scenarios, the maximum residual load exceeds the total thermal, transmission and storage capacity for that zone (Figure 6.1). However, most bidding zones in these scenarios are adequate by design [15]. In addition, we do not utilise the demand side response options that were defined to negate this.

To identify critical situations in which not all demand can be met by generation, we made the TYNDP scenarios more challenging by either increasing the demand (i.e. an increase in electrification) or decreasing the generation (i.e. a decrease in carbon-emitting generators). We define 12 scenarios: four alternatives of each of the 3 TYNDP scenarios: (i) unchanged, (ii) +10% demand, (iii) +20% demand and (iv) -20% generation capacity. For the latter, we only decrease the capacity of highly emitting generators that use as fuel either hard coal, lignite, or oil.

6.3.2 Power System Model

We used the unit commitment and economic dispatch problem (UCED) to simulate the hourly operation of the power system in Europe. The UCED is a mathematical optimisation model that finds the most cost-effective schedule for operating generators, ensuring that all demand is met at every time step and in every region. This method was chosen for its ability to simulate hourly market operations with

high technical detail, which is commonly used in the power industry [42, 2].

The UCED may incorporate many types of technical constraints, of which some can be omitted depending on the purpose of the study [45]. We therefore can use a simplified model which includes fewer constraints regarding the flexibility of thermal power plants. Moreover, we explicitly minimise the ENS in the power system and not the total system cost, which implicitly minimises the same amount of ENS. The complete model specification, our simplifications and the validation of the assumptions underlying these simplifications can be found in 8.5.4 and 8.5.5 respectively.

We simulate the hourly operation of the power system for a total of 28 weather years (1982-2010) in yearly segments from the 1st January to the 31st of December, i.e. 8760 hours in one model run. We set the storage levels at the start of the simulation at half capacity and enforce that the capacity is also at half capacity at the end of the year. This ensures that within a simulated year any storage discharged, e.g. hydro reservoirs are compensated by pumping or hydro inflow during that year.

6.3.3 Modelling weather dependent variables

The TYNDP scenarios contain, among others, technologies that depend on the weather, see Table 6.1. When the influence of the weather on an energy system is investigated, it is vital that the potential generation of these technologies is modelled accurately [9]. As the spatial distribution of measurements is sparse, climate model data is utilised. As the data for the different technologies was collected from various sources, care was taken to make sure that the underlying climate model is consistent across them.

For all weather dependent variables, data derived from the ERA5 reanalysis dataset is used [21]. Wind and solar energy generation was determined with the conversion models as described in Section 6.3.3.1 for the period 1950-2022. The hydrological data provided through by the E-Hype project, as described in Section 6.3.3.2, was only available from 1980-2010. The energy demand dataset, as described in Section 6.3.5, was only available from 1982-2016. The analysis is, therefore, limited to the period 1982-2010, as this is the period with maximum overlap.

6.3.3.1 Energy conversion models for wind and solar

To determine the electricity generation time series of RES per bidding zone, two things need to be determined. First, the potential generation profile per unit of installed capacity for solar photovoltaic and wind turbine technology must be determined for each climate model grid cell. Second, the potential generation of each technology must be multiplied by the distribution of installed capacity in each grid cell and summed up over all grid cells within a bidding zone.

Conversion models can be employed to calculate the potential generation of wind and solar energy. In previous work within the ACDC-ESM project [39], a number of conversion models were analysed and compared together with the TSO

stakeholder, TenneT TSO B.V., to determine which were representative yet computationally simple. For solar photovoltaic electricity generation we follow these recommendations and use the relatively simplified method as described by [25]. For comprehensiveness, 8.5.6 provides the exact description of the method used. More elaborate methods, like the one presented by [37], were not used, as these require additional information on panel tilt angle and solar radiation components that are not available within the TYNDP2020 scenario building guidelines.

For wind turbine electricity generation, we follow the recommendation laid out by [39] and use the method as described from [25]. However, we made four adjustments to this model to align it with the TYNDP2020 study. First, we reduced the effective maximum capacity factor (CF_e) by 5% to 95% to represent the wake and array losses in large scale wind-farms [27, 3, 19, 36]. Secondly, we let the capacity factor linearly decrease at high wind speeds to more accurately represent high windspeed operational conditions. The third change was that we tuned the power curve regimes based on stakeholder input. Finally, the wind speed provided by ERA5 (at 100 meter) does not match the hub heights of turbines within the TYNDP scenarios used, therefore it is scaled using the wind profile power law to 150 meters for offshore turbines and 120 meters for onshore turbines. See 8.5.7 for the formal definitions and more detailed discussion of the methods used.

For both technologies the total energy generation per bidding zone per hour was obtained by multiplying the weighted mean generation profile per bidding zone with the installed capacity as provided by the [15] for the scenario used. The weights in the averaging procedure for each bidding zone were determined by the mean capacity factor of each grid cell within that zone. Grid cells that were partially within a bidding zone got an additional weighting based on the percentage of the area within a zone.

6.3.3.2 Hydro inflow data

The hydro inflow data is based on historical river runoff reanalysis data simulated by the E-HYPE model [10]. E-HYPE is a pan-European model developed by The Swedish Meteorological and Hydrological Institute (SMHI), which describes hydrological processes including flow paths at the subbasin level. E-hype only provides the time series of daily river runoff entering the inlet of each European subbasin over 1980-2010. To match the operational resolution of the dispatch model, we linearly downscale these time series to hourly. By summing up runoff associated with the inlet subbasins of each country, we also obtain the country-level river runoff.

The hydro inflow time series per country as inputs of the UCED model is defined as the normalized energy inflows (per unit installed capacity of hydropower) embodied in the country-level river runoff. The dispatch model decides whether the energy inflows are actually used for electricity generation, stored, or spilled (in case the storage reservoir is already full). Specific details on the modelling method can be found in 8.5.8.

We explicitly consider three types of hydropower plants, namely storage hy-

dropower plant (STO), run-of-river hydropower plant (ROR) and pumped storage hydropower plant (PHS). For modelling purposes, we need to estimate the specific maximum energy storage content, for each type of hydropower. We obtain this by using an in-house database, containing the information of 207 hydropower plants, and calibrating this with present level of total storage size (220 TWh) in Europe given by [28].

6.3.4 Weather Regimes

In this study we use the classification of the atmospheric state from [18]. They revisited the identification of European weather regimes and showed that six clusters should be used in the classification, see 8.5.9. The six weather regimes used are defined for the whole of Europe at a daily interval for the period December-March from 1979-2018, but we only used the period 1982-2010 due to the availability of other datasets. The six regimes used have been labelled to indicate atmospheric state. Due to their symmetry, a name (Atlantic Ridge (AR), North Atlantic Oscillation (NAO) and Scandinavian Blocking (SB)) and state (+ and -) are used to label each of the six weather regimes.

While the specific weather can vary within a weather regime, the general flow of air is consistent within a weather regime, see also 8.5.11. The AR+ regime is associated with north-to-south air flow, sunny weather in north-eastern Europe and with calm weather in the Atlantic. The AR- regime is associated with sunny, but cold weather in north-eastern Europe, with a gradient to slightly warmer weather in the south-west. Under both AR regimes south-west Europe is characterised by decreased wind speeds and increased solar irradiance. The NAO+ regime is associated with a westerly flow, bringing warm temperatures and higher wind speeds to Scandinavia, while in the south colder temperatures and less sunlight is seen. Warmer and sunnier weather is observed in most of Europe during the NAO- state, due to easterly flow. On the other hand, the blocking pattern of the SB regimes, due to a stationary large high pressure system, generally brings cold and calm weather to central and northern Europe during the SB+ regime. While the SB- regime shows an increased wind speed in central Europe and the Atlantic. Both SB regimes show strongly reduced solar irradiance.

The persistence and occurrence of a specific weather regime is subject to decadal variability [11]. Therefore, we show in Table 6.2 the occurrence (the presence of weather regimes in the total number of days), how many times a persistent period of that weather regime occurs, the persistence (the average length) and maximum length for the six weather regime used.

6.3.5 Weather dependent demand

Weather not only influences the generation of electricity, but also the demand for electricity, primarily for heating, cooling and lighting. The effect of temperature based metrics like Heating Degree days on demand are known [34] and well established metrics in impact assessments [41, 7]. Scenarios for the future like the TYNDP2020, take into account system wide changes to an energy system. Not

Table 6.2: Prevalence of the daily defined European weather regimes (WR) in the winter months (December, January, February, March) from 1982 to 2010: the number of days the WR occurs, number of periods (consecutive days with the same WR), the average and maximum length of these periods.

WR	number of days	number of periods	avg length period	max length period
AR-	550 (15.6%)	114	4.8 days	23 days
AR+	562 (16.0%)	151	3.7 days	16 days
NAO-	611 (17.4%)	145	4.2 days	20 days
NAO+	697 (19.8%)	167	4.2 days	16 days
SB-	568 (16.2%)	157	3.6 days	22 days
SB+	528 (15.0%)	89	5.9 days	32 days

only the influence of temperature on the need for space heating and cooling related demand is taken into account, but also the transition to heat pumps and the additional demand from transport electrification (private cars, busses, passenger trains and heavy goods) [14].

In this study we use the hourly weather dependent demand time series for each bidding zone and scenario that were generated for the TYNDP2020. As the weather model that was used to obtain the an-European Climate Database version 3.1 (PECDv3.1) dataset is ERA5, the driving weather is consistent with the other data sources used. The PECDv3.1 initially released by ENTSO-E contained a few errors (countries missing data under specific scenarios), the specific updated datafiles used were provided by ENTSO-E through the ACDC-ESM project.

6.4 Results

In this section, we present our results in three stages. We first show the link between energy not served (ENS) and weather regimes for the 12 adjusted TYNDP scenarios. Then we discuss to what degree the sequence of weather regimes increases or reduces the risk for the energy system. And finally, we look deeper into what the meteorological link is between the weather regimes and ENS.

In the analysis we focus on two typical regions based on subsets of bidding zones. The first regions consist of Germany (*DE00*), France (*FR00*) and the Netherlands (*NL00*) and represents central Europe. The second regions consist of Lithuania (*LT00*), Latvia (*LV00*), the southern region of Norway (*NOM1*) and the northern region of Sweden (*SE01*) and represents the Scandinavian and Baltic region.

6.4.1 Scenario dependency

In Figure 6.2 the ENS as a percentage of the total demand is shown for all twelve scenarios. We can see that for the base scenarios of the TYNDP, Finland (*FI00*) and Norway (*NON1*, *NOS0*, *NOM1*) have some ENS (approximately 0.6% of the total demand), but for most countries the ENS is close to zero. When the base scenario is stretched, either by increasing the demand or decreasing the generation

capacity of dispatchable generators, then we indeed see more ENS. Especially the Scandinavian and Baltic countries have ENS in the altered scenarios. From the three scenarios provided by the TYNDP, National Trends has the least ENS while Distributed Energy has the most.

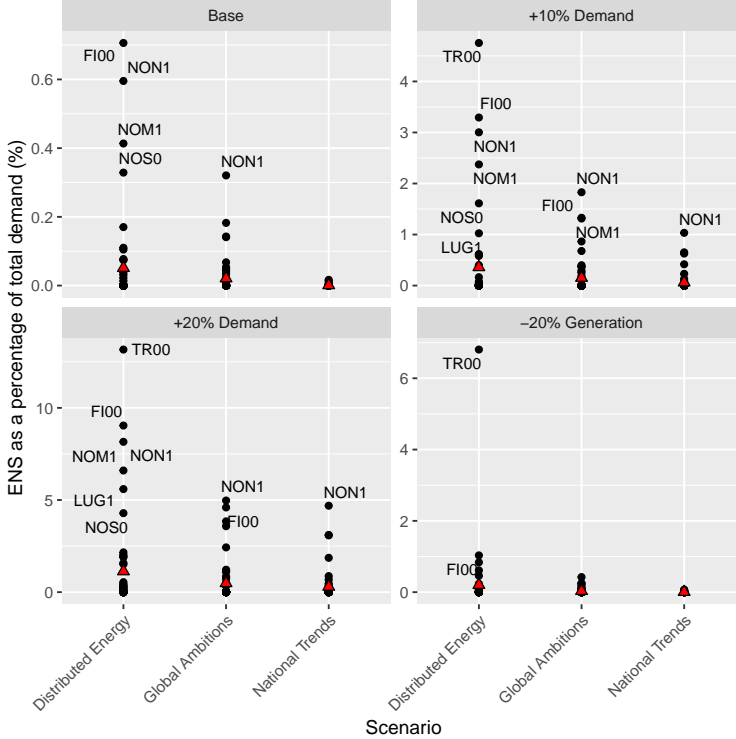


Figure 6.2: The Energy Not Served as a percentage of the total electricity demand of each bidding zone based on weather years 1982 to 2010. The red triangle represents the average over all bidding zones. The twelve scenarios are clustered by their variation. The regions with a high share of ENS are labelled with their region code. Please note that the *y-axes are on different scales*.

The distribution of ENS events throughout the year is given in Figure 6.3 for all twelve scenarios, showing that most ENS occurs in the winter months. As the ENS between bidding zones can differ in orders of magnitude, the total hours of loss of load expected (LOLH) is shown instead. When the demand increases, inevitably there would be some ENS in the non-winter months as can be seen in the third row. However, most LOLH and ENS occur in the winter time period, from December to March. As the meteorological variability in this winter period can be identified by using the definition of the weather regimes, a classification of the atmospheric state, we can analyse the relation between these regimes and the ENS events.

To investigate whether ENS events are not only caused by a single atmospheric

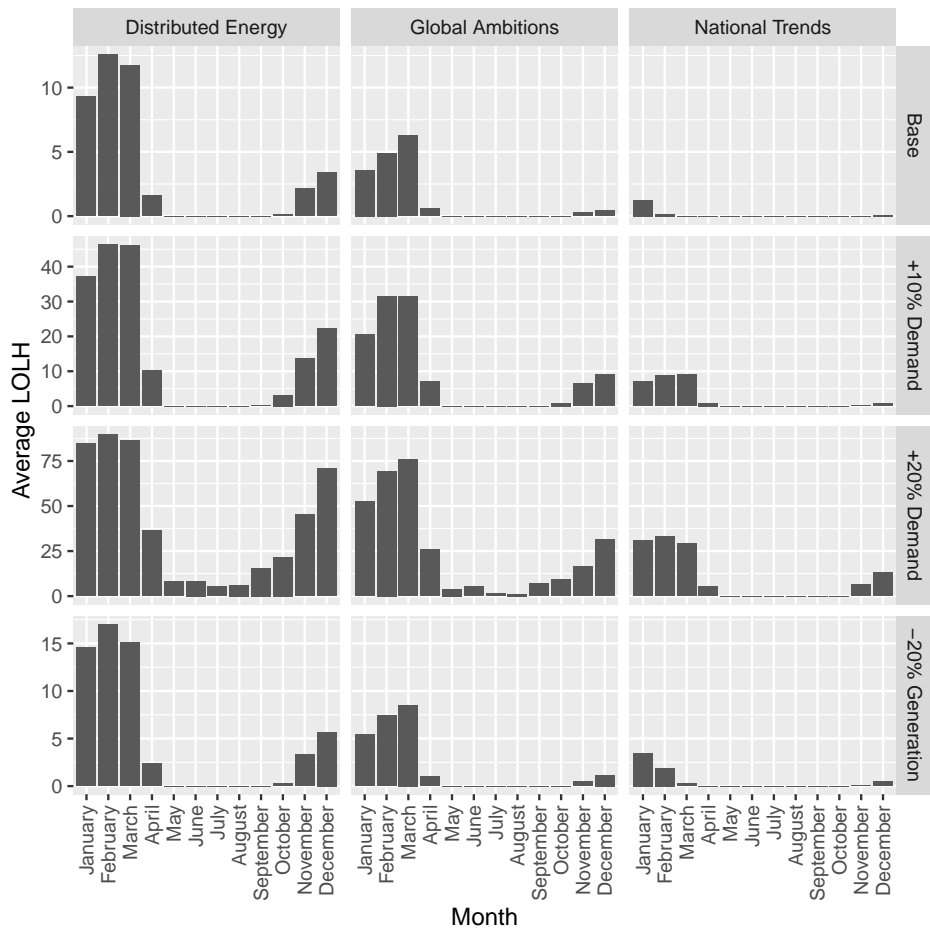


Figure 6.3: The average loss of load hours per year and bidding zone for each month and scenario based on the weather years 1982 to 2010.

state, but also by a specific sequence of atmospheric states, the weather regime occurrence preceding an ENS event is shown in Figure 6.4. We go back as far as 30 days before the ENS event to capture the impact of longer persisting weather regimes (see also Table 6.2). We observe that three weather regimes are most prevalent in this 30 day period: the positive state of Scandinavian Blocking (SB+) and the North Atlantic Oscillation (NAO+) weather regimes for the typical central European regions (Figure 6.4a), and the negative state of the Atlantic Ridge (AR-) regime for the Scandinavian and to a lesser degree at the Baltic zones (Figure 6.4b). In the northern European zones this behaviour is already detected in the original scenarios. However, for central European zones this behaviour is only detected during more challenging scenarios since those regions have almost no ENS in less demanding scenarios.

For the Netherlands in the scenarios DE+10%, GA+20% and NT+10%, presented in Figure 6.4a, the SB+ regime is present during 21.0%, 24.9% and 20.1% of the ENS events, respectively. While its average occurrence is 15.0% during the full period analysed (1982-2010). In the 30 days prior to an ENS event the prevalence of SB+ is even stronger for the Netherlands with 28.7%, 47.0% and 40.6% of the time, respectively.

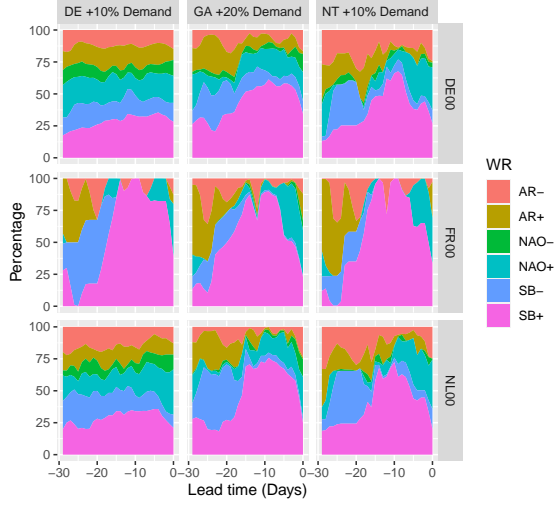
Similar behaviour is seen in most central European bidding zones, and while its absolute statistics differ between scenarios, it does not seem to depend on a specific scenario. Giving the fact that SB+ is the least frequent weather regime in our data set (Table 6.2), it is a clear signal that the SB+ weather regime is more likely to result in critical situations for central Europe.

6.4.2 Sequence of Weather Regimes

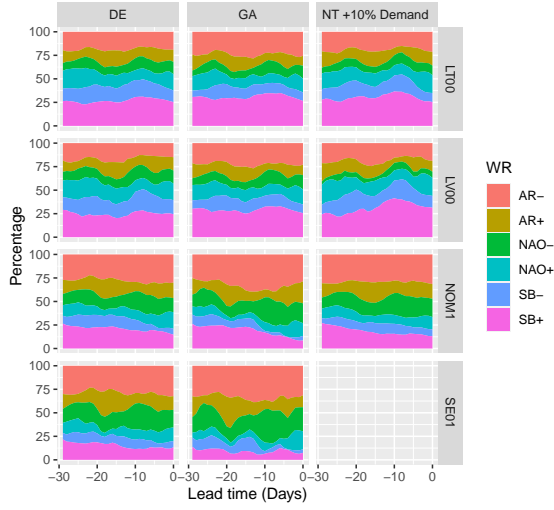
The central European regions mostly have a NAO+ or SB+ weather regime on the day of the ENS event (Figure 6.4a). In addition, even without the SB+ weather regime during the ENS event, this weather regime is prevalent 10 days before the ENS event. This suggests that a specific sequence or precedence of a weather regime could cause ENS.

To identify whether specific weather regimes are more prevalent in the period before ENS events, we assessed their occurrence during an ENS event, and 10 and 20 days before (see 8.5.10). We observe that ENS take place most of the time during the SB+ or NAO+ weather regimes across all scenarios (see Figure 6.5), and 10 or 30 days before the ENS events the weather is mostly in a SB+ regime. However, for the bidding zones in Norway and Sweden the AR- weather regime occurs slightly more in the 10 and 30 days before an ENS event. During or 10 days before an ENS event, no weather regime is clearly occurring the least. However, 30 days before an ENS event, NAO- is the least present.

The occurrence of a possible specific sequence of weather regimes leading to ENS is shown in Figure 6.6. For central European bidding zones, represented by Germany, there is a significant occurrence of SB+ in the period leading to an ENS event that happens during the weather regimes AR-, NAO+ or SB+. We observe a peak in the presence of SB+ at 10+ days prior to the ENS event. This is not something that is already present in the normal precedence of these weather



(a) Central European bidding zones



(b) Scandinavian and Baltic bidding zones

Figure 6.4: The distribution of daily weather regimes (WR) occurrence in the 30 days before an ENS event for a subset of scenarios and bidding zones based on the weather years 1982 to 2010.

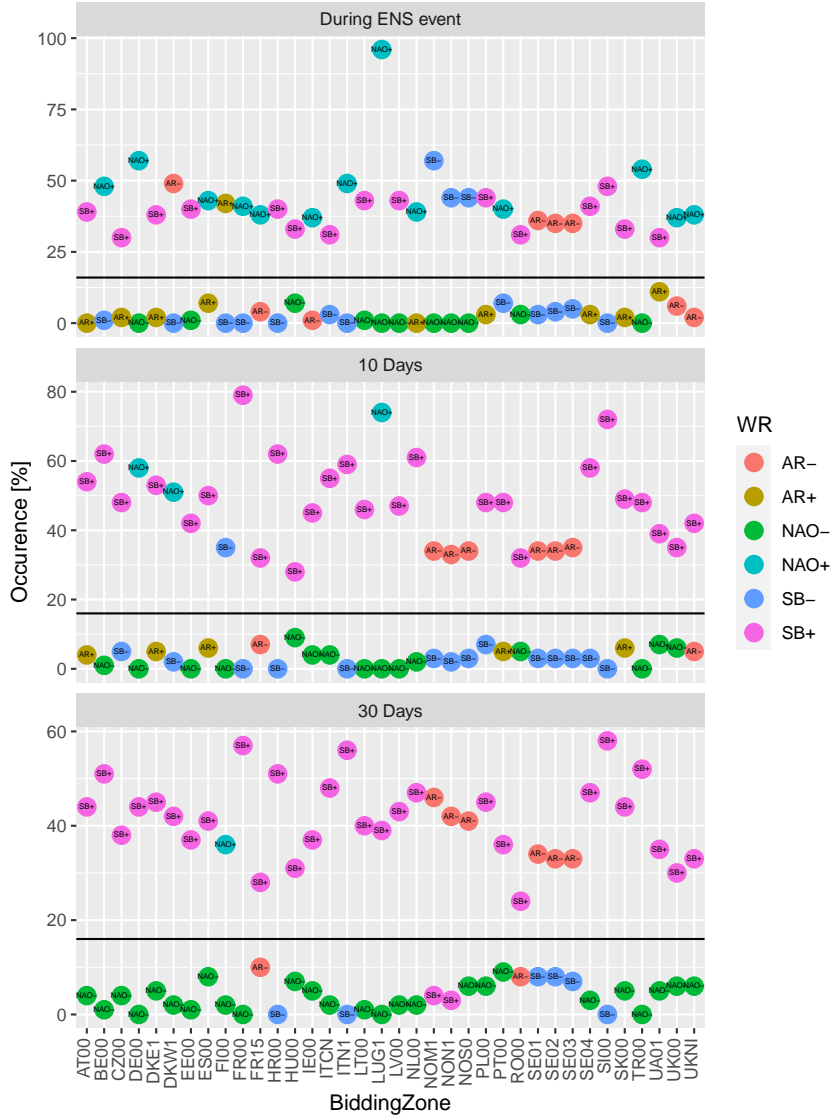


Figure 6.5: The occurrence of the two weather regimes that are present the most and the least during the day of the ENS event, and in the 10 and 30 days preceding it. Only the bidding zones with at least 50 ENS events across all scenarios and weather years based on 1982 to 2010 are presented. Naming convention are provided in Appendix B.

regimes.

For Scandinavian bidding zones, represented by Sweden in Figure 6.6, there is a significant occurrence of SB+ in the period leading to an ENS event that coincides with a NAO+ or SB+ weather regime. However, unlike the central European region this is not observed for ENS events during the AR- weather regime, which is most prominently associated with ENS events in northern Europe. In addition, we can see that the AR- regime is strongly present 20+ days prior to ENS events during SB- weather regime.

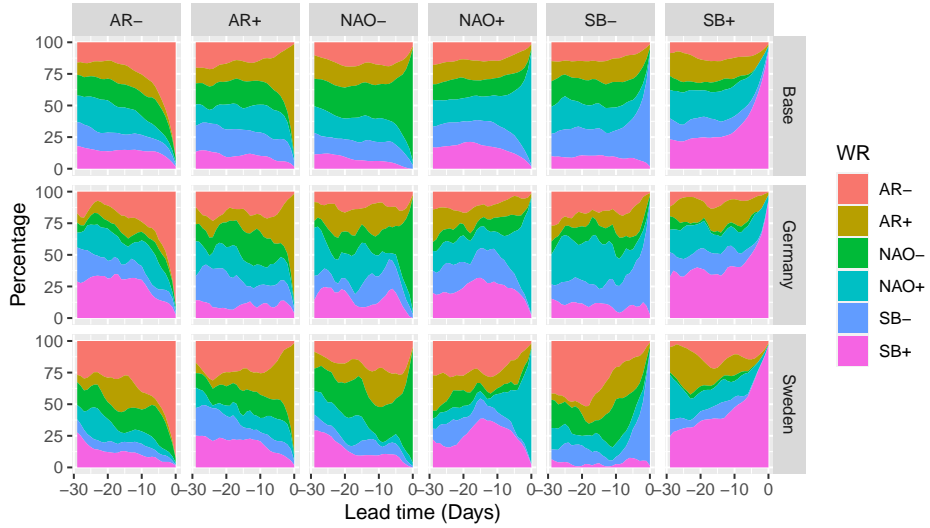


Figure 6.6: The daily relative occurrence of weather regimes (WR) before an ENS event grouped by the weather regime on the day of the ENS event in the analysed period (1982-2010). Base shows the normal precedence of weather regimes prior to a specific weather regime at day 0. For clarity, only Germany (DE00) and Sweden (SE01) are shown for the Distributed Energy +20% demand scenario.

6.4.3 Driving factors for Unserved Energy during Weather Regimes

That some weather regimes have a stronger link with ENS events can be expected as they are a way to analyse the meteorological variability at a synoptic scale², which influences the renewable electricity generation, hydro inflow and temperature, which in turn influences electricity demand. However, these weather regimes are defined over the whole of Europe, while their impact depends on the region considered.

²In meteorology, the synoptic or large scale is used to indicate weather systems ranging in size from several hundred to several thousand kilometres. This corresponds to a horizontal scale typical of mid-latitude high pressure systems, extra-tropical cyclones and storms.

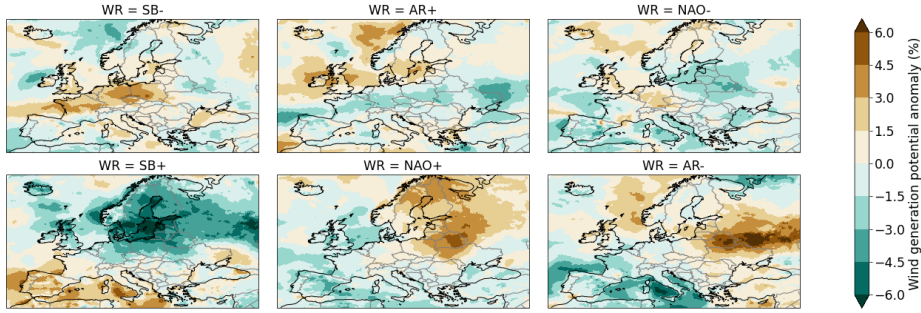


Figure 6.7: The average wind power generation anomaly from December to March (DJFM) in Europe for each weather regime with respect to the DJFM mean in the period 1982-2010.

Based on the spatial changes of meteorological circumstances during a specific weather regime, we can assess its potential impact on the energy system. For instance, on average during the SB+ weather regime a decrease in wind power potential is observed in parts of central Europe with respect to the December to March mean (Figure 6.7). This would likely impact the electricity system during this weather regime. Similarly, the NAO- weather regime is associated with small change in wind power potential over Europe. Additional Figures describing the anomaly over Europe in solar power potential and the meteorological drivers can be found in 8.5.11.

Compared to the average anomaly in renewable energy generation potential, demand, and residual load in the winter period (see Figure 6.8), the SB+ weather regime is on average associated with higher demand and lower generation from solar photovoltaic systems, onshore and offshore wind. This behaviour is observed in both representative regions. Consequently, the residual load during a SB+ regime in these zones is much higher on average compared to other weather regimes, for the Latvian region (LT00) it is even 50.8% higher.

For some bidding zones another weather regime is associated with increased residual load. For instance, in the Netherlands (NL00), the NAO+ weather regime is associated with an even higher residual load on average (25.9%) then under SB+ (18.2%), while most ENS events are found during the SB+ weather regime. In addition, while the AR- regime shows a strong relation with ENS for the Scandinavian and to a lesser degree at the Baltic zones, the driving factors cannot be deduced based on the finding in Figure 6.8.

Apparently, the weather regime is not the only driving factor for ENS events and part of it is associated with (the assumptions of) the specific technologies used or the energy system scenarios. In addition, although the European electricity grid is well interconnected between bidding zones, the relation between an ENS event and a specific weather regime can change from bidding zone to bidding zone. However, in general the SB+ and NAO+ weather regimes are associated with more ENS events compared to other weather regimes.

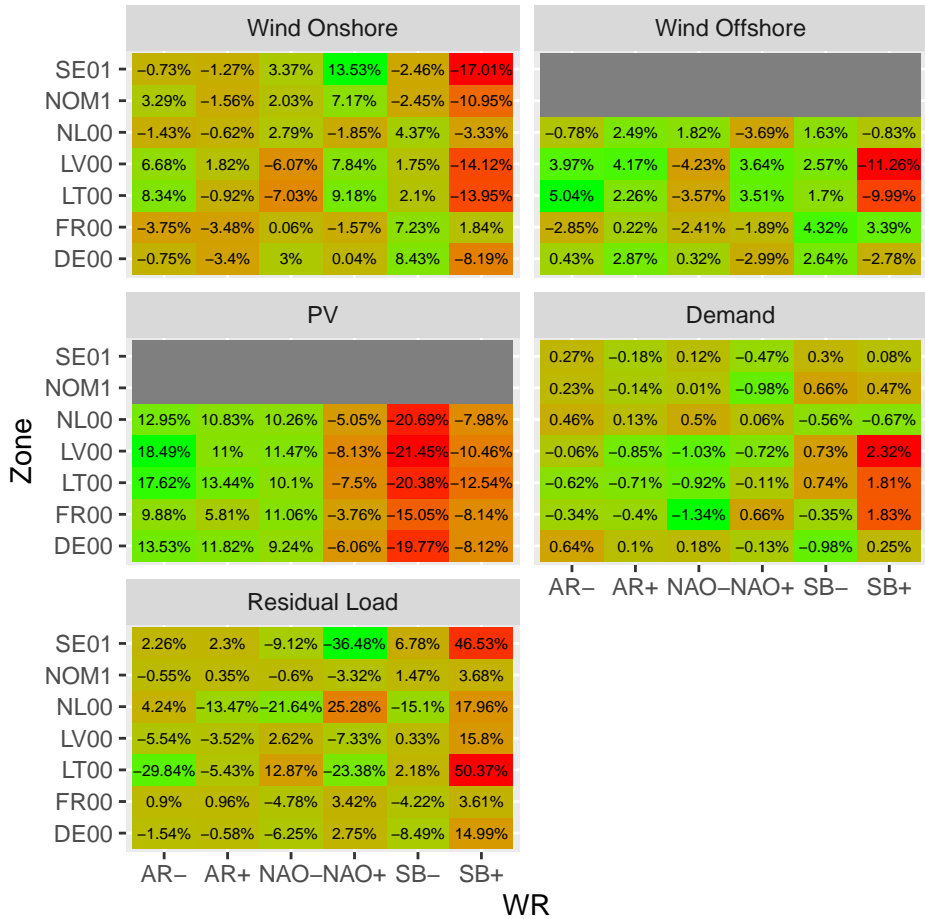


Figure 6.8: The average percentage anomaly, with respect to the December-March mean based on the weather years 1982-2010, in demand, solar photovoltaic (PV), residual load, onshore and offshore wind. The zones in the two typical regions for central Europe and northern Europe are shown. Note that residual load can be negative and the mean can be close to zero resulting in relative high changes

6.4.4 Role of storage

As we have shown in Section 6.4.1–6.4.3, the SB+ weather regime is prevalent in many bidding zones during ENS events. This weather regime can persist for a prolonged period (Table 6.2), and has a peak in relative occurrence in the 10+ days prior to an ENS event. The strong presence of the SB+ weather regime in the period prior to an ENS event could indicate that a build up or a specific sequence of weather regimes is needed for ENS to occur. This could indicate that storage plays a role, as it may be depleted during these weather regimes.

The evaluation of the average anomaly in storage level, the amount of charging and discharging during a specific weather regime (see Figure 6.9) shows that the average storage levels is higher during the SB+ weather regime in all bidding zones except for the Netherlands (NL00). In addition, we observe an increase in the discharge (all regions) *and* in the charging (central Europe) during these events. Similar behaviour is observed for the SB- weather regime and during the NAO+ regime for the Netherlands (NL00).

The earlier observation that SB+ is more challenging may be aligned with the observation in Figure 6.9 that storage is utilised more frequently during the SB+ weather regime to overcome these challenges. It should be noted that some regions, like Germany (DE00), France (FR00), Sweden (SE01) and Norway (NOM1), also show this behaviour to a lesser extend during the SB- and NAO+ weather regime.

In addition, while the AR- regime shows a strong relation with ENS for the Scandinavian and to a lesser degree at the Baltic zones, the driving factors cannot be deduced based on the finding in Figure 6.8.

In addition, we observe that the both states of the AR and the NAO- weather regime are associated with low storage levels in the Scandinavian and some central European regions. Especially the AR- weather regime can be linked to depleting storage for Sweden (SE01), Norway (NOM1), and France (FR00), with storage levels at -39.2%, -35.9%, and -46.0% respectively. As the AR- regime shows a strong relation with ENS for the Scandinavian and Baltic zones, storage is likely the driving factor in these zones.

6.4.5 Validation of power system model formulation

Model characteristics often included in the UCED problem such as ramping limits, minimum uptime, and binary commitment variables, are unnecessary when you are only interested in energy not served [45]. This was validated by running multiple months with 4 different models of varying degree in detail and similar values of ENS where found (see 8.5.4).

However, similar values of ENS do not imply that they occur at the same bidding zone or time [46]. Therefore, to make sure our results are robust under different model decisions, a more detailed model that includes generation cost (the Cost Model in 8.5.4) was simulated for analysed period of 1982-2010 for the Distributed Energy +10% demand scenario. The Cost Model is optimised by the interior-point barrier method while the ENS Model is optimised by the dual simplex method.

		Charge					
Zone	SE01	-2.23%	-2.22%	-2.76%	12.16%	5.94%	-14.51%
	NOM1	-5.51%	9.98%	-3.06%	20.92%	-3.53%	-25.1%
	NL00	-10.98%	-13.21%	-10.39%	18.99%	3.64%	8.73%
	LV00	-10.79%	-1.56%	-2.55%	5.27%	4.45%	4.17%
	LT00	-13.35%	4.6%	-4.01%	5.23%	11.21%	-5.25%
	FR00	-21.39%	-12.35%	-28.31%	12.19%	23.65%	26.9%
	DE00	-16.97%	3.39%	-17.67%	3.19%	8.45%	21.34%
		Discharge					
Zone	SE01	6.97%	-15.63%	0.83%	-4.94%	-0.85%	15.87%
	NOM1	-17.31%	-6.31%	-11.04%	2.31%	16.92%	16.39%
	NL00	-5.47%	-10.83%	0.5%	13.6%	-3.72%	2.8%
	LV00	-8.64%	3.04%	4.38%	-8.65%	5.2%	6.5%
	LT00	-9.4%	0.78%	1.98%	-16.13%	11.38%	15.68%
	FR00	-2.64%	-24.23%	-18.51%	20.43%	10.33%	12.08%
	DE00	-0.58%	-9.17%	-8.64%	4.18%	-1.93%	17.01%
		Storage Level					
Zone	SE01	-39.22%	-7.09%	-19.91%	15.24%	26.85%	22.69%
	NOM1	-35.89%	3.64%	-20.9%	-5.62%	30.4%	32.54%
	NL00	12.6%	-10.82%	5.3%	12.92%	-13.79%	-9.93%
	LV00	3.7%	-4.03%	-5.26%	0.43%	-2.18%	8.33%
	LT00	2.27%	-5.23%	-2.29%	-3.96%	1.54%	9.42%
	FR00	-45.99%	-5.76%	-31.8%	15.68%	39.27%	28.2%
	DE00	-25.75%	-7.35%	-19.99%	12.54%	26.24%	13.19%
		AR-	AR+	NAO-	NAO+	SB-	SB+
		WR					

Figure 6.9: The average percentile anomaly per weather regimes in charge, discharge and storage level, compared to the December to March mean during the 1982–2010, for the total storage from batteries and (pumped) storage hydropower plant. The zones in the two typical regions for central Europe and northern Europe are shown.

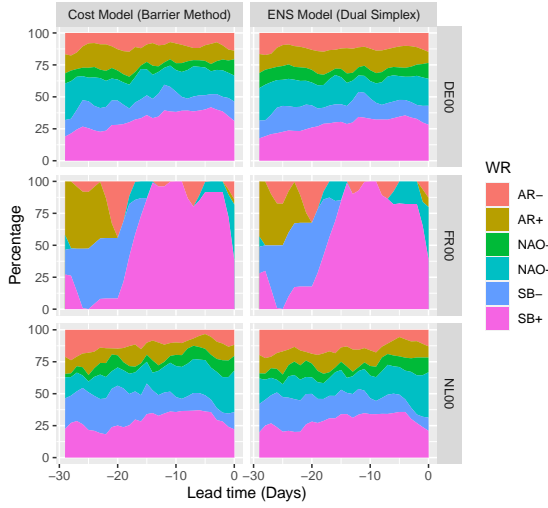


Figure 6.10: The distribution of daily weather regimes (WR) occurrence in the 30 days before an ENS event for the Cost and ENS Model formulations. Only the DE with 10% extra demand scenario DE00, FR00 and NL00 bidding zones are shown based on the weather years 1982 to 2010.

In line with the results shown in Figure 6.4 for the ENS Model, we observe that three weather regimes are most pronounced in the Cost Model (see Figure 6.10). While the exact timing might be shifted slightly within a day, we observe extremely similar occurrence rates of the weather regimes in the prior to ENS events. Both model formulations identify the same critical moments, indicating that cost plays no role for possible occurrence of an ENS events.

6.5 Limitations and discussion

The relation found between ENS events and the weather regimes is in line with previous studies [20, 41, 43, 6, 32, 30, 40]. Although changes in the absolute values of risk differ between studies, an increase in risk during a winter time period high pressure system over Scandinavia or north-west Europe is seen. Where previous work has focused on the relation between weather regimes with renewable energy resource generation [20, 35] or the residual load [43, 6, 32, 30, 40], we analysed this relation between weather regimes and critical situations identified in full power system simulations. The link between specific weather regimes and ENS can be used to inform policy maker or grid operators in the choices they make. For instance, when in the long-term forecast a strong and persistent Scandinavian Blocking is observed, an early warning could be given to the grid operators to adjust their short-term planning for the likely reduced availability of the wind and solar resources.

In our study, the analysed period is limited to 28 historical weather years due

to the availability of data. This is slightly shorter than the 30 years normally used when looking at the impact of weather. By using a dataset with a longer period of consistent data, the relation between ENS and weather regimes can be better evaluated [5]. At the same time, the analysis presented here covers a significantly larger number of weather years than used by Transmission System Operators (TSO) in their European resource adequacy assessments [13], and ten year network development plan (TYNDP) scenario assessment [14]. In line with the recommendations made by [9], the development of the new open access version of the Pan-European Climate Database (PECD) [12] will provide the European TSOs and other parties with the option to use a longer consistent dataset, covering past and future projections, that allows for similar and more advanced assessments than were made here.

The limited time-span of the period analysed imposed additional limitations on the study results, especially related to the uncertainties related to climate system. By only looking at a short historic period, we cannot adequately assess the aleatoric uncertainty, the year-to-year variability of weather, of our results. This interannual to multi-decadal variability of the state of the climate would preferably be addressed to obtain robust results [9]. For instance, the combined wind and solar resource shows multidecadal variability of around 5% [44], which is a similar order of magnitude as the change observed during the challenging weather regimes (see Figure 6.8). In addition, the occurrence, persistence and transition probabilities of a specific weather regime is dependent on decadal variability [11] and is linked to the state of the El Nino Southern Oscillation (ENSO) [17]. Consequently, by changing the specific decades analysed, the absolute values of the risk can differ.

By only looking at historical weather years, no assessment of the impact of climate change could be made. As the TYNDP scenarios cover different states of future, it would be better if climate state of the future would be used to drive the weather dependent parts of the energy system [9]. However, the climate state of the future is subject to three very strong sources of uncertainty that would need to be accounted for [38]. There is uncertainty in the specific pathway to the future and the emissions associated with this, these could be assessed by using multiple Representative Concentration Pathways (usually 3-4 RCP's are used). The epistemic uncertainty in the climate response to these emissions could be assessed by comparing the results from different climate models (depends on the region under consideration, usually 5-12 are used). And finally, the aleatoric uncertainty can be assessed by looking at a consecutive 30 year period. Assessing all three uncertainties for all TYNDP models used here (3 base or 12 with all adjustments) would require running at least 1350 and upwards to 17280 years through our Power System Model. Even if a consistent dataset of all weather dependent variables could be created, this is currently not feasible due to the running time of our simulations (on a small cluster this takes 20-45 minutes for the ENS Model). Although there is no agreement on how exactly [9], a different approach should thus be used to assess the impact of climate change.

Because specific modelling choices in the UCED have an effect on the decision variables and outcomes of the simulation [45], model choices matter. For instance,

the fixed storage level at start and end of the year might limit the use of storage in times of need, although similar assumptions are made in the [13]. In addition, the analysed period we use in a single run (8760 hours, or one year) is already an improvement compared to the two-stage simulation used within the [13]. To properly assess the impact of storage and its use during the ENS events a different start, and thus endpoint, of the simulated year would need to be considered. In addition, the level of storage defined in the scenarios might be subject to over planting with respect to the renewable energy resource capacity. As shown by [26] the ability to balance the potential of renewable generation with storage has a limit in the order of a couple of hours and additional storage will likely rarely be utilised by renewables.

6.6 Conclusion

The aim of this study was to investigate the relationship between weather regimes and energy not served (ENS). For this we analysed twelve future European capacity scenarios based on 2020 Ten Year Network Development Plan from the European transmission system operators. For each of these scenarios we simulated an hourly power system model with weather dependent demand and renewable energy generation from 28 historic weather years.

The different scenarios show slightly different results, but most ENS events occur in the period from December to March. We find that most bidding zones have a particular weather regime that causes the most ENS events. However, an ENS event can still occur in all regions during any weather regime but with a smaller probability. Different scenarios show some variation, but the weather regime associated most with an ENS event for a region is consistent across the scenarios analysed.

For western European bidding zones, ENS events tend to coincide with the positive Scandinavian Blocking (SB+) and positive North Atlantic Oscillation (NAO+) weather regime. During the SB+ weather regime persistent cold and calm weather is observed, leading to an increased electricity demand in conjunction with a decreased wind and solar energy potential, which leads to high residual loads. While the NAO+ regime is associated with stronger westerly flow, and thus increased wind energy potential in Scandinavia, it is associated with ENS events in central Europe. This could be due to the observed prevalence of SB+ in the 10+ days prior to an ENS event in these regions. While storage utilisation is increased significantly, storage levels are not depleted on average during this weather regime.

For Scandinavian and Baltic countries, the results indicate that the negative Atlantic Ridge (AR-) weather regime is more likely to be present during and leading up to ENS events. During the AR- weather regime the calm, sunny and cold weather in north-eastern Europe leads to a slightly increased demand in these regions. A significant decrease in charging of the storage system, and storage level of most regions is observed. This combination likely drives the ENS events in this region.

To conclude, this chapter shows a clear correlation between specific weather

regimes and unserved energy for some European countries. We found that the period preceding an ENS event is important. This indicates that for some ENS events a build-up is required, and this illustrates the variable nature of the energy system.

Bibliography

- [1] European Commission (EC). *European Green Deal*. European Union, Dec. 2019. URL: https://eur-lex.europa.eu/resource.html?uri=cellar:b828d165-1c22-11ea-8c1f-01aa75ed71a1.0002.02/DOC_1&format=PDF (visited on 08/11/2020).
- [2] Saleh Y Abujarad, Mohammad Wazir Mustafa, and Jasrul Jamani Jamian. “Recent approaches of unit commitment in the presence of intermittent renewable energy resources: A review”. In: *Renewable and Sustainable Energy Reviews* 70 (2017), pp. 215–223.
- [3] James Bleeg et al. “Wind Farm Blockage and the Consequences of Neglecting Its Impact on Energy Production”. In: *Energies* 11.6 (June 2018), p. 1609. DOI: 10.3390/en11061609. URL: <https://doi.org/10.3390/en11061609>.
- [4] BloombergNEF. *Power Transition Trends*. 2022.
- [5] H. C. Bloomfield et al. “The Importance of Weather and Climate to Energy Systems: A Workshop on Next Generation Challenges in Energy–Climate Modeling”. In: *Bulletin of the American Meteorological Society* 102.1 (Jan. 2021), E159–E167. DOI: 10.1175/bams-d-20-0256.1. URL: <https://doi.org/10.1175/bams-d-20-0256.1>.
- [6] Hannah C. Bloomfield, David J. Brayshaw, and Andrew J. Charlton-Perez. “Characterizing the winter meteorological drivers of the European electricity system using targeted circulation types”. In: *Meteorological Applications* 27.1 (Dec. 2019). DOI: 10.1002/met.1858. URL: <https://doi.org/10.1002/met.1858>.
- [7] HC Bloomfield et al. “Quantifying the sensitivity of european power systems to energy scenarios and climate change projections”. In: *Renewable Energy* (2021). DOI: 10.1016/j.renene.2020.09.125.
- [8] United Nations Framework Convention on Climate Change. *Paris Agreement*. UN Treaty. United Nations, Dec. 2015. URL: https://treaties.un.org/pages/ViewDetails.aspx?src=TREATY&mtdsg_no=XXVII-7-d&chapter=27&clang=_en (visited on 08/11/2020).
- [9] Michael T. Craig et al. “Overcoming the disconnect between energy system and climate modeling”. In: *Joule* 6.7 (2022), pp. 1405–1417. ISSN: 2542-4351. DOI: <https://doi.org/10.1016/j.joule.2022.05.010>. URL: <https://www.sciencedirect.com/science/article/pii/S2542435122002379>.

- [10] Chantal Donnelly, Jafet CM Andersson, and Berit Arheimer. “Using flow signatures and catchment similarities to evaluate the E-HYPE multi-basin model across Europe”. In: *Hydrological Sciences Journal* 61.2 (2016), pp. 255–273.
- [11] Josh Dorrington et al. “CMIP6 Models Trend Toward Less Persistent European Blocking Regimes in a Warming Climate”. In: *Geophysical Research Letters* 49.24 (Dec. 2022). DOI: 10.1029/2022gl100811. URL: <https://doi.org/10.1029/2022gl100811>.
- [12] Laurent Dubus et al. “Towards a future-proof climate database for European energy system studies”. In: *Environmental Research Letters* 17.12 (Nov. 2022), p. 121001. DOI: 10.1088/1748-9326/aca1d3. URL: <https://doi.org/10.1088/1748-9326/aca1d3>.
- [13] ENTSO-E. *European Resource Adequacy Assessment - 2021 Edition*. 2021.
- [14] ENTSO-E and ENTSO-G. *TYNDP2020—Scenario building guidelines*. 2020. URL: https://2020.entsos-tyndp-scenarios.eu/wp-content/uploads/2020/06/TYNDP_2020_Scenario_Building_Guidelines_Final_Report.pdf.
- [15] ENTSO-E and ENTSO-G. *TYNDP2020—Scenario Report*. 2020.
- [16] EC ETRI. “Energy Technology Reference Indicator Projections for 2010–2050”. In: *Joint research centre (JRC), European Commission (EC)* (2014).
- [17] Swinda K. J. Falkena et al. *A Bayesian Approach to Atmospheric Circulation Regime Assignment*. 2022. DOI: 10.48550/ARXIV.2206.11576. URL: <https://arxiv.org/abs/2206.11576>.
- [18] Swinda K.J. Falkena et al. “Revisiting the identification of wintertime atmospheric circulation regimes in the Euro-Atlantic sector”. In: *Quarterly Journal of the Royal Meteorological Society* May (2020), pp. 1–14. ISSN: 1477870X. DOI: 10.1002/qj.3818.
- [19] Jana Fischereit et al. “Review of Mesoscale Wind-Farm Parametrizations and Their Applications”. In: *Boundary-Layer Meteorology* 182.2 (Aug. 2021), pp. 175–224. DOI: 10.1007/s10546-021-00652-y. URL: <https://doi.org/10.1007/s10546-021-00652-y>.
- [20] Christian M. Grams et al. “Balancing Europe’s wind-power output through spatial deployment informed by weather regimes”. In: *Nature Climate Change* 7.8 (July 2017), pp. 557–562. DOI: 10.1038/nclimate3338. URL: <https://doi.org/10.1038/nclimate3338>.
- [21] H Hersbach et al. “ERA5 hourly data on single levels from 1959 to present”. In: *Copernicus Climate Change Service (C3S) Climate Data Store (CDS)* (2018). DOI: 10.24381/cds.adbb2d47.
- [22] International Energy Agency. *World Energy Outlook 2022*. 2022, p. 524. DOI: <https://doi.org/https://doi.org/10.1787/3a469970-en>. URL: <https://www.oecd-ilibrary.org/content/publication/3a469970-en>.

- [23] IPCC. “Summary for Policymakers”. In: *Climate Change 2021: The Physical Science Basis. Contribution of Working Group I to the Sixth Assessment Report of the Intergovernmental Panel on Climate Change*. Ed. by V. Masson-Delmotte et al. Cambridge, United Kingdom and New York, NY, USA: Cambridge University Press, 2021, pp. 3–32. DOI: 10.1017/9781009157896.001.
- [24] IRENA. *World Energy Transitions Outlook 2022: 1.5° C Pathway*. 2022.
- [25] S. Jerez et al. “The CLIMIX model: A tool to create and evaluate spatially-resolved scenarios of photovoltaic and wind power development”. In: *Renewable and Sustainable Energy Reviews* (2015). DOI: 10.1016/j.rser.2014.09.041.
- [26] Hannah G. Livingston and Julie K. Lundquist. “How many offshore wind turbines does New England need?” In: *Meteorological Applications* 27.6 (Nov. 2020). DOI: 10.1002/met.1969. URL: <https://doi.org/10.1002/met.1969>.
- [27] J. K. Lundquist et al. “Costs and consequences of wind turbine wake effects arising from uncoordinated wind energy development”. In: *Nature Energy* 4.1 (Nov. 2018), pp. 26–34. DOI: 10.1038/s41560-018-0281-2. URL: <https://doi.org/10.1038/s41560-018-0281-2>.
- [28] Tim Mennel et al. “The hydropower sector’s contribution to a sustainable and prosperous Europe”. In: *Main Report* (2015).
- [29] Paul-Antoine Michelangeli, Robert Vautard, and Bernard Legras. “Weather regimes: Recurrence and quasi stationarity”. In: *Journal of the atmospheric sciences* 52.8 (1995), pp. 1237–1256.
- [30] Fabian Mockert et al. *Meteorological conditions during Dunkelflauten in Germany: Characteristics, the role of weather regimes and impacts on demand*. 2022. DOI: 10.48550/ARXIV.2212.04870. URL: <https://arxiv.org/abs/2212.04870>.
- [31] Robert Neal et al. “A flexible approach to defining weather patterns and their application in weather forecasting over Europe”. In: *Meteorological Applications* 23.3 (2016), pp. 389–400.
- [32] Noelia Otero et al. “Characterizing renewable energy compound events across Europe using a logistic regression-based approach”. In: *Meteorological Applications* 29.5 (Sept. 2022). DOI: 10.1002/met.2089. URL: <https://doi.org/10.1002/met.2089>.
- [33] Kris Poncelet, Erik Delarue, and William D’haeseleer. “Unit commitment constraints in long-term planning models: Relevance, pitfalls and the role of assumptions on flexibility”. In: *Applied Energy* 258 (2020), p. 113843. ISSN: 0306-2619. DOI: <https://doi.org/10.1016/j.apenergy.2019.113843>. URL: <https://www.sciencedirect.com/science/article/pii/S0306261919315302>.

- [34] Robert G. Quayle and Henry F. Diaz. “Heating Degree Day Data Applied to Residential Heating Energy Consumption”. In: *Journal of Applied Meteorology* 19.3 (Mar. 1980), pp. 241–246. DOI: 10.1175/1520-0450(1980)019<0241:hdddat>2.0.co;2. URL: [https://doi.org/10.1175/1520-0450\(1980\)019%3C0241:hdddat%3E2.0.co;2](https://doi.org/10.1175/1520-0450(1980)019%3C0241:hdddat%3E2.0.co;2).
- [35] P Ravestein et al. “Vulnerability of European intermittent renewable energy supply to climate change and climate variability”. In: *Renewable and Sustainable Energy Reviews* 97 (2018), pp. 497–508.
- [36] Yves Marie Saint-Drenan and et al. “A parametric model for wind turbine power curves incorporating environmental conditions”. In: *Renewable Energy* (2020). DOI: 10.1016/j.renene.2020.04.123.
- [37] Yves-Marie Saint-Drenan et al. “An approach for the estimation of the aggregated photovoltaic power generated in several European countries from meteorological data”. In: *Advances in Science and Research* 15 (May 2018), pp. 51–62. DOI: 10.5194/asr-15-51-2018. URL: <https://doi.org/10.5194/asr-15-51-2018>.
- [38] Theodore G. Shepherd. “Storyline approach to the construction of regional climate change information”. In: *Proceedings of the Royal Society A: Mathematical, Physical and Engineering Sciences* 475.2225 (May 2019), p. 20190013. DOI: 10.1098/rspa.2019.0013. URL: <https://doi.org/10.1098/rspa.2019.0013>.
- [39] Laurens P. Stoop et al. “Detection of Critical Events in Renewable Energy Production Time Series”. In: *Advanced Analytics and Learning on Temporal Data*. 2021. DOI: 10.1007/978-3-030-91445-5_7.
- [40] Paulina Tedesco et al. *Gaussian copula modeling of extreme cold and weak-wind events over Europe conditioned on winter weather regimes*. 2022. DOI: 10.48550/ARXIV.2209.12556. URL: <https://arxiv.org/abs/2209.12556>.
- [41] K. van der Wiel et al. “Meteorological conditions leading to extreme low variable renewable energy production and extreme high energy shortfall”. In: *Renewable and Sustainable Energy Reviews* 111 (2019a), pp. 261–275. ISSN: 1364-0321. DOI: <https://doi.org/10.1016/j.rser.2019.04.065>.
- [42] Manuel Welsch et al. “Incorporating flexibility requirements into long-term energy system models—A case study on high levels of renewable electricity penetration in Ireland”. In: *Applied Energy* 135 (2014), pp. 600–615.
- [43] Karin van der Wiel et al. “The influence of weather regimes on European renewable energy production and demand”. In: *Environmental Research Letters* (2019B). DOI: 10.1088/1748-9326/ab38d3. URL: <https://dx.doi.org/10.1088/1748-9326/ab38d3>.
- [44] Jan Wohland, David Brayshaw, and Stefan Pfenninger. “Mitigating a century of European renewable variability with transmission and informed siting”. In: *Environmental Research Letters* 16.6 (May 2021), p. 064026. DOI: 10.1088/1748-9326/abff89. URL: <https://doi.org/10.1088/1748-9326/abff89>.

- [45] R.H. Wuijts, M. van den Akker, and M. van den Broek. “Effect of modelling choices in the unit commitment problem”. In: *Energy Systems* (2023). DOI: 10.1007/s12667-023-00564-5.
- [46] Rogier Hans Wuijts et al. “Pitfalls of Power Systems Modelling Metrics”. In: *2022 18th International Conference on the European Energy Market (EEM)*. IEEE. 2022, pp. 1–11.

Chapter 7

Conclusion

7.1 Summary

Mitigation efforts to avoid dangerous effects of climate change are leading to a shift in electricity production towards low carbon and intermittent renewable energy sources. This shift, along with the increasing use of electric heating, introduces more variable generation and demand in the power system that are both influenced by weather patterns.

To assess the adequacy of future power systems and identify potential problems, power system models are needed to simulate their operation.

The unit commitment problem (UC), also called the unit commitment and economic dispatch problem, is a well-known tool that simulates the operation of the power system with high technical detail, taking into account the flexibility of thermal generators, and the transmission and storage capabilities of the system. Solving the UC problem is not trivial as it is a hard optimization problem. Additionally, the size of the European power system models and the need to consider multiple weather years make it even more difficult. This results in high computation times which can be addressed by either increasing the efficiency of the algorithms or performing justified simplifications to the UC problem.

The goal of this thesis was to gain insights into how power system modelling based on the UC could be improved to accurately assess the operation of future power systems under many weather scenarios. We achieved this goal by addressing the following three sub-questions:

- How do modeling decisions influence the outcomes and computational performance of the UC in power system modeling? (**Chapter 2, 5 and 6**)
- How can solving the UC be algorithmically improved? (**Chapter 3 and 4**)
- What is the relationship between adequacy of European power systems and weather regimes? (**Chapter 6**)

In **chapter 2**, our aim was to assess the effect of modeling simplifications, which are often made to reduce computation times, and to find out which of these simplifications are justified. To this end, a comprehensive benchmark set of UC problem instances was created. An UC problem instance consist of a specific power system in a real or fictional geographic area which includes techno-economic parameters for each generator and, where relevant, data of transmission lines and storage units. Almost all the UC problem instances from literature (17 in total) were collected and put into a similar format. This benchmark was used to compare the quality of solutions and computation times between a base UC model and variations of this model with fewer constraints and/or characteristics. The base UC model was a Mixed Integer Linear Programming (MILP) problem that incorporated linear approximations of quadratic cost functions for generators¹, minimum up- and downtime, time-dependent startup costs, and ramping limits. In addition, the model included constraints to ensure sufficient reserves in the system, and a

¹A generation cost function describes the relation between fuel and variable O&M cost and the generation.

DC approximation of power flows for problem instances with transmission. The quality of the solutions was assessed based on total system costs, capacity factors, and the number of times the relaxed models violated omitted constraints.

Simplifications such as linear relaxation with or without the use of tighter generation constraints can significantly increase the speed of solving the UC problem, with an average speed-up factor of 32 and a small objective cost gap between the relaxation and the base model (almost always below 1% and for one third below 0.1%). However, the resulting schedules may not be realistic, as they can include fractional commitment decisions. Moreover, linear relaxation results in significant capacity factor differences for individual generators compared to the base model. On average, the capacity factor difference was 6.4% over 30 runs and 15 UC instances, with a maximum difference of 37.7% between the relaxation and the base model. Secondly, when the objective is to minimize energy not served instead of total system cost then the linear relaxation has the exact same amount of energy not served as the base model. Thirdly, we found that using a linear approximation of the quadratic generation cost function produced good results, average 0.11% cost difference. However, using a piece-wise linear approximation with multiple pieces further reduced the gap between the real evaluation and the approximation, but at a significantly higher computation cost: using 3 segments instead of 1 took roughly twice as long but with almost no gain with only 0.01% point improvement in the cost difference.

All other simplifications of the UC model are not recommended. First, omission of minimum up- and downtime mostly increased computation time and making start-up costs time-independent did not speed up the process, while both simplifications resulted in quality loss with regard to costs and significant differences in capacity factors. Secondly, omission of ramping limits and reserve constraints results in a model that is twice as fast on average, but at the expense of too much quality loss. Without the ramping limits the total cost for one problem instance was 5% lower on average than the cost of the base model and the dispatch of generators was significantly different with on average a 12% difference in capacity factors compared to those of the base model. Finally, while simplifications of the transmission system may speed up the computation time, the difference in total system cost was incredibly high. For one instance on average the total cost was underestimated by 50% when transmission constraints were omitted.

In chapter 3, two algorithms were developed that solve the single-unit commitment problem (1UC), a special case of the UC problem in which a least cost schedule is searched for only one generator subject to generation limits, minimum up- and downtime, and ramping limits. In this problem, the generator is not required to meet a demand, but a time series of electricity prices is given that determines how much revenue the generator can make at each time step. In this chapter two dynamic programming algorithms based on two different recurrence relations were introduced. The first algorithm is suitable for any convex generation cost function while the second one can only be applied to linear or piece-wise linear generation cost functions.

For the first recurrence relation we created multiple functions F_t^τ that for each valid power production level p_t returns the cost of the optimal schedule for which

the generator at time t , is on for the last τ time steps and produces p_t during timestep t . By creating these functions inductively, we were able to identify irrelevant functions and remove them. This results in a time complexity of $O(nmk^2)$ where k is the maximum number of relevant functions over all the timesteps and m is the maximum number of pieces of the piece-wise convex functions F_t^τ . We showed that for the UC benchmark set introduced in Chapter 2, k was at most 5 and m at most 10 and did not increase when we increased the amount of time steps. Moreover, we demonstrated experimentally that this results in a computation time that grows linear in the amount of time steps. This improves the quadratic growth of earlier algorithms.

For the second dynamic programming algorithm a different recurrence relation H_t^τ that requires fewer functions to be stored was introduced. These functions are harder to create than F_t^τ . However, we showed that in the special case where the generation cost function is piece-wise linear we only need to keep track of a limited number of points Q to represent these functions. The method of representing cost only at a limited number of points is not new. However, our method works for non-equal ramping limits, where previous work only considered the case in which the ramp-up and ramp-down limits were equal, and we showed how to efficiently compute the value at Q . This resulted in an improved algorithm in terms of generality and time complexity of $O(n \cdot |Q|)$.

Computational experiments with generator data from multiple power systems were performed. The results show that our algorithms outperform other methods for both piece-wise linear and quadratic generation cost. Both methods increase the time efficiency and solve the single-unit commitment problem for large time horizons (1000 timesteps) in a few milliseconds.

In chapter 4, a new alternating direction method of multipliers (ADMM) algorithm was developed that heuristically solves the UC. First, we transformed a standard UC formulation into the augmented Lagrangian by relaxing the demand coupling constraint. Next, we solved this new problem with ADMM, an iterative algorithm. In each iteration we solved the subproblems induced by the decoupling of the demand coupling constraint. These subproblems were comparatively easy to solve as many efficient methods exist for these subproblems. The use of our fast algorithm for the 1UC subproblem introduced in Chapter 3, for example, enables many iterations so that ADMM converges to a feasible solution of high quality.

Computational experiments on a large set of UC instances demonstrated that our algorithm produces high quality solutions on each UC instance and were on average 0.15% removed from the optimum. For the problem instances with quadratic cost, it is faster (on average ~ 195 times faster) than solving it with state-of-the-art Mixed Integer Quadratic Programming (MIQP) formulation for the UC. For linear instances it is competitive and starts to outperform MILP when the time horizon grows. The time complexity seems to grow almost linearly with the amount of time steps. When solving instances with long time horizons our method can find a high-quality solution in seconds while the MIP solver could not find any good solution after 1 hour. UC problems with long time horizons are common in large scale power system models covering more than a few days, i.e. weeks or even months, or in short-term UC problem with high temporal resolution. Moreover, due to

the decoupled nature of ADMM the subproblems can easily be changed to model elements of the power system in more detail or to improve the time complexity of the subproblems to achieve even faster results.

In chapter 5, the significance of widely used metrics was studied by examining various (sub)optimal solutions for the UC problem and it was found that the value of common metrics applied on these solutions were often arbitrary. This was illustrated by running multiple experiments on six scenarios of a future European power system for target years 2030 and 2040 created by ENTSO-E, the European Network of Transmission System Operators. Each scenario was run multiple times by adding additional objectives such as the minimization and maximization of capacity factors of generators, emissions, and loss of load hours (LOLH), while keeping the total dispatch costs the same. In this way, we found the maximum and minimum values of these metrics which could technically arise from the UC model when cost is minimized, and thus identified how much these metrics can vary within equivalent (sub)-optimal solutions.

We found that the difference in the LOLH metric could be as high as a factor 38 for individual instances and the total difference of the average minimum and the average maximum value, depending on the level of model detail, varied from a factor of 1.5 to 2.8 while all solutions had the same optimal objective cost.

In the experiments regarding capacity factors (CF) and CO₂ emissions, UC solutions were studied that were 0.1%, 0.5% and 1% removed from the optimum. The CF differences of coal-fired, gas-fired, and nuclear generators depend on how close the solutions were to the optimum. For example, we found two solutions for one UC instance within 1% of the optimum where the average CF of all coal-fired generators could either be 0% or 20%. The difference between the average minimum CF and the average maximum CF for coal-fired power plants was a factor of 5.3. For gas-fired and nuclear this was 2.8 and 1.2 respectively. Finally, for the CO₂ emissions the difference was less pronounced between equivalent cost solutions of a UC instance, as on average CO₂ emissions could vary by a factor 1.1 to 1.4.

In this chapter, we showed that we can minimize the spread of LOLH a little bit by including more detail in our model such as adding flexibility constraints, ramping limits and minimum up- and downtime, and a wheeling charge on the transmission lines. However, the takeaway from this chapter is that adding additional detail should not be done solely to avoid spread of these metrics, but rather, care should be taken when using any metric that is not explicitly optimized for. These metrics are secondary characteristics of the solution and are often not included in the objective, so they should not be used as the primary focus of the analysis of these solutions. A more robust approach might be to focus only on the elements included in the objective that are used in the optimization model. For example, using the total energy not served (ENS) as a metric for adequacy is more reliable than using loss of load hour expectation. ENS is explicitly modeled in the objective with a high coefficient, and as a result, (sub)optimal solutions tend to have the same or similar ENS values.

In chapter 6, the relationship between weather and energy not served (ENS) was investigated. We simulated 12 future European power system scenarios by

running an hourly power system model with demand and renewable energy patterns for 28 weather years. Next, the prevailing weather regimes at the times when ENS events occur were identified. Weather regimes refer to large-scale atmospheric patterns that in this research are grouped according to atmospheric states into six classifications, with each day being assigned to a specific weather regime. The results show that in most regions a particular weather regime causes the most ENS events. However, for any region ENS events can still occur in any weather regime but with a smaller probability. Our study found that in western and central European countries, ENS events coincide with the weather patterns positive Scandinavian Blocking (SB+) and positive North Atlantic Oscillation (NAO+). SB+ is characterized by cold and windstill weather with reduced incoming solar radiation and NAO+ is characterized by colder temperatures and reduced incoming solar radiation in the southern parts of Europe. Furthermore, we observed that the relative prevalence of SB+ reaches its peak about 10 days before an ENS event. This suggests that the long duration of the SB+ weather regime limits power storage in these countries. For Scandinavian and Baltic countries, the results indicate that the weather pattern negative Atlantic Ridge (AR-), which is associated with sunny, but cold weather in north-eastern Europe, with a gradient to slightly warmer weather in the south-west, is more likely to occur during and leading up to ENS events. To conclude, this chapter shows a clear correlation between specific weather regimes and unserved energy for some European countries.

7.2 Research Question 1: How do modeling decisions influence the outcomes and computational performance of the UC in power system modeling?

All model decisions influence the outcomes and computational performance of the UC in power system modeling. Based on the type of influence, these decisions can be grouped into the following three categories:

- **Decisions resulting in some speed up, large cost difference, and noticeable difference in decision variables:** (Tight) linear relaxation, linear approximation of the quadratic cost function, and any relaxation when the objective is changed to minimization of energy not served instead of total system cost.
- **Decisions resulting in large or some speed up, large cost difference, and noticeable difference in decision variables:** omission of ramping limits or reserve requirements, simplification of the transmission system by using a trade-based formulation or treating everything as a copperplate.
- **Decisions resulting in no or a small speed up, large cost difference, and noticeable difference in decision variables:** Omission of minimum up- and downtime and time-dependent startup costs.

Notice that in all categories the decision variables are noticeably different, this in turn influences the value of the metrics that are not included in the objective function. For example, our experiments highlight how sensitive the capacity factors of individual and groups of generators are. Even the linear relaxation, that has the least cost difference of the simplifications, results in large capacity factor differences. This difference is even larger for other model relaxations. Even for a tighter model, which has an equivalent search space, the capacity factor difference was high. These results imply that there are many different solutions with similar cost and that the actual generation pattern produced should not be considered as the unique way to achieve cost-efficient operation. For example, we found that the difference in the loss of load metric could be as high as a factor 38 for individual experiments. The combined capacity factors differences of coal, gas- and nuclear-powered generators show that these differences depend on the distance to the optimal value but are high for any suboptimal solution. This sensitivity decreases but does not disappear when more detail is added to the model. However, the takeaway from this thesis is not that additional detail should be added to avoid arbitrariness in these metrics, but rather, care should be taken when using any metric that is not explicitly included in the objective.

To conclude, some model simplifications are more valid than others. Moreover, it depends on the purpose of the model whether or not the model simplifications are valid. For example, if you are interested in ENS then even the most simplified model will give you equivalent results. However, if you are interested in the capacity factors or loss of load hours metric than you need to realise that these metrics may change significantly within equivalent cost solutions. Even without changes to the model, the input or the algorithm the value of these metrics can significantly change and therefore using UC with this purpose should be used with caution.

7.3 Research Question 2: How can solving the unit commitment problem be algorithmically improved?

In this thesis, we made significant algorithmic improvements for solving the UC. Specifically, we introduced a novel decomposition algorithm and in addition, we developed two separate algorithms to address the 1UC subproblem, which is frequently encountered in UC decomposition approaches. One of these algorithms is designed to handle linear or piece-wise linear generation cost functions, while the other is capable of dealing with any convex generation function. The latter 1UC algorithm is used in the decomposition algorithm introduced in Chapter 4 and the computational improvements of the 1UC are an important reason that this decomposition algorithm scales well in the length of the time horizon. In this thesis, it is experimentally shown that the computation time for our 1UC algorithm scales linearly with the amount of timesteps. Moreover, conditions are identified when the time complexity is linear, and it seems that these conditions are always

met in practice. As a consequence, the computation time of our decomposition algorithm also scales linear or near linear with the amount of timesteps. If instead we would use previous state-of-the-art dynamic programming algorithms for 1UC that in practice scale quadratic, then our decomposition algorithm would also scale quadratically with the amount of timesteps and would not be competitive. Our algorithm can solve UC instances with a time horizon of one week (168 hours) within seconds and produce a solution that is close to optimal. This is a major improvement given the limitations of MILP and MIQP solvers. If the time horizon is 24 hours then 7 out of 15 instances could be solved to optimality by an MIP solver within 1 hour. However, when the time horizon is 168 only 2 out of 15 instances could be solved to optimality by an MIP solver within 1 hour. Furthermore, while for some instances the MIP solver produces solutions that are close to optimal after 1 hour, 4 are still more than 1% removed from optimality and one even 31%. This illustrates the need for different algorithms besides MIP to solve the UC and hence we introduce a decomposition algorithm that can solve the UC within seconds and is close to optimal.

These computational improvements to the UC for long time horizons are promising in the context of power system modelling where long-time horizons are required. Long time horizons are important because the storage and use of large hydro plants can span weeks or even months and this interaction is not captured by shorter time horizons.

7.4 Research Question 3: What is the relationship between adequacy of European power systems and weather regimes?

With the knowledge and insight gained in Chapters 2-5 we simulated the future European power system and investigated the relationship between energy not served (ENS) and weather regimes. ENS was chosen as the model outcome because it is one of the key reliability indicators used in adequacy studies performed by transmission system operators in Europe and because it is less arbitrary than loss of load hours (LOLH). Since we want to minimize ENS, we made appropriate simplifications and were able to run 28 weather years on 12 scenarios.

The results show that all regions have a particular weather regime that causes the most ENS events. However, for any region ENS events can still occur for any weather regime but with a smaller probability. Our study found that in western and central European countries, ENS events coincide with the weather regime *positive Scandinavian Blocking* (SB+) and *positive North Atlantic Oscillation* (NAO+). Furthermore, we observed that the relative prevalence of SB+ reaches its peak about 10 days before an ENS event. This suggests that the long duration of the SB+ weather regime of SB+ limits power storage in these countries. For Scandinavian and Baltic countries, the results indicate that the weather pattern *negative Atlantic Ridge* (AR-) is more likely to occur during and leading up to ENS events.

7.5 Key Contributions and Impact

Simplifications of the unit commitment problem (UC) are made to reduce computation time. However, these are often made without analyzing their effect on solution quality. This thesis has significant implications for Transmission System Operators (TSOs), policy makers and researchers that use UC in power system modelling as it provides guidelines on which model simplifications are justified and effective, and which are not. Additionally, the investigation of power system modeling metrics, such as loss of load hours (LOLH) and associated loss of load expectation (LOLE), are crucial for policy makers in the EU. Currently, LOLE is a key metric in adequacy studies which is codified into EU law and guides the implementation of capacity mechanisms. However, this thesis demonstrates that this metric is unreliable, revealing a flaw in the methods used for conducting adequacy studies.

Our newly introduced algorithms to solve the 1UC problem enable researchers using decomposition algorithms based on the relaxation of the demand-generation balance constraint to use a faster algorithm. Since in most decomposition algorithms the bulk of the computation time is solving the 1UC problem for many iterations, the overall decomposition algorithm that solves the UC becomes faster.

Moreover, when solving UC with either quadratic generation or long-time horizons, the newly developed ADMM algorithm appears to be the preferred method for solving UCs for operational research or for power system modeling with high levels of detail.

In addition, in the last chapter we identify a clear relationship between weather regimes and adequacy. Earlier work around this topic tried to identify the relationship between weather regimes and residual load, the demand minus the renewable energy generations. This chapter takes it one step further and investigates the effect of weather regimes on the power system itself by simulating the European power system for multiple weather years and linking the critical moments with the weather regimes. This chapter takes the first steps in identifying critical weather patterns which will play a central role in the adequacy of the future European power system.

7.6 Future Work

Power system modeling relies on the availability of data. Transmission system data is only available from open-source projects that rely on educated guesses about high voltage transmission lines which in turn makes it impossible to model Europe at a high resolution. We settled for using the net transfer capacity (NTC) between countries, but this highly overestimates the transfer capacities within countries as it assumes each country as a copperplate. In future work, it would be valuable to represent the physical flows better by modelling the underlying transmission network between and within countries. However, this would be a data gathering challenge and an algorithmic challenge given the size of the resulting model

In this thesis, we assumed that MILP formulations solved by standard software like Gurobi represent state-of-the-art algorithms for solving the UC, as also con-

firmed by other researchers, and given the fact that MILPs for UC are often used in commercial settings. Therefore, we compared our ADMM algorithm to this approach. However, it is difficult to fully understand the current state-of-the-art since there are many different definitions of the UC problem. Moreover, many algorithms are not fully described or published online, and even when they are, they are often tested on different problem instances, making direct comparison difficult. There are some research papers that have compared their developed algorithm with others, but these comparisons have typically been performed on the simplest UC instances. One potential future research direction would be to conduct a detailed survey of the different UC algorithms and to perform a thorough comparison of these methods. This could give a clearer picture on the current state-of-the-art algorithms and inform the development of new approaches for solving the UC problem.

The last chapter suggests that some weather regimes co-occur more often with ENS events for some countries. Since weather regimes are predictable, it could be valuable to investigate to what extent these weather regimes can be used to predict future ENS events. Thus, we can know days or weeks in advance that a critical weather pattern with negative consequences for the power system may occur. Based on such an early warning system, preventative measures can be taken to mitigate the effect of a long positive Scandinavian blocking that result in a long duration of low renewable generation and higher demand.

Uncertainty in the UC has received a lot of academic attention but in power system studies this is largely ignored. While we did account for variability of the weather by looking at many weather years, we did not include the uncertainty of RES generation, hydro inflow, or demand patterns. However, keeping everything deterministic can still give much insight. If we find energy not served with perfect foresight, then without this perfect foresight we would also have energy not served and therefore it gives a lower bound. The unpredictability of RES, demand and the availability of generators remains a significant aspect of power system operation and will become even more critical with the increasing integration of renewable energy sources. It would be beneficial to incorporate uncertainty into future power system models in some way.

7.7 Nederlandse Samenvatting

Mondiale inspanningen om de verstreckende gevolgen van klimaatverandering te verminderen leiden tot een transitie in de elektriciteitsproductie richting koolstofarme en hernieuwbare energiebronnen. Dit zorgt samen met het toenemende gebruik van elektrische verwarming voor meer variabele opwek en vraag in het elektriciteitssysteem. Deze vraag en opwek wordt sterk beïnvloed door weerspatronen.

Om de leveringszekerheid van toekomstige elektriciteitssystemen te beoordelen en mogelijke problemen te identificeren, zijn er elektriciteitssysteem modellen nodig om hun werking te simuleren.

Het unit commitment probleem (UC) is een model dat de werking van het en-

ergiesysteem simuleert met een hoge technische nauwkeurigheid, rekening houdend met de flexibiliteit van thermische generatoren en de transmissie- en opslagcapaciteiten van het systeem. Het oplossen van het UC-probleem is een moeilijk optimalisatieprobleem. Bovendien maakt de omvang van de Europese elektriciteitssysteem en de noodzaak om meerdere weerjaren door te rekenen het nog moeilijker. Dit resulteert in lange rekentijd, die kunnen worden aangepakt door ofwel de efficiëntie van de algoritmen te vergroten ofwel gerechtvaardigde vereenvoudigingen aan te brengen in het UC-probleem. Het doel van dit proefschrift was inzichtelijk te maken hoe de modellering van elektriciteitssystemen op basis van UC verbeterd kan worden om de werking van toekomstige elektriciteitssystemen nauwkeurig te beoordelen onder verschillende weerscenario's. We hebben dit doel bereikt door de volgende drie deelvragen te beantwoorden:

- Hoe beïnvloeden modelleringsbeslissingen de resultaten en rekentijd van het UC-probleem in modellering van elektriciteitssystemen? (**Hoofdstuk 2, 5 en 6**)
- Hoe kan het oplossingsalgoritme van het UC-probleem verbeterd worden? (**Hoofdstuk 3 en 4**)
- Wat is de relatie tussen de leveringszekerheid van Europese elektriciteitssystemen en weerregimes? (**Hoofdstuk 6**)

Het doel van **hoofdstuk 2** was om het effect van vereenvoudigingen in de modellering van elektriciteitssystemen te beoordelen en te achterhalen welke van deze vereenvoudigingen gerechtvaardigd zijn. Hiertoe werd een uitgebreide verzameling van testproblemen van het UC gecreëerd. Een UC-testprobleem bestaat uit een specifiek energiesysteem in een echt of fictief geografisch gebied, waarbij techno-economische parameters worden gedefinieerd voor elke generator en, indien relevant, gegevens van transmissielijnen en opslag. Bijna alle UC-testproblemen uit de literatuur (in totaal 17) werden verzameld en in een vergelijkbaar format gezet. Deze testproblemen werden gebruikt om de kwaliteit van oplossingen en berekeningstijden te vergelijken tussen een basis UC-model en variaties op dit model met minder beperkingen en/of kenmerken. Het basis-UC-model was een geheeltallige lineair programmeringsprobleem (MILP) dat lineaire benaderingen van kwadratische kostenfuncties voor generatoren bevatten en ook minimale aan- en uit-tijd, tijdafhankelijke opstartkosten en op- en afregel limieten. Bovendien bevatte het model beperkingen om voldoende reserves in het systeem te waarborgen, en een gelijkstroom benadering van de fysische transmissielijnen. De kwaliteit van de oplossingen werd beoordeeld op basis van de totale systeemkosten, capaciteitsfactoren en het aantal keren dat de weggelaten randvoorwaarden overtreden werden.

Ten eerste vereenvoudiging door middel van lineaire relaxatie kan de snelheid van het oplossen van het UC-probleem aanzienlijk verhogen. Gemiddeld genomen werd de rekentijd een factor 32 sneller waarbij er maar een klein verschil in de waarde van de doelfuncties tussen de relaxatie en het basismodel plaatsvond (bijna altijd onder 1% en voor een derde zelfs onder 0,1%). Echter, de resulterende

productieschema's zijn mogelijk niet realistisch, omdat ze fractionele variabelen kunnen bevatten. Bovendien leidt lineaire relaxatie tot aanzienlijke verschillen in de capaciteitsfactoren voor individuele generatoren in vergelijking met het basismodel. Gemiddeld bedroeg het verschil in capaciteitsfactor 6,4% over 30 runs en 15 UC-probleemgevallen, met een maximaal verschil van 37,7% tussen de relaxatie en het basismodel. Ten tweede, wanneer het doel is om de niet-geleverde elektriciteit te minimaliseren in plaats van de totale systeemkosten, heeft de lineaire relaxatie exact dezelfde hoeveelheid niet-geleverde elektriciteit als het basismodel. Ten derde hebben we ontdekt dat het gebruik van een lineaire benadering van de kwadratische generatiekostenfunctie goede resultaten opleverde met gemiddeld maar een 0,11% kostenverschil. Het gebruik van een stuksgewijze lineaire benadering met meerdere segmenten verminderde het verschil tussen de werkelijke evaluatie en de benadering verder, maar tegen een aanzienlijk hogere rekentijd: het gebruik van 3 segmenten in plaats van 1 verdubbelde de rekentijd zonder significante verbetering (slechts 0,01% verschil in de doelfunctie).

Alle andere vereenvoudigingen van het UC-model worden niet aanbevolen. Ten eerste resulteerde het weglaten van minimale aan- en uit-tijd meestal in langere rekestijden en de opstartkosten onafhankelijk maken van de tijd versnelde het proces niet, terwijl beide vereenvoudigingen resulteerden in verlies van kwaliteit van de oplossingen. Ten tweede leidde het weglaten van opregel-limieten en reservebeperkingen tot een model dat gemiddeld twee keer zo snel was, maar ten koste van te veel kwaliteitsverlies. Zonder de opregel-limieten was de totale waarde van de doelfunctie voor een UC-testprobleem gemiddeld 5% lager dan de kosten van het basismodel en de inzet van generatoren was aanzienlijk anders met gemiddeld een verschil van 12% in capaciteitsfactoren in vergelijking met die van het basismodel. Tot slot, vereenvoudigingen van het transmissiesysteem kunnen de berekeningstijd versnellen maar het verschil in totale systeemkosten is buitengewoon hoog. Voor één geval werd de totale kostprijs gemiddeld met 50% onderschat wanneer gedetailleerde transmissiebeperkingen werden weggelaten.

In **hoofdstuk 3** worden twee algoritmes gepresenteerd die het single-unit commitment probleem (1UC) oplossen, een speciaal geval van het UC-probleem waarbij gezocht wordt naar een optimaal productieschema's voor slechts één generator, rekening houdend met productielimieten, minimum aan- en uit-tijd en opregel-limieten. In dit probleem is het niet nodig dat de generator aan een elektriciteitsvraag voldoet, maar wordt er een tijdreeks van elektriciteitsprijzen gegeven die bepaalt hoeveel opbrengst de generator kan maken als hij produceert. In dit hoofdstuk zijn twee dynamische programmeer algoritmen geïntroduceerd op basis van twee verschillende recursieve vergelijkingen. Het eerste algoritme is geschikt voor elke convexe kostenfunctie, terwijl het tweede algoritme alleen kan worden toegepast op lineaire of stuksgewijs lineaire kostfuncties.

Voor de eerste recursievergelijking hebben we meerdere functies F_t^τ gedefinieerd die voor elke geldige productieniveau p_t de kosten van het optimale schema teruggeven waarbij de generator op tijdstap t gedurende de laatste τ tijdstappen aan staat en p_t produceert tijdens tijdstap t . Door deze functies inductief te creëren konden we irrelevante functies identificeren en verwijderen. Dit resulteert in een tijdscomplexiteit van $O(nmk^2)$, waarbij k het maximale aantal relevante functies is

en m het maximale aantal stukken van de stuksgewijs convexe functies F_t^τ . We hebben aangetoond dat voor de UC-probleem verzameling die in hoofdstuk 2 is geïntroduceerd, k hoogstens 5 was en m hoogstens 10, en dat deze waarden niet toenamen wanneer het aantal tijdstappen werd verhoogd. Bovendien hebben we experimenteel aangetoond dat dit resulteert in een rekentijd die lineair toeneemt met het aantal tijdstappen. Dit verbetert de kwadratische groei van eerdere algoritmen.

Voor het tweede dynamische programmeeralgoritme werd een andere recursievergelijking H_t^τ geïntroduceerd. Deze functies zijn moeilijker te creëren dan F_t^τ . Er wordt in hoofdstuk 3 echter aangetoond dat het speciale geval waarin de generatie kostfunctie stuksgewijs lineair is, we slechts een beperkt aantal punten in de verzameling Q hoeven bij te houden om deze functies te representeren. De methode om de kosten alleen op een beperkt aantal punten weer te geven, is niet nieuw. Maar deze methode werkt voor ongelijke opwaartse en neerwaartse regellimieten, waar eerdere onderzoeken alleen de situatie behandelden waarin deze limieten aan elkaar gelijk waren, en we hebben laten zien hoe de waarde bij Q efficiënt berekend kan worden. Dit heeft geresulteerd in een verbeterd algoritme qua universaliteit en tijdscomplexiteit van $O(n \cdot |Q|)$.

Om de geïntroduceerde algoritmes te testen zijn experimenten uitgevoerd met generatorgegevens van meerdere energiesystemen. De resultaten tonen aan dat onze algoritmen beter presteren dan andere methoden voor zowel stuksgewijs lineaire als kwadratische generatiekosten. Beide methoden verbeteren de tijdefficiëntie en lossen het single-unit commitment probleem voor grote tijdsperiodes (1000 tijdstappen) in enkele milliseconden op.

In **hoofdstuk 4** wordt er een nieuw Alternating Direction Method of Multipliers (ADMM) algoritme gepresenteerd dat het UC-probleem oplost. Ten eerste hebben we een standaard UC-formulering omgezet naar de Augmented Lagrangian door de randvoorwaarde dat vraag en aanbod gelijk moet zijn te versoepelen. Vervolgens hebben we dit nieuwe probleem opgelost met ADMM, een iteratief algoritme. In elke iteratie hebben we de deelproblemen opgelost die ontstaan door het versoepelen van de vraag en aanbod gelijkheid. Deze deelproblemen waren relatief eenvoudig op te lossen omdat er veel efficiënte methoden bestaan voor deze problemen. Het gebruik van ons snelle algoritme voor het 1UC probleem dat geïntroduceerd werd in hoofdstuk 3, maakt veel iteraties mogelijk, zodat ADMM convergeert naar een kwalitatief hoogwaardige oplossing.

Experimenten met een grote set UC instanties hebben aangetoond dat ons algoritme op elke UC instantie hoogwaardige oplossingen produceert, die gemiddeld slechts 0,15% verwijderd zijn van het optimum. Voor probleeminstanties met kwadratische kosten is het sneller (gemiddeld ongeveer 195 keer sneller) dan het oplossen met een state-of-the-art Mixed Integer Quadratic Programming (MIQP) formulering voor UC. Voor lineaire instanties is het competitief en begint het beter te presteren dan een MILP solver wanneer de tijdshorizon groot wordt. De tijdscomplexiteit lijkt bijna lineair te groeien met het aantal tijdstappen. Bij het oplossen van instanties met een lange tijdshorizon kan onze methode in enkele seconden een hoogwaardige oplossing vinden, terwijl de MIP-solver na 1 uur geen goede oplossing kon vinden. UC-problemen met een lange tijdshorizon komen

veel voor in grootschalige energienetwerkmodellen die meer dan enkele dagen, bijvoorbeeld weken of zelfs maanden, beslaan, of in kort termijn UC-problemen met een hoge temporele resolutie. Bovendien kunnen de deelproblemen vanwege de losgekoppelde aard van een ADMM-algoritme gemakkelijk worden aangepast om elementen van het energienetwerk gedetailleerder te modelleren of om de tijdscomplexiteit van de deelproblemen te verbeteren en zo nog snellere resultaten te behalen.

In **hoofdstuk 5** wordt de significantie van veelgebruikte indicatoren onderzocht door (sub)optimale oplossingen van verschillende UC-problemen te genereren, en wordt er aangetoond dat de waarde van desbetreffende indicatoren in deze oplossingen vaak willekeurig is. Dit werd geïllustreerd door meerdere experimenten uit te voeren op zes scenario's van een toekomstig Europees energienetwerk voor de doeljaren 2030 en 2040, gecreëerd door ENTSO-E, het Europese netwerk van transmissiesysteembeheerders. Elk scenario werd meerdere keren uitgevoerd met extra doelfuncties, zoals het minimaliseren en maximaliseren van de capaciteitsfactoren van generatoren, emissies en het aantal loss of load hours (LOLH), terwijl de originele doelfunctie gelijk bleef. Op deze manier vonden we de maximale en minimale waarden van deze indicatoren die technisch gezien kunnen voorkomen in het UC-model wanneer systeemkosten worden geminimaliseerd, en identificeerde we zo hoeveel deze indicatoren kunnen variëren binnen equivalente (sub)optimale oplossingen.

We ontdekten dat het verschil in de LOLH-metrick tot wel een factor 38 kon zijn voor individuele probleeminstanties. Ook zagen we dat het totale verschil tussen de gemiddelde minimale en de gemiddelde maximale waarde, afhankelijk van het niveau van detail in het model, varieerde van een factor 1.5 tot 2.8, terwijl alle oplossingen dezelfde optimale doelkosten hadden.

Bij de experimenten met betrekking tot de capaciteitsfactoren (CF) en CO₂-emissies werden UC-oplossingen bestudeerd die 0,1%, 0,5% en 1% verwijderd waren van het optimum. De CF-verschillen van kolengestookte, gasgestookte en kerncentrale-generatoren zijn afhankelijk van hoe dicht de oplossingen bij het optimum lagen. Zo vonden we bijvoorbeeld twee oplossingen voor een UC-instantie binnen 1% van het optimum, waarbij de gemiddelde CF van alle kolengestookte generatoren 0% of 20% kon zijn. Het verschil tussen de gemiddelde minimale CF en de gemiddelde maximale CF voor kolencentrales was een factor 5.3. Voor gasgestookte en kerncentrale-generatoren waren deze respectievelijk 2.8 en 1.2. Ten slotte was het verschil in CO₂-emissies minder uitgesproken tussen equivalente kostenoplossingen van een UC-instantie, aangezien de CO₂-emissies gemiddeld konden variëren met een factor 1,1 tot 1.4.

In dit hoofdstuk hebben we laten zien dat we de spreiding van de metrick LOLH deels kunnen verminderen door meer details in ons model op te nemen, zoals het toevoegen van flexibiliteitsbeperkingen, op- en afregellimieten en minimale aan- en uittijden, en kosten op het gebruik van transmissielijnen. Het is echter niet aan te raden extra detail toe te voegen louter om deze spreiding te verminderen. Dit hoofdstuk laat in plaats daarvan zien dat er zorgvuldigheid betracht moet worden bij het gebruik van elke indicator die niet expliciet geoptimaliseerd is. Deze indicatoren zijn secundaire kenmerken van de oplossingen en worden vaak

niet opgenomen in de doelfunctie, dus ze moeten niet als primaire focus worden gebruikt bij de analyse van deze oplossingen. Een robuustere aanpak zou kunnen zijn om alleen te focussen op de elementen die zijn opgenomen in de doelfunctie en die worden gebruikt in het optimalisatiemodel. Bijvoorbeeld, het gebruik van de totale niet-geleverde elektriciteit (ENS) als maatstaf voor leveringzekerheid ten opzichte van het gebruik van LOLH. ENS wordt expliciet gemodelleerd in de doelfunctie met een hoge coëfficiënt, en als gevolg daarvan hebben (sub)optimale oplossingen doorgaans dezelfde of vergelijkbare ENS-waarden.

In **hoofdstuk 6** is de relatie tussen weer en niet-geleverde elektriciteit (ENS) onderzocht. We hebben 12 toekomstige scenario's voor het Europese elektriciteitssysteem gesimuleerd door een uur gebaseerd model van het elektriciteitssysteem te draaien met vraag- en hernieuwbare energiepatronen voor 28 weerjaren. Vervolgens zijn weerregimes geïdentificeerd op het moment dat er sprake is van niet-geleverde elektriciteit. Weerregimes verwijzen naar grootschalige atmosferische patronen die in dit onderzoek worden gegroepeerd volgens atmosferische toestanden in zes classificaties, waarbij elke dag wordt toegewezen aan een specifiek weerregime. De resultaten tonen aan dat in de meeste regio's een bepaald weerregime de meeste situaties veroorzaakt waarin niet alle elektriciteit geleverd kan worden. Echter, in elke regio kan niet-geleverde elektriciteit nog steeds voorkomen onder elk weerregime, zij het met een kleinere waarschijnlijkheid. Ons onderzoek heeft uitgewezen dat in West- en Centraal-Europese landen tijden met niet-geleverde elektriciteit samenvallen met de weerpatronen van positieve Scandinavian Blocking (SB+) en North Atlantic Oscillation (NAO+). SB+ wordt gekenmerkt door koud en windstil weer met minder zonne-energie en NAO+ wordt gekenmerkt door koudere temperaturen en minder zonne-energie in het zuidelijke deel van Europa. Bovendien hebben we waargenomen dat de relatieve prevalentie van SB+ ongeveer 10 dagen voorafgaand aan een ENS-gebeurtenis haar piek bereikt. Dit suggereert dat de langdurige SB+ weersituatie de opslag van energie beperkt in deze landen. Voor Scandinavische en Baltische landen geven de resultaten aan dat het weerpatroon negatieve Atlantic Ridge (AR-) vaker voorkomt tijdens en voorafgaand aan ENS-gebeurtenissen. Dit weerpatroon wordt geassocieerd met zonnig maar koud weer in Noordoost-Europa. Dit hoofdstuk toont een duidelijke correlatie tussen specifieke weerregimes en niet-geleverde energie voor enkele Europese landen.

Acknowledgements

I would like to express my sincere gratitude and appreciation to all those who have supported me throughout this challenging yet fulfilling journey of pursuing my PhD.

First and foremost, I would like to extend my deepest gratitude to my beloved wife, Roos. I am truly blessed to have her by my side and without her I could have never finished or started my PhD.

I would also like to thank Marjan. There were many times I barged into her room and unloaded one of my many “genius” ideas. Whether they were really genius is beside the point but she always listened and tried to poke holes in them. The first part made my PhD enjoyable and the second part improved my ideas, turned them into articles and in turn made me a better researcher.

Being a good listener also applies to Machteld. Whether it was spoken or written, no word was left unturned. In the form of feedback for which I am retroactively absolutely grateful for. Or in conversation where I sometimes tried to mumble away details but they never had a chance to slip by. This characteristic stems from a passion about the topic, the same passion that brought people together with PhD-meetings either online or at your home or in the form of trips to a trading floor (which inspired my current work).

I would also like to express my sincere appreciation to my promotor, Ernst Worrell, for his support and guidance throughout this research journey.

Furthermore, I would like to extend my heartfelt thanks to my dear work colleagues, Jing and Laurens. The countless discussions, brainstorming sessions, and shared experiences have enriched my research development. Moreover, I would like to express my sincere gratitude to the many people at KNMI and TenneT, Arno, Frank, Gerard amongst others, that guided the topics of the project.

I would also thank my friends that in varying degrees supported me during my PhD. In an undefined particular order I would like to thank: **Niels**, *Vincent*, Rijk, **Jetze**, Mart, *Jelle* and **Koos**. Especially those in bold or italics or underscored I would like to thank.

Lastly, I would like to thank my family and our newest family member: my son David. Although the substance of his feedback is often overstated I did feel unconditional support by him merely existing.

Curriculum vitae

Rogier Hans Wuijts was born on 14 April 1993 in Zevenaar. In 2016 he obtained a bachelor's degree in Artificial Intelligence from the Utrecht University. In 2018 he completed a masters degree Computing Science, cum laude, also from the Utrecht University. During the bachelor and master at the Utrecht University he worked as a teaching assistant for multiple courses and as a research assistant for a small programming project. In 2018 he started as a PhD student at the Copernicus Institute of Sustainable Development and at the Department of Information and Computing Science at the Utrecht University under the supervision of dr. ir. Marjan van den Akker, dr. ir. Machteld van den Broek and prof. dr. Ernst Worrell. As of May 2023 he works as Portfolio Quant at PZEM.

Chapter 8

Appendices

8.1 Appendix Chapter 2

8.1.1 Additional Tight Constraints

We will briefly describe these constraints here but to get a better understanding of what the effect is of using different but equivalent formulations we recommend the article of Knueven et al. [14].

The following equations only hold for generators with a minimum up time of 1 denoted with G^1 . The maximum generation is limited by a combination of the startup and shutdown limit.

$$\begin{aligned} p'_{gt} &\leq (\bar{P}_g - \underline{P}_g)u_{gt} - (\bar{P}_g - SU_g)v_{gt} \\ &\quad - [SU_g - SD_g]^+ w_{gt+1} \\ g &\in G^1 \end{aligned} \quad (8.1)$$

$$\begin{aligned} p'_{gt} &\leq (\bar{P}_g - \underline{P}_g)u_{gt} - (\bar{P}_g - SD_g)w_{gt+1} \\ &\quad - [SD_g - SU_g]^+ v_{gt} \\ g &\in G^1 \end{aligned} \quad (8.2)$$

where $[\cdot]^+$ is defined as the maximum of 0 and the value within the brackets.

For the generators with a minimum up time larger than 1, $G^{>1}$, we can limit the maximum generation with the startup limit plus the ramping limit times the number of timesteps the generator is on (iRU_g in the equation).

$$\begin{aligned} p'_{gt} &\leq (\bar{P}_g - \underline{P}_g)u_{gt} - (\bar{P}_g - SD_g)w_{gt+1} \\ &\quad - \sum_{i=0}^{\min\{UT_g-2, \lfloor \frac{\bar{P}_g - SU_g}{RU_g} \rfloor\}} (\bar{P}_g - SU_g - iRU_g)v_{t-i} \\ g &\in G^{>1}, t \in T \end{aligned} \quad (8.3)$$

$$\begin{aligned} p'_{gt} &\leq (\bar{P}_g - \underline{P}_g)u_{gt} \\ &\quad - \sum_{i=0}^{\min\{UT_g-1, \lfloor \frac{\bar{P}_g - SU_g}{RU_g} \rfloor\}} (\bar{P}_g - SU_g - iRU_g)v_{gt-i} \\ g &\in G^{UT_g > 1, (UT_g - 2) < \lfloor \frac{\bar{P}_g - SU_g}{RU_g} \rfloor}, t \in T \end{aligned} \quad (8.4)$$

We can do something similar for the shutdown and ramp down limit:

$$\begin{aligned}
p'_{gt} &\leq (\bar{P}_g - \underline{P}_g)u_{gt} \\
&\quad - \sum_{i=0}^{K^{SD_t}} (\bar{P}_g - SD_g - iRD)w_{t+1+i} \\
&\quad - \sum_{i=0}^{K^{SU_t}} (\bar{P}_g - SU_g - iRU)v_{t-i} \\
g &\in G^{>1}, t \in T
\end{aligned} \tag{8.5}$$

$$\begin{aligned}
K^{SD_t} &= \min\{\lfloor \frac{\bar{P} - SD}{RD} \rfloor, UT - 1, |T| - t - 1\} \\
K^{SU_t} &= \min\{\lfloor \frac{\bar{P} - SU}{RU} \rfloor, UT - 2 - [K^{SD_t}]^+, t - 1\}
\end{aligned}$$

where K^{SD_t} is the amount of timesteps to go from \bar{P}_g to SD_g at time t and K^{SU_t} is the amount of timesteps it takes to go from SU_g to \bar{P}_g at time t .

The inequalities of (8.1) and (8.2) come from Gentile et al. [8], (8.3) comes from Pan and Guan [20] and (8.4) and (8.5) are novel constraints from Kneuen et al. They all constrain the production level range reflecting the prolonged effect of ramping limits over multiple timesteps. For example, two timesteps after a generator has been started the total production level can never exceed $SD_g + 2RU$.

8.1.2 Additional Figures and Tables

Instance	Model	Time	MIP-Gap	L1Norm	ACFD	MCFD	Cost-Gap	% Fractional	% Ramp Up Violation	% Ramp Down Violation	% Min Up Violation	% Min Down Violation
GA10	Base	1.98	0.0012	0	0	0	0	0	0	0	0	0
	$Model^{Tight}$	1.81	0.0014	0	0.01	0.03	0	0	0	0	0	0
	$Model_{LP}$	0.06	0	0.14	5.24	18.37	0.017	39.35	0	0	0	0
	$Model_{LP}^{Tight}$	0.1	0	0.09	4.03	11.16	0.0098	31.07	0	0	0	0
	$Model^{Ramp}$	0.26	0.0013	0.19	12.18	25.93	0.051	0	6.47	6.64	0	0
	$Model^{MUMD}$	7.24	0.0013	0	0.19	0.9	0.0002	0	0	0	0	2.21
	$Model^{TDSUC}$	1.55	0.0011	0	0.15	0.77	0.001	0	0	0	0	0
	$Model^{Reserve}$	0.97	0.0038	0.17	8.44	19	0.0463	0	0	0	0	0
	$Model^{All}$	0.07	0.0005	0.28	15.32	36.69	0.0785	0	12.76	12.91	17.43	8.98
RTS26	Base	4.03	0.0073	0	0	0	0	0	0	0	0	0
	$Model^{Tight}$	3.68	0.0078	0.01	0.2	1.71	0	0	0	0	0	0
	$Model_{LP}$	0.26	0	0.11	5.26	22.78	0.0214	11	0.26	0	0	0
	$Model_{LP}^{Tight}$	0.32	0	0.1	4.98	26.92	0.0209	9.08	0.27	0	0	0
	$Model^{Ramp}$	4.36	0.008	0.13	5.52	20.86	0.022	0	3.1	0.83	0	0
	$Model^{MUMD}$	9.29	0.0091	0.01	0.27	2.09	0	0	0	0	0	4.66
	$Model^{Reserve}$	2.98	0.0071	0.02	0.57	3.32	0.0008	0	0	0	0	0
	$Model^{All}$	1.02	0.0059	0.11	5.01	27.67	0.0235	0	3.19	0.73	3.67	2.76
TAI38	Base	3.37	0.0079	0	0	0	0	0	0	0	0	0
	$Model^{Tight}$	3.38	0.0074	0.01	0.38	5.89	0	0	0	0	0	0
	$Model_{LP}$	0.26	0	0.03	1.5	13.45	0.0017	6.88	0	0.1	0	0
	$Model_{LP}^{Tight}$	0.28	0	0.02	1.3	13.18	0.0015	6.45	0	0.06	0	0
	$Model^{Ramp}$	1.91	0.0065	0.04	4.52	32.91	0.018	0	3.76	3.26	0	0
	$Model^{MUMD}$	3.09	0.0074	0.02	1.46	17.83	0.0005	0	0	0	0	6.95
	$Model^{Reserve}$	3.65	0.0043	0.06	4.04	46.01	0.0196	0	0	0	0	0
	$Model^{All}$	1.08	0.0063	0.08	5.54	49.17	0.0328	0	4.13	4.12	0	14
RCUC50	Base	81.58	0.0093	0	0	0	0	0	0	0	0	0
	$Model^{Tight}$	67.15	0.0086	0.01	0.95	13.86	0	0	0	0	0	0
	$Model_{LP}$	0.52	0	0.11	5.54	19.82	0.0065	32.45	0.79	1.43	0	0
	$Model_{LP}^{Tight}$	0.77	0	0.09	4.37	17.41	0.004	23.94	0.01	0.39	0	0
	$Model^{Ramp}$	31.05	0.0089	0.09	6.34	27.53	0.0109	0	2.76	2.66	0	0
	$Model^{MUMD}$	465.92	0.0121	0.06	4.25	24.68	0.0026	0	0	0	12.82	15.65
	$Model^{Reserve}$	46.3	0.0088	0.08	6.49	38.81	0.0168	0	0	0	0	0
	$Model^{All}$	8.41	0.0095	0.11	7.87	32.76	0.0306	0	2.92	2.75	18.64	19.09
RTS54	Base	600.47	0.0623	0	0	0	0	0	0	0	0	0
	$Model^{Tight}$	600.5	0.0615	0.03	1.31	14.69	0	0	0	0	0	0
	$Model_{LP}$	6.57	0	0.09	5.25	26.34	0.0127	20.19	1.18	1.57	0	0
	$Model_{LP}^{Tight}$	7.1	0	0.06	3.59	27.97	0.0091	14.09	0.16	0	0	0
	$Model^{Ramp}$	600.62	0.0365	0.05	2.05	17.73	0.0066	0	5.37	4.64	0	0
	$Model^{MUMD}$	600.5	0.0539	0.05	3.17	19.41	0.003	0	0	0	1.55	1.76
	$Model^{TDSUC}$	600.57	0.0649	0.05	3.45	27.88	0.0082	0	0	0	0	0
	$Model^{Reserve}$	600.37	0.0596	0.03	1.47	13.93	0.0011	0	0	0	0	0
	$Model^{All}$	558.89	0.0234	0.09	6.04	32.16	0.0193	0	6.19	5.26	0	2.64

Table 8.1: The performance indicators of $Model$, $Model^{Tight}$ model and the 7 relaxed models for 15 instances of the power system. Values represent the averages over 30 runs of the model-instance combination.

Instance	Model	Time	MP-Gap	L1Norm	ACFD	MCFD	Cost-Gap	% Fractional	% Ramp Up Violation	% Ramp Down Violation	% Min Up Violation	% Min Down Violation
GMLC73	Base	12.51	0.006	0	0	0	0	0	0	0	0	0
	$Model^{Tight}$	16.2	0.0052	0	0.25	5.63	0	0	0	0	0	0
	$Model_{LP}$	0.71	0	0.01	0.7	11.19	0.0026	1.61	0	0.12	0	0
	$Model_{LP}^{Tight}$	0.72	0	0.01	0.7	11.41	0.0025	1.93	0	0.13	0	0
	$Model^{Ramp}$	1.56	0.0047	0.01	1.83	18.24	0.0079	0	4.45	4.87	0	0
	$Model^{MUMD}$	10.88	0.0053	0	0.28	6.8	0	0	0	0	0	0
	$Model^{TDSUC}$	12.96	0.0069	0	0.24	5.79	0	0	0	0	0	0
	$Model^{Reserve}$	1.93	0.0058	0.02	2.72	31.73	0.0207	0	0	0	0	0
	$Model^{All}$	0.27	0.002	0.02	3.16	34.26	0.026	0	4.63	5.97	3.33	0
RTS96	Base	302.89	0.012	0	0	0	0	0	0	0	0	0
	$Model^{Tight}$	305.66	0.0115	0	0.21	7.33	0	0	0	0	0	0
	$Model_{LP}$	4	0	0.02	1.3	33.39	0.0009	6.84	0	0	0	0
	$Model_{LP}^{Tight}$	3.57	0	0.02	1.16	24.76	0.0007	6.35	0	0	0	0
	$Model^{Ramp}$	205.81	0.0101	0.01	0.58	15.06	0.0003	0	0.87	0.98	0	0
	$Model^{MUMD}$	600.51	0.0512	0.02	1.21	23.86	0.0019	0	0	0	23.52	0
	$Model^{TDSUC}$	170.26	0.01	0.02	1.39	31.82	0.0048	0	0	0	0	0
	$Model^{Reserve}$	248.36	0.0108	0	0.22	6.74	0	0	0	0	0	0
	$Model^{All}$	78.45	0.0093	0.03	2.18	47.34	0.009	0	1.26	1.14	25.6	1.74
A110	Base	10.37	0.0072	0	0	0	0	0	0	0	0	0
	$Model^{Tight}$	11.84	0.0071	0.01	0.35	5.84	0	0	0	0	0	0
	$Model_{LP}$	1.13	0	0.05	1.58	14.49	0.0014	13.87	0	0	0	0
	$Model_{LP}^{Tight}$	1.19	0	0.03	1.03	10.7	0.0006	8.13	0	0	0	0
	$Model^{Ramp}$	6.72	0.0079	0.09	4.24	35.14	0.0096	0	9.06	8.74	0	0
	$Model^{MUMD}$	15.88	0.0085	0.07	2.24	12.88	0.0053	0	0	0	17.04	15.25
	$Model^{TDSUC}$	10.54	0.0066	0.01	0.45	6.89	0.0002	0	0	0	0	0
	$Model^{Reserve}$	5.64	0.0068	0.11	3.64	22.8	0.0126	0	0	0	0	0
	$Model^{All}$	0.34	0.007	0.16	6.44	34.42	0.0209	0	12.46	11.75	19.94	17.73
KOR140	Base	600.43	0.0576	0	0	0	0	0	0	0	0	0
	$Model^{Tight}$	600.41	0.0546	0.03	0.87	15.26	0	0	0	0	0	0
	$Model_{LP}$	1.39	0	0.04	1.37	14.83	0.0026	7.39	0.49	0.09	0	0
	$Model_{LP}^{Tight}$	1.38	0	0.04	1.08	15.78	0.0013	5.95	0.1	0.09	0	0
	$Model^{Ramp}$	479.35	0.0119	0.05	2.04	19.96	0.0317	0	1.73	1.4	0	0
	$Model^{MUMD}$	572.75	0.014	0.08	3.86	19.51	0.0543	0	0	0	3.31	23.41
	$Model^{TDSUC}$	600.36	0.0515	0.03	0.95	14.91	0.0017	0	0	0	0	0
	$Model^{Reserve}$	513.29	0.0134	0.08	4.87	40.68	0.031	0	0	0	0	0
	$Model^{All}$	6.7	0.0092	0.12	6.62	35.07	0.088	0	1.64	1.01	0.43	24.86
OSTRO182	Base	196.83	0.0086	0	0	0	0	0	0	0	0	0
	$Model^{Tight}$	115.8	0.0079	0.06	5.44	42.25	0	0	0	0	0	0
	$Model_{LP}$	0.87	0	0.1	6.44	37.71	0.003	24.59	0.09	0.81	0	0
	$Model_{LP}^{Tight}$	1.07	0	0.1	5.97	40.34	0.0023	23.02	0.11	0.96	0	0
	$Model^{Ramp}$	26.86	0.0086	0.11	8.31	46.47	0.0068	0	6.48	6.39	0	0
	$Model^{MUMD}$	411.62	0.0086	0.06	5.63	41.42	0.0002	0	0	0	1.47	4.42
	$Model^{TDSUC}$	163.7	0.0086	0.06	5.75	41.81	0.0008	0	0	0	0	0
	$Model^{Reserve}$	348.2	0.0098	0.15	10.24	50.82	0.0226	0	0	0	0	0
	$Model^{All}$	522.72	0.011	0.19	11.18	55.79	0.029	0	4.32	4.17	28.12	3.86

Table 8.2: Table continued

Instance	Model	Time	MIP-Gap	LiNorm	ACFD	MCFD	Cost-Gap	% Fractional	% Ramp Up Violation	% Ramp Down Violation	% Min Up Violation	% Min Down Violation
RCUC200	Base	598.62	0.0176	0	0	0	0	0	0	0	0	0
	<i>Model^{Tight}</i>	583.14	0.0174	0.01	0.9	23.03	0	0	0	0	0	0
	<i>Model_{LP}</i>	3.55	0	0.09	4.73	25.82	0.0045	25.92	1.21	1.34	0	0
	<i>Model_{LP}^{Tight}</i>	5.39	0	0.07	3.63	22.98	0.0025	19.25	0.19	0.54	0	0
	<i>Model_{Ramp}</i>	600.45	0.0171	0.07	5.38	30.03	0.0103	0	2.43	2.36	0	0
	<i>Model^{MUMD}</i>	600.83	0.0199	0.04	2.95	24.03	0.0013	0	0	0	9.63	13.18
	<i>Model^{Reserve}</i>	268.23	0.0083	0.06	5.2	40.7	0.0147	0	0	0	0	0
	<i>Model^{All}</i>	365.52	0.0099	0.1	6.76	37.62	0.0277	0	2.25	2.01	15.59	16.37
HUB223	Base	600.4	0.2682	0	0	0	0	0	0	0	0	0
	<i>Model^{Tight}</i>	600.41	0.2735	0.01	0.29	21.31	0	0	0	0	0	0
	<i>Model_{LP}</i>	6.14	0	0.02	0.93	48.84	0.009	5.69	0.08	0	0	0
	<i>Model_{LP}^{Tight}</i>	6.58	0	0.02	0.91	51.8	0.009	5.53	0	0	0	0
	<i>Model_{Ramp}</i>	600.31	0.171	0.08	3.01	62.64	0.1024	0	3.21	3.13	0	0
	<i>Model^{MUMD}</i>	600.36	0.2711	0.01	0.34	22.28	0	0	0	0	0	0
	<i>Model^{TDSUC}</i>	600.47	0.246	0.03	1.3	63.87	0.0168	0	0	0	0	0
	<i>Model^{Reserve}</i>	33.31	0.0082	0.21	8.35	64.35	0.4348	0	0	0	0	0
DSET304	Base	21.95	0.0056	0.26	11.64	66.18	0.4921	0	12.17	5.89	0.03	0
	Base	13.79	0.0055	0	0	0	0	0	0	0	0	0
	<i>Model^{Tight}</i>	9.56	0.0047	0.02	2.43	79.53	0	0	0	0	0	0
	<i>Model_{LP}</i>	2.6	0	0.02	2.61	82.49	0.0001	0.69	0	0.21	0	0
	<i>Model_{LP}^{Tight}</i>	2.75	0	0.02	2.67	86.8	0	0.54	0	0.05	0	0
	<i>Model_{Ramp}</i>	5.67	0.005	0.05	3.97	83.46	0.0001	0	3.14	4.41	0	0
	<i>Model^{MUMD}</i>	13.3	0.0072	0.02	2.35	76.88	0	0	0	0	0	0
	<i>Model^{Reserve}</i>	14	0.0052	0.07	5.12	82.55	0	0	0	0	0	0
CA610	<i>Model^{All}</i>	3.3	0.0038	0.07	5.21	86.16	0.0001	0	2.24	3.77	0	0
	Base	100.07	0.0066	0	0	0	0	0	0	0	0	0
	<i>Model^{Tight}</i>	111.25	0.0067	0.01	0.63	42.09	0	0	0	0	0	0
	<i>Model_{LP}</i>	11.96	0	0.01	1.84	49.53	0.0006	1.47	0	0.01	0	0
	<i>Model_{LP}^{Tight}</i>	15.98	0	0.01	1.7	48.71	0.0006	1.31	0.01	0.03	0	0
	<i>Model_{Ramp}</i>	33.69	0.0073	0.01	1.61	47.35	0.0006	0	0.56	0.7	0	0
	<i>Model^{MUMD}</i>	123.08	0.0053	0.01	0.73	42.04	0	0	0	0	0	0
	<i>Model^{TDSUC}</i>	102.8	0.0062	0.02	1.36	44.64	0.0015	0	0	0	0	0
FERC934	<i>Model^{Reserve}</i>	24.53	0.0075	0.02	1.67	50.56	0.0116	0	0	0	0	0
	<i>Model^{All}</i>	4.83	0.0043	0.03	3.39	52.81	0.0138	0	0.63	0.83	0	0
	Base	30.75	0.0043	0	0	0	0	0	0	0	0	0
	<i>Model^{Tight}</i>	27.85	0.003	0	0.04	6.2	0	0	0	0	0	0
	<i>Model_{LP}</i>	21.78	0	0.04	1.72	100	0.0057	1.25	0.12	0.03	0	0
	<i>Model_{LP}^{Tight}</i>	23.84	0	0.04	1.71	100	0.0057	1.18	0.11	0.01	0	0
	<i>Model_{Ramp}</i>	19.45	0.0067	0.06	3.17	100	0.0134	0	1.98	1.92	0	0
	<i>Model^{MUMD}</i>	42.58	0.0066	0.02	0.49	55.56	0.0012	0	0	0	17.96	16.46
	<i>Model^{TDSUC}</i>	30.31	0.0037	0	0.12	33.11	0	0	0	0	0	0
	<i>Model^{Reserve}</i>	19.02	0.0059	0.06	2.74	100	0.0122	0	0	0	0	0
	<i>Model^{All}</i>	1.31	0.0031	0.08	3.58	100	0.0171	0	1.75	1.52	18.9	11.16

Table 8.3: Table continued

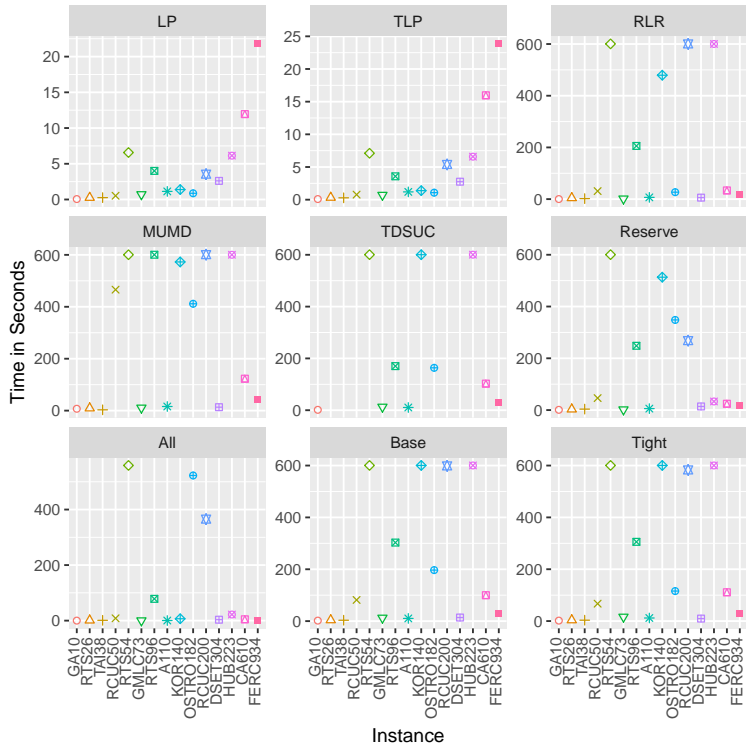


Figure 8.1: Average time in seconds of 30 runs for 15 instances and 9 models.

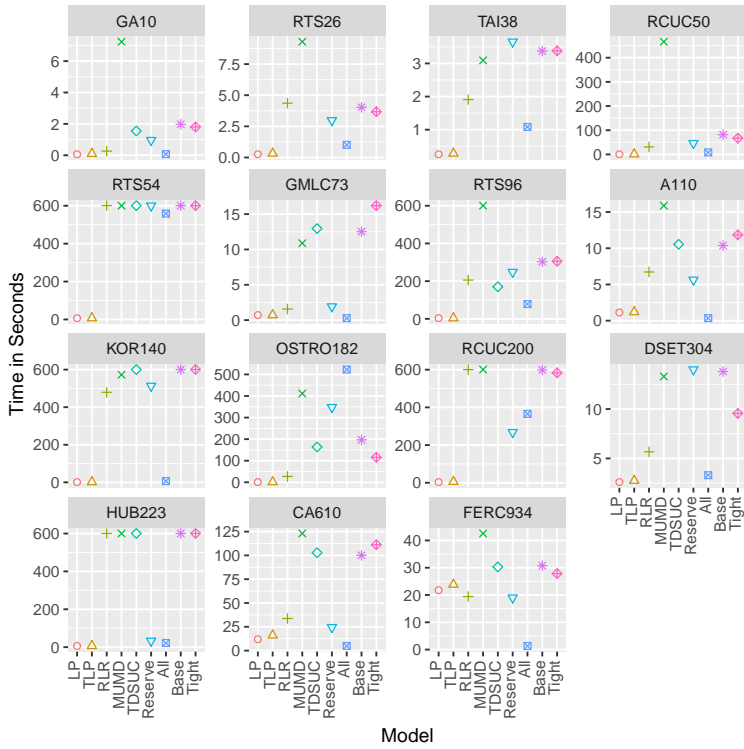


Figure 8.2: Average time in seconds of 30 runs for 9 models and 15 instances.

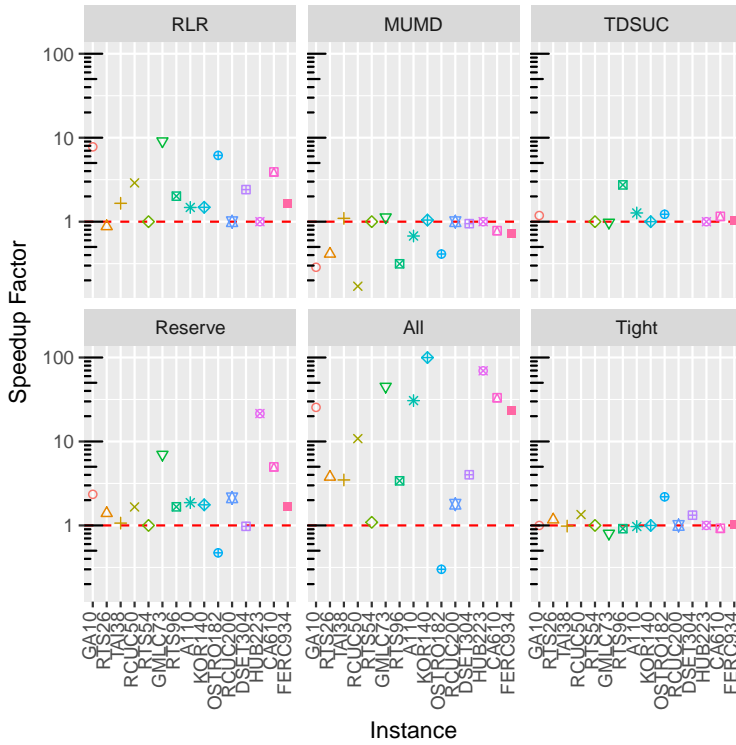


Figure 8.3: The geometric mean(because we are averaging ratio's) of the speedup factor compared to the Base model for 6 models on 15 instances.

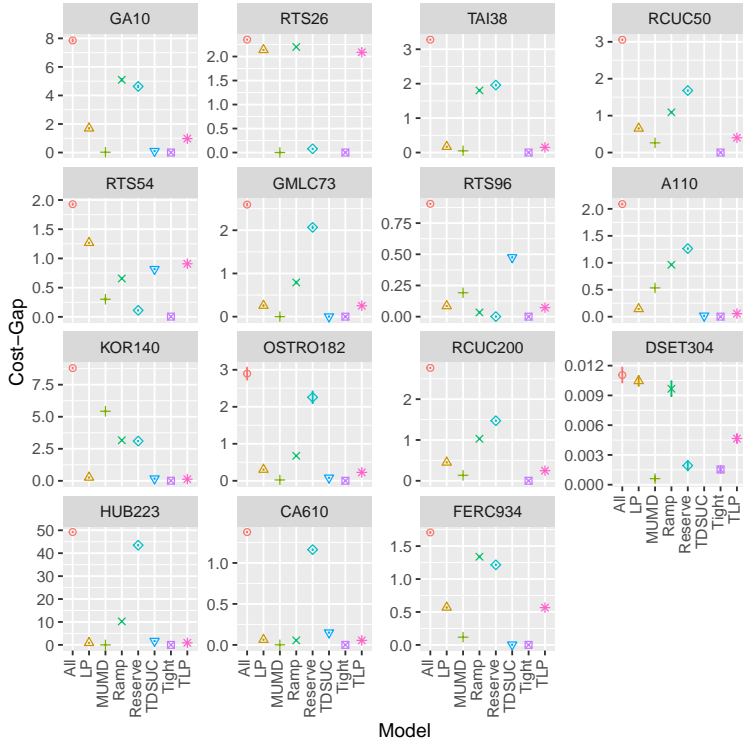


Figure 8.4: Average Cost-gap compared to the Base model of 30 runs with the 8 models for 15 instances.

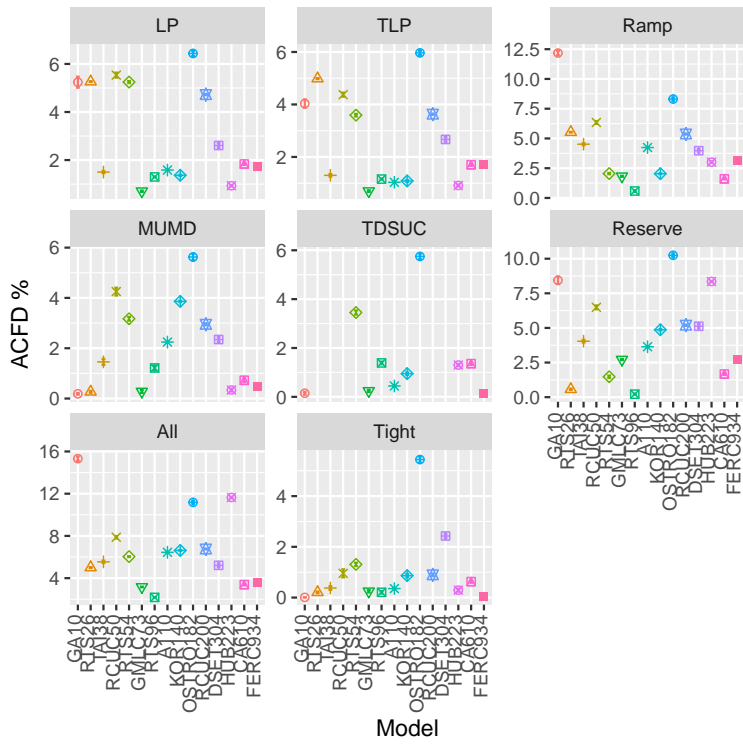


Figure 8.6: Average ACFD of 30 runs with the 8 models for 15 instances.

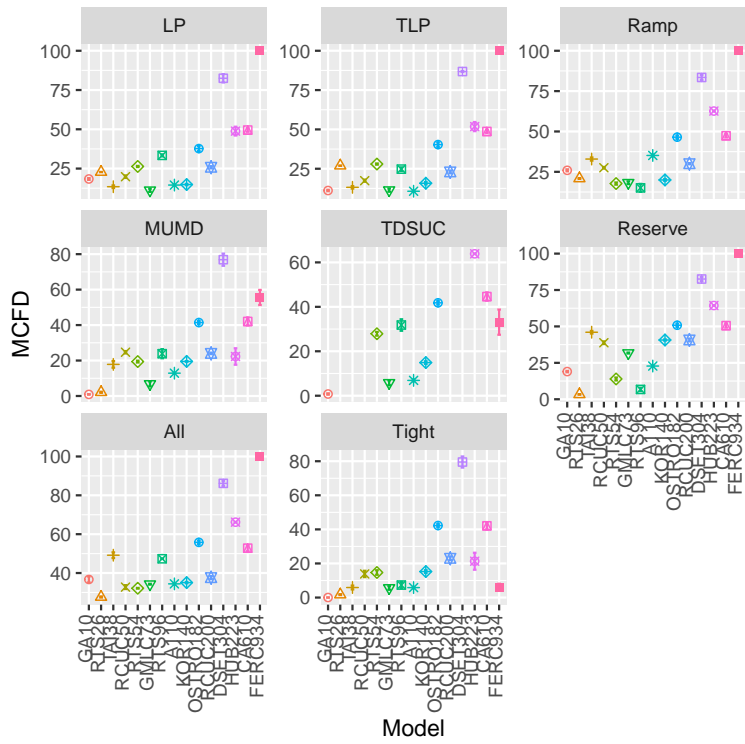


Figure 8.7: Average MCFD of 30 runs with the 8 models for 15 instances.

Instance	Number Pieces	Time (seconds)	MIP-Gap	L1Norm	ACFD	MCFD	% Gap	% Quadratic-Gap
GA10	1	0.832	0.0001	0	0	0	0	0.0770118
	2	1.214	0	0	0	0	0.0006	0.0179208
	3	1.578	0	0	0	0	0.0007	0.0075764
	4	1.731	0	0	0	0	0.00072	0.0045426
	5	1.821	0	0	0	0	0.00073	0.0027844
	10	2.845	0	0	0	0	0.00074	0.0007338
RTS26	1	1.375	0.0001	0	0	0	0	0.0320985
	2	2.124	0	0.01	0.757	4.533	0.0003	0.0083127
	3	2.549	0.0001	0.013	1.204	6.709	0.00039	0.0031116
	4	2.93	0.0001	0.009	0.899	4.62	0.00039	0.0020292
	5	3.312	0	0.012	0.993	5.349	0.0004	0.0012238
	10	4.202	0	0.01	0.977	4.407	0.0004	0.0003504
TAI38	1	2.951	0	0	0	0	0	0.4880275
	2	4.446	0.0001	0.018	2.78	23.962	0.00467	0.1397739
	3	5.392	0.0001	0.017	3.193	22.336	0.00595	0.0467517
	4	7.649	0.0001	0.013	3.066	19.548	0.00622	0.0290308
	5	7.42	0.0001	0.017	3.067	21.768	0.00638	0.0175016
	10	15.359	0.0001	0.023	3.512	25.467	0.00658	0.0042991
RCUC50	1	60.823	0.0001	0	0	0	0	0.053523
	2	103.043	0.0001	0.013	1.521	12.993	0.00052	0.0124765
	3	117.835	0.0001	0.018	2.044	17.143	0.00064	0.0044369
	4	134.615	0.0001	0.009	1.35	13.033	0.00066	0.0030241
	5	171.076	0.0001	0.011	1.555	15.168	0.00069	0.0017665
	10	313.916	0.0001	0.014	1.775	15.872	0.0007	0.0004742
A110	1	4.893	0.0001	0	0	0	0	0.216543
	2	6.056	0.0001	0.01	1.336	15.08	0.00304	0.0293861
	3	6.641	0.0001	0.01	1.448	23.84	0.00344	0.0124286
	4	7.541	0.0001	0.011	1.443	21.084	0.00363	0.0063244
	5	7.679	0.0001	0.01	1.411	21.027	0.00366	0.0049364
	10	11.88	0.0001	0.01	1.464	22.114	0.00377	0.0014096
KOR140	1	594.69	0.00018	0	0	0	0	0.0115792
	2	586.701	0.00024	0.022	0.986	21.962	0.0001	0.0036314
	3	597.28	0.00028	0.021	1.07	23.69	0.0001	0.0017275
	4	601.381	0.00026	0.02	1.082	19.98	0.00013	0.0009015
	5	601.16	0.00032	0.023	1.143	20.211	0.00011	0.000536
	10	601.045	0.00033	0.022	1.085	21.466	0.0001	0.0001702
OSTRO182	1	527.487	0.00013	0	0	0	0	0.0079862
	2	538.12	0.00016	0.072	6.575	44.9	0.00011	0.0010644
	3	589.407	0.0003	0.076	6.923	49.629	0.00013	0.000548
	4	600.499	0.00025	0.071	6.545	47.09	0.00014	0.0002805
	5	600.552	0.00025	0.071	6.667	49.146	0.00018	0.0001827
	10	600.843	0.00037	0.075	6.802	48.42	0.00013	0
RCUC200	1	203.597	0.0001	0	0	0	0	0.0523796
	2	462.718	0.0001	0.01	1.119	27.678	0.00049	0.0113307
	3	490.46	0.0001	0.009	1.254	27.508	0.00059	0.0045818
	4	511.845	0.0001	0.009	1.2	26.294	0.0006	0.0029522
	5	574.803	0.00014	0.01	1.287	27.936	0.00056	0.0018212
	10	600.629	0.00074	0.015	1.595	31.274	0.00055	0.0004569

Table 8.4: The performance indicators of models with different amounts of pieces at the piece-wise linear approximation on the quadratic generation. Values represent the averages over 30 runs of the model-instance combination.

Instance	Model	Time (seconds)	MIP-Gap	L1Norm %	ACFD %	MCFD %	Cost-Gap %	Line Constraint
D2SET1442	<i>Model</i> (PTDF)	22.075	0.0001	0	0	0	0	0
	<i>Model</i> ^{Copper}	1.364	0.0001	1.472	12.62	100	10.8739	44.2469
	<i>Model</i> ^{Trade}	7.222	0.0001	0.953	8.865	100	7.8334	20.1835
	Angles	23.274	0.0001	0.046	0.435	19.053	0.0015	0
RTS26	<i>Model</i> (PTDF)	3.693	0.0001	0	0	0	0	0
	<i>Model</i> ^{Copper}	1.804	0	0.008	0.352	3.335	0.001	0
	<i>Model</i> ^{Trade}	5.29	0.0001	0.011	0.444	4.604	0.001	0
	<i>Model</i> ^{Angles}	8.913	0.0001	0.012	0.471	4.998	0.0007	0
RTS54	<i>Model</i> (PTDF)	600.377	0.0006	0	0	0	0	0
	<i>Model</i> ^{Copper}	180.728	0.0001	0.016	1.075	10.101	0.0193	0.2398
	<i>Model</i> ^{Trade}	600.386	0.0007	0.029	1.705	15.039	0.0116	0.2351
	<i>Model</i> ^{Angles}	600.469	0.0007	0.013	1.061	10.64	0.0099	0
RTS96	<i>Model</i> (PTDF)	300.938	0.0001	0	0	0	0	0
	<i>Model</i> ^{Copper}	27.897	0.0001	0.03	2.55	51.729	0.2021	1.0764
	<i>Model</i> ^{Trade}	486.894	0.0002	0.004	0.233	8.163	0.0003	0
	<i>Model</i> ^{Angles}	500.695	0.0002	0.003	0.26	8.643	0.0004	0
DSET304	<i>Model</i> (PTDF)	18.39	0.0001	0	0	0	0	0
	<i>Model</i> ^{Copper}	7.359	0	0.09	8.53	91.511	3.3542	39.7321
	<i>Model</i> ^{Trade}	4.68	0	0.07	6.441	90.217	3.3438	25.1786
	<i>Model</i> ^{Angles}	12.421	0	0.062	5.813	93.326	0.002	0
ZUI1905	<i>Model</i> (PTDF)	0.657	0.0001	0	0	0	0	0
	<i>Model</i> ^{Copper}	0.295	0	5.182	10.814	31.543	56.9935	60.3056
	<i>Model</i> ^{Trade}	0.462	0.0001	3.24	4.987	27.96	37.5199	40.75
	<i>Model</i> ^{Angles}	0.551	0.0001	1.929	2.862	28.495	0.0017	0

Table 8.5: Performance indicators of the 4 transmission models for the 6 instances with transmission. Values represent the averages over 30 runs of the model-instance combination.

8.2 Appendix Chapter 3

Proposition 8.2.1. *If f_t is a piece-wise linear function then the break points of F_t^τ are only in B*

Proof. For $\tau = 1$ its trivial. For $\tau > 1$ assume $F_{t-1}^{\tau-1}$ only has breakpoints in B . Recall that $\min_{p_{t-1} \in [p_t - \Delta^+, p_t + \Delta^-]} F_{t-1}^{\tau-1}(p_{t-1})$ is constructed from $F_{t-1}^{\tau-1}$ by shifting the intervals of $F_{t-1}^{\tau-1}$ and introducing one new interval in the case where f_t is a piece-wise linear cost function. The new breakpoints are those already in B but shifted down by Δ^- or up by Δ^+ and if they exceed \underline{P} or \bar{P} they become \underline{P} or \bar{P} . In the first case those new points are in B by definition 2) and 3), in the later case they are in B by 1). The addition of f_t can add breakpoints caused by the fact that f_t is piece-wise linear with breakpoints at B^{f_t} . \square

Proposition 8.2.2. *If F_t^τ is a piece-wise linear function then a minimal point in interval $[p, p']$ of F_t^τ is in $B \cup \{p, p'\}$*

Proof. Suppose the optimal point p_t^* lies in $[p, p']$. Then from Proposition 8.2.1 we know $p_t^* \in B$. Suppose $p_t^* \notin [p, p']$ since F_t^τ is convex the minimal point in $[p, p']$ is as close as possible to p_t^* bounded by the interval, this is either p or p' . \square

Proposition 8.2.3. *If F_t^τ is a piece-wise linear function then the minimum value at the end of a on-period has a production value in $B \cup \{SD\}$.*

Proof. If the generator is last on at t then it can only produce $p_t \in [\underline{P}, SD]$. Combined with Proposition 8.2.2 this is minimal in $B \cup \{SD\}$. \square

The minimum value at the end of a *on-period* has a production value in $B \cup \{SD\}$. These points however do not only depend on points in $B \cup \{SD\}$. Optimal points can also depend on non-optimal points. We can iteratively capture these additional points by the set Q . That is a set of all the points from which F_t^τ is minimal plus all the points that are needed to compute the minimal points.

The recursive rules of Q come from the following observation: suppose we want to know the value of $F_t^\tau(p_t)$ for some point $p_t \in \{B \cup SD\}$. The value of this point is constructed from the minimum in $[p_t - \Delta^+, p_t + \Delta^-]$. From Proposition 8.2.2 we know this minimum is in $Q \cup \{p_t - \Delta^+, p_t + \Delta^-\}$. The set Q therefore needs to contain all the points that are on the path found by backtracking from optimal points.

From (3.28) its easy to see the three propositions also hold for H_t^τ . Moreover Q are the only points we need to store to represent H_t^τ .

8.3 Appendix Chapter 4

8.3.1 Multi-block ADMM by Variable Splitting

Another way to decompose a problem with n (sets) of variables is by variable splitting. First, we can rewrite the optimization problem of (4.2) and (4.3) (or a

problem with n variables) to the following equivalent optimization problem that has additional variables z_i that are copies of p_i :

$$\min \sum_{i=1}^n f_i(p_i) \quad (8.6)$$

s.t.

$$D - \sum_{i=1}^n z_i = 0 \quad (8.7)$$

$$p_i = z_i \quad \forall i \in \{1, \dots, n\} \quad (8.8)$$

Afterwards, we can define the augmented Lagrangian by relaxing (8.8):

$$\mathcal{L}(\mathbf{p}, \mathbf{z}, \pi) = \sum_{i=1}^n f_i(p_i) + \pi_i(p_i - z_i) + \frac{\rho}{2}(p_i - z_i)^2 \quad (8.9)$$

$$\text{s.t. } D - \sum_{i=1}^n z_i = 0 \quad (8.10)$$

The ADMM iterations are presented in Algorithm 7. The optimal values for any

Algorithm 7 Multi-block by Variable Splitting

```

1: while Stopping criteria have not been met do
2:   for all  $i = 1, \dots, n$  do
3:      $p_i^{k+1} \leftarrow \operatorname{argmin}_{p_i} \{f_i(p_i) + \pi_i^k p_i + \frac{\rho}{2}(p_i - z_i^k)^2\}$ 
4:   end for
5:    $\mathbf{z}^{k+1} \leftarrow \operatorname{argmin}_{z_1, \dots, z_n} \{\sum_{i=1}^n \pi_i^k (p_i^{k+1} - z_i) + \frac{\rho}{2}(p_i^{k+1} - z_i)^2 | D = \sum_{i=1}^n z_i\}$ 
6:   for all  $i = 1, \dots, n$  do
7:      $\pi_i^{k+1} \leftarrow \pi_i^k + \rho(p_i^{k+1} - z_i^{k+1})$ 
8:   end for
9:    $k \leftarrow k + 1$ 
10: end while

```

p_i does not depend on the other production variables because only the copied variables are coupled in (8.7). Therefore, at each iteration a similar subproblem is solved as when we used the Gauss-Seidel method. However, the difference is that the optimal value for all the copied variables must be found and more Lagrange multipliers must be updated. A main advantage of this method is that:

- At its core it is still 2-block which has convergence guaranties.
- The updates on p_1, p_2 ect. can be done in parallel instead of sequential because only the values from iteration k and not from $k + 1$ are used.

There seems to be a disadvantage of introducing multiple additional variables and Lagrange multipliers and finding the optimal values of the copied variables at

line 5 in Algorithm 7. However, it is possible to achieve the same effect with only one copied variable and one Lagrange multiplier for each relaxed constraint.

We can rewrite the z_i minimization step as follows:

$$\sum_{i=1}^n \pi_i^k (p_i^{k+1} - z_i) + \frac{\rho}{2} (p_i^{k+1} - z_i)^2 = \quad (8.11)$$

$$\sum_{i=1}^n \frac{\rho}{2} \left[(p_i^{k+1} - z_i)^2 + 2 \frac{\pi_i^k}{\rho} (p_i^{k+1} - z_i) + \left(\frac{\pi_i^k}{\rho} \right)^2 - \left(\frac{\pi_i^k}{\rho} \right)^2 \right] = \quad (8.12)$$

$$\sum_{i=1}^n \frac{\rho}{2} \left((p_i^{k+1} - z_i) + \frac{\pi_i^k}{\rho} \right)^2 - \frac{(\pi_i^k)^2}{2\rho} \quad (8.13)$$

For z_i to be optimal, we need to minimize subject to $\sum_i^n z_i = D$. We are minimizing a sum of quadratic differences $p_i^{k+1} + \frac{\pi_i^k}{\rho} - z_i$. It is easy to show (by e.g the KKT conditions) that the minimum is attained if all the differences are equal, i.e., the difference would be the same for every i and would be equal to the average difference, which implies

$$p_i^{k+1} + \frac{\pi_i^k}{\rho} - z_i = \frac{\sum_{j=1}^n (p_j^k + \frac{\pi_j^k}{\rho} - z_j)}{n} \quad (8.14)$$

Since the total sum $\sum_i^n z_i$ must be equal to D we can get z_i^{k+1} by calculating:

$$z_i^{k+1} = \frac{D}{n} + p_i^{k+1} + \frac{\pi_i^k}{\rho} - \frac{\sum_{j=1}^n (p_j^{k+1} + \frac{\pi_j^k}{\rho})}{n} \quad (8.15)$$

which simplifies to:

$$z_i^{k+1} = \frac{D}{n} - \bar{p}^{k+1} + p_i^{k+1}, \quad (8.16)$$

where $\bar{p}^{k+1} = \sum_{i=1}^n p_i^{k+1}$

If all multipliers π_i start with the same value at the beginning of the iteration then the update (Algorithm 3 line 7) would be the same for every multiplier due to (8.14). This implies that all multipliers have the same value and can be replaced by a single multiplier. Moreover, since the optimal value of z_i^{k+1} has an analytical form (8.16), we can simplify Algorithm 3 to Algorithm 4.

In fact Algorithm 4 is called the *optimal exchange* problem which in turn is a special case of the *sharing problem* [3]. *Optimal exchange* is similar to Gauss-Seidel, they both have a quadratic constant that is based on the residual load. However, they differ with respect to convergence, as *optimal exchange* is proven to be convergent, but Gauss Seidel not necessarily. Moreover, finding the optimal value of p_1, \dots, p_n can be done in parallel with *optimal exchange* but not with Gauss Seidel.

Algorithm 8 Optimal Exchange

```
1: while Stopping criteria have not been met do
2:   for all  $i = 1, \dots, n$  do
3:      $p_i^{k+1} \leftarrow \operatorname{argmin}_{p_i} \{f_i(p_i) + \lambda^k p_i + \frac{\rho}{2}(p_i - \frac{D}{n} + \bar{p}^k - p_i^k)^2\}$ 
4:   end for
5:   for all  $i = 1, \dots, n$  do
6:      $\lambda^{k+1} \leftarrow \lambda^k + \rho(\bar{p}^{k+1} - \frac{D}{n})$ 
7:   end for
8:    $k \leftarrow k + 1$ 
9: end while
```

8.3.2 Gauss Seidel Compared to Variable Splitting

An unexpected result is that the Gauss Seidel outperformed the Exchange ADMM variation by a large margin. Gauss Seidel converged faster and found heuristic solutions of better quality. For most instances the solution found by the Exchange algorithm was far from optimal (Figure 8.8), while Gauss Seidel found high-quality solutions. Therefore, for the remainder of the results and figures we only show the results of our Gauss Seidel variant.

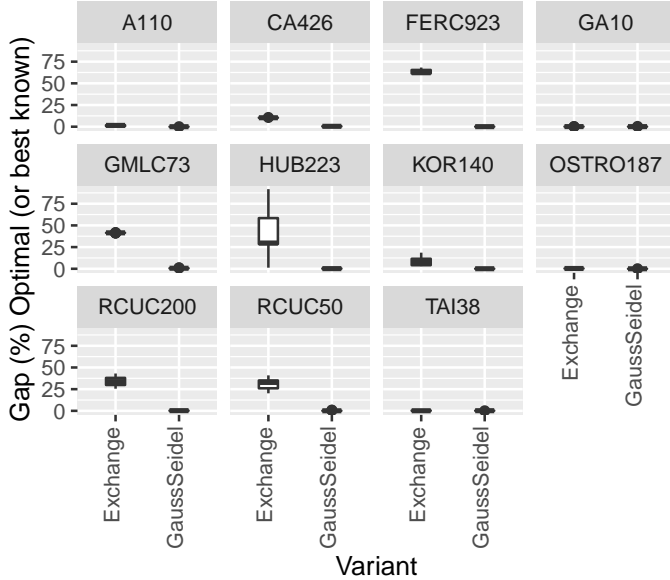


Figure 8.8: Gap when using the Exchange or Gauss Seidel ADMM variation. Time horizon for experiments were 24 hours. All instances were repeated 10 times.

8.4 Appendix Chapter 5

8.4.1 UC problem description

Our UC description contains generators, RES, storage and transmission lines. The entire UC formulation is presented in (8.17) - (8.37).

$$\min \sum_{t \in T} \sum_{g \in G} a_g u_{gt} + b_g p_{gt} + c_g p_{gt}^2 + v_{gt} cost_{start} \quad (8.17)$$

$$+ \sum_{t \in T} \sum_{n \in N} ENS_{nt} VOLL \quad (8.18)$$

$$+ \sum_{t \in T} \sum_{l \in L} f_{lt} WC \quad (8.19)$$

s.t.

$$p_{gt} \geq u_{gt} \underline{P}_g, g \in G, t \in T \quad (8.20)$$

$$p_{gt} \leq \bar{P}_g u_{gt}, g \in G, t \in T \quad (8.21)$$

$$\sum_{i=t-UT_g+1}^t v_{gi} \leq u_{gt}, t \in T, g \in G \quad (8.22)$$

$$\sum_{i=t-DT_g+1}^t w_{gi} \leq 1 - u_{gt}, t \in T, g \in G \quad (8.23)$$

$$p_{gt} - p_{gt-1} \leq (SU_g - RU_g) v_{gt} + RU_g u_{gt}, t \geq 2, g \in G \quad (8.24)$$

$$p_{gt-1} - p_{gt} \leq (SD_g - RD_g) w_{gt} + RD_g u_{gt-1}, t \geq 2, g \in G \quad (8.25)$$

$$p_{rt} \leq AF_{rt} \bar{P}_{rt}, r \in R, t \in T \quad (8.26)$$

$$0 \leq pc_{st} \leq \bar{PC}_s, t \in T, s \in S \quad (8.27)$$

$$0 \leq pd_{st} \leq \bar{PD}_s, t \in T, s \in S \quad (8.28)$$

$$p_{st} = pd_{st} - pc_{st}, t \in T, s \in S \quad (8.29)$$

$$\underline{PE}_s \leq pe_{st} \leq \bar{PE}_s, t \in T, s \in S \quad (8.30)$$

$$pe_{st} = pe_{st-1} + pc_{st} * \eta_{st}^c - \frac{pd_{st}}{\eta_{st}^d}, t \in T, s \in S \quad (8.31)$$

$$inj_{nt} = \sum_{l=(n' \rightarrow n), n' \in N} f_{lt}, t \in T, n \in N \quad (8.32)$$

$$\underline{f}_l \leq f_{lt} \leq \bar{f}_l, l \in L, t \in T \quad (8.33)$$

$$\sum_{g \in G_n} p_{gt} + \sum_{r \in R_n} p_{rt} + \sum_{s \in S_n} pd_{st} + inj_{nt} = \quad (8.34)$$

$$D_{nt} + \sum_{s \in S_n} pc_{st}, t \in T, n \in N \quad (8.35)$$

$$u_{gt} - u_{gt-1} = v_{gt} - w_{gt}, t \in T, g \in G \quad (8.36)$$

$$u_{gt}, v_{gt}, w_{gt} \in \{0, 1\}, p_{gt}, p_{rt}, p_{st}, pe_{st}, inj_{nt}, f_{lt} \in \mathbb{R} \quad (8.37)$$

(8.17) is the objective function of the UC it includes the generation and start cost. (8.18) is the system wide cost every energy that is not served, ENS_{nt} at node n and time t is multiplied by the value of lost load (VOLL) which is set at $10.000 \frac{\$}{MWh}$. (8.19) is the an additional wheel charge (WC) of $1 \frac{\$}{MWh}$ on the power flow between countries. Constraint (8.20) and (8.21) ensures the minimum and maximum production of a generator. Constraint (8.22) and (8.23) ensures the minimum up and downtime of the generators. Constraint (8.24) and (8.25) ensures the ramping limits of generators between timesteps. Constraint (8.26) ensures that the RES production is lower than the availability at that hour. (8.27), (8.28) and (8.30) ensure the charge, discharge and energy storage limits for storage units. Equation (8.29) is the sum of charge and discharge i.e. the net storage production. Equation (8.31) describes the relation between the charge, discharge and net power production of a storage unit. Equation (8.36) describes the logic between the binary commitment, start and stop variables of the generators. Equation (8.32) describes the relation between the flow on transmission lines and the power injection at nodes. Constraint (8.33) ensures flow limits on transmission lines. Equation (8.35) ensures that the total generation meets the total demand at every node and timestep. At last, the commitment variables are binary while the production are real numbers (8.37).

8.4.2 Overview of experiments

variant	ENS	Cost	Full
function f	(8.18)	(8.17),(8.18)	(8.17),(8.18),(8.19)
constraints	(8.20),(8.21),(8.27)-(8.37)	(8.20),(8.21),(8.27)-(8.37)	(8.20)-(8.37)
α		1	
function g_{max}		$\min \sum_{t \in T, g \in G} ENS_{gt}^2$	
function g_{min}		$\min \sum_t LOLH_t$	
extra constraints		$LOLH_t \in \{0,1\}$ $ENS_{nt} \leq D_{nt} LOLH_t$	
variant	CF Gas Coal Nuclear	CO ₂	
function f	(8.17),(8.18)	(8.17),(8.18)	
constraints	(8.20)-(8.37)	(8.20)-(8.37)	
α	$\alpha \in \{1.001, 1.005, 1.01\}$	$\alpha \in \{1.001, 1.005, 1.01\}$	
function g_{max}	$\max \sum_{t \in T, g \in G_{type}} p_{gt}$	$\max \sum_{g \in G, t \in T} FCP_g u_{gt} + VCP_g p_{gt}$	
function g_{min}	$\min \sum_{t \in T, g \in G_{type}} p_{gt}$	$\min \sum_{g \in G, t \in T} FCP_g u_{gt} + VCP_g p_{gt}$	

Table 8.6: The explicit details of all the experiments.

8.4.3 Additional Figures

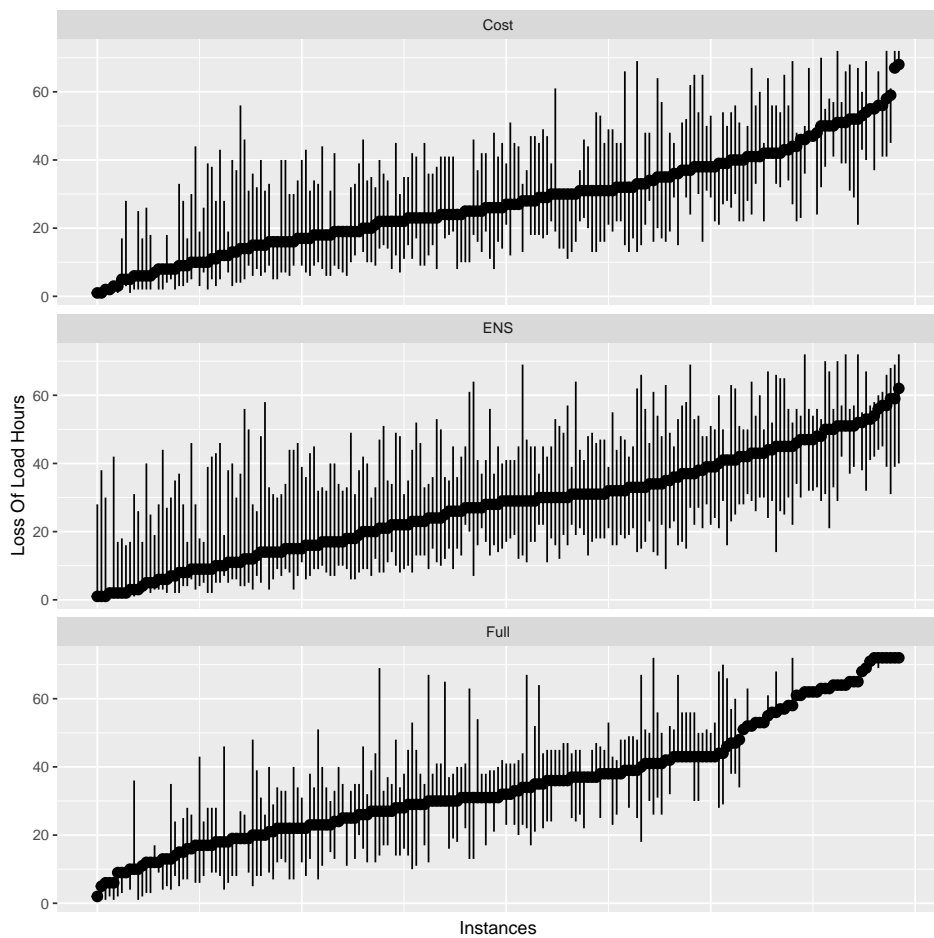


Figure 8.9: LOLH for all instances, ordered by the LOLH, for the Cost-Model, ENS-Model and Full-Model

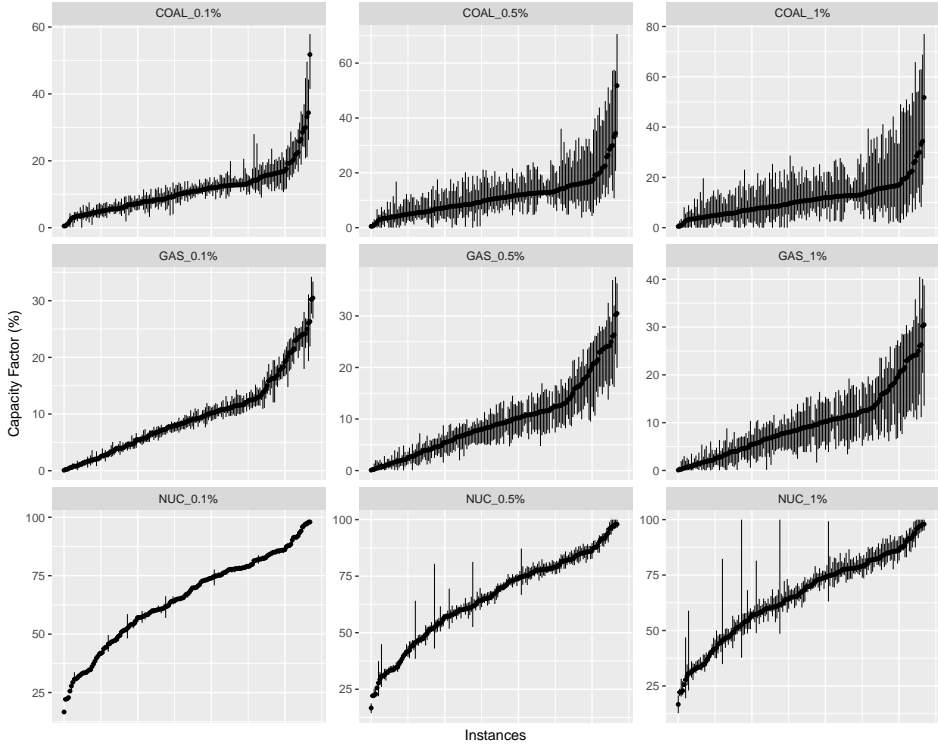


Figure 8.10: CF for all instances, ordered by the CF, for the Coal, Gas and Nuclear for different values of α

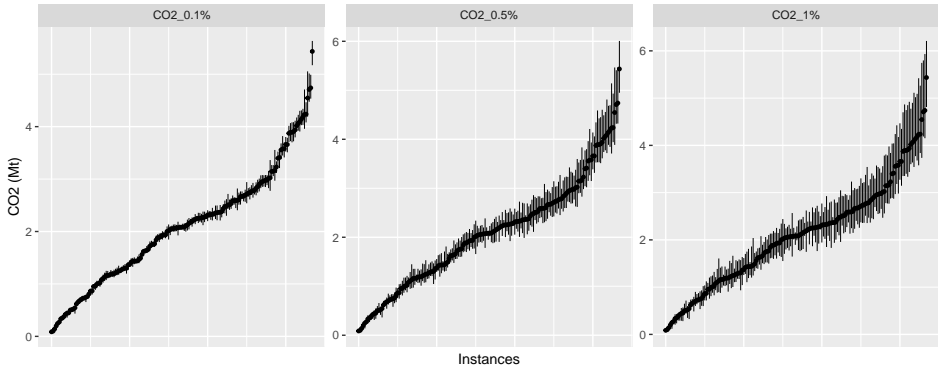


Figure 8.11: CO₂ for all instances, ordered by the CO₂, for different values of α

8.5 Appendix Chapter 6

8.5.1 Open Research

The ERA5 data used for to obtain the RES potentials in the study are available at the Climate Data Store via <https://www.doi.org/10.24381/cds.adbb2d47> under the License to use Copernicus Products [10, 11]. The conversion to renewable energy generation potential data used as input for the energy system model in the study are available at Github respectively via <https://github.com/laurensstoop/CapacityFactor-CF>

and <https://github.com/laurensstoop/EnergyVariables> with the MIT license. The Electricity Demand data used within the analysis is available at Zenodo via <https://www.doi.org/10.5281/zenodo.5780184> with the CC 4.0 license [4]. The RES generation and demand data used in this study are available at ZENODO via <https://www.doi.org/10.5281/zenodo.7390479> with CC-4.0 [21].

The Weather Regime data used for the categorisation of weather in the study are available upon request from dr. S.K.J. Falkena, the method describing their creation is presented in [7].

To obtain the hydro inflow data used in this study, please get into contact with dr. Jing Hu.

All the capacity data used and information about their origin is included in an online dataset at <https://github.com/rogierhans/TYNDP2040ScenarioData>.

8.5.2 Region definition and naming convention

The bidding zone codes of the bidding zones used is shown in Table 8.7, and their spatial location in Figure 8.12.

Table 8.7: Mapping between bidding zone codes and countries.

AL00	Albania	FR15	France	NL00	Netherlands
AT00	Austria	HR00	Croatia	NOM1	Norway
BA00	Bosnia	HU00	Hungary	NON1	Norway
BE00	Belgium	IE00	Ireland	NOS0	Norway
BG00	Bulgaria	ITCN	Italy	PL00	Poland
CH00	Switzerland	ITCS	Italy	PT00	Portugal
CY00	Cyprus	ITN1	Italy	RO00	Romania
CZ00	Czech Republic	ITS1	Italy	RS00	Serbia
DE00	Germany	ITSA	Italy	SE01	Sweden
DKE1	Denmark	ITSI	Italy	SE02	Sweden
DKKF	Denmark	LT00	Lithuania	SE03	Sweden
DKW1	Denmark	LUB1	Luxemburg	SE04	Sweden
EE00	Estonia	LUF1	Luxemburg	SI00	Slovenia
EL00	Greece	LUG1	Luxemburg	SK00	Slovakia
EL03	Greece	LV00	Latvia	TR00	Turkey
ES00	Spain	ME00	Montenegro	UA01	Ukraine
FI00	Finland	MK00	North Macedonia	UK00	United Kingdom
FR00	France	MT00	Malta	UKNI	United Kingdom

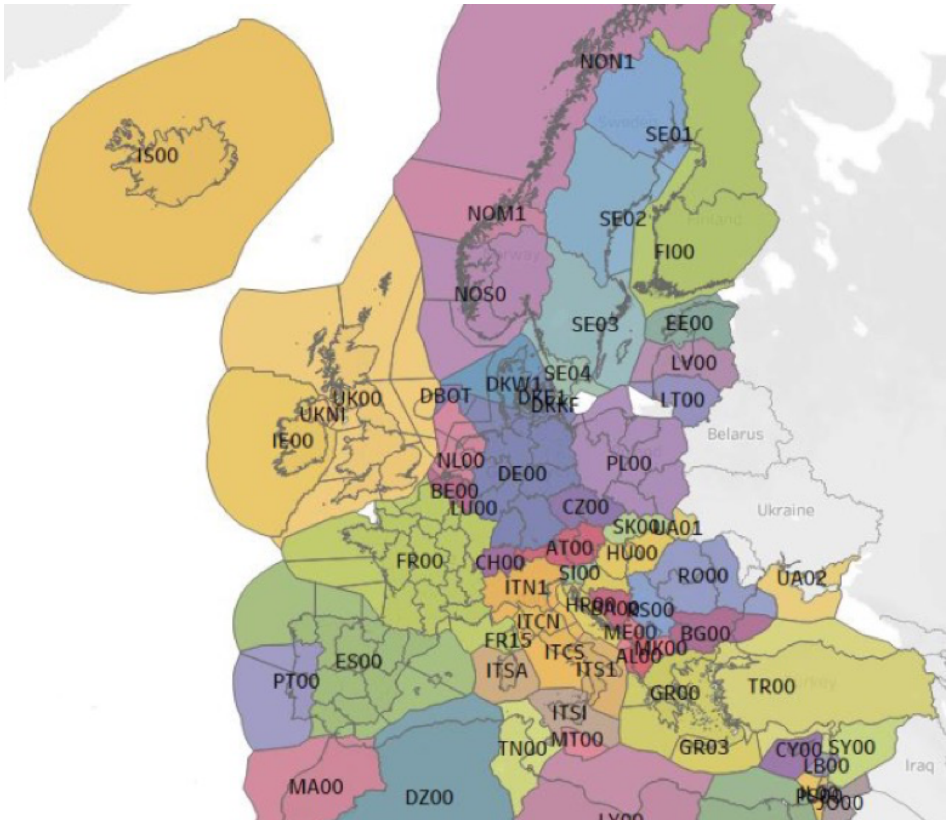


Figure 8.12: Location of the bidding zones used in this study. Figure provided by ENTSO-E.

8.5.3 Specified capacity of the main bidding zones used

The specific installed capacities for the main bidding zones used in the analysis are shown in Figure 8.13. The technologies are clustered based on their core principle in Hydro, Other, Solar, Thermal and Wind. The zones shown are the central European subset represented by Germany (*DE00*), France (*FR00*) and the Netherlands (*NL00*), and the Scandinavian countries represented by the southern region of Norway (*NOM1*) and the northern region of Sweden (*SE01*). For the Scandinavian countries any region in Norway or Sweden could be used, for simplicity the first zone was thus chosen.

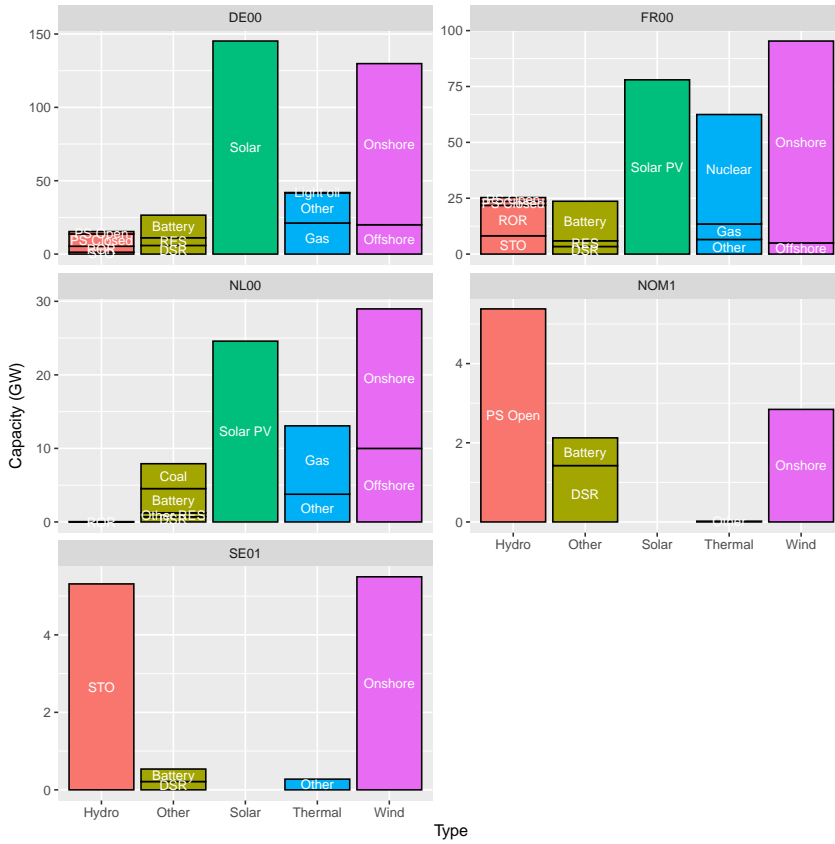


Figure 8.13: Installed capacity for a subset of bidding zones in the TYNDP Distributed Energy 2040 scenario is shown. The technologies listed are clustered according to their driving principle.

8.5.4 Unit Commitment Model

In this section, we define the Unit Commitment and Economic Dispatch (UCED) model that we use in this paper. Our UCED description is based on a Mixed Integer Linear Program (MILP) formulation with detailed thermal generators, Renewable Energy Sources (RES), storage, and transmission lines. The decision variables p_{gt} , p_{rt} , p_{st} are the generation of thermal generator (g), RES (s), and storage (s) unit at time step t . Other variables are added to narrow down the feasible state space of these variables. We use the well-known 3-bin formulation [15] which is given in:

$$\min \sum_{t \in T} \sum_{n \in N} VOLL \cdot ENS_{nt} + \sum_{g \in G} a_g u_{gt} + b_g p_{gt} + v_{gt} cost_{start} \quad (8.38)$$

s.t.

$$p_{gt} \geq u_{gt} \underline{P}_g, g \in G, t \in T \quad (8.39)$$

$$p_{gt} \leq \overline{P}_g u_{gt}, g \in G, t \in T \quad (8.40)$$

$$\sum_{i=t-UT_g+1}^t v_{gi} \leq u_{gt}, t \in T, g \in G \quad (8.41)$$

$$\sum_{i=t-DT_g+1}^t w_{gi} \leq 1 - u_{gt}, t \in T, g \in G \quad (8.42)$$

$$p_{gt} - p_{gt-1} \leq (SU_g - RU_g) v_{gt} + RU_g u_{gt}, t \geq 2, g \in G \quad (8.43)$$

$$p_{gt-1} - p_{gt} \leq (SD_g - RD_g) w_{gt} + RD_g u_{gt-1}, t \geq 2, g \in G \quad (8.44)$$

$$p_{rt} \leq AF_{rt} \overline{P}_{rt}, r \in R, t \in T \quad (8.45)$$

$$0 \leq pc_{st} \leq \overline{PC}_s, t \in T, s \in S \quad (8.46)$$

$$0 \leq pd_{st} \leq \overline{PD}_s, t \in T, s \in S \quad (8.47)$$

$$p_{st} = pd_{st} - pc_{st}, t \in T, s \in S \quad (8.48)$$

$$\underline{PE}_s \leq pe_{st} \leq \overline{PE}_s, t \in T, s \in S \quad (8.49)$$

$$pe_{st} = pe_{st-1} + pc_{st} * \eta_{st}^c - \frac{pd_{st}}{\eta_{st}^d}, t \in T, s \in S \quad (8.50)$$

$$inj_{nt} = \sum_{l=(n' \rightarrow n), n' \in N} f_{lt}, t \in T, n \in N \quad (8.51)$$

$$\underline{f}_l \leq f_{lt} \leq \overline{f}_l, l \in L, t \in T \quad (8.52)$$

$$\sum_{g \in G_n} p_{gt} + \sum_{r \in R_n} p_{rt} + \sum_{s \in S_n} p_{st} + inj_{nt} = D_{nt} - ENS_{nt}, t \in T, n \in N \quad (8.53)$$

$$u_{gt} - u_{gt-1} = v_{gt} - w_{gt}, t \in T, g \in G \quad (8.54)$$

$$u_{gt}, v_{gt}, w_{gt} \in \{0, 1\}, p_{gt}, p_{rt}, p_{st}, pe_{st}, inj_{nt}, f_{lt} \in \mathbb{R} \quad (8.55)$$

(8.38) is the objective function of the UC consisting the system wide cost of Energy not Served (ENS) times the Value of Lost Load (VOLL) and the generation cost and start cost, a_g is the constant cost and b_g is the linear cost coefficient.

Constraint (8.39) and (8.40) ensure the minimum and maximum production of generators. Constraint (8.41) and (8.42) ensure the minimum up and downtime of generators. Constraint (8.43) and (8.44) ensure the ramping limits of generators between time steps. Constraint (8.45) ensures that the RES production is lower than the availability at that hour. (8.46), (8.47) and (8.49) ensure the charge, discharge, and energy storage limits for storage units. Equation (8.48) is the sum of charge and discharge i.e. the net storage production. Equation (8.50) describes the relation between the charge, discharge, and net power production of a storage unit. Equation (8.54) describes the logic between the binary commitment, start and stop variables of the generators. Equation (8.51) describes the relation between the flow on transmission lines and the power injection at nodes. Constraint (8.52) ensures flow limits on transmission lines. Equation (8.53) ensures that the total generation meets the total demand at every node and time step. At last, the commitment variables are binary while the generation are real numbers (8.55).

8.5.5 Validating Assumptions

We assume that most model characteristics normally included in the unit commitment problem such as ramping limits, minimum uptime, and binary commitment variables, are unnecessary when you are only interested in energy not served [26]. To validate this assumption, we ran four models with two different objective functions and two levels of detail to check whether this results in equivalent solutions. The first objective function minimises ENS directly, and the second one indirectly through the minimisation of total system costs in which ENS is heavily penalised with a Value of Loss of Load (VOLL). Both types of minimisation's were applied to a full, and a simplified version of the UCED model. In the simplified version the ramping limits, minimum uptime, and binary commitment variables are omitted. We ran the four UCED models in chunks of 720 timesteps at the time for the weather years 1982–2010 and original 3 TYNDP scenarios.

We use the following naming convention to indicate the four different models used:

- Detailed ENS Model, including ramping limits, minimum up- and downtime and with binary variables. ENS minimisation.
- Detailed Cost Model, including ramping limits, minimum up- and downtime but without binary variables. Cost minimisation.
- ENS Model, simplified model without binary variables. ENS minimisation.
- Cost Model, simplified model without binary variables. Cost minimisation.

The results, see Table 8.8, show that in all models the average ENS is almost the same. Moreover, the individual differences in all instances are smaller than 1 MWh, a negligible percentage of the total demand. The average computation time per weather year for these models differs significantly. As expected, a simplified model with ENS minimisation is significantly faster than running the model with more detail. Consequently, as the solution metrics that are relevant for our analysis

(EENS) are the same, this is the preferred model to use as it allows us to run many power system configurations and weather years in order to get robust results.

Table 8.8: For the four different model formulations, the averaged total ENS in the system, the maximum difference in ENS of model run on a single weather compared to the average ENS of the same year and the average computation time of a year are shown. The average is calculated over all 720 hour chunks for the weather years 1982–2010.

Model	Detailed ENS	Detailed Cost	ENS	Cost
Average ENS (MWh)	5246374.8	5246375.0	5246374.8	5246374.9
Max difference (MWh)	0.28	0.61	0.28	0.22
Avg. Computation time (s)	1051.9	593.6	52.7	190.9

8.5.6 Method for determining photovoltaic panel generation potential

To obtain the solar photovoltaic potential generation, we follow the method as set out by [13] Explicitly, the potential PV_{pot} is calculated by formula (8.56).

$$PV_{pot} = P_R \frac{I}{I_{std}} \quad (8.56)$$

where I is the short-wave downward radiation at the surface, I_{std} is the incoming short-wave downward radiation under the standard test condition for solar photovoltaic cells ($I_{std} = 1000 \text{ W/m}^2$) and the performance ratio is given by P_R .

The performance ratio can be modelled in a number of ways [13]. Here, see Eq. (8.57), we take into account the cooling effect of the wind on a solar panel cell temperature, which in turn is also influenced by the irradiance and the ambient air temperature, see Eq. (8.58).

$$P_R = 1 + \gamma (T_{cell} - T_{ref}) \quad (8.57)$$

where $\gamma = -0.5 \text{ }^\circ\text{C}$ and the $T_{ref} = 25 \text{ }^\circ\text{C}$ is the standard test condition temperature for photovoltaic cells. The cell temperature T_{cell} is modeled by formula (8.58).

$$T_{cell} = c_1 + c_2 T + c_3 I + c_4 V \quad (8.58)$$

where T is the air temperature around the cell, I the short-wave downward irradiance on the cell and V the wind around the cell. The constants c_1 to c_4 have been determined by [22] to be $c_1 = 4.3 \text{ }^\circ\text{C}$, $c_2 = 0.943$, $c_3 = 0.028 \text{ }^\circ\text{C m}^2 \text{ W}^{-1}$ and $c_4 = -1.528 \text{ }^\circ\text{C s m}^{-1}$.

8.5.7 Method for determining wind turbine generation potential

To convert windspeeds to wind turbine generation potential we use an adjusted version of the power curve method from [13]. We made three adjustments to this

model. First, we reduced the effective capacity factor (CF_e) with 5% to 95% to represent the wake losses in large scale wind-farms. Secondly, we introduce a linear decay in the capacity factor at high wind speeds to more accurately represent high windspeed operational conditions. The third change was that we tuned the power curve regimes. Equation (8.59) gives the capacity factor for wind turbines (CF_{wind}) used in this study.

$$CF_{wind}(t) = CF_e \times \begin{cases} 0 & \text{if } V(t) < V_{CI}, \\ \frac{V(t)^3 - V_{CI}^3}{V_R^3 - V_{CI}^3} & \text{if } V_{CI} \leq V(t) < V_R, \\ 1 & \text{if } V_R \leq V(t) < V_D, \\ \frac{V_{CO} - V(t)}{V_{CO} - V_D} & \text{if } V_D \leq V(t) < V_{CO}, \\ 0 & \text{if } V(t) \geq V_{CO}. \end{cases} \quad (8.59)$$

Here $V(t)$ is the wind speed at the height of the wind turbine and the power curve regimes are given by the cut-in ($V_{CI}=3$ m/s), rated ($V_R= 11$ m/s), decay ($V_D=20$ m/s) and cut-out ($V_{CO}= 25$ m/s) wind speed. The windspeed provided by ERA5 (at 100 meter) did not match the hub height for the wind turbines used in the TYNDP scenario. Using the wind profile power law we scaled the windspeed to 120 and 150 meters for on- and offshore turbines. The surface roughness was set to a constant value for both onshore ($\alpha = 0.143$) and offshore regions ($\alpha = 0.11$) in line with the reported values in [12].

8.5.8 Method for determining Hydropower generation potential

The hydro inflow data are based on historical river runoff reanalysis data simulated by the E-HYPE model [5]. E-HYPE is a pan-European model developed by The Swedish Meteorological and Hydrological Institute (SMHI), which describes hydrological processes including flow paths at the subbasin level. A subbasin in the context of hydrology is the region from which all surface run-off flows through to a particular point, this is generally a the collection of upstream streams, rivers and lakes.

E-hype only provides the time series of daily river runoff (in m^3/s) entering the inlet of each European subbasin over 1980-2010. To match the operational resolution of the dispatch model, we linearly downscale the time series to hourly. By summing up runoff associated with the inlet subbasins of each country, we also obtain the country-level river runoff.

The hydro inflow time series per country as inputs of the dispatch model is defined in this study as normalized energy inflows (per unit installed capacity of hydropower) embodied in the country-level river runoff. Therefore, it resembles an input capacity factor time series that can be extracted from water (CFW_t). The UCED model decides whether the energy inflows are actually used for electricity generation, stored, or spilled (in case the storage reservoir is already full). The hydro inflows CFW_t at a given time t is proportional to the instantaneous river

runoff Q_t :

$$CFW_t = \frac{Q_t}{Q_{avg}} CFW_{avg} \quad (8.60)$$

Where Q_{avg} is the long-term average river runoff and CFW_{avg} is the corresponding average energy inflow. However, the long-term average data of CFW_{avg} are not available and cannot be calculated due to the lack of plant-level hydrological details such as hydraulic head; active storage volume. For practical reasons, we use the long-term capacity factors based on the actual electricity outputs of aggregated hydropower plants to replace CFW_{avg} . They can be calculated based on the average of reported yearly capacity factors CF_{avg} [6]. The calculation would be ideally carried out for the entire 30-year period 1980-2010, but yearly capacity factors reported for many European countries are not readily available prior to 1990. Therefore, we calculated the ratio between the CFW_{avg} and Q_{avg} for the period 1990-2010 and used it as a scalar for the entire 30-year Q_t time series.

In reality CF_{avg} may be smaller than CFW_{avg} , because not all energy embedded in the river runoff is always converted into electricity due to spillage or non-energy usage. As a result, the values in the CFW_t time series used as inputs in the UCED model may be underestimated.

We explicitly consider three types of hydropower plants, namely storage hydropower plant (STO), run-of-river hydropower plant (ROR) and pumped storage hydropower plant (PHS). For modelling purposes, we need to estimate the specific maximum energy storage content (or specific storage size [$\frac{GWh}{MW}$]), for each type of hydropower. This is performed by deriving an EU-average specific energy storage content $\frac{GWh}{MW}$ per hydropower type based on an in-house database containing 207 large power plants. The derived specific energy storage content is calibrated to the present level of total storage size (220 TWh) of STO, RoR, and PHS together in Europe reported by [16]. The resulting specific energy storage contents for STO, RoR and PHS are 2.05, 0.43 and 0.18 $\frac{GWh}{MW}$.

8.5.9 Classification of weather into regimes

To classify the European winter time period meteorological variability at the synoptic scale, a number of different criteria can be used. Although this classification is generally according to the anomaly of the geopotential height at the 500 hPa level, they have a strong relation with the variability at the surface [9, 24, 2]. Recently the Grosswetterlagen method [1] has gained more traction due to the use of machine learning to classify the weather [18]. However, the large number of regimes used limits the interpretability of a single regime [18, 7]. For this reason, the use of the four European weather regimes based on a k -means clustering as set out in [17] is still prevalent in many impact studies (e.g. when considering the impact of the variability of weather on the renewable energy resource [25, 2, 19, 23]). On the other hand, when only four weather regimes are used to describe the full variability in surface weather, it is difficult to separate partially mixed signals that are present due to the coarse classification of the meteorological variability [9].

The use of four regimes to classify the winter time period weather in Europe is mostly due to the initial work by [17] on using k -means clustering on the first

few empirical orthogonal functions of the geopotential height at the 500hPa level. While the granularity of the meteorological data has increased by 3-orders since then. Recently, [7] revisited the identification of European weather regimes. They found that when the full field data is used, instead of only the first few empirical orthogonal functions, the optimal number of weather regimes is six when looking at the Bayesian Information Criterion. In addition, they show that by incorporating a weak persistence constraint instead of using a low-pass filter to stabilise the regime identification, the classification of a specific regime cluster is better and thus more defined.

8.5.10 Summary of relative occurrence of weather regimes for all bidding zones

An overview of the relative occurrence of the weather regimes in the 1, 10 and 30 days prior to an ENS event for all bidding zones and scenarios is provided in figures 8.14, 8.15 and 8.16.

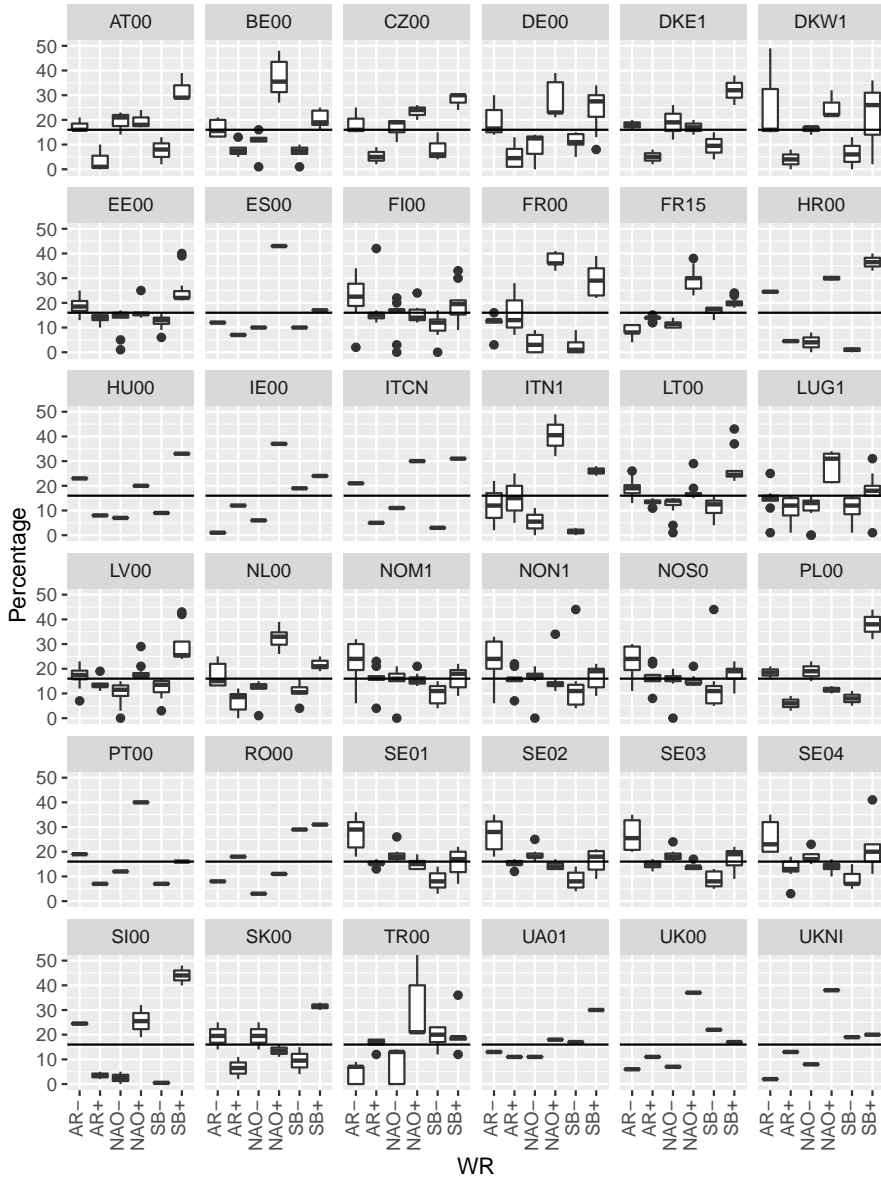


Figure 8.14: For each bidding zone and for all 12 scenarios the occurrence of weather regimes within a 1 day period before the ENS event.

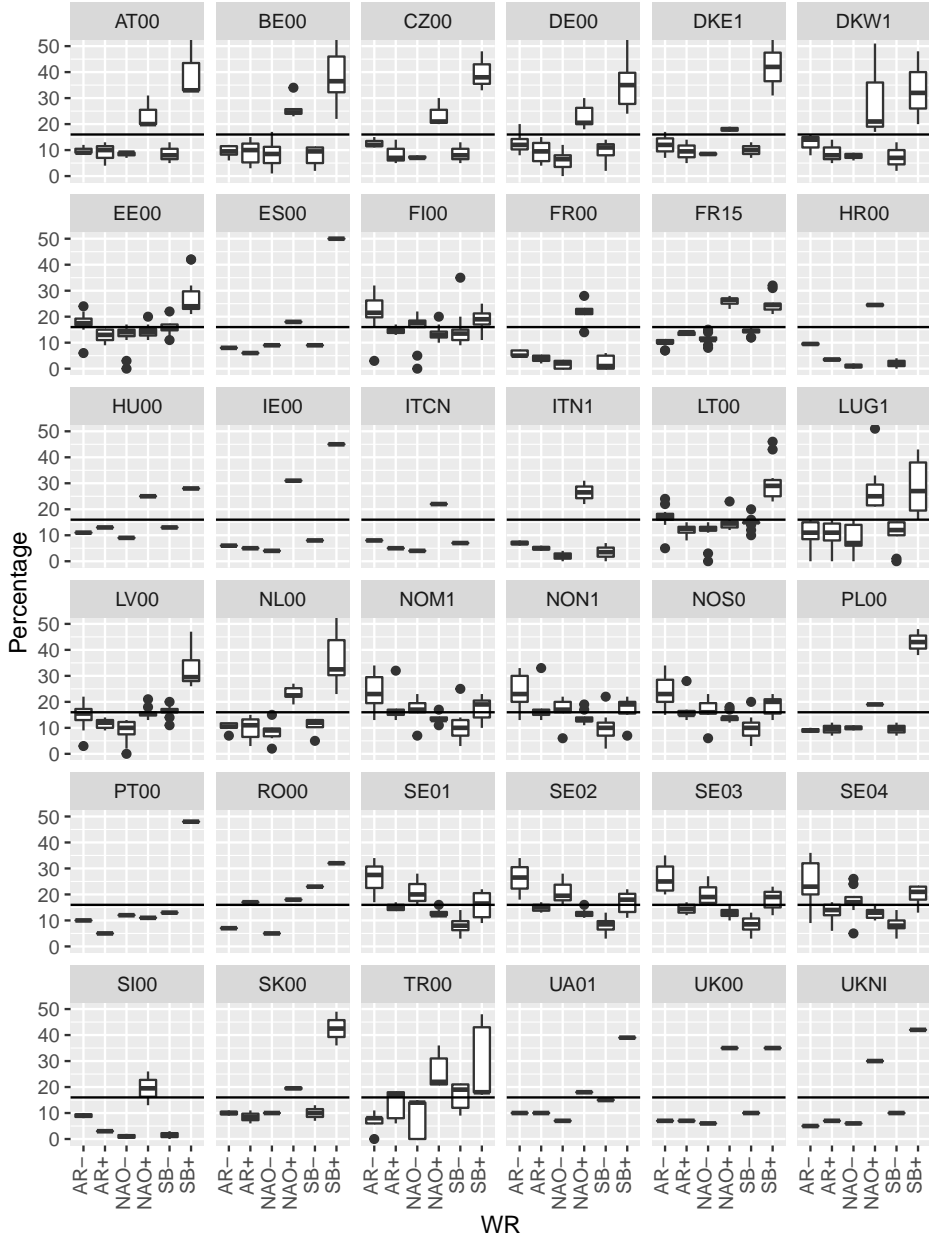


Figure 8.15: For each bidding zone and for all 12 scenarios the occurrence of weather regimes within a 10 day period before the ENS event.

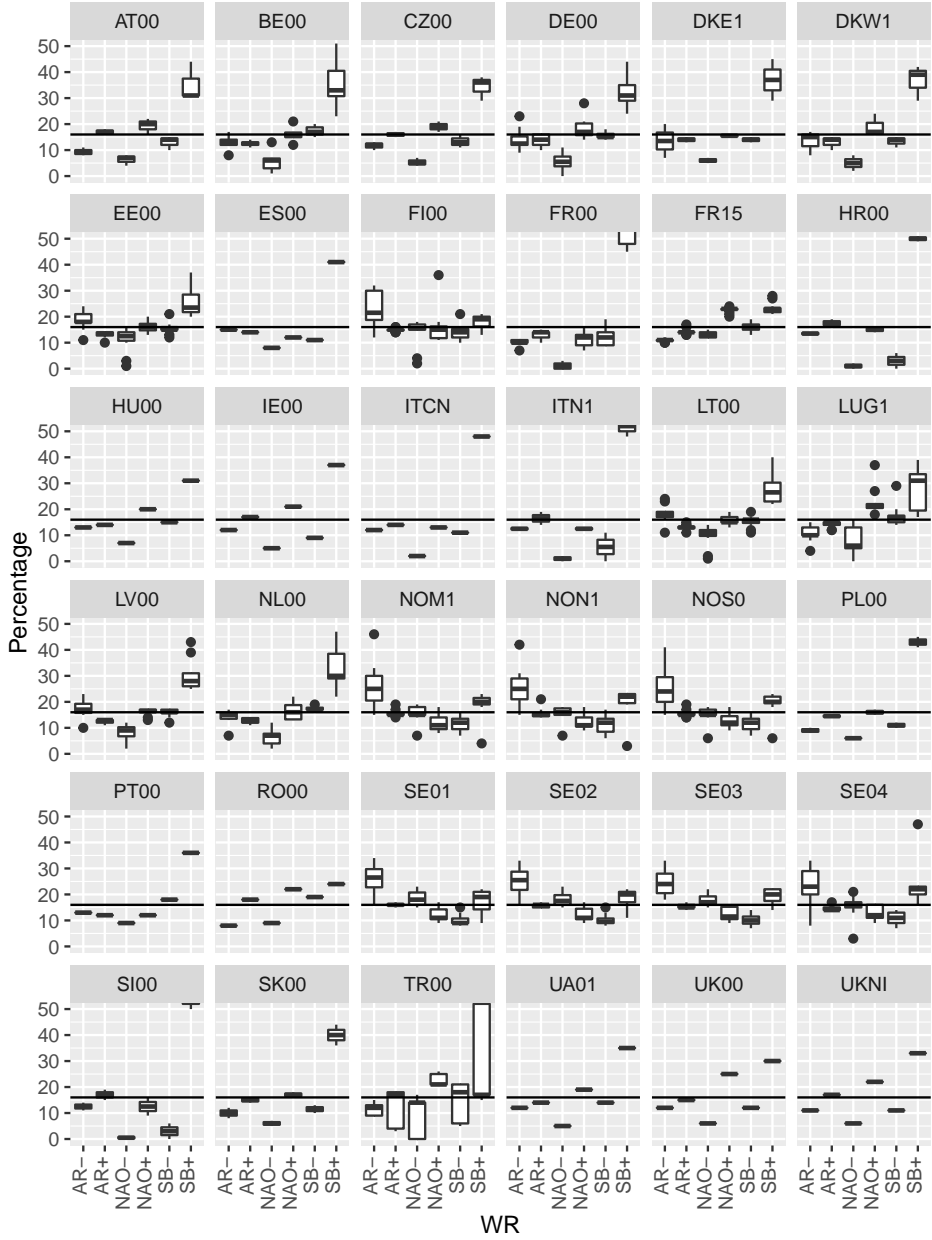


Figure 8.16: For each bidding zone and for all 12 scenarios the occurrence of weather regimes within a 30 day period before the ENS event.

8.5.11 Meteorological changes between different weather regimes

An overview of anomaly in the wind speed at 100 meter height, solar irradiance and air temperature at 2 meter height over Europe can be found in Figures 8.17, 8.18, and 8.19, respectively. The anomaly in solar photovoltaic potential is shown in Figure 8.20, the anomaly of the wind turbine potential was provided in Figure 6.7.

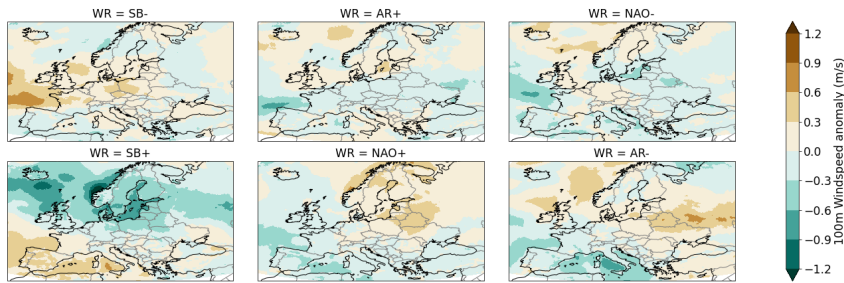


Figure 8.17: The average 100 meter windspeed anomaly from December to March (DJFM) in Europe for each weather regime with respect to the DJFM mean over 1982-2010.

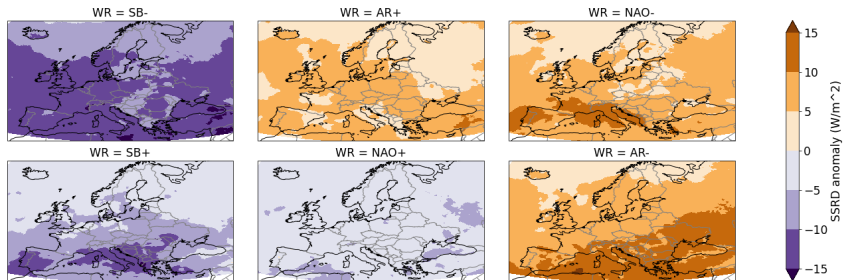


Figure 8.18: The average solar irradiance anomaly from December to March (DJFM) in Europe for each weather regime with respect to the DJFM mean over 1982-2010.

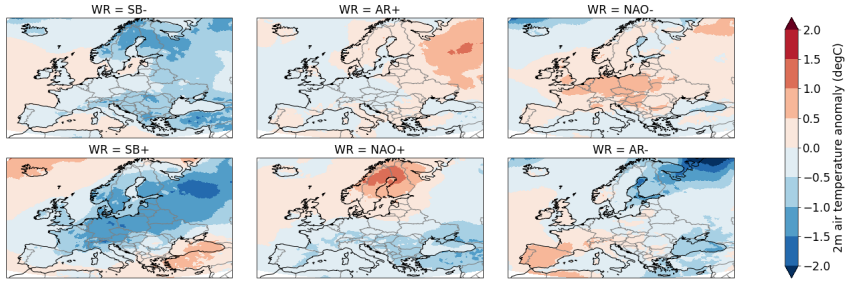


Figure 8.19: The average 2 meter air temperature anomaly from December to March (DJFM) in Europe for each weather regime with respect to the DJFM mean over 1982-2010.

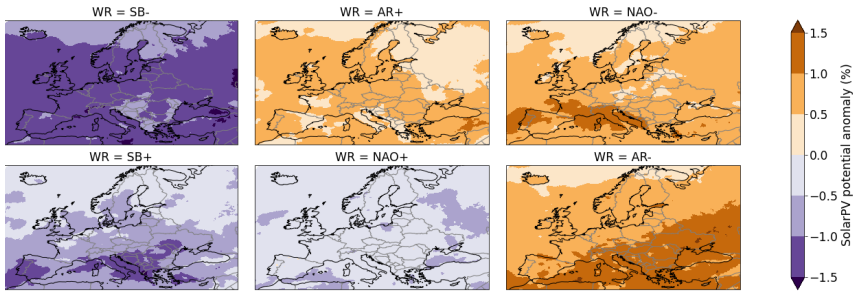


Figure 8.20: The average solar photovoltaic power generation anomaly from December to March (DJFM) in Europe for each weather regime with respect to the DJFM mean over 1982-2010.

Bibliography

- [1] F Baur, P Hess, and H Nagel. “Kalender der grosswetterlagen Europas 1881–1939”. In: *Bad Homburg* 35 (1944).
- [2] Hannah C. Bloomfield, David J. Brayshaw, and Andrew J. Charlton-Perez. “Characterizing the winter meteorological drivers of the European electricity system using targeted circulation types”. In: *Meteorological Applications* 27.1 (Dec. 2019). DOI: 10.1002/met.1858. URL: <https://doi.org/10.1002/met.1858>.
- [3] Stephen Boyd, Neal Parikh, and Eric Chu. *Distributed optimization and statistical learning via the alternating direction method of multipliers*. Now Publishers Inc, 2011.
- [4] Matteo De Felice. *ENTSO-E Pan-European Climatic Database (PECD 2021.3) in Parquet format*. Dec. 2021. DOI: 10.5281/zenodo.5780185. URL: <https://doi.org/10.5281/zenodo.5780185>.
- [5] Chantal Donnelly, Jafet CM Andersson, and Berit Arheimer. “Using flow signatures and catchment similarities to evaluate the E-HYPE multi-basin model across Europe”. In: *Hydrological Sciences Journal* 61.2 (2016), pp. 255–273.
- [6] Eurostat. *Renewable energy statistics*. 2021. URL: https://ec.europa.eu/eurostat/statistics-explained/index.php?title=Renewable_energy_statistics.
- [7] Swinda K.J. Falkena et al. “Revisiting the identification of wintertime atmospheric circulation regimes in the Euro-Atlantic sector”. In: *Quarterly Journal of the Royal Meteorological Society* May (2020), pp. 1–14. ISSN: 1477870X. DOI: 10.1002/qj.3818.
- [8] Claudio Gentile, Germán Morales-España, and Andrés Ramos. “A tight MIP formulation of the unit commitment problem with start-up and shut-down constraints”. In: *EURO Journal on Computational Optimization* 5.1-2 (2017), pp. 177–201.
- [9] Christian M. Grams et al. “Balancing Europe’s wind-power output through spatial deployment informed by weather regimes”. In: *Nature Climate Change* 7.8 (July 2017), pp. 557–562. DOI: 10.1038/nclimate3338. URL: <https://doi.org/10.1038/nclimate3338>.

- [10] H Hersbach et al. “ERA5 hourly data on single levels from 1959 to present”. In: *Copernicus Climate Change Service (C3S) Climate Data Store (CDS)* (2018). DOI: 10.24381/cds.adbb2d47.
- [11] Hans Hersbach et al. “The ERA5 global reanalysis”. In: *Quarterly Journal of the Royal Meteorological Society* (2020). DOI: 10.1002/qj.3803.
- [12] S. A. Hsu, Eric A. Meindl, and David B. Gilhousen. “Determining the Power-Law Wind-Profile Exponent under Near-Neutral Stability Conditions at Sea”. In: *Journal of Applied Meteorology* 33.6 (June 1994), pp. 757–765. DOI: 10.1175/1520-0450(1994)033<0757:dtplwp>2.0.co;2. URL: [https://doi.org/10.1175/1520-0450\(1994\)033%3C0757:dtplwp%3E2.0.co;2](https://doi.org/10.1175/1520-0450(1994)033%3C0757:dtplwp%3E2.0.co;2).
- [13] S. Jerez et al. “The CLIMIX model: A tool to create and evaluate spatially-resolved scenarios of photovoltaic and wind power development”. In: *Renewable and Sustainable Energy Reviews* (2015). DOI: 10.1016/j.rser.2014.09.041.
- [14] Bernard Knueven, James Ostrowski, and Jean Paul Watson. “On mixed integer programming formulations for the unit commitment problem”. In: *E-print, Department of Industrial and Systems Engineering University of Tennessee, Knoxville, TN 37996* (2018).
- [15] Bernard Knueven, James Ostrowski, and Jean-Paul Watson. “A novel matching formulation for startup costs in unit commitment”. In: *Mathematical Programming Computation* (2020), pp. 1–24.
- [16] Tim Mennel et al. “The hydropower sector’s contribution to a sustainable and prosperous Europe”. In: *Main Report* (2015).
- [17] Paul-Antoine Michelangeli, Robert Vautard, and Bernard Legras. “Weather regimes: Recurrence and quasi stationarity”. In: *Journal of the atmospheric sciences* 52.8 (1995), pp. 1237–1256.
- [18] Robert Neal et al. “A flexible approach to defining weather patterns and their application in weather forecasting over Europe”. In: *Meteorological Applications* 23.3 (2016), pp. 389–400.
- [19] Noelia Otero et al. “Characterizing renewable energy compound events across Europe using a logistic regression-based approach”. In: *Meteorological Applications* 29.5 (Sept. 2022). DOI: 10.1002/met.2089. URL: <https://doi.org/10.1002/met.2089>.
- [20] Kai Pan and Yongpei Guan. “A polyhedral study of the integrated minimum-up/-down time and ramping polytope”. In: *arXiv preprint arXiv:1604.02184* (2016).
- [21] Laurens P. Stoop. *Energy Climate dataset consistent with ENTSO-E TYNDP2020 studies (CSV & NetCDF)*. Version 1. Laurens P. Stoop received funding from the Netherlands Organization for Scientific Research (NWO) under Grant No. 647.003.005. Dec. 2022. DOI: 10.5281/zenodo.7390479. URL: <https://doi.org/10.5281/zenodo.7390479>.

- [22] G TamizhMani et al. “Photovoltaic Module Thermal/Wind Performance: Long-Term Monitoring and Model Development for Energy Rating”. In: *NCPV and Solar Program Review Meeting Proceedings, 24-26 March 2003, Denver, Colorado (CD-ROM)* (2003). URL: <https://www.osti.gov/biblio/15006842>.
- [23] Paulina Tedesco et al. *Gaussian copula modeling of extreme cold and weak-wind events over Europe conditioned on winter weather regimes*. 2022. DOI: 10.48550/ARXIV.2209.12556. URL: <https://arxiv.org/abs/2209.12556>.
- [24] Hazel E Thornton et al. “The relationship between wind power, electricity demand and winter weather patterns in Great Britain”. In: *Environmental Research Letters* 12.6 (June 2017), p. 064017. DOI: 10.1088/1748-9326/aa69c6. URL: <https://doi.org/10.1088/1748-9326/aa69c6>.
- [25] Karin van der Wiel et al. “The influence of weather regimes on European renewable energy production and demand”. In: *Environmental Research Letters* (2019B). DOI: 10.1088/1748-9326/ab38d3. URL: <https://dx.doi.org/10.1088/1748-9326/ab38d3>.
- [26] R.H. Wuijts, M. van den Akker, and M. van den Broek. “Effect of modelling choices in the unit commitment problem”. In: *Energy Systems* (2023). DOI: 10.1007/s12667-023-00564-5.